SPECTROPOLARIMETRY OF THE SUN AND F, G AND K TYPE STARS

by

S. R. FULLERTON, B.Sc.

A THESIS SUBMITTED TO THE UNIVERSITY OF GLASGOW
FOR THE DEGREE OF DOCTOR OF PHILOSOPHY

Department of Physics and Astronomy,
University of Glasgow.
September, 1994.

ProQuest LLC.
789 East Eisenhower Parkway
P.O. Box 1346
Ann Arbor, MI 48106 – 1346

CONTENTS

SUMMARY

In this thesis the role of polarimetry in investigating the effects of active regions on the Sun, and similar magnetic regions on late-type stars, have upon the emitted radiation is pursued, and which forms an important part of understanding solar-stellar connections.

A whole-disk solar polarimeter incorporating a tilt-tunable interference filter was used to measure the polarization at the centre of the absorption profile due to Fe I lines near 4782Å and at Hβ. Significant polarizations of up to 2.10^{-4} were measured with accuracies of 7.10^{-5} or better in p for both spectral regions, and were found to vary between the days of observations.

It was postulated that the positions of active regions on the visible hemisphere of the Sun were causing these variations. A theoretical argument was that a combination of magnetic intensification in magnetically sensitive lines and of resonance scattering were producing the measurable polarization. A model was devised that was consistent with the observed data, and was extended to predict how the observed polarization from the Sun, or any star upon which magnetic regions exist, would vary as these regions traversed the star's visible hemisphere.

To attempt to show observational evidence that these postulations were correct a double beam polarimeter was designed and constructed for use in measuring the polarization from small areas on the disk of the Sun, including sunspots and areas of quiet photosphere. However this investigation did not come to fruition.

It is clear that further studies in many areas of solar polarization are required to confirm the variations, with more advanced detection systems and procedures of investigation into magnetic and scattering effects.

A number of F, G and K type stars were observed to investigate whether similar polarimetric variations existed for them. Measurements made with the Glasgow polarimeter showed that α Tau was polarized at 4500Å, while α Boo exhibited different levels of polarization at four wavelengths, and evidence of temporal

variations were found. The current instrumental polarization of the instrument was also found.

On finding that the results of stellar observations showed large anti-correlations between the two channels of the Glasgow polarimeter, it was argued that atmospheric effects could cause these correlations when the design of the instrument and the data acquisition method were taken into account. Although the argument seemed sound, an attempt to show these effects numerically by using dummy data was not conclusive.

ξ Boo A, for which magnetic fields have been reported and which has a 6.2 day rotation period, and χ Her were observed with the Multi-purpose Fotometer at the Jacobus Kapteyn Telescope. However the instrument appeared to have a large and varying instrumental polarization. An attempt was made to formulate this variation and subtract those measurements of an unpolarized standard star from those of the target stars, but no reasonable formulation could be estimated, and the polarization measurements of ξ Boo A and χ Her are therefore inconclusive.

The effect of dead-time upon polarimetric measurements acquired using photometric techniques was considered, and it was found that for increasing photon count rates the observed polarization and its error were underestimated. A correction procedure was formulated, and the dead-time of the solar whole-disk instrument was estimated to be 100ns.

It is of great importance to follow up the findings in this thesis with improved polarimetric observations of both the Sun and solar-type stars to further understand the mechanisms behind the observed polarizations, and to explore "solar-stellar connections".

PREFACE

The work in this thesis was carried out by the author at the University of Glasgow Observatory during the period 1990-93, being funded by the Science and Engineering Research Council (now PPARC) and supervised by Dr. D. Clarke.

Whilst many of the instruments used by the author had already been built by Dr. Clarke and previous members of the Observatory, the author made refinements to both the instrumentation and the computational side of the data acquisition. Due to the primitive nature of the existing data reduction programs, however, the author devised and wrote practically all software used in the analyses.

The first two chapters cover the background to the work, the theory behind the production of solar and stellar polarizations, and the instrumentation used. Although only devising one instrument himself, for which a full description is made, the author also describes the other instruments for which knowledge is required to understand how the author's own work contributed during the analysis of data acquired with those instruments.

Chapters 3, 4 and 5 describe the observations and analyses of solar and stellar data. The author wishes to thank Dr. Clarke for supplying the raw data used for the material in Chapter 3. The stellar data was obtained personally, and for those measurements made with the Jacobus Kapteyn Telescope in April 1992 thanks are extended to the support astronomer, Rene Rutten, for his help with the various problems encountered with the polarimeter. All analyses in these chapters were performed by the author, but Dr. Clarke supplied the formulation for the dead-time corrections.

Chapter 6 contains the theoretical argument and model that magnetic active regions are responsible for solar and/or stellar polarizations, and finally chapter 7 then discusses the work in the thesis.

The author has published part of this thesis from section 3.3:-

"Studies in Solar Polarimetry": Fullerton, S.R., 1993, in "*X-ray and Ultraviolet Polarimetry*", *Proc. SPIE*, **2010**, 60, ed. Fineschi, S.

ACKNOWLEDGEMENTS

I should first of all like to thank Dr. David Clarke for his ideas and input into my work, his electronics expertise, and for supplying the raw solar data that was analysed in Chapter 3. Also thanks go to Colin Hunter, the technician at the Observatory, who constructed the double-beam polarimeter (a number of times!) from my various designs, and also for his footballing arguments. I am also grateful to Jaber Naghizadeh, Geoff Fox, Tom Kelly, Bob Loney and Margaret Morris at the Observatory for ideas, chat and generally keeping me sane in the loneliness of the Observatory!

Also thanks go to the many other members of the Astronomy department at the University, and to the other many friends I have made since my arrival in Glasgow, especially Ricky, Marianne, Eddie, Laura, James, Jane, and Laura.

A special mention should be made of my parents for their continuing support in many ways during my University years, and also to my parents-in-law, who have helped me greatly over the past five years.

Finally I should like to thank Ruth, my new wife, for putting up with the late observing nights and me in general.

Stephen R. Fullerton

September, 1994

Department of Astronomy

Glasgow University

CHAPTER 1

INTRODUCTION

1.1 Astronomical Polarimetry

The majority of astronomical investigations in the ultra-violet to near infra-red range of the electromagnetic spectrum are either photometric or spectroscopic in nature, purely measuring the intensity of the incoming radiation, in the latter case with respect to wavelength. However, a vital piece of information about the radiation is frequently overlooked, that being the state of the electric vectors of the light. Polarimetry is the measurement of these states which gives direct information on the source of the light.

There are many aspects of stellar physics for which the Sun is the only accessible source of information, such as the structure of sunspots and magnetic fields, differential rotation, and chromospheric and coronal effects. Although these phenomena are not directly visible on other stars, evidence of them may be seen, such as the detection of x-rays that are a signature of flares, increases in Ca II emission which shows chromospheric activity, and these and many other pieces of information are used to make "solar-stellar connections". In this thesis the role of polarimetry in finding observational evidence of the existence of magnetic regions analogous to sunspots is investigated by observing polarimetric effects in the light from the sun both as a star and as a spatially resolved object, and searching for similar effects in the light from solar and late-type stars.

In 1896 a discovery was made by Zeeman that concerns much of this study. He found that spectral lines could be broadened when the radiating atoms were in the presence of an intense magnetic field. Spectral line splitting and their associated polarization were then observed in the laboratory a few years later, and in 1908 Hale showed from the Zeeman effect that sunspots had strong magnetic fields. Round about the same time Mie and Debye independently developed theories of light scattering by arbitrarily sized spherical particles that produce polarization, and theories were incorporated by van de Hulst in his fundamental

text of light scattering by small particles almost 50 years later.

From the 1940's onwards discoveries of polarization in the light of a number of astronomical objects have been made. Öhman (1942) found polarization in the Andromeda Galaxy (M31), while the first discovery of stellar polarization was by Babcock (1947), his observations of 78 Vir showing that peculiar A-type stars have strong magnetic fields, a finding which opened up the field of stellar polarimetry. Two years later Hall (1949) and Hiltner (1949) made independent measurements of linear interstellar polarization and subsequently published extensive catalogues of polarized starlight. Dombrovskij discovered large polarization in the Crab Nebula in 1952, which had been predicted in association with synchrotron radiation in the previous year, and three years later radio polarization from the Crab Nebula was detected by Mayer, McCullogh and Sloanaker.

In 1959 strong wavelength dependence of linear polarization was found for planets, stars and nebulae, an account of which was published by Gehrels and Teska (1963). The importance of knowing the wavelength dependence of the polarization under investigation is highlighted in this and many other works as it provides a method of establishing which mechanisms are responsible for the observed polarization.

1.2 Polarimetric Definitions

In 1852, Stokes formulated the four parameters that completely describe the state of light. An electromagnetic wave can be described in terms of the components of its electric vector in two orthogonal planes perpendicular to the direction of propagation of the wave. For a wave propagating along the z-axis of an x,y,z, right-handed, co-ordinate system, these components may be written as:

$$E_x = E_{x_0} e^{i(\omega t - \frac{2\pi z}{\lambda} + \delta_x)} \qquad (1.1)$$

$$E_y = E_{y_0} e^{i(\omega t - \frac{2\pi z}{\lambda} + \delta_y)}$$

where

E_x and E_y are the values of the electric field vector in the x and y-directions at the position z and time t,

E_{x_0} and E_{y_0} are the amplitudes of the x- and y- vibrations,

δ_x and δ_y are the phases of the x- and y-vibrations at $z = 0$,

ω is the angular frequency,

λ is the wavelength, and

i is the square root of minus 1.

The polarization of such waves is related to these electric vectors by the Stokes parameters, I, Q, U and V, which are defined as

$$\begin{aligned} I &= < E_{x_0}^2 > + < E_{y_0}^2 > \\ Q &= < E_{x_0}^2 > - < E_{y_0}^2 > \\ U &= < 2\, E_{x_0} E_{y_0} \cos(\delta_y - \delta_x) > \\ V &= < 2\, E_{x_0} E_{y_0} \sin(\delta_y - \delta_x) > \end{aligned} \qquad (1.2)$$

where I represents the total intensity of the waves, Q and U the intensities associated with linear polarization, and V the intensity associated with circular polarization. The work presented in this thesis concerns only the measurement of linear polarization. The degree of linear polarization, p, is defined by

$$p = \frac{(Q^2 + U^2)^{1/2}}{I} \; . \qquad (1.3)$$

For a particular observing system Q and U take on values according to the chosen reference axes. For astronomical sources, an obvious choice of reference

axes are those of declination (x-axis), right ascension (y-axis), with the direction of propagation being the z-axis in the right-handed co-ordinate frame. The direction of vibration, also known as the position angle, can then expressed as an angle running from 0° to 180°, increasing from north, through east, to south. The Q and U parameters then define an angle θ relating the direction of vibration of the linear polarization to this frame, where

$$\tan 2\theta = {}^{U}/_{Q} , \tag{1.4}$$

and note has to be taken of the individual signs of U and Q to identify the correct quadrant. If the linear polarization is measured in a different frame (x′,y′), then the values of Q and U have to be rotated into this reference frame.

The work in this thesis deals with the *normalized Stokes' parameters*, q and u, which are defined as

$$q = {}^{Q}/_{I} \quad \text{and} \quad u = {}^{U}/_{I} , \tag{1.5}$$

and the degree of linear polarization may now be written as

$$p = (q^2 + u^2)^{1/2} , \tag{1.6}$$

where $p = 0$ corresponds to unpolarized light, and $p = 100\%$ linearly polarized light. The angle θ is defined as the position angle of the direction of vibration, giving the orientation of the linear polarization measured anti-clockwise with respect to the positive q-axis, the relations between q, u, p and θ being expressed by:

$$\begin{aligned} q &= p \cos 2\theta \\ u &= p \sin 2\theta \\ \theta &= {}^{1}/_{2} \tan^{-1}({}^{u}/_{q}) \end{aligned} \tag{1.7}$$

When a beam of light passes through an optical element then the Stokes' parameters will be affected. To calculate these effects it is best practice to use matrix algebra. By writing the parameters in matrix notation as a Stokes' column vector {I Q U V}, the effect of the optical element can be represented by a 4 x 4 matrix, which operate on the column vector to provide a column vector describing the emerging beam. The process is known as *Mueller calculus* and the matrix describing the optical element is known as its *Mueller matrix*. Denoting the matrix of an element as [𝔼], the Stokes' column vector of the emerging beam {I* Q* U* V*} is calculated thus:

$$\begin{bmatrix} I^* \\ Q^* \\ U^* \\ V^* \end{bmatrix} = [\,\mathbb{E}\,] \begin{bmatrix} I \\ Q \\ U \\ V \end{bmatrix} \tag{1.8}$$

with [𝔼] denoted by:

$$[\,\mathbb{E}\,] = \begin{bmatrix} a_{11} & a_{12} & a_{13} & a_{14} \\ a_{21} & a_{22} & a_{23} & a_{24} \\ a_{31} & a_{32} & a_{33} & a_{34} \\ a_{41} & a_{42} & a_{43} & a_{44} \end{bmatrix} \tag{1.9}$$

The values of the elements within the Mueller matrices describing the various optical parts of the instruments used in this study can be found in Appendix A.

1.3 Solar Polarimetry

Broad-band linear polarization connected with solar magnetic regions was first discovered over 30 years ago by Dollfus (1958) and Leroy (1962). They attributed the polarization to self-absorption in the transverse Zeeman effect, where the π component suffers a greater saturation leaving a net polarization for the whole line. But since a broad-band measurement includes many lines of

different strengths and Landé factors, it is difficult to calibrate such measurements to determine the strength of the transverse magnetic field. Other sources of polarization in both lines and the continuum, such as coherence scattering, are probably also important in sunspots. Dollfus compared the polarization measured in wavelength bands containing few and many lines, finding a factor of two greater polarization in the latter.

Detailed analyses of sunspot magnetic fields can now be made with filter magnetographs, giving excellent spatial resolution. An example of this is given in figure 1.1 which shows the transverse magnetic field superimposed on a Hα filtergram (taken from Wang, 1990). Balasubramaniam *et al.* (1990) used such magnetograms to measure the Stokes' profiles across the Fe I 5250.2Å line in a sunspot umbra, using the data to derive the magnetic field strength and other parameters (figure 1.2). The complexity of a sunspot magnetic field is readily apparent with field lines in all directions, meaning that if similar spectral profiles are taken using the light combined from all parts of a sunspot, then the directions of vibrations will tend to cancel out and leave only small levels of polarization.

Kemp and Henson (1983) measured the broadband circular polarization of sunspots between 0.37-4.5μm in 0.1μm passbands, the results of which clearly showed that polarization decreases as a function of increasing wavelength with the B and V band polarizations of 0.08% and 0.04% respectively being much greater than those in the infra-red of less than 0.01%.

Dollfus also studied solar limb polarization. In 1959 his group made radial scans from the centre of the solar disk out to about 20 arc seconds from the limb in a range of wavelength bands, four of which are shown in figure 1.3. These graphs not only show clearly the centre-to-limb variation (CLV) of polarization, but also highlight the wavelength dependence as the magnitude of p decreases by a factor of about 2 at the limb itself between the measurements at 0.41μm and 0.60μm.

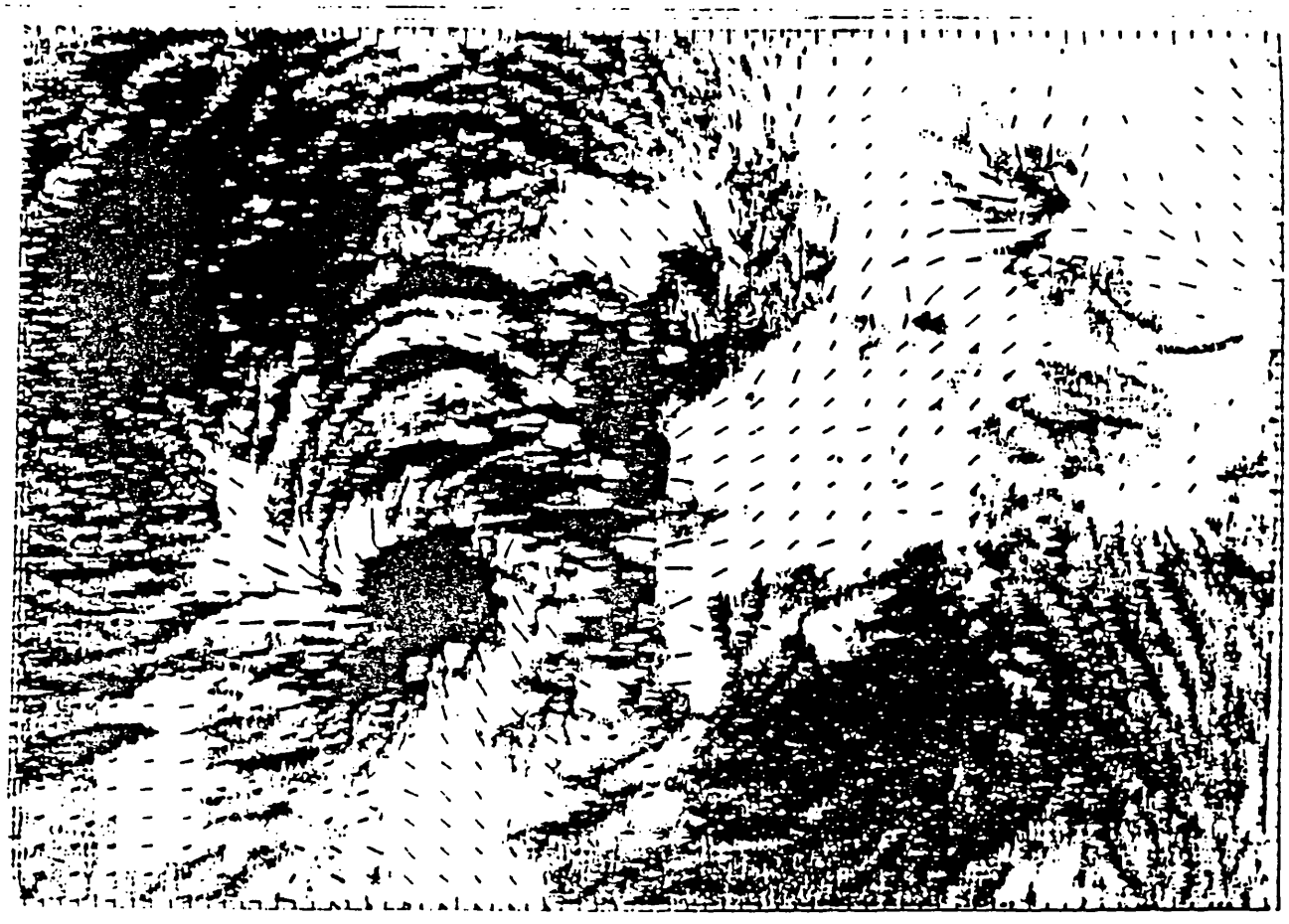

Fig. 1.1 Comparison of the transverse magnetic fields and an Hα filtergram obtained at BBSO, 2200UT, September 22, 1989. (Taken from Wang, 1990)

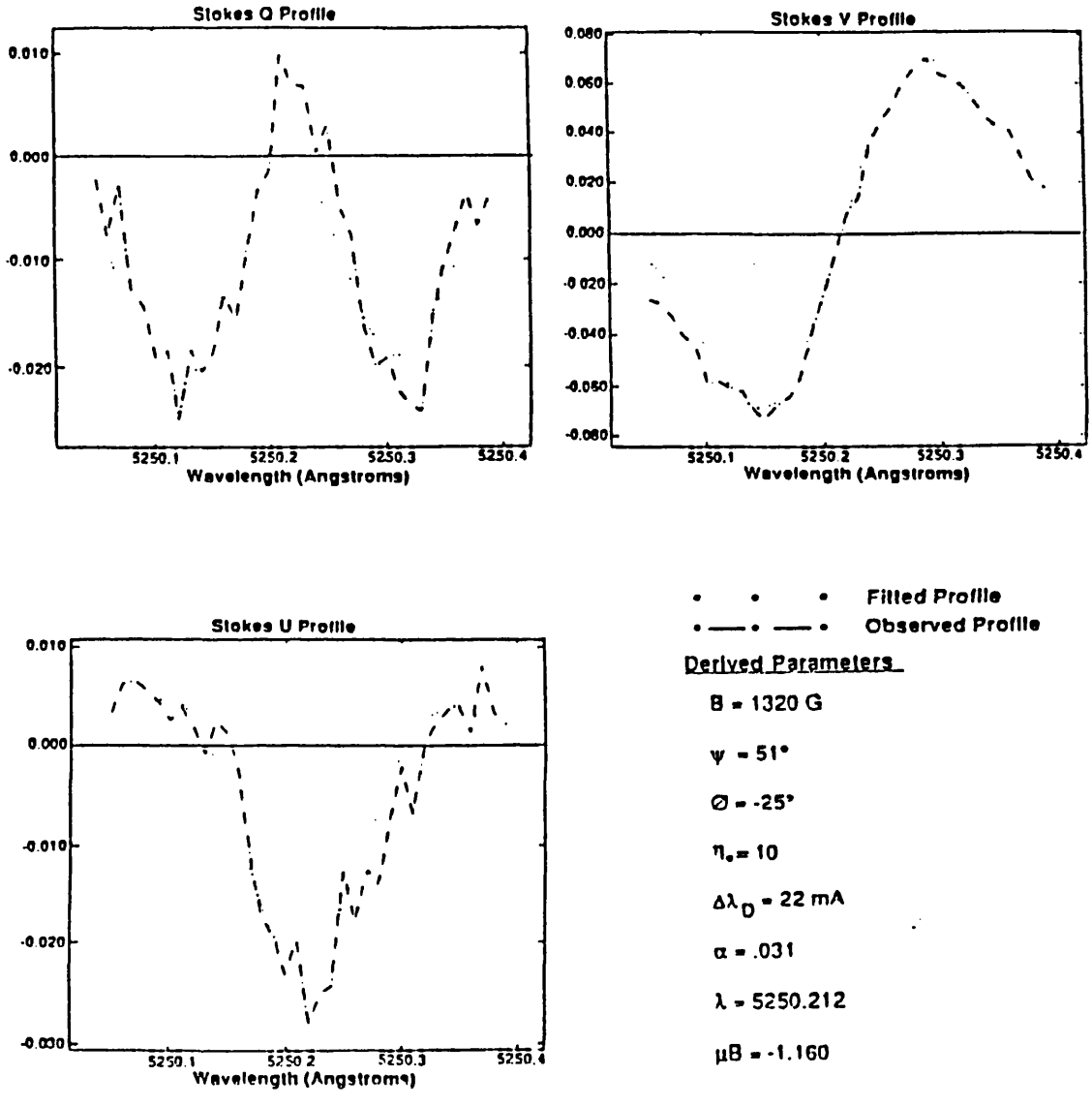

Fig. 1.2 Stokes' polarization profiles in sunspot umbra acquired with the MSFC vector magnetograph (dot-dashed lines), compared with fitted profiles resulting from the non-linear least square inversion (dotted lines), with the values of the fitting parameters being shown in the bottom right (Taken from Balasubramaniam *et al.*, 1990)

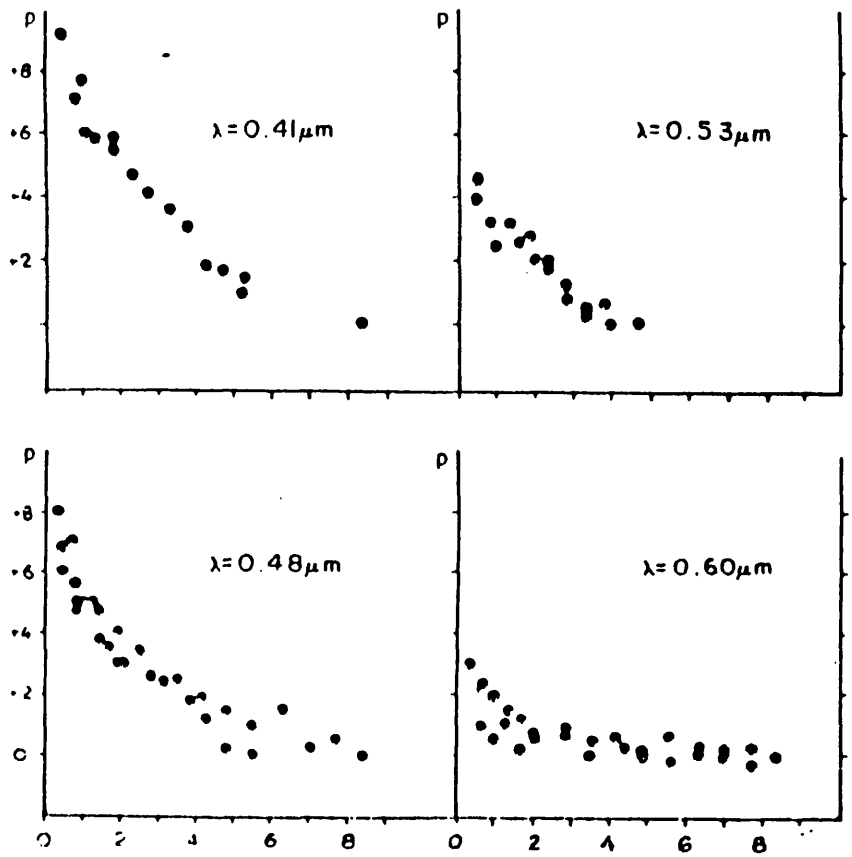

Fig. 1.3 Polarization p (in units of 10^{-4}) as a function of distance, d, inside the solar limb (in arcmins) at four wavelengths. (Taken from Dollfus, 1974)

Stenflo *et al.* (1980) measured polarized line profiles of 10 non-magnetic resonance lines (including Ca II H and K and Ca I 4227Å) and their centre-to-limb variation. They concluded that the steep increase of the CLV curves towards the limb is partly due to the dependent geometry of scattering, but also partly due to the decrease in collision rate with height leading to an increased ratio of coherent to incoherent scattering in the higher layers. They also showed that in strong lines with pronounced dampening in the wings the polarization had a maxima in the wings, typically about 0.6Å from the line centre, and a few strong lines such as Ca II K and Ca I had narrow polarization peaks in the Doppler core, whereas the absence of core polarization in some resonance lines is likely to be connected with magnetic depolarization.

A recent review of broadband solar and stellar polarizations by Clarke (1991) include results of whole-disk measurements made at 5000Å over a period of a few weeks, which suggest that solar polarimetric variations connected with the movement of active regions are just about measurable. The magnitude of the measured polarization seemed to be correlated with the AVSO activity index. These results contrast the claim by Leroy and LeBorgne (1989) that summing the broad-band polarized signals from many active regions in which the directions of vibration will not be parallel (as seen in figure 1.1) will lead to extremely low levels of polarization (less than 0.0001%) that would not be measurable. They conclude that magnetic saturation has little role to play as a diagnostic within astrophysics. In the same paper they also claim that it is not obvious that the net broad-band polarization of a region is larger near to the solar limb.

It must be questioned, therefore, whether previous reported detections of whole-disk, broad-band polarization are indeed real, or if Leroy and LeBorgne's simplistic view of summing the effects of many active regions is valid in estimating such polarizations. The structure of a sunspot magnetic field is not circularly symmetric, nor truly random, but the bipolar nature of sunspot groups will also serve to cancel polarization when measured on a global scale. It is of

great interest therefore to gain further knowledge of the global and sunspot polarizations, both in broad-band and within spectral lines.

1.4 Polarization of Solar and Late-type Stars

Intrinsic linear polarization is a well known observational phenomenon associated with stars at the extremes of spectral classification (i.e. early- and late-types). Its measurement provides valuable information for models associated with stellar atmospheres, their geometries and aspects, with reviews being found in Coyne and McLean (1979) for luminous, red variables, Coyne and McLean (1982) on Be stars, Schwarz (1986) on late-type stars, and by Landolfi *et al.* (1992) and Leroy *et al.* (1993) on Ap star models.

For stars in the middle of the spectral sequence, including solar-type stars, general intrinsic polarization is small. Many solar-type stars have been included in unpolarized standard star surveys, but in a couple of cases variable intrinsic polarizations were found. Piirola (1977) measured a number of F, G, and K stars within 25 parsecs of the Sun, finding that one star, χ Her (F9V), showed temporal variations in polarization over 5 nights. Kemp *et al.* (1986) discovered variable polarization over 65 nights in α Boo (Arcturus; K2IIIp) in the blue band with an amplitude of about 0.005%, and indicated possible periodicities. They also concurrently measured the Ca II H and K emission which clearly showed variability, indicating magnetic activity during the period of the observations (figure 1.4).

In his thesis, Stewart (1984) analyzed Hβ and Ca II K polarization for α Boo and found indicative but inconclusive evidence of polarization variability across the lines. He also suggested a marginal detection of a small Hβ polarization for α Tau (K5III) on one occasion, but no such polarization in any Ca II K measurements.

Huovelin *et al.* (1985) claimed that there are weak wavelength dependent

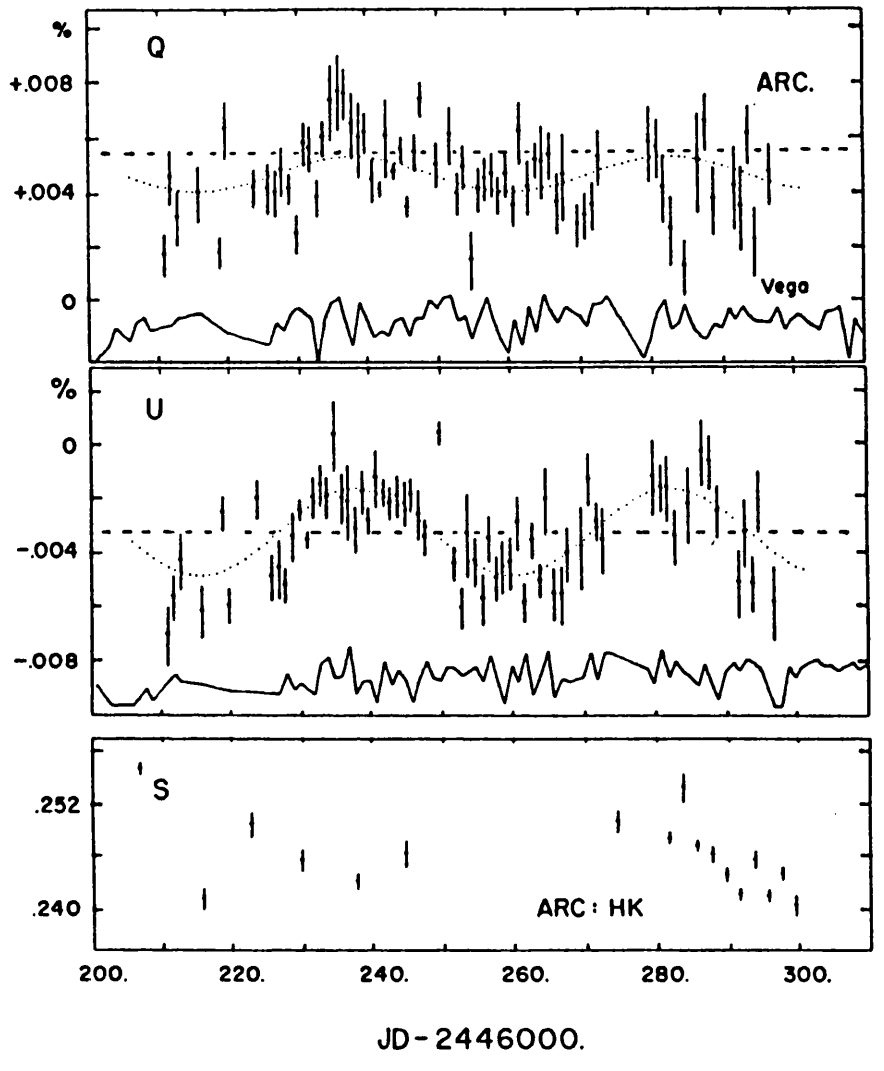

Fig. 1.4 Polarization variations in B band in Arcturus during 1985 May-August. Dashed horizontal lines indicate approximate instrumental polarization levels. Dotted curves are from least-mean-squares fit to 44.5 day sinusoids. Polarization of Vega (α Lyr) is also shown for comparison, using 87 contemporaneous data points connects by continuous lines. Lower panel shows Mount Wilson measurements of the Ca II H and K emission in Arcturus over the same time span. The rapid variability on time scales of 1-5 days tends to obscure the longer period effects, indicating the need for dense coverage in future observations. (Taken from Kemp *et al.* 1986)

polarizations in three solar-type stars, whereas other observers are not convinced (e.g. Leroy 1989b postulated that the observations were influenced by parasitic polarization from scattered moonlight). However further work by Huovelin, Saar and Tuominen (1988) again found wavelength dependent polarizations in a sample of F5-G5 dwarfs including the G8 dwarf ξ Boo A, a star well known for controversy over the possible detections of a magnetic field.

The question of whether ξ Boo A has a magnetic field, and if so whether it is variable, has been debated for over a decade. Robinson *et al.* (1980) pioneered a new spectroscopic technique to detect magnetic fields in stellar photospheres using the shapes of absorption line profiles rather than by making polarization or associated measurements. Although a magnetically sensitive line would be broadened in a magnetic field by the Zeeman effect (see section 1.4), even for a field strength of a few thousand Gauss, the thermal broadening of the line will be greater than the magnetic broadening, so normal spectroscopy is not adequate. Robinson's group showed that the deconvolution of a magnetically insensitive absorption line profile, which shows no Zeeman splitting, from a magnetically sensitive line profile could show the existence of the Zeeman shifted components. They estimated the strength of the magnetic field from the wavelength shifts, and estimated the coverage of a "magnetic region" (called the *filling factor*) on the visible hemisphere of the star by the relative strengths of the shifted to the unshifted lines. These "magnetic regions" could be likened to sunspots, but are of greater surface area.

From the profiles of Fe I lines measured in 1979, the group derived fields of 2550 ± 390 Gauss covering 20-45% of the surface of ξ Boo A, and of 1880 ± 350 Gauss covering 10% of 70 Oph. Comparison observations of solar active regions yielded 1800 ± 550 Gauss covering 10% of the region. They compared their results to those of Boesgard (1974) whose Lick spectrograms indicated essentially zero fields, while Mauna Kea spectrographs indicated positive fields of ~170 Gauss for ξ Boo A. They also noted that Boesgard (1974) reported that Ca II

emission flux from this star seemed to show a 6 to 7 year cycle.

Marcy (1981) took five high-resolution, high signal-to-noise spectra of the magnetically sensitive and insensitive Fe I lines at 6137.34Å and 6240.65Å respectively, which have similar strengths to those of the Sun, to detect Zeeman splitting for ξ Boo A, but none of the observations showed positive evidence of magnetic fields. Marcy did, however, draw attention to other solar related phenomena on ξ Boo A, in that Vaughan and Preston (1980) had monitored the chromospheric variability of Ca II H and K emission which, over the previous ten years, had shown large variations in activity on a time scale of 5 years as well as shorter variations over periods of weeks.

Zirin (1976) observed a corona around ξ Boo A via the helium line at 10830Å in absorption in 1975. He marginally detected it in 1971 but it was not present in 1966, suggesting comparison with Boesgard's temporal variation time scale. The corona was confirmed by soft x-ray detection by HEAO 1 in January 1978 (Walter *et al.* 1978), with a higher flux then measured in August 1979 by the *Einstein* observatory. The higher x-ray flux was measured within 4 months of Robinson's magnetic field measurements mentioned previously, but in August 1980, two months after magnetic field null results were obtained by Marcy, the soft x-ray flux had fallen ten times lower than those of the 1979 measurement.

In his paper of 1984 Marcy described a search for Zeeman broadening in 29 G and K main sequence dwarfs, using the same technique and Fe I lines as before, and revealed 19 positive detections. Observations of solar light (using the daytime sky as the source) showed no significant Zeeman broadening, as was the case for α Boo (for which Marcy argued that because of the low thermal energy density of its photospheric gas, a field of more than about 700 Gauss would destabilize the vertical gas structure).

Marcy also took profiles of a sunspot group (Mount Wilson group number 22952) which had a magnetic field strength of about 2 kilogauss and showed clear Zeeman splitting. The splitting was also asymmetric, for which he accorded to

downdrafts in solar magnetic regions. He found similar field strengths for 70 Oph A, ξ UMa B and ε Eri, the latter star according to Timothy *et al.* (1981) displaying significant field changes over time periods of a day, and Smith (private communication, 1982) claiming to have found Zeeman broadening yielding a field strength of 1000 Gauss.

For ξ Boo A itself, Marcy found field strengths on average to be 100 Gauss with filling factors greater than 60%. He also showed that the magnetic fluxes seemed to increase towards later spectral types, and allowing for this, the magnetic fluxes were found to correlate with rotation rates. They also correlated with chromospheric Ca II H and K emission and with soft x-ray fluxes.

Gray (1984) also measured the magnetic fields of a sample of F, G and K type dwarfs, and detected fields in 7 out of 18 stars. All of these positive detections were in stars of type G6 or later and had strengths of about 1900 Gauss, but the results for ξ Boo A were ambiguous. χ Her showed no field present in this sample.

Gondoin *et al.* (1985) used infra-red lines for the deconvolution technique. Higher spectral resolution is attained and the Zeeman splitting is greater, being dependent upon the square of the wavelength, allowing easier detection of the splitting. Using the Fe I lines at 16486.62Å and 16316.90Å (insensitive), and 15662.00Å and 15621.66Å (sensitive), no relative broadening was found for ξ Boo A, estimating an upper limit of 1100 Gauss and a filling factor of 20%, deduced from an average of four days spectra. They also found a suggestive result of 600 Gauss and a filling factor of 20% for λ And, but as it was near to the limit of detection the result was deemed not conclusive. A high resolution optical spectrum of ξ Boo A also found no evidence of Zeeman broadening at that time.

Basri and Marcy (1988) re-examined the infra-red Fe I line measurements taken by Marcy in 1984 using an improved model atmosphere code which included all the relevant line and stellar physics instead of the approximate treatment of

radiative transfer previously used. They examined the possibility that the observed broadenings could be due to deficiencies in the past or then present methods of analysis, concluding that magnetic fields were indeed detected. In particular, for ε Eri they derived a field strength of 1000 Gauss covering 35% of the stellar surface, and for ξ Boo A a field of 1200 Gauss covering 40% of the surface.

They then searched for Zeeman broadening in the profiles of 11 late G and K dwarfs (Marcy and Basri, 1989), again using infra-red lines to obtain high signal-to-noise, and their analysis included the separate treatment of each Stokes' parameter, improved oscillator strengths and a disk integration of velocity broadening. Six of the 11 stars sampled showed magnetic fields present, the most extreme being ε Eri (B = 1000 G and filling factor = 40%) and ξ Boo A (B = 1600 G and filling factor = 22%) The quantity B × (filling factor) correlated with chromospheric Ca II emission and with stellar rotation rate. They suggested that magnetic fields increase with declining stellar mass as well as with rotation rate. They also found two stars, σ Dra and 54 Psc, that exhibited no Zeeman broadening at all, proving that magnetically weak stars do exist later than type K0, and that 61 Cyg showed clear broadening which was not expected for an old, slow rotator.

Toner and Gray (1988) spectroscopically monitored ξ Boo A for four observing seasons and found systematic variations in the spectral line asymmetries and equivalent widths with a period of 6.43 ± 0.01 days. They reported no evidence of a change in period or phase shift over the four seasons, and were unable to detect any variation in the magnetic field strength. They claim that these observations are understandable in terms of a surface feature that is carried across the apparent disk of the star by rotation. They developed a numerical simulation that reproduced both the asymmetry variations and the line strength variations deducing that the gross characteristics of the feature were: $T_{\rm eff}$ 200K cooler than the rest of the photosphere covering 10 ± 5 % of the surface at a

latitude of +55 ± 8°. Due to the apparent lack of Zeeman broadening they believed that they had discovered a new type of surface feature distinct from active magnetic regions (sunspots), and called it a "starpatch".

In his review of magnetic field measurements, Saar (1990) highlighted the fact that the deconvolution method has an advantage over polarization measurements because line broadening does not depend upon magnetic field orientation, whereas the probably dipolar nature of magnetic fields would cancel circular polarization and dramatically reduce linear polarization, which is also diluted by unpolarized light from non-magnetic regions. However Saar did simultaneously measure Ca II H and K emission and broad-band linear polarization of a sample of F5 - K5 dwarfs, including ξ Boo A, to investigate activity variations and to permit a rough spatial distribution of active areas on the stars (see Huovelin *et al.* 1988).

Huovelin's group measured the polarization of ξ Boo A in the U, B and V bands and the Ca II H and K emission, with the results being shown in figure 1.5. The H and K measurements were made over a period of 163 nights, overall variations being well above the significant level. It is easily seen that the H and K emission seems to have a near 6 day cycle (remembering that the rotation period is 6.2 days), and that the polarization measurements made over 5 nights also show variations which were significant in the V band, while being indicative in the U and B bands. They also estimated that the wavelength dependence of the polarization varies as $\lambda^{-5.9\pm0.6}$. Their theoretical calculation of the polarization due to magnetic intensification yields a $\lambda^{-4.9}$ dependence, and the observed dependence argues strongly that the polarization mechanism for ξ Boo A is not Rayleigh scattering ($p \propto \lambda^{-4}$). In the analysis, they also stated that the steepness of the dependence may well be underestimated as the effects of noise may give overestimates of the magnitudes of p(B) and p(V). The variations of the H and K emission suggested active areas in more than one longitude position.

It is obvious from the above reports that ξ Boo A must have a variable

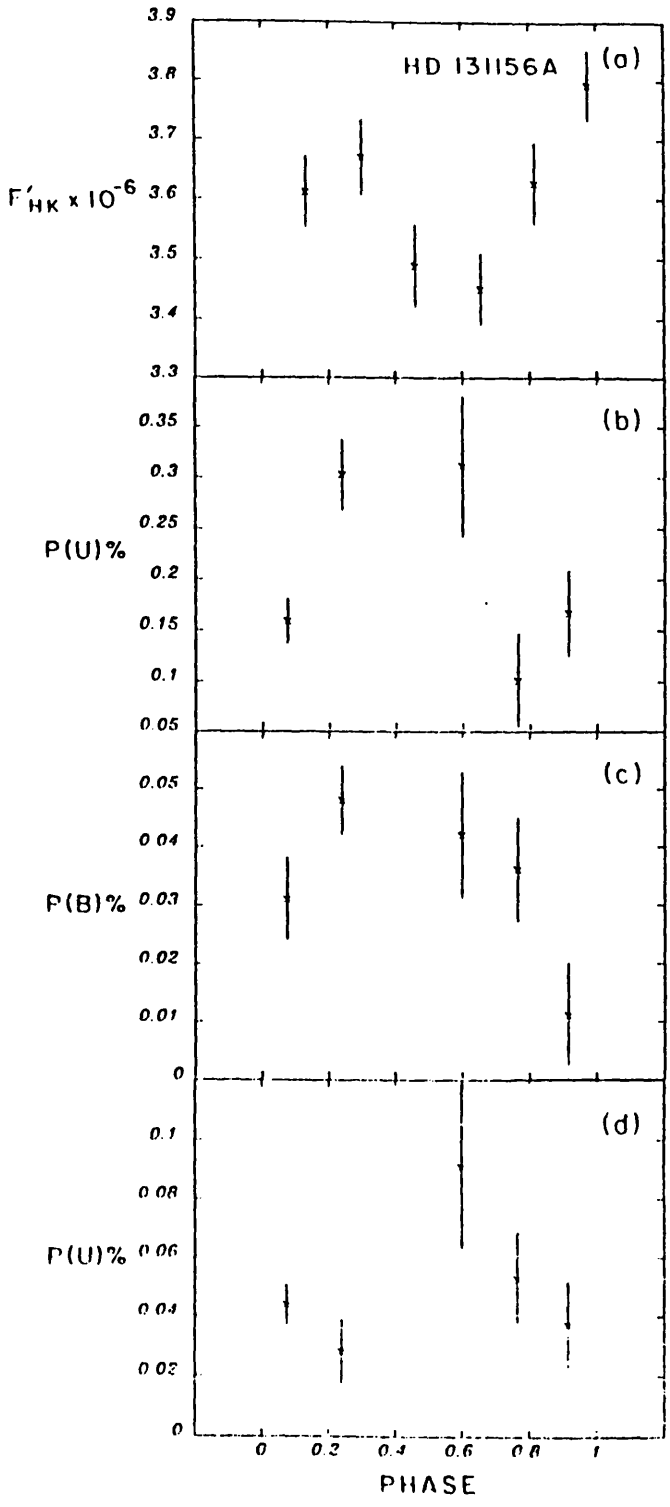

Fig. 1.5 (a) Ca II flux, and degree of polarization (b), (c) and (d) vs. rotational phase for ξ Boo A. (Taken from Huovelin *et al.*, 1988)

magnetic field. It may be enhanced in regions (likened to "patches") which show rotational modulation, and a more global field may well exist which produces chromospheric and coronal effects similar to those of the Sun. The detections and non-detections may well be accounted for by a similar phenomena to that of the Sun, i.e. the 11-year magnetic cycle, but over a period of about 6-7 years in this case. This star would seem to provide an ideal test case for comparison with solar data with the possibility of taking polarimetric observations over full rotation periods and being able to investigate wavelength dependence.

1.5 Mechanisms that Produce Polarization Relevant to this Work

1.5.1 The Magnetic Zeeman Effect and Magnetic Intensification

The Zeeman effect in a transverse magnetic field is a well known phenomena. The energy levels of atomic electrons in an external magnetic field are split into several components according to their total magnetic dipole moment, μ, due to the orbital and spin magnetic dipole moments. For a magnetic field strength, B, of less than several tenths of 1 Tesla (i.e. a few thousand Gauss) the splitting is proportional to B and given by

$$\Delta E = -\underline{\mu} \cdot \underline{B} \tag{1.10}$$

If we consider a transition from a singlet state to a higher energy level, the spectral line will be split into 3 components. The central component has the same energy as the single zero-field line, is twice the intensity of the two components displaced in energy by ΔE and is of the orthogonal polarization to them. In a saturated stellar absorption line the Zeeman splitting is much smaller than the Doppler broadening and so is not seen, but the three components may be unequally absorbed producing a net polarization in the observed line with a direction of vibration parallel to the magnetic field. This process is known as

differential absorption or *magnetic intensification*, and its possible detection in starlight has been addressed by Leroy and LeBorgne (1989), and has been modeled by Landi Degl'Innocenti (1982).

As there are more spectral lines towards shorter wavelengths, linear polarization produced by this method is greater in the ultra-violet region of the electromagnetic spectrum. Leroy (1989) calculated the polarization produced by the combination of 6000 solar absorption lines and showed that the wavelength dependence of the polarization has a high degree at short wavelengths, decreasing steadily to a trough near 4800Å, increasing slightly to a peak near 5200Å and falling towards zero at longer wavelengths (figure 1.6). The observations made in this study are confined to wavelengths between 4000Å and 5600Å in an attempt to observe this dependence and confirm that this mechanism does produce observable amounts of linear polarization.

1.5.2 Polarization due to Scattering

Outside of solar active regions with large magnetic fields it is not possible to measure line polarizations due to the Zeeman effect. However resonant and fluorescent scattering does generate polarization all over the solar disk, with increasing amplitude near the solar limb. The scattered radiation will only be polarized if there is an anisotropy in the radiation field, which is provided by limb darkening or brightening. The solar limb is darkened, which for dipole-type scattering results in linear polarization oriented parallel to the limb.

Stenflo *et al.* (1983a; 1983b) recorded a linear polarization spectrum 10 arc seconds inside the solar limb across the wavelength ranges 3165-4230Å and 4200-9950Å to explore the physics of such scattering in spectral lines. Their results which are of most interest to this study include:

i) the polarization peak in the Doppler core of the Ca I 4227Å line, with $p_{max} = 1.10\%$ (fig 1.7a);

ii) polarization in the two Balmer lines Hα and Hβ, $p_{max} = 0.17\%$ and 0.20%

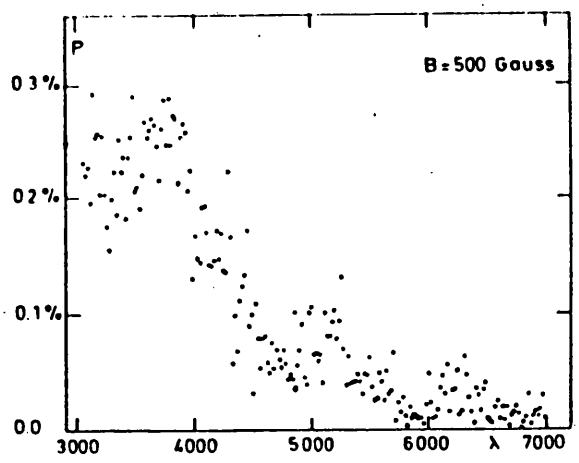

Fig. 1.6 The degree of linear polarization P due to magnetic intensification computed for a transverse magnetic field of 500 G. P has been determined for every 20Å interval in the solar spectrum, starting from 3080Å up to 6980-7000Å. (Taken from Leroy, 1989)

(a)

(b)

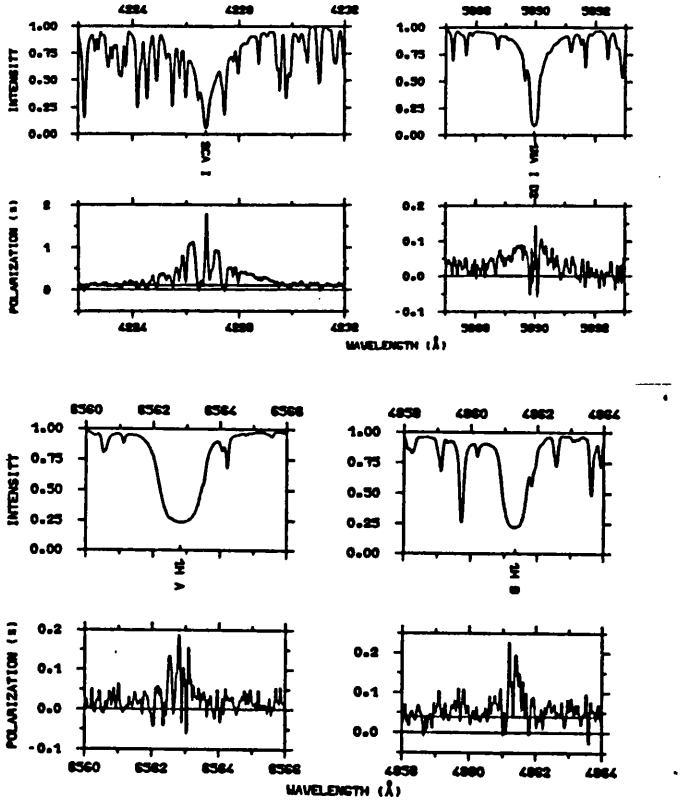

Fig. 1.7 Polarization in (a) Ca I 4227Å and (b) Hα and Hβ, due to resonant and fluorescent scattering. (Taken from Stenflo *et al.* 1983b)

respectively (fig 1.7b), a case of fluorescent scattering in which emission of a Hα photon seems to be preceded by excitation by a Lyβ photon, and similarly photons scattered in Hβ representing scattering of Lyγ photons;

iii) Fe I polarization is very common, for example the 4871.33Å multiplet has $p_{max} = 0.17\%$, for which they believed that this is because electron levels with high excitation potentials are often metastable in Fe I.

Scattering by atoms and molecules, Rayleigh scattering, has a strong angular dependence and a wavelength dependence of linear polarization given by $p \propto \lambda^{-4}$. Free atoms show very strong scattering of their resonance lines, the peak polarization depending upon the Zeeman sub-levels of the states involved. Rayleigh scattering due to the radiation field in a star's atmosphere above the photosphere being non-isotropic will, like resonance scattering, be greatest near the limb, and with a direction of vibration tangential to the limb.

Only for the Sun can the disk be spatially resolved to investigate the centre-to-limb (CLV) variation of polarization, reviewed by Leroy (1972) and Mickey and Orrall (1974). For observations of a whole stellar disk it would be expected that, as the direction of vibration is tangential to the limb, the total polarization would be almost zero, even allowing for some oblateness due to rotation.

Scattering by dust particles is the cause of interstellar polarization. It results from the alignment of grains causing preferential extinction in one direction of vibration. Serkowski (1971) showed that the wavelength dependence of this polarization can be expressed as

$$p(\lambda) = p_{max} \exp[-1.15\, ln^2(\lambda_{max}/\lambda)] \qquad (1.11)$$

where p_{max} is the maximum degree of polarization and λ_{max} is the wavelength at which p_{max} is measured. The polarimetric standard stars used to find the position

angle of a polarimeter owe their observed polarization to this interstellar effect and not to any intrinsic effects.

1.6 Aims of the Investigations into Solar and Stellar Polarization

From the observations previously been made by others it appears that further work is required in many areas. Measurable polarization from solar-type stars has been difficult to verify, with many claims that either observations have been affected by sources not intrinsic to the star or that global polarization due to effects similar to those on the Sun are not measurable because of cancellation. It has been postulated that magnetic regions much larger than sunspots and with stronger field strengths must exist on some stars.

Polarization has been shown to exist in the light from solar active regions as a result of the Zeeman effect and the Stokes' profiles of spectral lines are readily measurable in observations of discrete regions of sunspots, in which the magnetic field will have a specific direction. However, observations of more extended regions, for which the magnetic fields direction are more random leading to cancellation of linear polarization, have not been conclusive as showing polarization in lines or in broad-band.

Extending this to the whole solar disk, while some authors claimed polarimetric variations in both broad and narrow-bands, others came to the conclusion that simply adding the polarization from various regions vectorially resulted in such small levels that the Sun may be classed as an unpolarized standard star. In the former case it was shown that broad-band variations correlated with sunspot movement which suggested not only that sunspots exhibit a net polarization of their own, but that their global effect was not totally cancelled by either random position angles or by dilution by unpolarized light from other parts of the solar disk. The latter conclusion was based exactly on those arguments of randomness and dilution, but the authors neglected to consider

effects near to the limb (scattering) that were later shown to produce polarization both in lines and in broad-band.

The work undertaken and described in this thesis was performed to extend the current knowledge of both solar and stellar polarizations and to discuss possible links between the two, so contributing to other investigations into solar-stellar connections. Stellar polarimetry was performed on solar and late-type stars that had previously indicated variable and/or wavelength dependent polarizations, to confirm or deny previous reports of polarimetric detection. If any such variation is due to magnetic regions on a rotating star then the modulation of the polarimetric signal would allow rotation periods to be deduced. An observed wavelength dependence can be considered a diagnostic of the polarization mechanism being either magnetic or as a result of scattering, thus providing distinctive dependencies. Observations were made both from Glasgow and La Palma, for which an application for time for performing polarimetry on solar-type stars was made based on the arguments made above.

Whole disk polarimetry of the Sun may be directly compared to polarization from stars because in both cases the entire radiation from the object is used. Measurements were made in narrow spectral bands to observe effects in a magnetically sensitive iron line and Hβ. But to gain an insight into which mechanism produces the polarization and the reasons for its variation required the study of the solar disk polarization in more detail, accomplished by measuring the normalized Stokes' parameters for different, small, isolated areas of the photosphere. While instruments already existed to measure stellar and solar whole-disk polarization both in lines and in broad-band, a new solar polarimeter was designed and constructed to undertake solar measurements over small areas of the solar disk specifically for this work. It was important for such an instrument to be able to not only explore the intrinsic polarization of sunspots, but also to investigate the temporal variations as a spot traversed the solar disk (simultaneously gaining information on the centre-to-limb variation),

the spectral dependence of polarization, and the comparison with quiet areas of the photosphere that may exhibit limb polarization due to scattering.

The effects of the atmosphere upon the measurements of stellar polarizations were also considered. As noise due to scintillation and seeing, for example, may set a limit of detectability of polarization using the stellar polarimeter, it was of great benefit to see whether observational or data reduction techniques could be improved in an effort to measure smaller levels of polarization. The instrumental polarization of the Glasgow polarimeter was unknown at the beginning of this work, and for that reason a sample of unpolarized standard stars was used to find its current value.

A model in which sunspots, and their respective positions on the visible hemisphere of the Sun, give rise to measurable whole disk polarization was formulated. The model included the effects of both magnetic intensification and of scattering near the limb to attempt to indicate that magnetic regions may break the circular symmetry in the radiation field of the Sun, when treated as a star in whole-disk observations, and of stars. Polarization measurements for single active regions were incorporated into the model, which attempted to predict polarization variations from the whole-disk, and subsequently from stellar observations. All of the above topics are explored in the development of this thesis.

CHAPTER 2

INSTRUMENTATION AND ANALYSIS TECHNIQUES

2.1 Continuously Rotating Half Wave Plate Polarimeters

Serkowski (1974) stated that the only way to reduce or eliminate polarimetric errors caused by atmospheric seeing or bad telescope guidance is by rapid modulation of the signal. This is achieved by one of two methods,

(i) using a rapidly rotating, superachromatic half-wave plate placed in front of a stationary polarizer, as incorporated by Lyot in 1948, which modulates the signal at 4 times the frequency of the mechanical rotation, or,

(ii) using active optics whose state may be altered by electrical currents and so have their fast axis orientation controlled.

The polarimeters used for making observations in this work incorporated a superachromatic half-wave plate, allowing a large wavelength coverage and simultaneous or quasi-simultaneous measurements of both normalized Stokes' parameters, q and u.

Application of Mueller calculus allows the effect of the polarizing optics to be investigated. It is usual to define a Cartesian co-ordinate system with the x-axis as the polarizing axis and the z-axis parallel to the direction of the incoming light. Defining an angle θ between the axis of the polarizer and the fast axis of the half-wave plate, measured anti-clockwise from x to y in this frame, the effect on the Stokes' vector, [S], for the incoming light beam is found by rotating the reference axis through an angle θ, [R(θ)], applying the half-wave plate matrix, [H], rotating back through θ to the original frame, [R(-θ)], and finally applying the polarizer matrix, [P]. The outgoing Stokes' vector, [S]′, can therefore be written as

$$[S]' = [P]\,[R(-\theta)]\,[H]\,[R(\theta)]\,[S] \qquad (2.1)$$

and the relevant Mueller matrices can be found in Appendix A.

Evaluating [S]′ gives

$$\begin{bmatrix} I \\ Q \\ U \\ V \end{bmatrix}' = \frac{1}{2} \begin{bmatrix} I + Q\cos 4\theta + U \sin 4\theta \\ I + Q\cos 4\theta + U \sin 4\theta \\ 0 \\ 0 \end{bmatrix} \tag{2.2}$$

Letting the measured signal be $S(\theta)$,

$$S(\theta) = \frac{G}{2} \left\{ I + Q\cos 4\theta + U \sin 4\theta \right\} \tag{2.3}$$

where G is the gain, or the instruments response to unpolarized light of unit intensity. When dealing with the normalized Stokes parameters knowledge of G is not required as it is cancelled out. $S(\theta)$ is therefore a constant signal superimposed with modulated components at four times the rotation rate of the half-wave plate, resulting in rapid modulation of the Stokes' parameters.

Two of the polarimeters used in this study incorporated this technique and used the same method of recording the I, Q and U signals. It involved using three scalars which integrate over specific phases of the half-wave plate rotation period.

The first scalar counts during the entire cycle to record the total intensity, I, and so over N cycles, letting C_1 be a measure of the signal,

$$C_1 = N \int_0^{2\pi} S(\theta)\, d\theta = N\, \pi\, I \tag{2.4}$$

The second scalar integrates for the same N rotations over specific values of θ, i.e. $0 \rightarrow \frac{\Pi}{4}$, $\frac{\Pi}{2} \rightarrow \frac{3}{4}\Pi$, $\Pi \rightarrow \frac{5}{4}\Pi$, $\frac{3}{2}\Pi \rightarrow \frac{7}{4}\Pi$. Letting C_2 be this signal strength, then

$$C_2 = 4N \int_0^{\pi/4} S(\theta)\, d\theta = N \left(\frac{\pi}{2} I + U \right) \tag{2.5}$$

giving U in terms of C_1 and C_2.

The third scalar integrates for the same N rotations over the following values of θ, $\frac{\pi}{8} \rightarrow \frac{3}{8}\pi$, $\frac{5}{8}\pi \rightarrow \frac{7}{8}\pi$, $\frac{9}{8}\pi \rightarrow \frac{11\pi}{8}$, $\frac{13\pi}{8} \rightarrow \frac{15\pi}{8}$, so letting C_3 be this signal strength then

$$C_3 = 4N \int_{\pi/8}^{3\pi/8} S(\theta)\, d\theta = N \left(\frac{\pi}{2} I - Q \right) \tag{2.6}$$

and hence giving Q in terms of C_1 and C_3.

The normalized Stokes' parameters, q and u, are then given by

$$q = \frac{Q}{I} = \pi \left(\frac{1}{2} - \frac{C_3}{C_1} \right) \tag{2.7}$$

$$u = \frac{U}{I} = \pi \left(\frac{C_2}{C_1} - \frac{1}{2} \right) \tag{2.8}$$

An alternative way of denoting the acquisition of the signal divides the rotation phase into sixteen parts which are associated with four intensities x, y, z and w, whose phase coverage correspond to

$$\begin{aligned}
x\text{: } \theta = {} & 0 \rightarrow \pi/8 \,, \quad \pi/2 \rightarrow 5\pi/8 \,, \quad \pi \rightarrow 9\pi/8 \,, \quad 3\pi/2 \rightarrow 13\pi/8 \\
y\text{: } \theta = {} & \pi/8 \rightarrow \pi/4 \,, \quad 5\pi/8 \rightarrow 3\pi/4 \,, \quad 9\pi/8 \rightarrow 5\pi/4 \,, \quad 13\pi/8 \rightarrow 7\pi/4 \\
z\text{: } \theta = {} & \pi/4 \rightarrow 3\pi/8 \,, \quad 3\pi/4 \rightarrow 7\pi/8 \,, \quad 5\pi/4 \rightarrow 11\pi/8 \,, \quad 7\pi/4 \rightarrow 15\pi/8 \\
w\text{: } \theta = {} & 3\pi/8 \rightarrow \pi/2 \,, \quad 7\pi/8 \rightarrow \pi \,, \quad 11\pi/8 \rightarrow 3\pi/2 \,, \quad 15\pi/8 \rightarrow 2\pi
\end{aligned} \tag{2.9}$$

The three scalar intensities can now be written as

$$\begin{aligned} C_1 &= x + y + z + w \\ C_2 &= x + y \\ C_3 &= y + z \end{aligned} \tag{2.10}$$

and hence the normalized Stokes' parameters are given by

$$\begin{aligned} q &= \pi \left(\frac{1}{2} - \frac{y + z}{x + y + z + w} \right) \\ u &= \pi \left(\frac{x + y}{x + y + z + w} - \frac{1}{2} \right) \end{aligned} \tag{2.11}$$

Using this description it is easier to model data from the polarimeters for the investigations into dead-time problems (section 2.4) and atmospheric effects (section 4.4) later in this study.

2.1.1 The Tilt-scanning Interference Filter Solar Whole-disk Polarimeter

Wyllie (1976) investigated the technique of tilt-scanning across spectral lines with a narrow band interference filter to observe line-profile fluctuations in early-type stars. When a filter is tilted from the perpendicular with respect to the direction of an incoming parallel light beam, its effective central wavelength is shifted towards shorter wavelengths, and thus a simple wavelength monochromator can be constructed. A disadvantage is that the bandwidth (or full-width at half-maximum, FWHM) of the filter also increases with increasing tilt angle. The technique is incorporated into the Glasgow whole-disk solar polarimeter to measure the normalized Stokes parameters at the centre of solar absorption lines and in the nearby continuum.

For a filter orientated at an angle θ to the normal to the direction of an incident, collimated light beam, its wavelength of peak transmission is

approximately given by

$$\lambda_\theta = \lambda_0 \left(1 - \frac{\sin^2\theta}{\mu^{*2}} \right)^{1/2} \qquad (2.12)$$

where λ_0 is the wavelength of peak transmittance at normal incidence and μ^* is the effective refractive index of the interfering layers. For small θ this reduces to

$$\lambda_\theta = \lambda_0 \left(1 - \frac{\sin^2\theta}{2\mu^{*2}} \right) \qquad (2.13)$$

which is easier to use for a calibration curve, as Clarke *et al.* (1975) found that it fits wavelength/tilt calibrations more closely than the equation 2.12.

Light is gathered by a telescope apparatus incorporating the polarimetric optics and an integrating sphere, and is fed by an optical fibre to a light-tight box containing the tilting filter apparatus.

The telescope apparatus uses a continuously rotating half-wave plate, modulating the signal at 56Hz, placed in front of a 100% sheet polarizer. Behind the polarizing optics is a 15mm objective lens which produces a 1mm image of the Sun that is then isolated by a diaphragm slightly larger than 1mm at the entrance of the integrating sphere. Therefore light from the entire solar disk is collected in the integrating sphere which also serves the purpose of reducing the photon flux and scrambling any structure within the solar image. This will reduce any polarimetric modulations that may be caused by an "image wobble" due to the rotating half-wave plate or by bad tracking of the telescope. A diagram of the polarimeter is shown in figure 2.1.

The apparatus had been constructed initially for use with a spectrograph to monitor whole-disk solar polarization with a spectral resolution of 50Å, and had had its instrumental polarization investigated (see section 3.2). The polarimeter was set up so that the positive Q axis of the telescope apparatus corresponds to

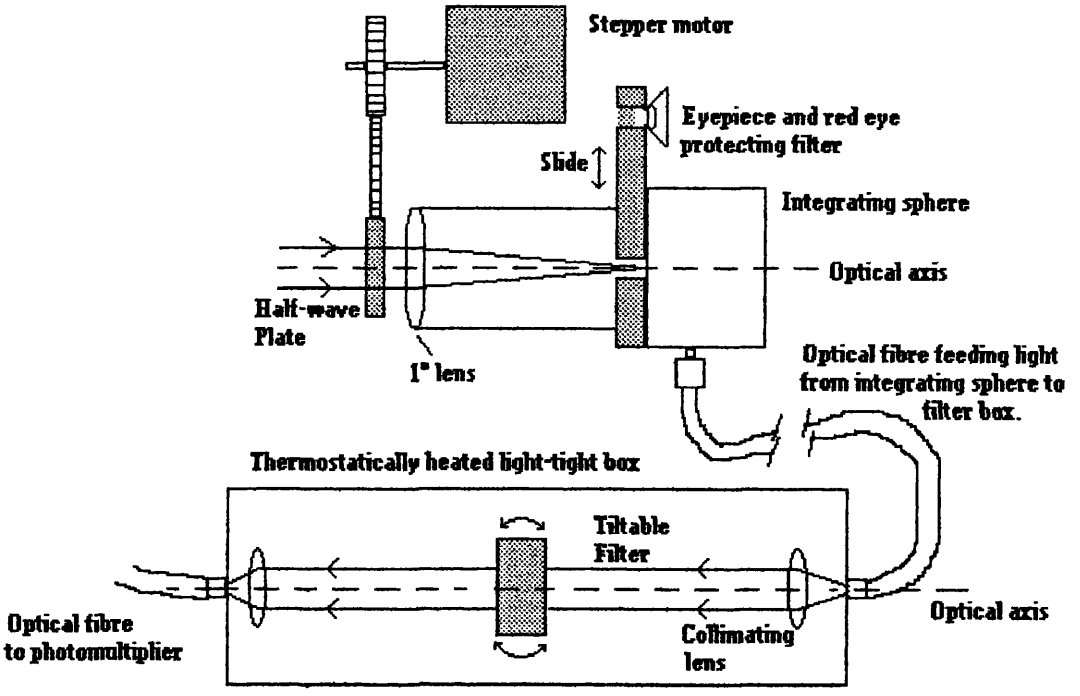

Fig. 2.1 Schematic of the whole-disk solar polarimeter

the polarization vibration, or position angle, being in the North-South direction in the equatorial frame. A subsequent experiment by Clarke (1991) confirmed this to within 1°, so it will be assumed that the instrumental frame is indeed in the equatorial frame. The polarimeter was attached to the side of the 50cm telescope at the University of Glasgow Observatory on an equatorial mount driven in hour angle to allow tracking of the Sun.

2.1.2 The Stellar Polarimeter

The Glasgow University Photometer/Polarimeter (GUPP) was designed and built by Dr. D. Clarke. It uses a superachromatic quartz/magnesium fluoride half-wave plate rotating at 5Hz at the focal point of a 50cm, f/8, reflecting telescope to modulate the signal polarimetrically at 20 Hz. The telescope sits on an equatorial mount and is driven in hour angle to track the object being observed (stellar, solar or lunar), with adjustment in right ascension and declination performed by push-buttons.

The collimated incoming beam passes through an analyzing prism, with the ordinary ray passing straight through and the extraordinary ray being deviated by 90°. Each beam then passes through an interference filter so that the instrument is capable of performing simultaneous two-colour polarimetry. Fabry lenses are used to direct the light onto photomultipliers and photon counting techniques are used to measure the polarimetric intensities. One photomultiplier has its maximum sensitivity at blue wavelengths and has a very low dark current (about 10 counts per second) at the operating voltage used (1600V from an EHT supply) and is not cooled, whereas the second photomultiplier has its maximum sensitivity at longer wavelengths and is cooled to about -20°C so that its dark current is less than 50 counts per second. Any dark current fluctuations at this level will then affect the polarimetric data by less than 1 part in 10^4 for expected count-rates of a few times 10^5, and a mean dark current is recorded several times during an observing session. The polarimeter is shown in figure 2.2.

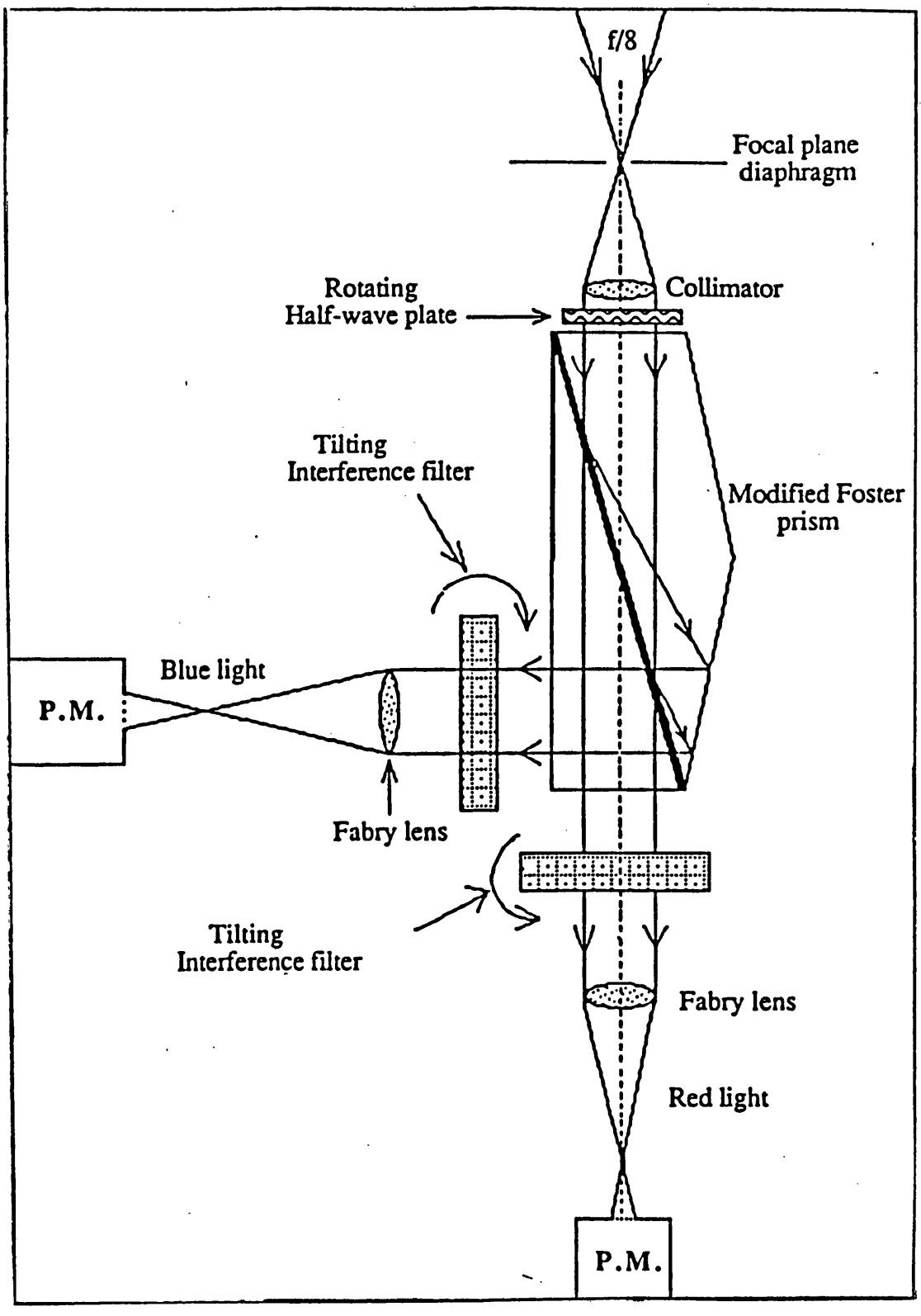

Fig. 2.2 Schematic diagram of the Glasgow University Photometer/Polarimeter

The method of measuring the normalized Stokes parameters is as given in section 2.1. As a polarizing prism is used instead of a sheet polarizer as the analyzer, two sets of three scalars are needed, and the measurements from them can be denoted by C_1, C_2 and C_3 as before for the ordinary ray, and C_4, C_5 and C_6 for the extraordinary ray. The prism matrix is the same as the sheet polarizer matrix for the ordinary ray, but as the extraordinary ray is deviated by 90° it undergoes a phase change, so that counter C_5 will be measuring -U when C_2 measures +U, and C_6 measures +Q while C_3 measures -Q. Therefore the signals are given by

$$\begin{aligned} C_4 &= N\,\pi\,I \qquad \text{(total intensity as for } C_1\text{)} \\ C_5 &= N\,(\tfrac{\pi}{2}I - U) \\ C_6 &= N\,(\tfrac{\pi}{2}I + Q) \end{aligned} \tag{2.14}$$

and finally the normalized Stokes' parameters for the extraordinary ray are given by

$$q = \frac{Q}{I} = \pi \begin{bmatrix} \frac{C_6}{C_4} & \frac{1}{2} \end{bmatrix} \tag{2.15}$$

$$u = \frac{U}{I} = \pi \begin{bmatrix} \frac{1}{2} & \frac{C_5}{C_4} \end{bmatrix} .$$

2.2 The use of a Savart Plate with a Rotatable Half-wave Plate: A Double Beam Solar Polarimeter

2.2.1 Outline of the experiment

Double-beam polarimeters have an advantage over single-beam instruments due to the fact that when the ratio of the intensity of one beam to the other is

taken the atmospheric effects upon the incident radiation during the integration are cancelled (Serkowski 1974). If the intensities of two orthogonally polarized rays are measured, say I_o (ordinary ray) and I_e (extraordinary ray), then the Stokes parameter (say q if the half-wave plate fast-axis is in the north-south direction) for that orientation is found by

$$q = \frac{I_o/I_e - 1}{I_o/I_e + 1} \tag{2.16}$$

This principle was used in the construction of a new solar polarimeter to investigate isolated areas on the solar disk, an instrument that had to be capable of measuring the normalized Stokes' parameters with short temporal resolution and in specific wavelength bands.

For a beam of light travelling along the optical axis a Savart plate will deviate both the ordinary ray and the extraordinary ray by equal amounts on opposite sides of the axis, the emerging rays being parallel to it. The intensity of each ray can then be detected separately by photomultipliers. The instrument does not use a half-wave plate as a modulator, but instead to rotate the electric vector of the incident light with respect to the orientation of the stationary Savart plate between integrations so that the Stokes Q and U parameters can be measured in turn.

Appendix A gives the Mueller matrix for a half-wave plate having its fast axis at an angle θ measured anti-clockwise from the polarizing direction of the analyzer which lies along the x-axis of a Cartesian frame whose z-axis is in the direction of the incoming radiation. The effect of the optics upon the Stokes vector [S] of the incoming radiation is found using Mueller calculus, first by rotating the frame by θ, given by [R(θ)], then applying the half-wave plate matrix, [H], rotating back into the original frame, [R(-θ)], and then applying the matrix for the ordinary ray [O] or the extraordinary ray [E]. Evaluating the

resulting Stokes vector $[S_o]'$ and $[S_e]'$ gives

$$\begin{bmatrix} I_o \\ Q_o \\ U_o \\ V_o \end{bmatrix}' = \frac{1}{2} \begin{bmatrix} I + Q \cos 4\theta + U \sin 4\theta \\ I + Q \cos 4\theta + U \sin 4\theta \\ 0 \\ 0 \end{bmatrix} \tag{2.17}$$

$$\begin{bmatrix} I_e \\ Q_e \\ U_e \\ V_e \end{bmatrix}' = \frac{1}{2} \begin{bmatrix} I - Q \cos 4\theta - U \sin 4\theta \\ I - Q \cos 4\theta - U \sin 4\theta \\ 0 \\ 0 \end{bmatrix} \tag{2.18}$$

A number of instrumental effects need to be incorporated into the equations in order to calculate the measured signals $S_o(\theta)$ and $S_e(\theta)$. The two photomultipliers that measure the ordinary and extraordinary rays have gains G_o and G_e respectively, which are the responses of each photomultiplier to unpolarized light of unit intensity. F_o and F_e denote the transmission of the filter to each orthogonal direction of vibration, and T_o and T_e are the transmissions of the Savart plate for each ray. The two emergent beams then have signals given by

$$S_o(\theta) = \frac{1}{2} G_o F_o T_o \left\{ I + Q \cos 4\theta + U \sin 4\theta \right\} \tag{2.19}$$

$$S_e(\theta) = \frac{1}{2} G_e F_e T_e \left\{ I - Q \cos 4\theta - U \sin 4\theta \right\}$$

Initially the half-wave plate will be orientated with its fast axis parallel to the direction of vibration of the ordinary ray in the stationary Savart plate, i.e. $\theta = 0°$ (set in the north-south direction), so that the ordinary ray contains a positive Q component and the extraordinary ray negative Q. Let these measured intensities be denoted by Q_{o1} and Q_{e1}, so that

$$Q_{O1} = \frac{1}{2} G_O F_O T_O \left\{ I + Q \right\} \qquad (2.20)$$

$$Q_{e1} = \frac{1}{2} G_e F_e T_e \left\{ I - Q \right\}$$

If the half-wave plate is then rotated by 22.5° the measurements can now be denoted by U_{O1} and U_{e1}, so

$$U_{O1} = \frac{1}{2} G_O F_O T_O \left\{ I + U \right\} \qquad (2.21)$$

$$U_{e1} = \frac{1}{2} G_e F_e T_e \left\{ I - U \right\}$$

To cancel out the values of G, F and T another measurement of Q and U must be taken such that the incident radiation with a certain direction of vibration is measured with the second photomultiplier if it was previously measured with the first, and vice versa. Rotating the half-wave plate a further 22.5° means that the light which previously became the ordinary ray is retarded to become the extraordinary ray when it now passes through the Savart plate. This gives the second set of Q measurements, denoted by Q_{O2} and Q_{e2},

$$Q_{O2} = \frac{1}{2} G_O F_O T_O \left\{ I - Q \right\} \qquad (2.22)$$

$$Q_{e2} = \frac{1}{2} G_e F_e T_e \left\{ I + Q \right\}$$

A final rotation of 22.5° similarly allows measurement of U_{O2} and U_{e2}, given by

$$U_{O2} = \frac{1}{2} G_O F_O T_O \left\{ I - U \right\} \qquad (2.23)$$

$$U_{e2} = \frac{1}{2} G_e F_e T_e \left\{ I + U \right\}$$

To calculate the normalized Stokes parameters q and u, and to cancel atmospheric effects and the efficiencies G_i, T_i and F_i, the two measurements for each *incident* direction of vibration are added, i.e. $Q_{O1} + Q_{e2}$, which both measure $(I + Q)$, and take the ratio of it to $Q_{e1} + Q_{O2}$ for $(I - Q)$, hence from eq. 2.16 for q and u

$$q = \frac{\dfrac{Q_{O1} + Q_{e2}}{Q_{e1} + Q_{O2}} - 1}{\dfrac{Q_{O1} + Q_{e2}}{Q_{e1} + Q_{O1}} + 1} = \frac{\dfrac{[G_OF_OT_O(I+Q)/2]+[G_eF_eT_e(I+Q)/2]}{[G_eF_eT_e(I-Q)/2]+[G_OF_OT_O(I-Q)/2]} - 1}{\dfrac{[G_OF_OT_O(I+Q)/2]+[G_eF_eT_e(I+Q)/2]}{[G_eF_eT_e(I-Q)/2]+[G_OF_OT_O(I-Q)/2]} + 1}$$

$$= \frac{\dfrac{(I+Q)(G_OF_OT_O+G_eF_eT_e)/2}{(I-Q)(G_eF_eT_e+G_OF_OT_O)/2} - 1}{\dfrac{(I+Q)(G_OF_OT_O+G_eF_eT_e)/2}{(I-Q)(G_eF_eT_e+G_OF_OT_O)/2} + 1} = \frac{\dfrac{(I+Q)}{(I-Q)} - 1}{\dfrac{(I+Q)}{(I-Q)} + 1} = \frac{\dfrac{I+Q-I+Q}{I-Q}}{\dfrac{I+Q+I-Q}{I-Q}} = \frac{Q}{I} \quad (2.24)$$

$$u = \frac{\dfrac{U_{O1} + U_{e2}}{U_{e1} + U_{O2}} - 1}{\dfrac{U_{O1} + U_{e2}}{U_{e1} + U_{O1}} + 1} = \frac{\dfrac{[G_OF_OT_O(I+U)/2]+[G_eF_eT_e(I+U)/2]}{[G_eF_eT_e(I-U)/2]+[G_OF_OT_O(I-U)/2]} - 1}{\dfrac{[G_OF_OT_O(I+U)/2]+[G_eF_eT_e(I+U)/2]}{[G_eF_eT_e(I-U)/2]+[G_OF_OT_O(I-U)/2]} + 1}$$

$$= \frac{\dfrac{(I+U)(G_OF_OT_O+G_eF_eT_e)/2}{(I-U)(G_eF_eT_e+G_OF_OT_O)/2} - 1}{\dfrac{(I+U)(G_OF_OT_O+G_eF_eT_e)/2}{(I-U)(G_eF_eT_e+G_OF_OT_O)/2} + 1} = \frac{\dfrac{(I+U)}{(I-U)} - 1}{\dfrac{(I+U)}{(I-U)} + 1} = \frac{\dfrac{I+U-I+U}{I-U}}{\dfrac{I+U+I-U}{I-U}} = \frac{U}{I} \quad (2.25)$$

and therefore the polarization state of the light may be calculated.

2.2.2 Initial Design

A simplistic design was initially drawn up in which the rotation of the Savart plate by discrete steps of 45° would allow the measurement of the Stokes' parameters of a thin light beam in four integrations. The thin beam of sunlight would be isolated from a solar image by an aperture, the image being formed by a

telescope. The two orthogonally polarized beams emerging from the Savart plate could then pass through a filter for wavelength selection and then pass through optical fibres to two photomultipliers. This scheme would allow a minimum of optical elements in a small light-tight container and would require a motor to rotate the optical elements.

For consistency it was decided that the holder made to contain the filter should be attached to the holder of the Savart plate so that it would co-rotate, and in this way the ordinary and extraordinary rays would pass through the same part of the filter at all times. Similarly, the holder for two optical fibres would also need to co-rotate so that each beam entered a single fibre at all times.

The physical nature of the Savart plate appeared to favour this design as it was held inside a cylinder, around which a ball race could be fitted that itself could be firmly held to the box for support while the Savart was rotated by connection via cogs to a motor, and the cog ratio could be chosen so that discrete rotations of 45° could be easily made.

The first problem was of how to get the two beams into the two optical fibres. For a beam of light travelling parallel to its optical axis the Savart plate deviates the orthogonally polarized beams' centres by 3mm, the beams emerging parallel to the optical axis , 1.5mm either side of it. The proposed aperture isolating solar light would give an incident beam 1mm in diameter which would only be slowly diverging (as the aperture is at a focal point), so the optical fibre apertures would need to be over 1mm in diameter, and their centres 3mm apart.

This was found to be impossible as no such fibres could be found. Instead two fibres with apertures of diameter 4mm, total diameter 5mm, would have to be used. If two such optical fibres were to be used and held side by side then this would require magnification of the separation of the beams by a factor of at least 10/3 using a lens.

2.2.3 The Final Design

The polarimeter is composed of a refracting telescope which produces an image of the Sun onto a screen which has a 1mm hole at its centre and which is the front face of a light-tight box. The optical arrangement inside this box consists of the polarizing optics, an imaging lens and two filters, and two optical fibres are placed in holes at the rear of the box to feed light to the detection system. These components are situated on a base attached to an equatorial mount which is mechanically driven in hour angle and declination. A schematic diagram of the instrument is shown in figure 2.3.

2.2.4 The Telescope

The refracting telescope has as its objective a 75mm diameter lens with a 315mm focal length, held in a plastic and rubber holder which has a threaded plastic hoop at one side. A 9mm diameter and focal length eyepiece is used. As these lenses were obtained separately a metal tube was made, of length 300mm and blackened on the inside, to connect the two lenses. The objective lens is connected to the tube by use of its thread and a threaded hoop placed over one end of the tube. The eyepiece is set into the tube by a threaded holder so that it can be moved slightly towards or away from the objective by rotation to allow the focusing of an image of the solar disk upon the face of a light-tight box.

The telescope is supported by a metal cup and a track whose teeth pass across a cog which may be rotated to move the telescope parallel to its optical axis. The cup and the axle of the cog are joined to a solid, wooden, rectangular base onto which the light-tight box is also fixed.

2.2.5 The Polarimetric Apparatus

The front of the light-tight box is a screen of thin metal painted white. The screen has a 1mm aperture aligned with the optical axis of the telescope through which the solar light passes to the rest of the optics. The distance

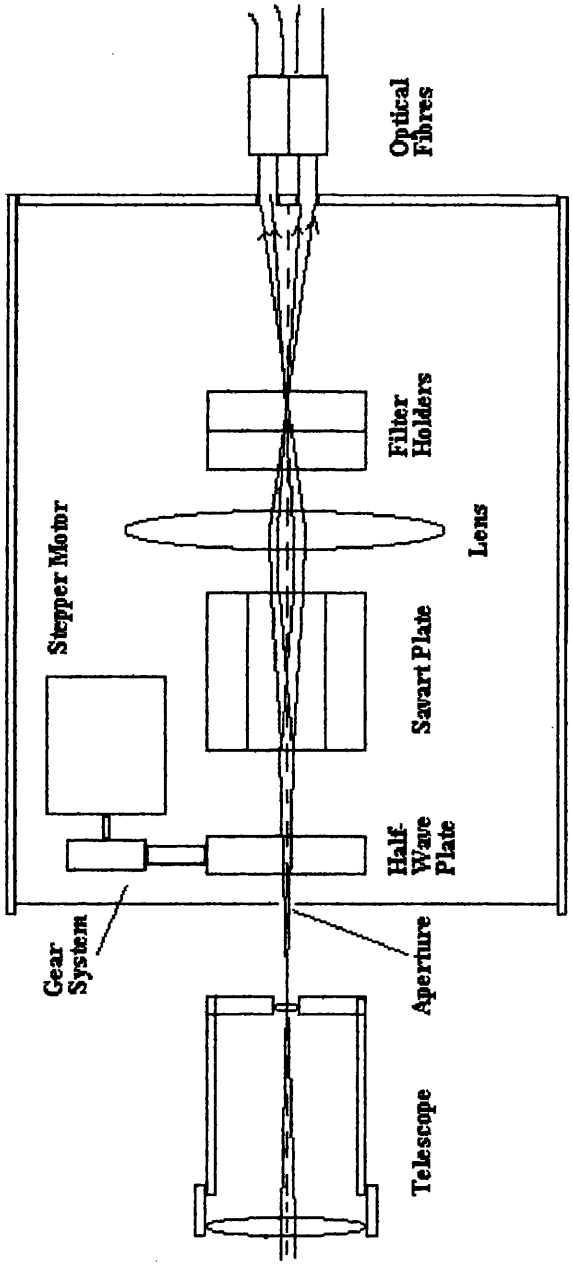

Fig. 2.3 Schematic of the double-beam solar polarimeter

between the telescope eyepiece and the screen may be varied by moving the telescope along its track in the direction of the incoming light, and hence the size of the solar image on the screen may be altered. This provides a method of varying the area of the solar disk that is being passed through the aperture on the screen so that active regions of different sizes may be observed in their entirety, or that small parts of large regions may be isolated. The maximum distance from the eyepiece to the screen is 60mm, which gives a solar image of diameter 50mm. Most active regions cover a few percent of the angular extent of the solar disk and so have an image of about 1mm on the screen. The rectangular box is completed by 3 thick metal walls, measuring 280mm long by 155mm wide by 155mm high, and a metal lid that screws down upon them, all of which are blackened on their insides. The box is screwed firmly onto on the wooden base, and the optical axis is parallel to the centreline of the base at a height of 70mm.

Inside the box, immediately behind the screen, is a rotatable, superachromatic, 10mm diameter half-wave plate. It is held in place by a 10mm thick holder which is screwed down onto the wooden base and which contains a ball race which allows the half-wave plate inside it to be rotated. An RS Components stepper motor controls the rotation. It has 200 steps per revolution so three spur gears are incorporated so that a final ratio of 2:1 means that the half-wave plate may be rotated in discrete steps of 0.9°. This allows it to be rotated by 22.5°, necessary to retard the incoming light by $\pi/4$ radians, in 25 steps. The electronic control of the rotation is described later.

The half-wave plate has its centre aligned with the 1mm aperture, and it should be strictly in the plane perpendicular to the optical axis so that during rotation it does not deviate the path of the light off the axis by prismatic effects, a cause of "image wobble". This is extremely difficult to achieve in practice, and its problems will be dealt with later in this section.

The Savart plate measures 20mm square by 40mm long and is held by rubber

inside a surrounding metal cylinder of 30mm diameter and length 40mm. It is placed immediately after the half-wave plate and acts as the analyzer, with its centre along the optical axis, and is held firmly on the wooden base. It splits the incoming light into its two orthogonally polarized beams, and is orientated such that the two beams are approximately in the plane parallel to the plane of the equatorial mount so that the two emerging polarized beams have their directions of vibration parallel to the equatorial and polar axes respectively. The centres of the two emerging beams are displaced by 1.5mm either side of the optical axis.

As the incident beam is not collimated a lens of focal length 50mm is placed immediately after the Savart plate to focus the two emerging beams onto the apertures of two liquid optical fibres. The dispersion of the beam emerging from the aperture is small so it was not thought necessary to collimate it as that would mean adding another optical element to the system and making its design more difficult. It was also known that it would be difficult to feed the separate beams emerging from the Savart plate into separate optical fibres, so the lens also allows magnification of the diameter of the light beams and their separation.

The two fibres are 5mm in diameter with an entrance apertures of 4mm. The 50mm lens magnifies the system so that when the emerging beams are focused upon the entrance of the fibres, which are held side by side into the back of the light-tight box, they have a diameter of 3.33mm and a separation 10mm.

It was earlier mentioned that the line along the centre of the Savart plate was not parallel to the line along the centre of its cylindrical housing, so not permitting rotation of the Savart in this experiment. The effect here is that the emergent beams are no longer parallel to the optical axis but are deviated slightly. For this reason the entrances of the optical fibres had to be positioned at the points where the two beams hit the back face of the light-tight box. These two positions should not move as the Savart plate is not rotated, but

the possible "image wobble" by the half-wave plate may have an effect on them. Shining a light source through the system allowed the marking of these positions and the holes were bored for the fibres.

Between the lens and the optical fibres are two holders, again fixed to the wooden base, which can each house an interference filter so that wave bands can be selected. As narrow band filters may be required, an overlapping broad band filter is placed in front of it to shield it from harmful UV light.

The optical fibres feed the light to two IP21 photomultipliers, whose operating voltages are -900V supplied by two EHT sources. They are each enclosed in a light-tight container. On one side of each container is a holder for the end of the optical fibre, and a manual shutter can be placed in front of the end of the fibre to prevent light from passing through a hole in the container wall to the photocathode inside.

The voltage pulses from the two photomultipliers are each passed through a pre-amplifier and onto a circuit containing the electronics required to count the voltage pulses using two scalars. The scalar gates could be opened and closed by electronic pulses sent from the operating computer.

2.2.6 The Mounting

The instrument was designed so that it could be used on any suitable equatorial mounting for portability and yet be totally self-contained. In one dome at the University Observatory is a coelostat mirror holder connected to a rotatable axle and set in a mounting designed specifically for the Observatory, and set at the correct angle to be an equatorial mount. It has two large gears that allow the mirror holder to be driven in hour angle and declination by stepper motors connected to threaded axles. The polarimeter could be bolted directly onto this mounting.

The motor steps were controlled by electronic pulses. The rate of the pulses for the hour angle motor could be set by a variable resistor (allowing solar,

stellar or lunar tracking), and four buttons on a control panel and handset could either speed up or slow down the hour angle drive, or drive the otherwise stationary declination motor in either direction.

2.7 Electronic Control of the Polarimeter

Previous polarimeters made by members of the University Observatory were controlled by in-house electronics commanded by Sinclair QL computers, and a fully detailed description of the all the electronic circuits can be found in Clarke (1989 a and b). Copies of the circuits for pre-amplifiers, control of scalars for photon counting, integration timing, data read-out and the control of all stepper motors were made. One of the serial ports of the Sinclair QL is used for transmitting commands for the various tasks by connecting it to the electronics rack containing the circuit boards.

A program was written in QL BASIC to issue the commands in the correct sequence for data acquisition, the order of which was as follows:

1. On starting the program, prepare a channel to the serial port in readiness for issuing commands, then initialize the electronics racks, clear scalars and electronic buffers, and inhibit movement of the half-wave plate motor.
2. Prompt for correct date and time (GMT).
3. Open a channel to store the data onto a floppy disk, prompting for the required name of the file. The current date, time and the name of the file is written to the file.
4. Prepare a screen window for data information.
5. The starting position of the half-wave plate is prompted for.
6. Prompt observer as to whether measurement of the photomultiplier dark current is required, whether polarimetric measurements are required, or to quit.

6a. Recording Dark Current. The manual shutters on the photomultiplier containers are kept in the closed position. The number of integrations are prompted for. A command is then sent to begin the integration and the two scalars are opened for a period of two seconds (set electronically). When the scalars are closed a signal is sent to the computer which then sends a command to keep the digits of the scalars in a buffer. When completed the scalars can be re-opened and begin counting again if necessary. The contents of the scalars are then read-out and stored in the computers memory during the next integration, and the two buffers are cleared in readiness to store the new values from this integration. This cycle continues until the required number of dark integrations have been made and the final read-out is made. The data are then sent to the floppy disk file.

6b. Recording Polarimetric Signal. The position of the half-wave plate is shown and the observer is prompted as to whether it should be rotated. The number of cycles of integrations is prompted for. Each cycle consists of 4 integrations. The manual shutters are opened. A command is sent to begin the first 2 second integration, and at the end of it a signal is sent back to the computer. The signal is then sent to store the digits of the scalars in the buffers. A command is sent to prepare the half-wave plate motor for anti-clockwise rotation, and a series of 25 commands are then sent to the stepper motor, one for each step. On completion of the half-wave plate rotation the scalars are re-opened, and the read-out of the buffers is performed. Integrations 2 and 3 are performed similarly, but when integration 4 of the cycle is complete and the scalar digits stored in the buffers then the stepper motor is prepared for clockwise rotation and a series of 75 commands steps the motor back to its original position before integration 1 of the cycle commenced. The first integration of the following cycle is then started

and the read-out of the previous integration performed. This chain of events continues until after the 4th integration of the final cycle when the motor is stepped back to its original position and the final read-out performed. The data are then sent to the floppy disk file.

7. Step 6 is repeated for as long as desired. On quitting a terminating line is added to the floppy disk file, and the file is then closed.

The scalar read-out is in the form of two concatenated 8 digit character strings separated by a space. Concatenated onto the end of the scalar digits is the current time (GMT), which is accessed in character string form by a command in the computer from its internal clock.

The character string actually starts as a single digit which acts as a label for each integration, with the data and time added after it. A digit 0 label means that the rest of the string is a comment line (for the date, time and file name header), digit 1 means that the values are for dark current, digits 2, 3, 4 and 5 point to the values of data corresponding to integrations 1, 2, 3 and 4 of each cycle respectively, and finally digit 9 is used for the start of the termination line which is filled with zeros for the scalar counts and the time.

The whole array of strings can then be easily written to the floppy disk file on the QL computer at the end of the integration cycles or dark current integrations. In writing such a simple ASCII file the data can then be easily reduced. An example of the format of each file is as follows:

0 suntest1 17-05-93 12:49:55	*file header*
1 10000123 20000123 12:51:32	*dark integrations*
.....:.....	*more dark integrations*
2 10783467 20783978 12:55:21	*source integrations*
3 10783467 20783978 12:55:24	
4 10783467 20783978 12:55:27	

5 10783467 20783978 12:55:32

..... *more dark or source integrations*

9 10000000 20000000 15:05:43 *file termination line*

2.2.8 Reduction of the data

After conversion to IBM format, the reduction programs, written entirely by the author, sort the data into arrays of dark counts and source counts, with the average of the dark counts being subtracted from those of the source. The termination line can used to tell the program that there is no further data and prevents end-of-file errors occurring.

The dark subtracted source counts are then converted into normalized Stokes' parameters using equations 2.24 and 2.24, making the substitutions:-

Q_{o1} = counts from channel 1 from integration labelled 2;

Q_{e1} = counts from channel 2 from integration labelled 2;

Q_{o2} = counts from channel 1 from integration labelled 4;

Q_{e2} = counts from channel 2 from integration labelled 4;

U_{o1} = counts from channel 1 from integration labelled 3;

U_{e1} = counts from channel 2 from integration labelled 3;

U_{o2} = counts from channel 1 from integration labelled 5;

U_{e2} = counts from channel 2 from integration labelled 5.

The data can now be processed in the required way.

2.2.9 Calibration problems

Calibration and testing began on an optical bench with the light-tight box, optical fibres, photomultipliers, and the electronics required to rotate the half-wave plate and perform the photon counting. A lamp was used as a light source, shining the lamp through the 1mm aperture previously allowed the position of the optical fibres to be determined. The performance of the IP21

photomultipliers with the complete optical system was investigated.

It was obvious at an early stage that a lamp did not provide a high enough signal for this testing to be done, even without a filter in the optical path. It was therefore decided to test the system with the Sun itself, using a quiet part of the solar disk near to its centre to provide an "unpolarized" source.

The complete polarimeter was secured on the mount. A narrow band filter was used initially to make sure that not too much light was incident to overload the photomultipliers. A broad band filter placed in front of the narrow band one shielded it from potentially harmful ultra-violet radiation. The EHT was switched on but the voltages supplied to the photomultipliers, which could be varied by dials and the voltages shown on voltmeters on the electronics rack face, were kept at zero. The shutters were opened to allow light to be incident upon the photocathode, and a run of integrations was started with the half-wave plate kept static. The supplied voltages were then slowly increased towards -900V, and the count rates could be monitored on the scalars to make sure no overload occurred which would damage the photomultipliers.

Once -900V was reached for each photomultiplier without a reasonable count rate being observed it was obvious that the variable resistors in the pre-amplifiers needed to be tuned so that a favourable count rate for the forthcoming investigation could be achieved. Most observations would be done with intermediate band filters, i.e. between 10Å and 50Å, and in extreme cases with 100Å passbands.

So it was decided to set up the system so that count rates on the verge of being influenced by dead-time when using 100Å passbands near the peak of the solar spectrum were possible, knowing that narrow band observations should not then be affected by dead-time. This meant tuning the variable resistors so that the read-out of two second integrations would be in the region of half a million counts.

Tuning was accomplished by turning a screw on one side of the variable

resistor. This could be accomplished with a screw driver through a hole in the case of the pre-amplifying circuit. It is not favourable to allow direct sunlight to be incident upon any of the electronics or photomultiplier cases in case of light leaks (although the cases were tested and assumed light-tight), so they were kept inside a container that allowed only the optical fibres and co-axial cables to enter. But due to the current problems of pre-amplifier tuning their cases were kept outside the container so that the tuning could be performed whilst monitoring continuous integrations so that the current count rate could be determined.

When the count rates of the two channels were roughly equal and above 10^5 counts per second a test needed to be performed to make sure that the detection systems were linear, that is that a doubling in the number of incident photons doubles the observed counts. If this is not achieved for both channels then the amplification system would need further tuning until it was correct.

To perform the test a sheet polaroid was placed ahead of the objective lens of the telescope so that only linearly polarized light passed through the entire system. Its direction of vibration was marked on the polaroid and it was placed on the telescope such that it was approximately in the north-south direction, to line up with the ordinary ray of the Savart plate. When the half-wave plate's fast axis is at the correct orientation, the linearly polarized light will pass totally through the ordinary channel, and when the half-wave plate is rotated from that position by 45° (50 steps) the light will pass totally through the extraordinary channel. At other angles the intensity in each channel will follow the usual $\cos^2(2\theta)$ law. At an angle of 22.5°, therefore, the two intensities should be equal.

It was very quickly seen that the two intensities did not rise and fall in the correct manner as the half-wave plate was rotated. This meant that either the detection systems were indeed not linear, that the optical paths were not constant or the efficiencies of the optical elements to each beam were not equal.

This could be due a number of effects. The half-wave plate may not be rotating in the plane exactly perpendicular to the direction of the light, which incur prismatic effects and would lead to the two beams emerging from the Savart plate to wobble. This may then result in only part of each beam entering their respective optical fibres, reducing the number of photons detected.

The Savart plate, as already stated, is not set strictly parallel to the axis of its cylindrical holder, so the emerging beams may not be parallel to the optical axis. This should not be a problem as the entrances to the optical fibres were placed where the two beams hit the back face of the light-tight box, and the Savart plate had not been moved. But if there was image wobble then this misalignment might be a problem. Although image wobble could not be seen visually on inspection, the half-wave plate holder was nevertheless replaced, but the accuracy to which it must be perpendicular to the optical axis was possibly still not attained.

Other possible factors were filter efficiency and photomultiplier response, but as shown earlier in this chapter these factors cancel out when calculating the normalized Stokes' parameters. Therefore observations were made to check whether reasonable results were being obtained. Again it was immediately obvious that this was not the case as the polarizations "measured" were extremely large and variant!

As the first instrument design had been found to be impractical, due to the Savart plate crystal not having its optical axis along the centreline of its cylindrical holder, thus not allowing Savart plate rotation, redesign and reconstruction was required during the winter of 1992/3 in readiness for the spring and summer observing season in 1993. The above proceedings had now taken up many of the already scarce clear or partly clear days in the spring of 1993.

Assuming an electronic reason the tuning of the pre-amplifiers was restarted when observations were possible. This brought about a new persistent problem where at a certain value of the variable resistor a count run-away is produced,

not a product of the amount of incident light. The correct configuration could not be found and the apparatus was brought back into the laboratory for more similar testing before it became obvious that the set-up was inadequate and it was too late for reconstructing the instrument.

The problems highlight the inherent difficulty in producing double beam polarimeters in which each beam is individually detected. One answer was briefly pursued using a charge coupled device (CCD) as a detector. The two orthogonal beams would be incident upon different parts of the chip at the same time, and each illuminate a small circle of pixels. If the total number of counts from each "circle" was found, then the intensity of each beam is known. If the image wobbled slightly then it would only be required to add up surrounding pixels to eliminate the problem. A possible drawback is "cross-talk", whereby photons from one beam have a parasitic effect upon the other. This could also be eliminated if the two beams were far apart and/or a baffle used between the beams.

A 1mm diameter circular beam of light would be incident upon about 6500 pixels measuring 22μm square, each pixel being capable of recording 255 counts for 8-bit read-outs, or up to 65535 for 16-bit read-outs, which would correspond to about 10^5 electrons depending upon its analogue-to-digital converter. Thus the maximum number of counts for 6500 pixels of an 8-bit CCD is over 1.5 million, so the two intensities would be at a good level to perform polarimetry to high accuracy with the inherent problems of photon counting. However time did not permit the application of this idea in practice.

Such a double-beam polarimeter would have been of great benefit and it is regrettable that this part of the project could not be brought to a suitable conclusion. It is imperative that the polarization of small regions of the solar disk are studied in more detail, and the information gained from such an experiment would have been extremely useful in understanding some of the results described in the following chapters.

2.3 Effects of Noise: Scintillation Noise, Seeing and Image Movement

The atmosphere will have an effect upon the measurements of such small levels of polarization as it affects the number of photons counted during integrations. Seeing, or the fluctuation and spread in the direction from which light is received, causes the image of a star to move around and not be point like when viewed. If the incident radiation does not illuminate the same part of a photocathode for the whole duration of an integration, then inhomogeneities in the sensitivity over the photocathode surface will introduce a noise effect unless steps are taken to reduce the motion. Such movement may also be introduced by bad tracking of the telescope or if a rotating optical element is not perfectly aligned with the optical axis, causing an "image-wobble", and will affect point sources and extended objects alike. The photometric errors for the integration may therefore not be photon shot-noise dominated, for which signal-to-noise ratio is given by the square root of the number of photons counted, but may be greater and possibly not uniformly distributed.

For the double-beam solar polarimeter, fully described in section 2.2, taking the ratio of the intensities of the two orthogonal beams cancels scintillation effects as air is not birefringent, so scintillation is the same for both orthogonally polarized components when the signals are measured simultaneously.

Meanwhile seeing and image-wobble effects are reduced in two ways. First, the instrument is observing an extended object filling the aperture at all times, and hence the light should remain incident upon a single area of the photocathode. Secondly, the half-wave plate does not rotate during an integration and light from the optical fibres being employed accept the whole of each orthogonal beam and the light is not focused onto the photocathode, which should result in negligible image movement across the photocathode during each integration.

In the case of continuously rotating half-wave plate polarimeters observing point sources, scintillation noise is cancelled by the rapid modulation of the signal. Serkowski (1974) shows the unpublished calculations by A.T. Young which state that the sinusoidal modulation with frequency f diminishes the errors of atmospheric origin in the amplitude of this modulation by a factor of $(f/f_c)^{5/6}$, where f_c is a "cut-off" frequency given by

$$f_c = V_\perp/\pi D \qquad (2.26)$$

where D is the telescope diameter and $V_\perp$ is the speed at which the atmospheric turbulence crosses the line of sight, typically 3000 cm s^{-1}. For the 50cm telescope the critical frequency is 20Hz, but as this treatment only applies to stellar-like sources and telescope diameters greater than a few centimetres we do not calculate f_c for the whole-disk solar polarimeter.

The stellar polarimeter modulates the signal at 20Hz so should be free of atmospheric effects at lower frequencies, but may be affected by higher frequency effects. Also, there is no correction for inaccurate telescope tracking or "image-wobble" due to the rotating half-wave plate, both of which may introduce noise into the data.

In the case of the whole-disk solar instrument the use of the integrating sphere negates both the effect of "image-wobble" created by the rotating half-wave plate not being perfectly aligned and the movement of the light source due to inaccurate telescope tracking. As the Sun is an extended object, measurements will not suffer from atmospheric effects due to the large angular extent.

2.4 The Effect of Dead-time on Polarimetric Precision

The number of photon counts recorded by photometric detection techniques relies upon the electronics of the photomultiplier, pre-amplifier and counting system. For most systems, the arrival of a photon will generate a voltage pulse

which will be counted by a scalar. There will then be a short "relaxation period" during which the system will be oblivious to other incoming photons and will not record them, and this is known as the *dead-time* of the system.

Typically, the dead-time is measured in tens of nanoseconds and so will not affect photon counting at lower count rates (less than 100,000 photons per second). However in the polarimetric systems used at Glasgow we may be dealing with count rates in excess of 100,000 photons per second when observing the Sun or bright stars. Therefore it is likely that some of the incoming photons will arrive during such a "relaxation period" and not be counted, leading to a distorted measurement of the Stokes' parameters.

The effect of dead-time has been formulated as follows: if the true rate of photons incident upon the photomultiplier is given by N, and the dead-time of the system is given by τ, then the observed rate of incident photons, n, is found from the relationship

$$n = N e^{-N\tau} \tag{2.27}$$

The effect is shown in figure 2.4 which is a plot of n against N for various values of τ ranging from 50ns to 200ns, showing that when N approaches $1/\tau$ the value of n levels off and then decreases, with the maximum n being at $N = 1/\tau$. It can be seen that, even for τ = 200ns, count rates below 10^5 photons per second are not affected to any great degree.

There is no analytical solution to the problem of calculating N knowing n, but an iterative technique was devised which estimates a value, x, to a desired accuracy, to which n is multiplied to estimate the true counts, N.

Knowing n and τ, the following steps give a reasonable estimate of N.

1. Initialize variables: $x = 1.1$ and $i = 0.1$
2. Let $t = \log_{10}(x)/x/n$

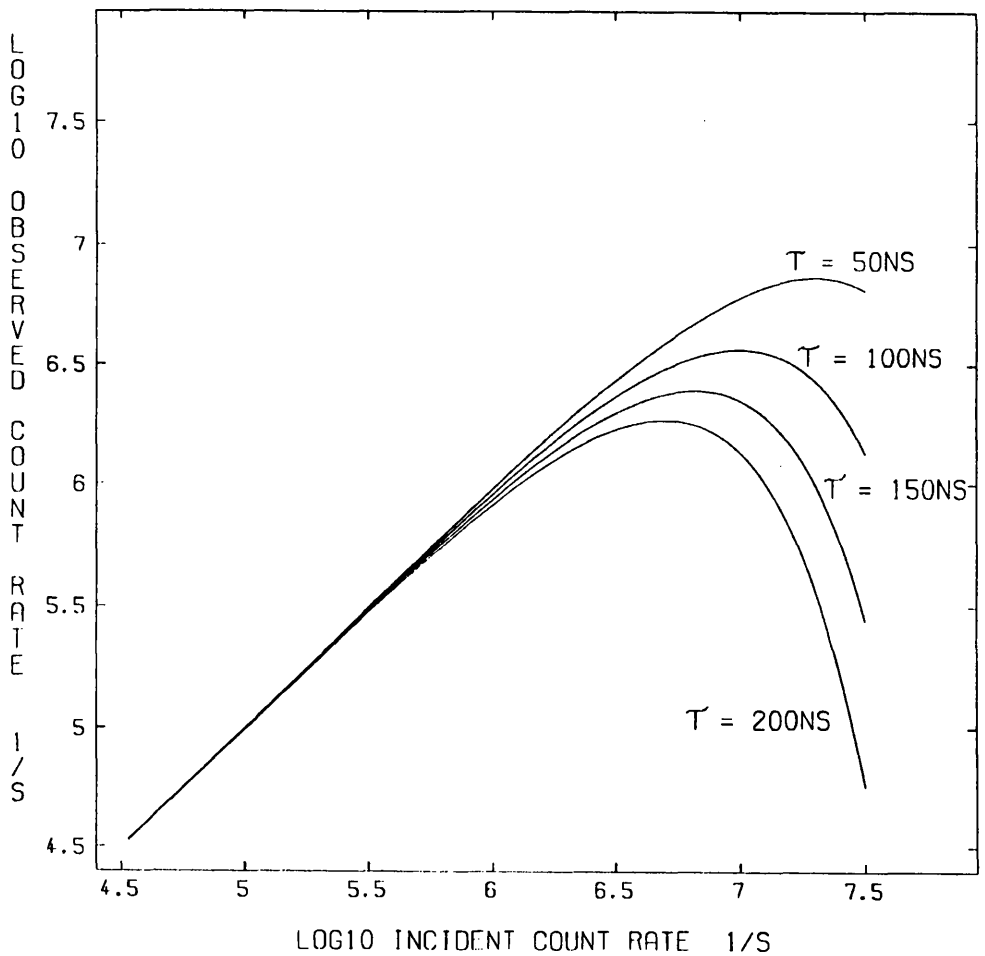

Fig. 2.4 Logarithm of observed photon count rate, $\log_{10}(n)$, against incident photon count rate, $\log_{10}(N)$, for various values of dead-time, τ (ns). (Units in s^{-1})

3. If $t < \tau$, increment x by i, (i.e. $x = x + i$) and repeat step 2.
4. When $t > \tau$ then make the following calculations,

$$x = x - i + i/10$$

$$i = i/10$$

which sets x back to the value before $t > \tau$ plus one tenth of the increment, and sets the increment to one tenth of its previous value. As i becomes smaller then x becomes closer and closer to the required value to use to correct n, and a minimum value of i needs to be set otherwise the loop will be infinite. A minimum value of 0.0001 is used here so that the estimated N should equal its true value to an accuracy of 1 part in 10^4, which would be well within the FWHM of a Gaussian distribution about 10^6 counts s^{-1} if photon shot noise dominated. If $i > 0.0001$ then step 2 onwards is repeated with the new x and i values used.

5. Finally, when i is 0.0001 and the calculated $t > \tau$, then the final calculation $x = x - i$ is used, and N is given by $N = nx$.

It is desirable to know what the value of the *dead-time* is for the system in use so that corrections may be made. This may be done experimentally using a bright light source, a half-wave plate and two fixed 100% linear polarizers. The light would need to be bright enough to register at least 1 million photons per second by the photometric detection system so that the effect of the dead-time is easily seen. If the two fixed polarizers are placed either side of the half-wave plate, then a particular orientation of the fast-axis of the half-wave plate would allow a maximum number of photons to pass through the optical system to the detector, and stepping through discrete angles of the half-wave plate would decrease the throughput until, at 45° from the original position, a minimum throughput would be reached (which should be zero). A plot of photon counts versus position angle of the half-wave plate would show a sinusoidal variation in the count rate.

As mentioned above, dead-time will not affect low photon count rates and so a true sinusoidal shape should be seen in this region, whereas in the near maximum count rate region the plot would show a leveling off of the observed rate. If a sinusoidal fit, or to be more precise a $\cos^2(2\theta)$ fit, to the observed count rates below about 10,000 per second were performed, and the values plotted for the complete cycle, then it is intuitive to conclude that this plot would have its maximum at higher count rates than that of the observed plot. Equation 2.27 could then be used to find which value of τ needs to be used to make the fitted curve equal to the observed curve.

This value of τ will only be an estimate, however, because the low signal-to-noise at low photon count rates will give a large spread of values, and so the fitted curve will be imperfect. Therefore it would be necessary to make repeated measurements at each position of the half-wave plate fast-axis and to use mean values of photon counts at each position.

This method was used as an attempt to estimate the dead-time of the detection system used with the solar whole-disk polarimeter. The half-wave plate of the system could be rotated in discreet steps of 0.9°, so 400 steps completed a full rotation of the half-wave plate during which the signal was modulated four times.

The Sun was used as a bright source, the maximum count rate being almost 10^6, and measurements were made after each rotation step so producing four periods. However the number of points with a count rate below 10^4 was small, and the low signal-to-noise ratio meant that they had a large scatter, so it was difficult to fit a smooth curve. It was found that a dead-time between 80ns and 150ns could be used for the fit to the data, possibly larger than the expected value of a few tens of nanoseconds. A value of 100ns will therefore be employed throughout for the stellar and solar whole-disk polarimeters to be consistent with previous data reduction by Dr. Clarke who employed this value.

The correction for dead-time also affects the calculated degree of

polarization (hence the Stokes' parameters q and u) and its error. Unfortunately it seems that many authors do not respect this fact and do not correct their data accordingly. To highlight this fact, data for the stellar/solar polarimeter has been simulated.

Using the NAG workstation routines for generating random numbers from a normal distribution, 500 data points were produced to mimic real data (500 points was the usual number of integrations used in observing a star with a particular set of filters). The modulation of the signal by the half-wave plate can be split into 4 sections, namely x, y, z and w, corresponding to orientations of the half-wave plate given by

$$\begin{aligned} \text{x: } \theta &= 0 \rightarrow {}^{\pi}/_{8} \\ \text{y: } \theta &= {}^{\pi}/_{8} \rightarrow {}^{\pi}/_{4} \\ \text{z: } \theta &= {}^{\pi}/_{4} \rightarrow {}^{3\pi}/_{8} \\ \text{w: } \theta &= {}^{3\pi}/_{8} \rightarrow {}^{\pi}/_{2} \end{aligned} \qquad (2.28)$$

as described in section 2.1.

The actual count rate, N_1, during each orientation of the half-wave plate rotation came from a random normal distribution, centred on 10^4, 5.10^4, 10^5, 5.10^5, 10^6 and 2.10^6 counts per second respectively, with an FWHM equal to its square root, and which would correspond to unpolarized light. Equation 2.27 was used with the four values of τ, 50ns, 100ns, 150ns and 200ns to give the observed intensities x, y, z and w for each value of N_1. The iteration technique was then used to correct these values to estimate the true values generated, and are denoted by x_c, y_c, z_c and w_c.

The Stokes' parameters were calculated by

$$q_o = \pi \left(\frac{1}{2} - \frac{y+z}{x+y+z+w} \right) \qquad (2.29)$$

$$u_o = \pi \left(\frac{x+y}{x+y+z+w} - \frac{1}{2} \right) .$$

and similarly for q_c and u_c with x_c, y_c, z_c and w_c. The means of q_o, u_o, q_c and u_c for the 500 integrations were calculated, as were their standard mean errors, and then p_o and p_c were calculated. To show how the corrections for dead-time affect p and the error, σ, the ratio is made of the corrected p_c (and σ_c) to the uncorrected p_o (and σ_o) for each value of observed count rate n and dead-time τ.

Figures 2.5 (a) and (b) show how the ratios p_c/p_o and σ_c/σ_o respectively vary with incident count rate N for the four values of τ. It is immediately apparent that the corrected values of p_c and σ_c are higher than the uncorrected values, and the difference between the two increases quite sharply with increasing count-rate and dead-time. It should be noted that for the designated dead-time of 100ns used in the following analyses, count rates below 10^5 s^{-1} will be barely affected, whereas above 10^5 s^{-1} it is very important to correct for dead-time, otherwise both p and σ will be underestimated.

This process was repeated with polarization added to the data, and it was found that the two ratios p_c/p_o and σ_c/σ_o did not vary when an intrinsic polarization of levels 0.01%, 0.1% and 1.0% were added.

2.5 Normality Testing and the Detection of Polarization

The statistics used in the following sections will be those explored by Stewart (1984). As a bias will be introduced in calculating the polarization, p, from the normalized Stokes' parameters, q and u, analysis will be concerned with q and u only.

2.5.1 Normality Testing by Skewness and Kurtosis

It is assumed that for each observation of n integrations the calculated mean values of the Stokes' parameters, $\hat{q}$ and $\hat{u}$, have estimated squared standard errors, $\hat{\sigma}_q^2$ and $\hat{\sigma}_u^2$, that come from the same parent statistical distribution. To test the normality of the distribution the skewness and kurtosis of each data set

(a) p_c/p_o

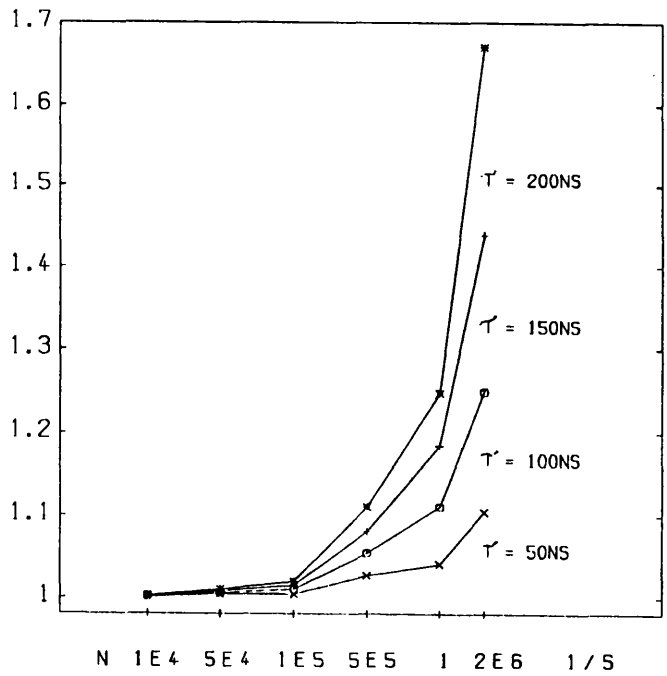

(b) σ_c/σ_o

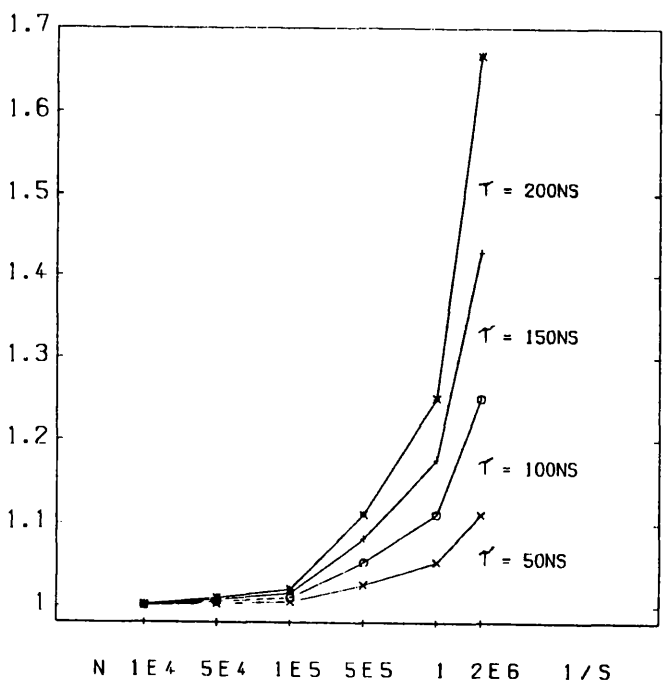

Fig. 2.5 (a) The behaviour of the ratio of corrected to observed degree of polarization, p_c/p_o (above), and (b) of the ratio of corrected to observed error upon the degree of polarization, σ_c/σ_o (below), with true incident photon count rate, N (s^{-1}).

are calculated, which can then be compared to tables by Brooks (1985) at the required confidence level.

If (q_0, u_0) are the true values of the Stokes' parameters, Stewart states that the confidence region for the point (q_0, u_0) for data which has $\hat{\sigma}_q^2 \neq \hat{\sigma}_u^2$ and $n_q = n_u$ at the (1-α)100% level is given by

$$\frac{(\hat{q} - q_0)^2}{\hat{\sigma}_q^2} + \frac{(\hat{u} - u_0)^2}{\hat{\sigma}_u^2} = z_{(1-\alpha)} \qquad (2.30)$$

which is an ellipse with centre $(\hat{q}, \hat{u})$ and semi-major and semi-minor axes given by $\sqrt{\hat{\sigma}_q^2 z_{(1-\alpha)}}$ or $\sqrt{\hat{\sigma}_u^2 z_{(1-\alpha)}}$. The observed data point is said to be unpolarized if the origin is contained within the ellipse at a chosen (1-α) confidence level. Values of $\sqrt{z_{(1-\alpha)}}$ as a function of sample size were calculated and tabulated by Stewart, and are used in this analysis. For the purpose of this study a confidence level of 95% will be used, and as each sample size is greater than 140 a value of $\sqrt{z_{(1-\alpha)}} = 2.46$ can be employed as it is almost invariant for larger sample sizes (at $n = \infty$ it is 2.45).

2.5.2 Testing for Spectral or Temporal Variability of Polarization: the Welch Test

Temporal changes in the normalized Stokes' parameters may not be visually apparent, so a test is needed to detect any significant difference in the data points. Brown and Forsythe (1974) concluded that in terms of size and power (power being the probability of rejecting the hypothesis of equality of means when it is indeed false), the Welch test is the recommended statistical test .

For a set of g data points for q (and/or u), with unequal sample sizes $n_1 \neq n_2 \neq \ldots \neq n_g$ and standard mean errors $\hat{\sigma}_1^2 \neq \hat{\sigma}_2^2 \neq \ldots \neq \hat{\sigma}_g^2$, the Welch statistic, W, is calculated from

$$W = \frac{\sum_i w_i (q_i - \tilde{q})^2 / (g - 1)}{\left[1 + \frac{2(g-2)}{(g^2-1)} \sum_i (1 - w_i/u)^2 / (n_i - 1) \right]} \qquad (2.31)$$

where

$$\begin{aligned} w_i &= 1/\hat{\sigma}_i^2 \\ u &= \sum_i w_i \\ \tilde{q} &= \sum_i w_i q_i / u \end{aligned} \qquad (2.32)$$

with the summations over i = 1, 2, ..., g.

When all the population means are equal (the standard mean errors being equal or unequal) W is approximately distributed as an F-statistic with g-1 and f degrees of freedom, where f is defined by

$$\frac{1}{f} = \left(3/(g^2 - 1) \right) \sum_i \left(1 - w_i/u \right)^2 / (n_i - 1) \qquad (2.33)$$

and the hypothesis of equality of the population means is rejected at the 95% confidence level.

The Welch test may show a polarimetric difference between observed data points when in fact none of the individual data points are polarized because the test weights observations with respect to their mean values and standard mean errors. The test may be applied to polarimetric measurements in different spectral passbands to investigate wavelength dependence of polarization, or to find temporal variations in measurements made over periods of days.

CHAPTER 3

POLARIMETRIC OBSERVATIONS OF THE SUN

3.1 Introduction

In section 1.3 it was seen that broad-band polarization has been registered in and around sunspots and at the solar limb and spectral line polarization in active regions and again at the solar limb. Similar phenomena must also occur in stars but the magnitude of any effect will be substantially reduced by the global radiation which is essentially unpolarized. If the effects from localized regions on the Sun can be detected from the measurement of the integrated light of the whole solar disk, then monitoring stars by polarimetry would allow rotation periods, scale times for activity, geometries, etc., to be deduced in a similar manner to that of the Sun.

With the above in mind, investigations of the total light from the whole disk of the Sun have been made in an attempt to make "solar-stellar connections". Estimates of the magnitude of any global effect made by Leroy (1989b) are discouraging, but Stewart (1984) has shown that readily detectable levels of polarization might be apparent within lines which are sensitive to resonance or fluorescent scattering.

Innovative equipment had been designed at Glasgow to investigate the global levels of polarization but the experiment provided null results at the time of solar minimum. Later it had been claimed by Clarke (1991) that a variable broad-band (50Å) polarization had been detected in association with the appearance and rotational progression of spot activity. Here an experiment aimed at investigating the detection of whole solar disk polarization within two solar absorption lines associated with the effect of magnetic intensification is described.

Spectral line profile scanning using narrow-band tilting interference filters has been used for many years to observe rapid line profile variations in Ap and Be stars. The technique is described in Clarke (1975), which shows that the tilt-scanning of a filter has many advantages in measuring spectral detail

over spectrographs, such as the high throughput of the system and the ability to accept the whole seeing disk, thus having a higher resolving power, but has the disadvantage of being non-linear in wavelength.

For this study the technique is used to detect whole solar disk polarization which may best be achieved by measuring the polarization in the centre of solar absorption lines when compared to that measured in the nearby continuum, which should be essentially unpolarized. Magnetic intensification produces a non-zero net polarization resulting from differentially saturated absorption lines that are subject to the transverse Zeeman effect: the π and σ components being unequally absorbed in a saturated line. Leroy (1989a) calculated the linear polarization for 6000 solar spectral lines due to this effect, which included the Fe-line at 4872.14Å for which the calculated polarization measured in a 20Å spectral band is 0.0115% for a magnetic field strength of 500 Gauss. It is the polarization of this line, including the minor effects of other Fe/Ni lines contained within the band pass of the selected filter, and the Hβ line at 4861.34Å that is studied in this chapter.

3.2 Investigation into the Instrumental Polarization

The problem with all polarimeters is that their optical elements can introduce polarization. Although many methods may be incorporated to try and cancel this effect, in this case by measuring the difference between a possibly partially polarized source (at the line centre) and an incident unpolarized source (the continuum), so that, in theory,

$$(I_{pol}+I_{unpol}+I_{instrumental})_{line}-(I_{unpol}+I_{instrumental})_{contnm} = I_{pol}$$

It is good practice to understand and estimate the instrumental effect on the state of polarization of the incident light.

To do this a glass pellicle was placed in front of the solar whole disk polarimeter. When a pellicle is tilted from the plane perpendicular to the direction of the incident light it will introduce partial polarization which can be calculated using Fresnel's laws. At any particular orientation, the measurement of the polarization at different tilt angles of the pellicle should give a set of points lying on a straight line when plotted on a q,u diagram. The quadrant in which this straight line lies is dependent upon the orientation of the pellicle.

If a series of measurements are made with respect to tilt angle at one orientation, and this is repeated at an orientation 45° clockwise or anticlockwise from the original, then when the two respective straight lines are plotted they should cross at the zero-polarization point, where both tilt angles would be zero, and should be perpendicular to each other in the q,u plane. If the instrument is introducing polarization it should be at a constant value and would be unaffected by the pellicle position (as it is placed in front of all the polarimeter optics), and therefore the zero-polarization point would not be at the origin in the q,u plane. The value of the zero-polarization point then gives us the instrumental polarization which can be subtracted from subsequent polarimetric measurements.

In order to perform the experiment a pellicle holder had to be made such that it would allow the pellicle to be tilted, and it must be able to be attached to the front of the polarimeter so that it could be rotated. A square housing for the pellicle was attached at the centre of two of its opposing sides by axles to a hollow cylinder, thus allowing the pellicle to be tilted. This cylinder was adjoined to a further hollow cylinder so that they could be rotated with respect to one another, and marks used to denote angles of 0, 45 and 90 degrees. The second cylinder could be bolted onto the telescope in front of the continuously rotating half-wave plate. This configuration is shown in figure 3.1.

Observations were made on 29 May 1991 using the Sun as a bright, unpolarized

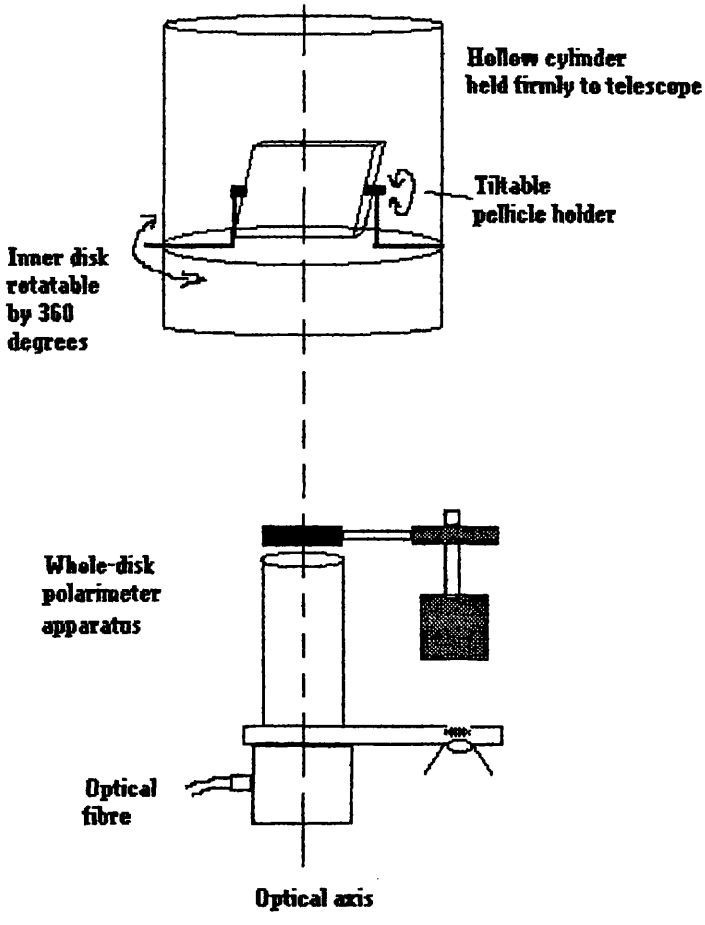

Fig. 3.1 Schematic of pellicle set-up in front of whole-disk polarimeter

light source as the polarimeter was already mounted on the telescope. Measurements were made of the q,u values at three different tilt angles at the orientations denoted by 0, 45 and 90 degrees. It does not matter at which angle of tilt the measurements are made because, as stated above, at a particular orientation the measured q,u values at each tilt angle will lie on a straight line on a q,u diagram.

The results are shown Table 3.1 which gives the q,u values and their standard errors for each measurement. The standard errors are seen to be just less than 0.01%, and as this is the minimum accuracy that will be required for the solar measurements, it is doubtful that the instrumental polarization can be calculated to a few times 0.001%. Drawing the best straight line through the points gives us an estimate of the gradient and intercept on the u axis for the three lines. Immediately apparent is that the three lines do not cross either at a single point or even within a small area (to allow for the observational errors). Also important is that the line measured at the 45 degree point is not perpendicular to either of the 0 or 90 degree lines, and these two lines themselves are not nearly parallel. It was decided not to try to calculate the gradients and intercepts by a least squares method due to only having three points per line and the obvious fact that it would not lead to any positive result. Instead their values were measured from the lines drawn on the graph shown in figure 3.2, and are included in Table 3.1.

It is therefore beneficial to look at the possibilities of making this experiment more precise.

First, the apparatus may not have been made to a high enough accuracy. The tilt axis of the pellicle *must* be in a plane perpendicular to the direction of the incident light, this may not have been the case. To highlight the importance of the effect of non-alignment, remember that a 1 degree rotation of the orientation of the tilt-axis results in a 2 degree rotation in the q,u plane, so if the tilt-axis is not perpendicular then in tilting the pellicle a slight shift

Orientation = 0 degrees

q_1 = +1.7304 ± 0.0093 % u_1 = +1.4668 ± 0.0088 %

q_2 = +2.1945 ± 0.0069 % u_2 = +1.7821 ± 0.0090 %

q_3 = +2.6481 ± 0.0061 % u_3 = +2.1113 ± 0.0094 %

Gradient = +0.7023 u intercept = +0.2480 %

Orientation = 45 degrees

q_1 = -1.6967 ± 0.0078 % u_1 = +1.6398 ± 0.0086 %

q_2 = -2.2171 ± 0.0076 % u_2 = +2.3205 ± 0.0077 %

q_3 = -2.5236 ± 0.0080 % u_3 = +2.7433 ± 0.0064 %

Gradient = -1.3320 u intercept = -0.6238 %

Orientation = 90 degrees

q_1 = -1.6282 ± 0.0081 % u_1 = -1.7683 ± 0.0072 %

q_2 = -2.3824 ± 0.0060 % u_2 = -2.5617 ± 0.0085 %

q_3 = -2.9346 ± 0.0079 % u_3 = -3.1534 ± 0.0101 %

Gradient = +1.0590 u intercept = -0.0430 %

Table 3.1 Measurements of q and u at three tilt angles for three orientations

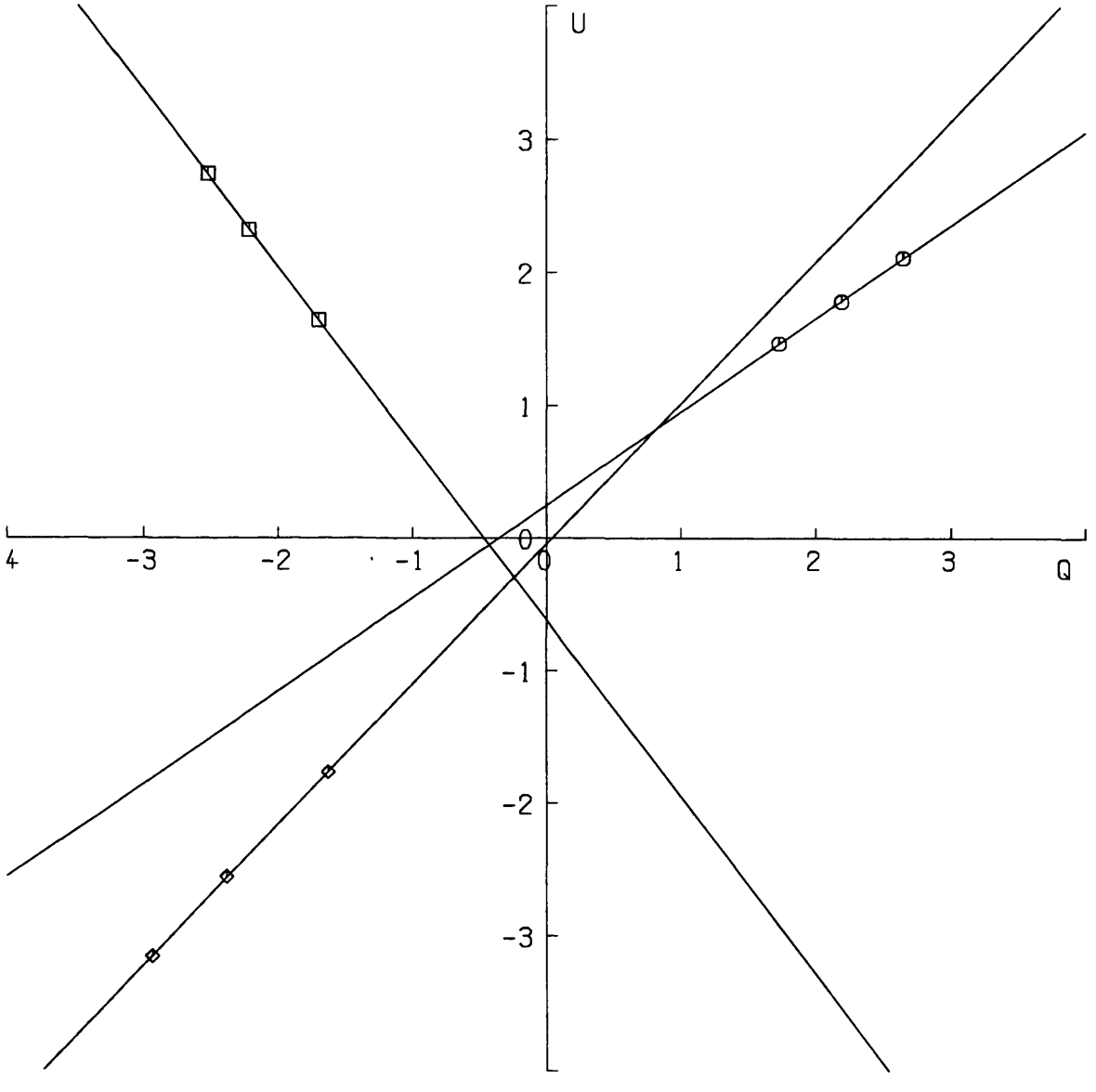

Fig 3.2 *q,u* diagram showing the measured values for three tilt angles at three orientations of the pellicle.

in orientation is produced whose effect is doubled in the q,u plane. The apparatus would also need to be very rigidly connected to the telescope so that there is no shift in orientation during the course of the day when the orientation of the telescope obviously changes due to the equatorial mount.

Secondly, the observational errors would need to be of the order of a few times 0.001% in order to estimate the zero-polarization point to a similar accuracy. This requires inordinately longer integration runs at each tilt and orientation position.

Thirdly, at least six different tilt angles should be used at each orientation so that an accurate least-squares fit can be used to find the gradient and u intercept. Measurements should be made at all tilt positions in one orientation before moving to the next orientation.

Points two and three require that this experiment would take many hours to complete. If count rates of just over 10^5 photons per second are assumed, together with integration times of 7.5 seconds, then assuming photon shot noise dominates the S/N ratio, then the error on each integration will be of the order of 10^3 photons/integration. An error of 1 part in 10^5 is desirable, requiring about 10,000 integrations of 7.5 seconds which is nearly 21 hours! A compromise is obviously needed, and it can be shown that 1000 integrations takes just over 2 hours, which will give an accuracy of about 3.5 parts in 10^5. Therefore the six measurements at a single orientation would take one whole days daylight hours, whereas the nine observations taken here were undertaken in only about six hours!

It is also desirable to know the relationship between the instrumental polarimetric frame and the equatorial frame. This can be achieved using a dangling 100% polarizer, which is weighted by a plumb-bob to keep its axis at a constant orientation with respect to the Earth. Measurements were made by Dr. Clarke on 20 July 1990 with the polaroid alternately set with face in and face out. In the q,u plane the bisector of a pair of such measurements corresponds to the position angle of an equivalent polaroid set with its axis parallel to the

vertical. At local noon this corresponds to the north-south axis of the equatorial frame, and the data suggested that the instrumental frame was set to within 1° of the $+q$ direction; there was little or no u component.

Prior to noon, the bisector of the polaroid's axis, which still remains set parallel to the vertical, will introduce a small component in the west direction. The data showed that the instrument interprets this as providing a negative u component. In the afternoon, the vertically oriented polaroid will provide a small component in the east direction, which corresponded to a small positive u value.

Dr. Clarke concluded that polarizations set N through E give positive u components and vibrations set N through W give negative u components. This conclusion will be referred to in later analysis of solar data.

3.3 Observations at Hβ and the Fe I lines near 4872Å, September 1991

3.3.1 The Light-tight box housing the filter apparatus

The light from the integrating sphere of the polarimeter apparatus is fed to a light-tight metal box by an optical fibre and is collimated by a lens. The collimated beam passes through the chosen filter, through a Fabry lens leading to a photomultiplier, the photons being recorded as described in section 2.2.

The filter is housed in a frame that may be tilted from the perpendicular to the light beam by a RS Components motor and a gear system whose ratio is 60:1, set up so that each 7.5° turn of the motor rotates the filter by 0°.125. The stepping motor is electronically controlled, the circuitry designed and built by Dr. D. Clarke.

3.3.2 Calibration of the filter wavelength with tilt angle

It is obvious from equation 2.13 that the relationship between the wavelength of peak transmission and tilt angle of the filter is non-linear and so

calibration needs to be undertaken. Also the physical properties of the filter will depend upon the conditions of its surroundings, e.g. temperature, which may affect both the peak transmission wavelength at normal incidence and the refractive index.

For the following experiment, a filter with a central wavelength of peak transmission, λ_c, of 4875.0Å, a FWHM, $\Delta\lambda$, of 1.9Å, and effective refractive index, μ^*, of 1.43, measured at 20°C, was used. The filter box was thermostatically controlled, but as the ambient temperature within the box housing the filter was lower than 20°C these parameters would be slightly different during the observing conditions. A spectral profile scan was made by observing the Sun and recording the photon counts made at 60 successive tilt positions from the normal position. This also allowed the tilt angles at the positions of the troughs corresponding to the centre of the complex of Fe I lines (the FWHM of the filter being too wide to resolve the lines individually) and of the Hβ line to be found, and two other tilt angles corresponding to parts of the continuum on the red and blue sides of the Fe I trough could be chosen. This spectral profile is shown in figure 3.3. The Fe I trough is denoted by FE, the Hβ trough by HB, while the continuum positions on the red and blue sides of the Fe I trough were chosen to be at CR and CB.

The wavelength of Hβ is well known to be 4861.34Å, but the actual wavelength of the trough due to line blending of the Fe I lines had to be estimated. The wavelengths, absorption depths and line widths of the individual lines were found in "The Solar Spectrum 2935Å to 8770Å" (Moore, C.E. *et al.*, N.B.S. Monograph 61), and the major lines that would fall within the bandwidth of the filter are shown in Table 3.2. The approximate wavelength of the recorded trough will be taken as 4871.5Å.

Using the positions of the two troughs FE and HB and the small absorption feature (containing Fe, Ti, Ni and Y lines and shown as AF in fig. 3.3) on the shorter wavelength side of the Hβ line, taken to be at approximately 4855.7Å, a

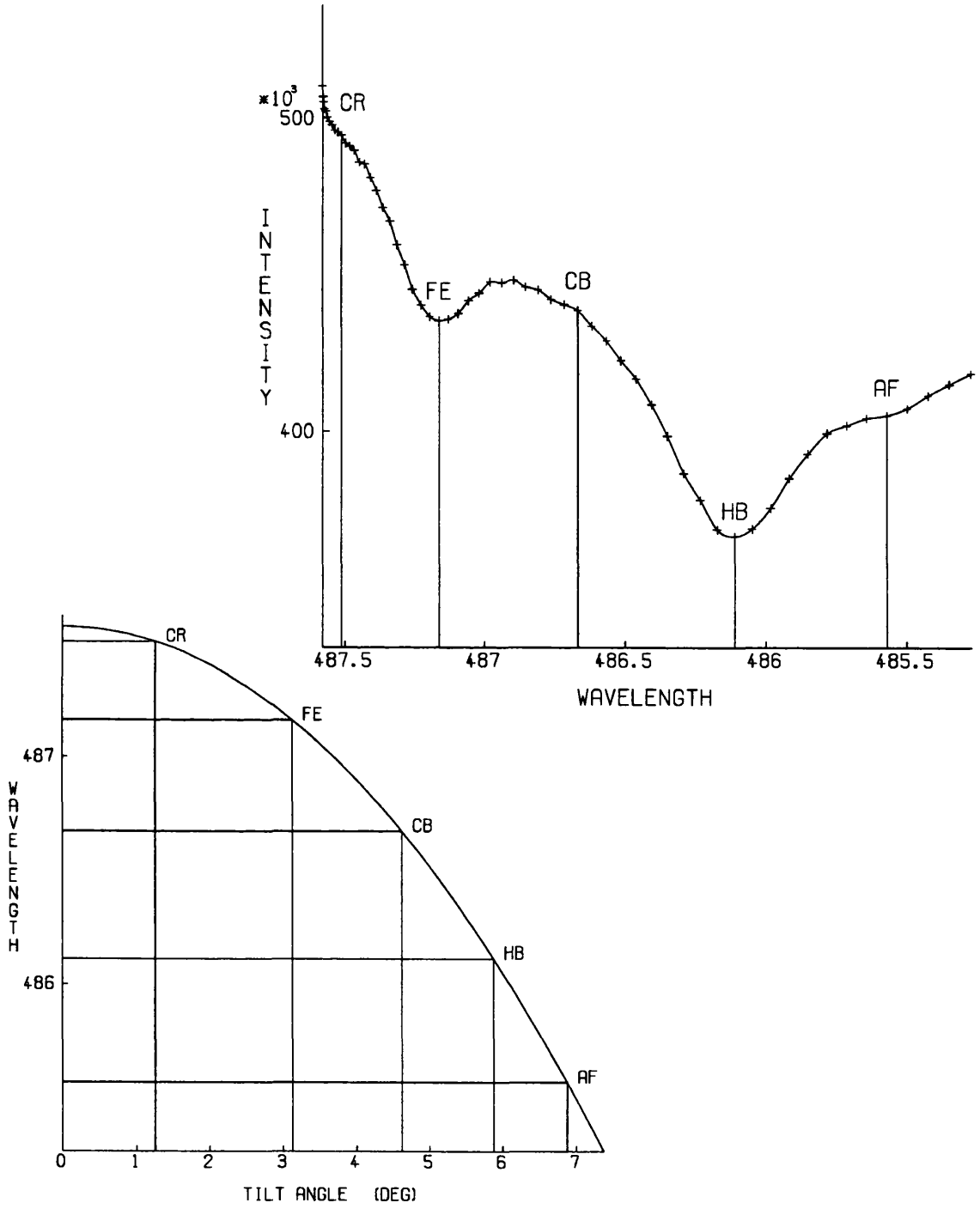

Fig. 3.3 Profile of the solar spectrum over 60 tilt steps (after x-axis had been calibrated for wavelength). (Upper figure)

Fig. 3.4 Calibration curve for wavelength against tilt angle for the 4875Å filter. (Lower figure)

Wavelength (Å)	Equivalent Width (mÅ)	Line
4873.45	58	Ni I
4873.26	24	Ni I
4872.14	195	Fe I
4871.94	45	Fe I
4871.33	228	Fe I
4870.82	74	Cr I & Ni I
4870.14	36	Ti I
4869.47	20	Fe I

Table 3.2 Solar spectral lines contained within filter bandwidth at Fe-line (The Solar Spectrum 2935Å to 8770Å, Moore, C.E., *et al.*, NBS Monograph 61)

Tilt angle θ	Effective wavelength		
1.250°	4875.29 Å	red continuum	(CR)
3.125°	4871.77 Å	Fe lines	(FE)
4.625°	4866.78 Å	blue continuum	(CB)
5.875°	4861.17 Å	Hβ line	(HB)

Table 3.3 Effective wavelengths of the filter at different tilt angles

least squares fit to the observed profile was used to find the best values of λ_c and μ under the observing conditions, and these were found to be:

$$\lambda_c \simeq 4875.53\text{Å} ; \qquad \mu \simeq 1.33 . \tag{3.1}$$

Equation 2.19 was then used to create a plot of wavelength against tilt angle, which is shown in figure 3.4. The effective central wavelength of the filter corresponding to the four tilt positions used for the observations are then given in Table 3.3.

3.3.3 The Polarimetric Measurements

The observations were made on 1991 September 2, 3, 4 and 11. Two sets of observations were made on each day, each corresponding to three of the four chosen spectral positions, either

(A) in the continuum on the red side of the Fe-line (hereafter referred to as CR),
at the Fe-line centre (FE)
and in the continuum on the blue side of the Fe-line (CB),
the set denoted 2A, 3A, 4A and 11A, or

(B) at the Fe-line centre (FE),
the blue continuum (CB)
and at the Hβ-line centre (HB),
which will be denoted 2B, 3B, 4B and 11B.

Observations at the three chosen filter positions were made cyclically, with either 10, 15 or 20 integrations being made at the first position before tilting to the second position and observing, then to the third position, before returning to observe again at the first position. As a single integration lasted about 7.5 seconds, each spectral position was observed for up to 150 seconds at a time, so the complete cycle was performed in about 450 seconds. This allowed

direct comparisons of the measured polarization between the various positions with a temporal resolution of 7.5 minutes.

Count rates of a few million counts per integration allowed a signal to noise ratio of greater than 3.10^3 to be expected for each cycle of integrations at each spectral point, given a normal S/N $\propto \sqrt{}$(photon counts) law (image wobble and seeing effects being reduced by the fact that the Sun is an extended object and that an integrating sphere scrambled the signal). Therefore groups of up to 25 cycles of integrations should allow polarimetric accuracies of better than 1 part in 10^4 by this method.

The polarimetric errors will be affected by dead-time at count-rates of a few times 10^5, so the data was treated as explained in section 2.4 with a value of τ = 100ns.

The rationale for this method of data acquisition is as follows. The degrees of polarization attempting to be measured are very small (about 0.01% or less) and the precision, at best, will be a few times 0.001%. Also the instrumental polarization of the instrument is not known to sufficient accuracy (see section 3.2) and may well vary from day to day. Therefore it is better to measure the difference of the measured polarization at two spectral positions, and to monitor the variations of this difference. For this study the difference in the Stokes q and u parameters were found to avoid any bias in calculating p and the position angle, ϕ, from q and u, as the measurements for each spectral position are made almost simultaneously. This negates the need to know the true instrumental polarization as it will be cancelled out in taking the difference, and knowledge of the position angle of a polarized source can be deduced from a measurement's position in the q,u plane.

The majority of the polarized light is produced in the absorption lines, while the continuum should be practically unpolarized, so the differences are made in the following way:

(i) between the Stokes parameters measured at FE and CR (hereafter denoted by [FE-CR]), i.e. $q_{[FE-CR]} = q_{FE} - q_{CR}$, etc.,

(ii) FE and CB ([FE-CB]),

(iii) HB and CB ([HB-CB]).

(Note: Hβ and red continuum measurements are not made simultaneously so the difference [HB-CR] is not made)

The individual values of the Stokes parameters at each spectral point were calculated from the total counts made during one cycle of 10, 15 or 20 integrations at that point, so that they were calculated with the maximum possible signal-to-noise ratio, i.e.

$$q_{cycle} = \pi \left(\frac{1}{2} - \frac{\Sigma C_{3_j}}{\Sigma C_{1_j}} \right) \qquad (j = 1, N) \qquad (3.2)$$

$$u_{cycle} = \pi \left(\frac{\Sigma C_{2_j}}{\Sigma C_{1_j}} - \frac{1}{2} \right) \qquad (j = 1, N)$$

where N is 10, 15 or 20 as described above.

The error upon the value q_{cycle} (and u_{cycle}) can be calculated from the dispersion of the individual values of q_j (and u_j) for each integration, j, during the cycle, about the value q_{cycle}. Therefore the standard mean error on the value q_{cycle}, $\sigma_{q_{cycle}}$, is given by

$$\sigma_{q_{cycle}} = \frac{1}{\sqrt{N}} \sqrt{\frac{\sum_{j=1}^{N} (q_j - q_{cycle})^2}{(N - 1)}} \quad \text{and} \qquad (3.3)$$

$$\sigma_{u_{cycle}} = \frac{1}{\sqrt{N}} \sqrt{\frac{\sum_{j=1}^{N} (u_j - u_{cycle})^2}{(N - 1)}}$$

The difference in q (or u) between the line centre and the continuum measurement could then be made,

$$q_{[\text{line-continuum}]} = q_{\text{line}} - q_{\text{continuum}} \qquad (3.4)$$
$$u_{[\text{line-continuum}]} = u_{\text{line}} - u_{\text{continuum}}$$

and the error upon them calculated by

$$\sigma q_{[\text{line-continuum}]} = \left(\sigma q_{\text{line}}{}^2 + \sigma q_{\text{continuum}}{}^2 \right)^{1/2} \qquad (3.5)$$

$$\sigma u_{[\text{line-continuum}]} = \left(\sigma u_{\text{line}}{}^2 + \sigma u_{\text{continuum}}{}^2 \right)^{1/2}$$

The weighted means and standard errors of these differences taken for all cycles of integrations could then finally be found.

3.3.4 Results

The results of the observations are listed in Table 3.4, which shows the date and run designation (A for CR, FE and CB; B for FE, CB and HB), the mean value of the differences in the degree of the Stokes' parameters q and u, with their standard errors, between the Fe-line centre and the red or blue continuum positions, and between the Hβ-line centre and blue continuum position. The q and u values recorded for each measurement were tested to see whether they belonged to a normal distribution by calculating their skewness and kurtosis and comparing them with the tables by Brooks (1985). Only three measurements failed at the 95% level, those being 2/9/91 A u [FE-CB]; 3/9/91 A q [FE-CR]; and 4/9/91 B q [FE-CB].

The standard mean errors on the parameters show that this method of measuring polarization is capable of a precision of better than 0.007% in 90

Date & run	Spectral Position	N	$q \pm \sigma_q$ (%)	$u \pm \sigma_u$ (%)	Normal q u
2/9/91	FE - CR	45	− 0.0063 ± 0.0035	+ 0.0042 ± 0.0038	Y Y
A	FE - CB		− 0.0031 ± 0.0038	+ 0.0035 ± 0.0040	Y N
B	FE - CB	19	+ 0.0008 ± 0.0068	+ 0.0148 ± 0.0062	Y Y
	HB - CB		− 0.0050 ± 0.0071	+ 0.0139 ± 0.0070	Y Y
3/9/91	FE - CB	20	− 0.0052 ± 0.0044	− 0.0099 ± 0.0044	Y Y
B	HB - CB		− 0.0004 ± 0.0048	− 0.0100 ± 0.0044	Y Y
A	FE - CR	25	+ 0.0042 ± 0.0044	+ 0.0015 ± 0.0045	N Y
	FE - CB		+ 0.0045 ± 0.0045	− 0.0026 ± 0.0048	Y Y
4/9/91	FE - CR	25	+ 0.0050 ± 0.0032	− 0.0050 ± 0.0033	Y Y
A	FE - CB		+ 0.0018 ± 0.0033	− 0.0079 ± 0.0035	Y Y
B	FE - CB	13	+ 0.0055 ± 0.0051	+ 0.0001 ± 0.0054	N Y
	HB - CB		− 0.0009 ± 0.0053	+ 0.0011 ± 0.0056	Y Y
11/9/91	FE - CR	18	− 0.0056 ± 0.0039	+ 0.0030 ± 0.0035	Y Y
A	FE - CB		− 0.0041 ± 0.0039	+ 0.0033 ± 0.0037	Y Y
B	FE - CB	10	+ 0.0068 ± 0.0050	+ 0.0124 ± 0.0045	Y Y
	HB - CB		+ 0.0013 ± 0.0052	+ 0.0157 ± 0.0049	Y Y

Table 3.4 Stokes' q and u values for September 1991 observations

minutes of observations, and as good as 0.003% in 3 hours, which is imperative when attempting to measure very low-level polarizations (i.e. $p < 0.01\%$).

To detect whether there was any significant change in the Stokes' parameters for each spectral difference (i.e. [FE-CR], [FE-CB] or [HB-CB]) during the observing runs over a period of about 2 hours, the Welch test was performed on the means of each Stokes' parameter for each cycle of integrations. For the observed data, only one set failed at the 95% confidence level, that of 3/9/91 B q [FE-CB], and none at the 99% level. This suggests that the whole solar disk polarization in these absorption lines does not significantly vary over time scales of a couple of hours at these levels of detection (≤0.007%).

Figures 3.5 to 3.12 (a) and (b) show the q,u diagrams for each day's observations, (a) showing the values at the three spectral positions [CR], [FE], and [CB] or [FE], [CB], and [HB], and (b) showing the respective differences, [FE-CR], etc. The axes are in units of 0.01% in both q and u.

The following symbols denote each respective spectral position:-

- Δ - [CR] red continuum
- ⊛ - [FE] Fe-line centre
- ◊ - [CB] blue continuum
- □ - [HB] Hβ line centre
- ⧖ - [FE-CR] Fe - red continuum
- ⌑ - [FE-CB] Fe - blue continuum
- * - [HB-CR] Hβ - blue continuum

It can be seen from the figures 3.5(a), 3.8(a), 3.9(a) and 3.11(a) that the red and blue continuum measurements are equal to within the standard errors (the error bars are one standard error in magnitude), and remain in the same quadrant. This tells us that either:

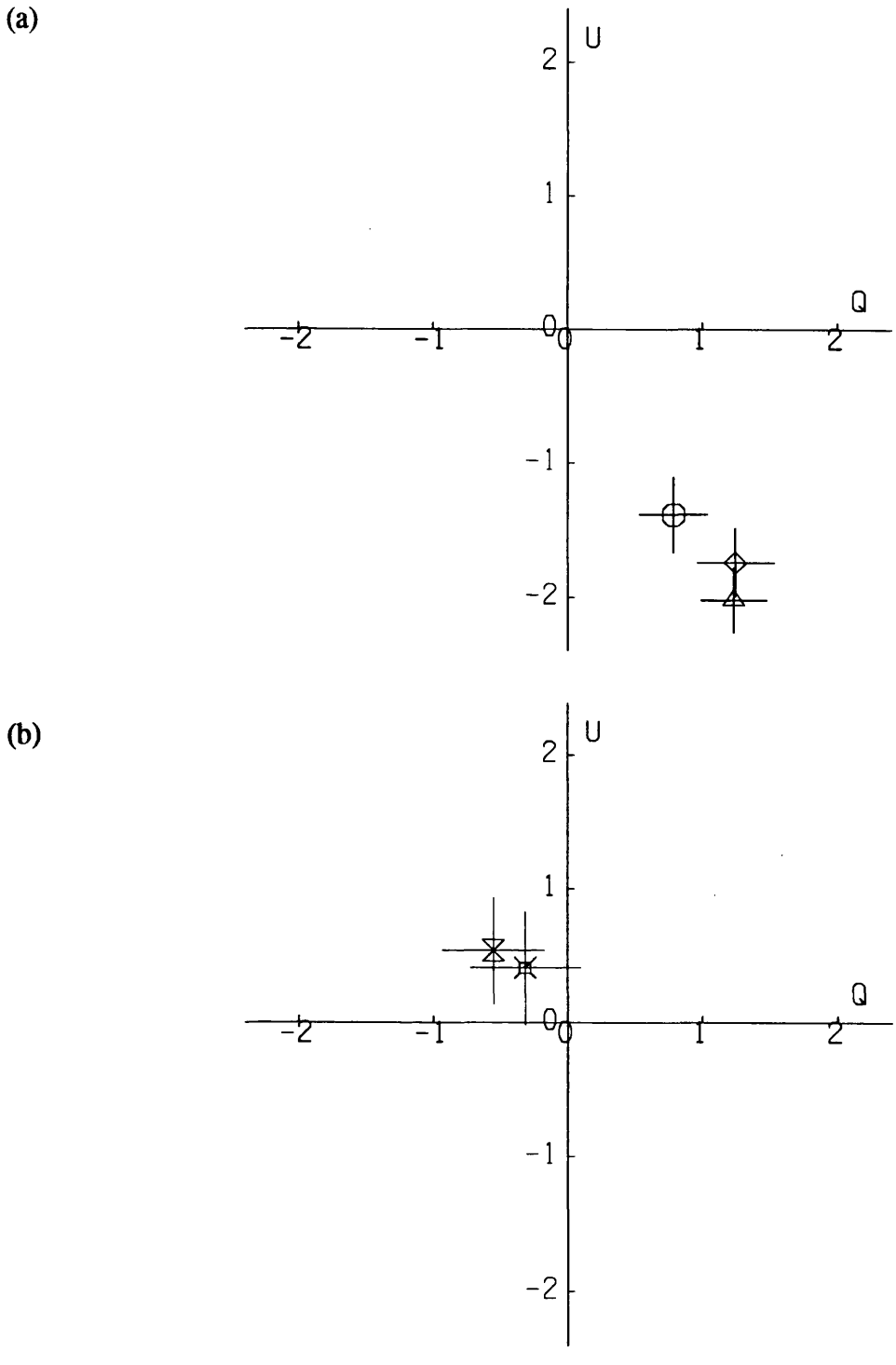

Fig. 3.5 *q,u* diagrams to show (a) measurements at the three spectral positions [CR], [FE] and [CB] (above), and (b) the two spectral differences [FE–CR] and [FE-CB] (below), made on 2/9/91, run A. (Units 0.01%)

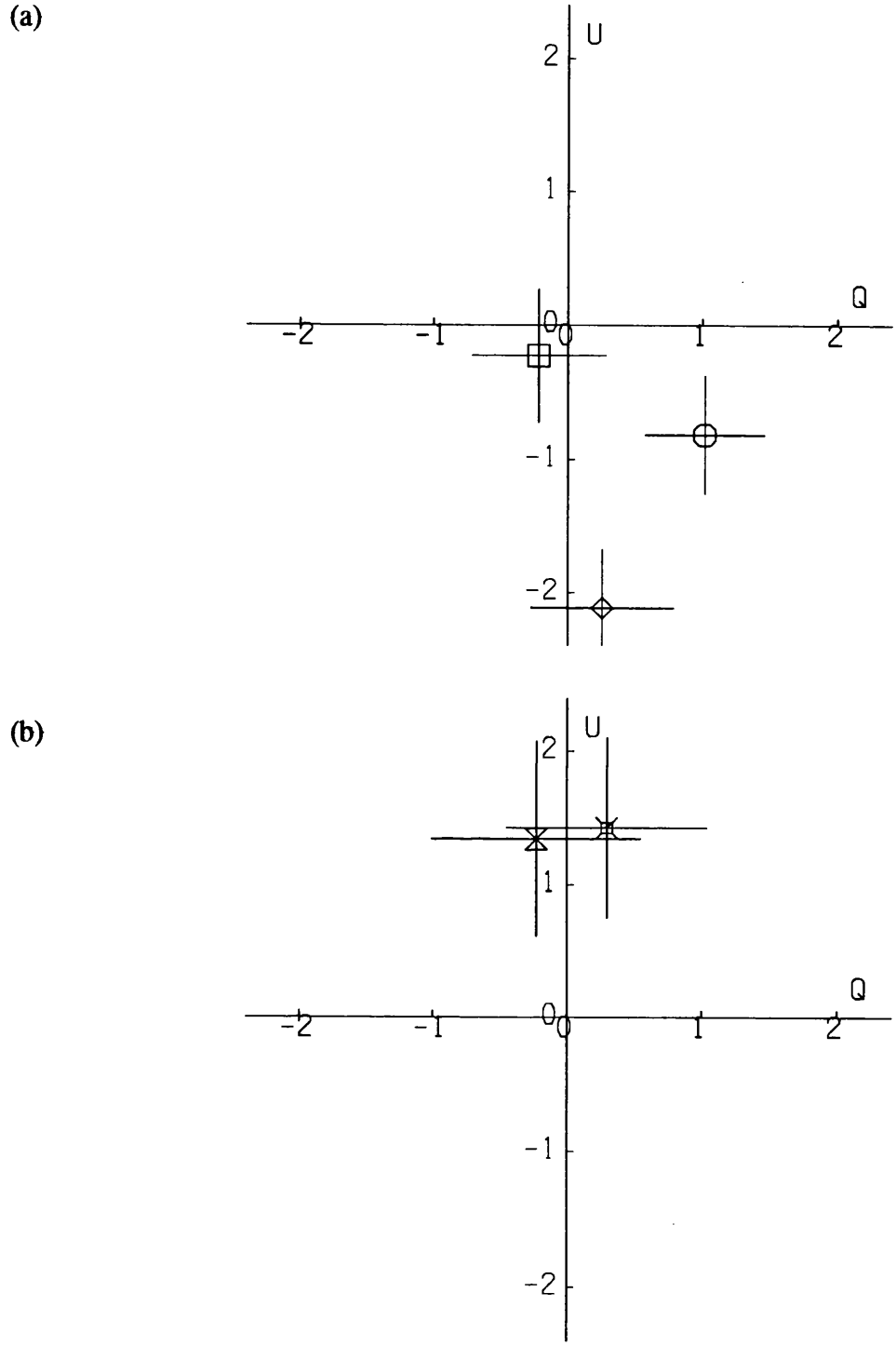

Fig. 3.6 *q,u* diagrams to show (a) measurements at the three spectral positions [FE], [CB] and [HB] (above), and (b) the two spectral differences [FE–CB] and [HB-CB] (below), made on 2/9/91, run B. (Units 0.01%)

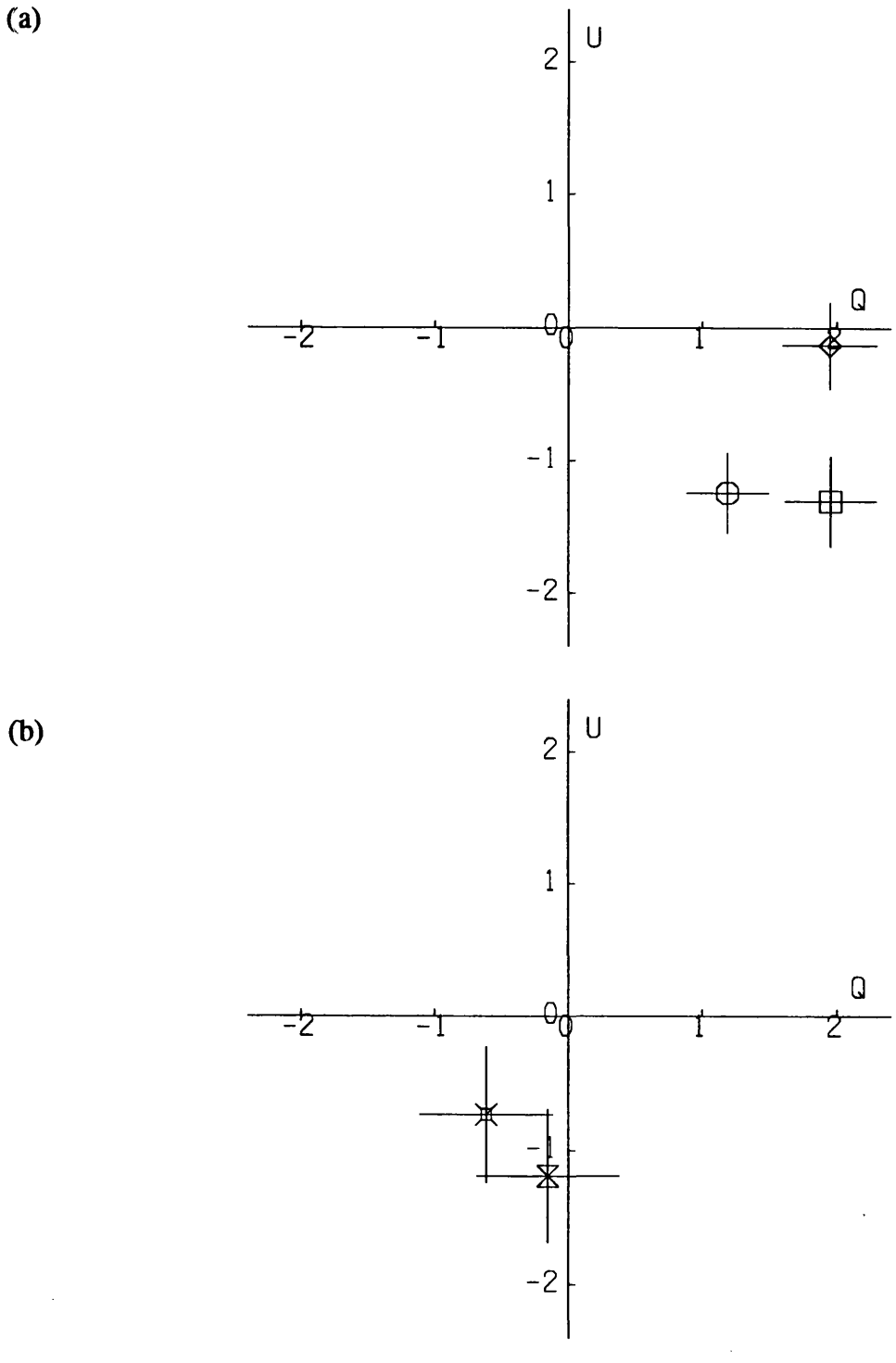

Fig. 3.7 As for figure 3.6 for observations made on 3/9/91, run B.

(a)

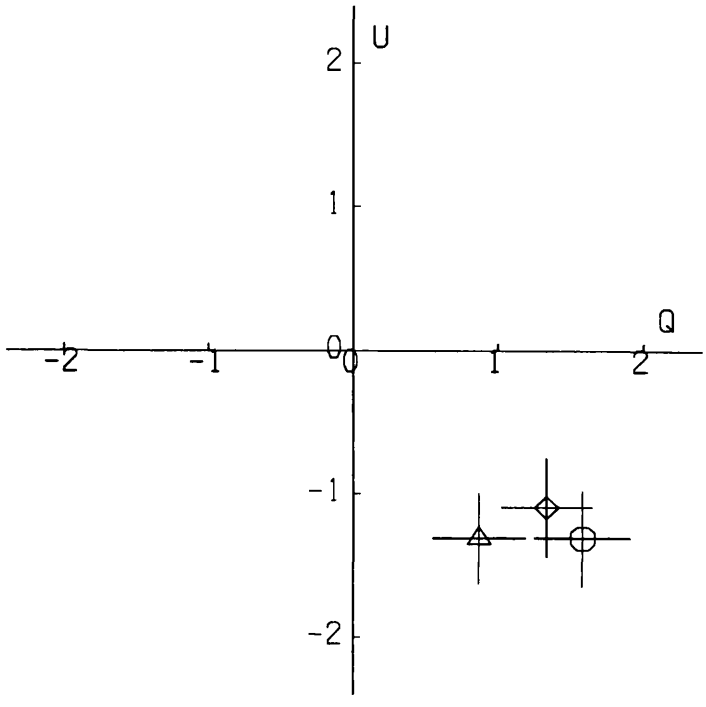

(b)

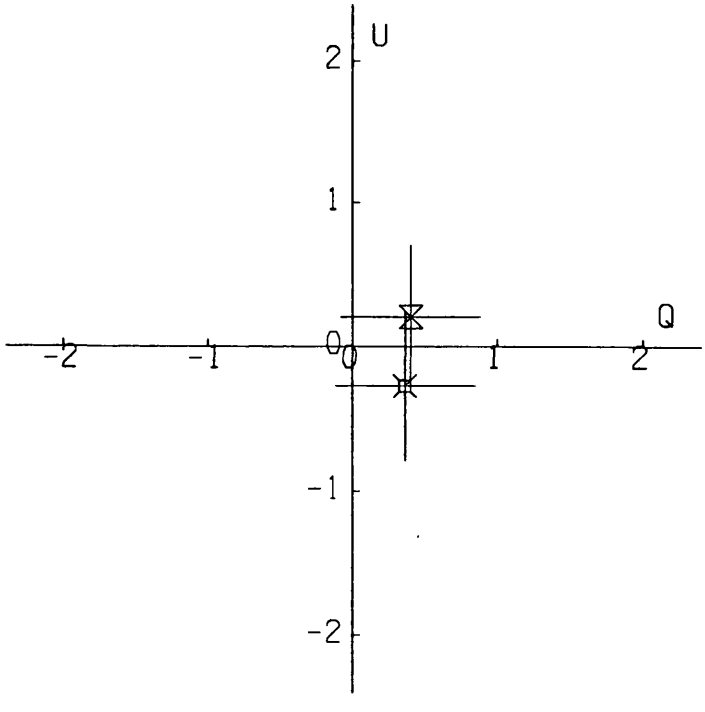

Fig. 3.8 As for figure 3.5 for observations made on 3/9/91, run A.

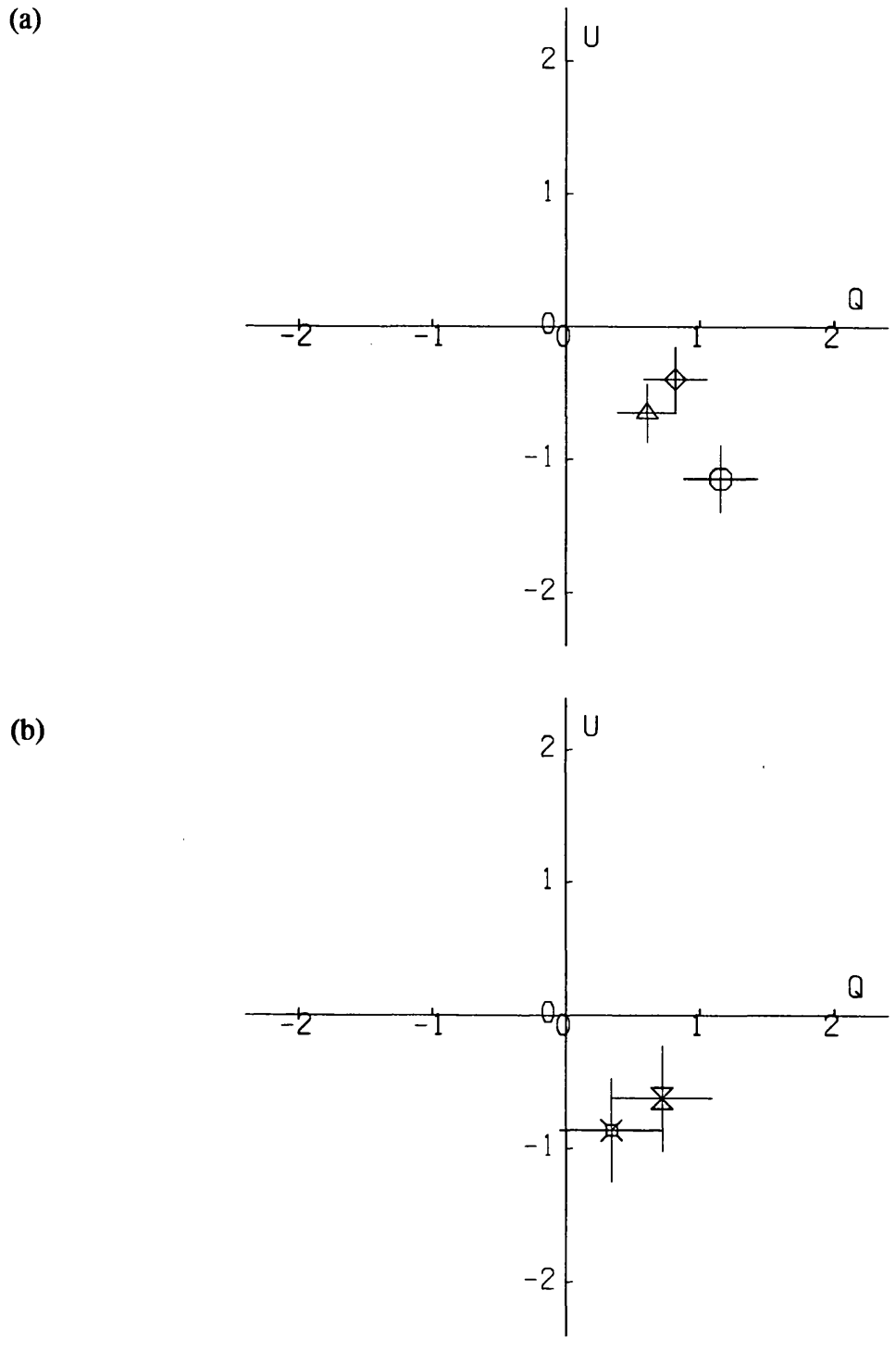

Fig. 3.9 As for figure 3.5 for observations made on 4/9/91, run A.

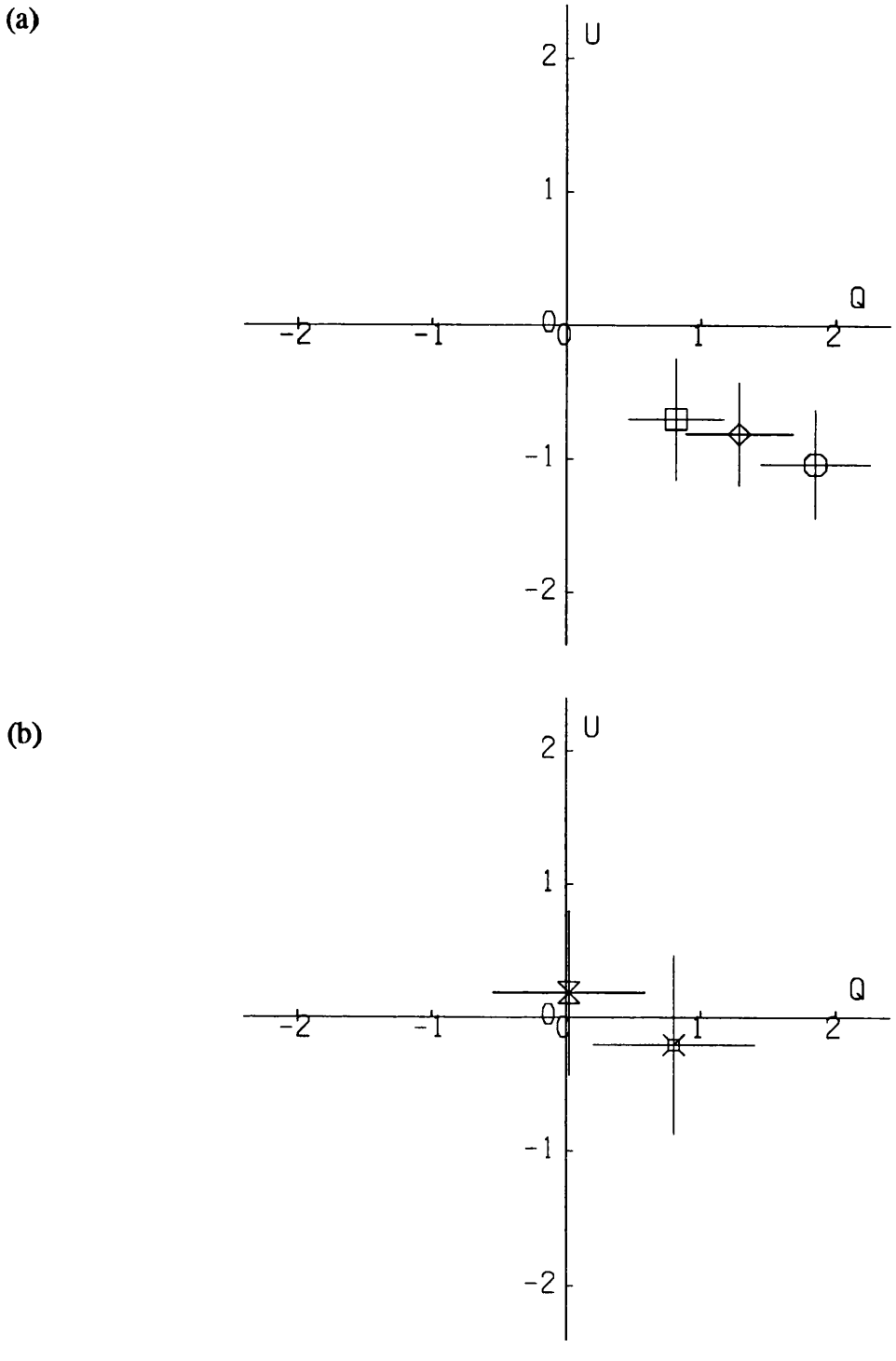

Fig. 3.10 As for figure 3.6 for observations made on 4/9/91, run B.

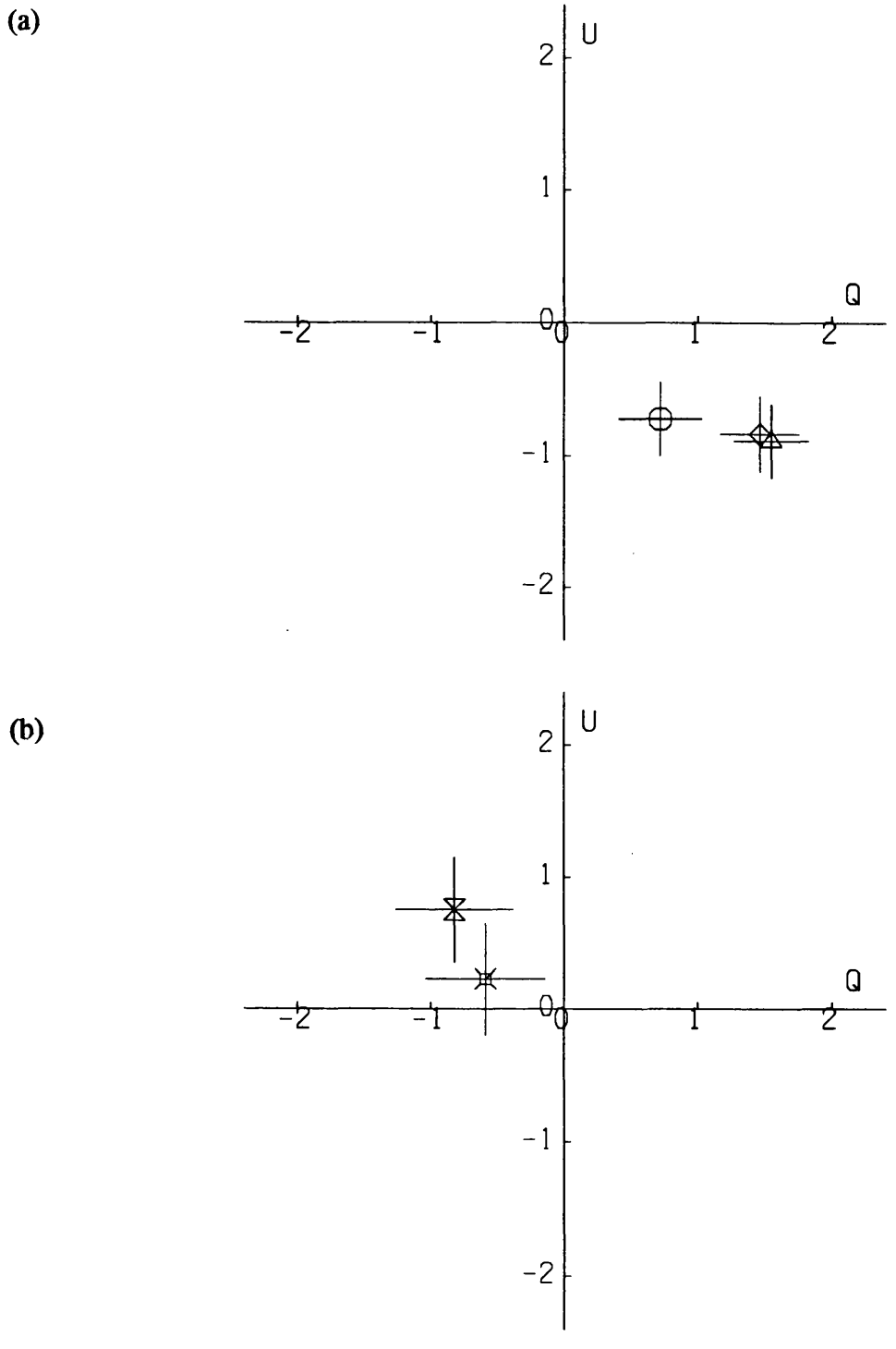

Fig. 3.11 As for figure 3.5 for observations made on 11/9/91, run A.

(a)

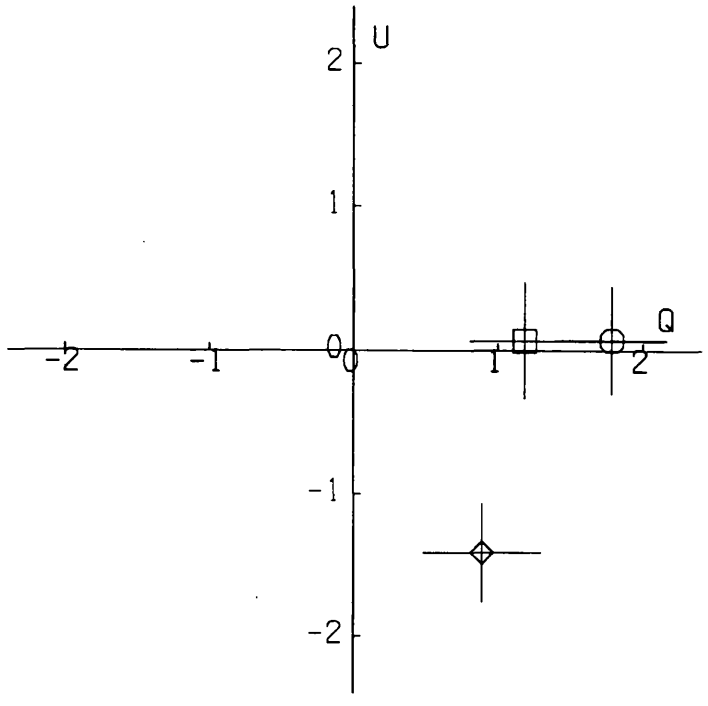

(b)

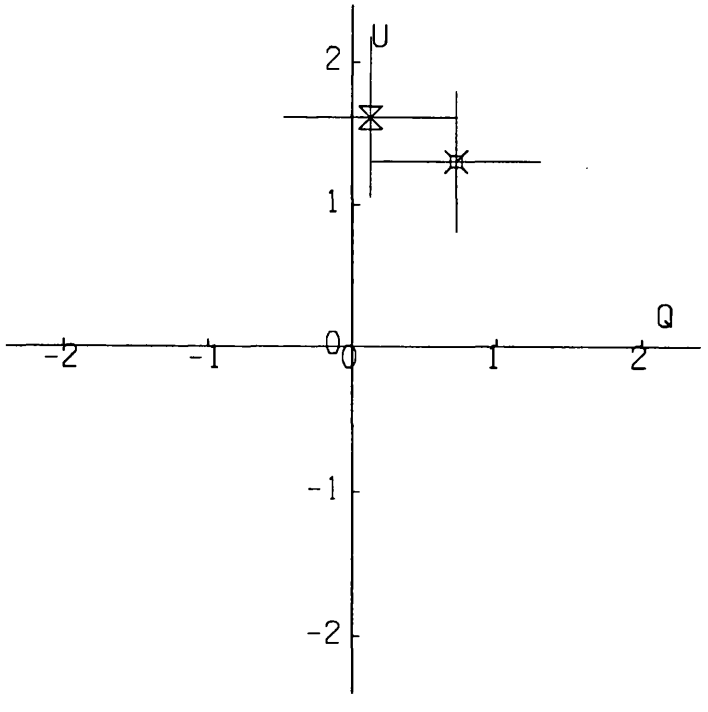

Fig. 3.12 As for figure 3.6 for observations made on 11/9/91, run B.

i) if a global continuum polarization exists at this low level it remains roughly constant, or

ii) if there is zero global continuum polarization then the instrumental polarization is less than 0.02% in both q and u and remains roughly constant.

However the Fe I and Hβ measurements do vary in their relative position to the continuum measurements, but it is obvious that their departure is of only a small amount. The (b) figures show that the differences do move in the q,u plane over the course of the 9 days of observations. The day to day changes are more easily seen in figures 3.13 to 3.15, showing the differences [FE-CR], [FE-CB] and [HB-CB] respectively, and can be summarized as follows:

[FE-CR] : Three observations found that the Stokes' q parameter at FE departed by more than 1 standard error (1-σ) from those at CR (2A, 4A and 11A). For the Stokes' u parameter, two measurements departed by more than 1-σ (2A and 4A). Those of 3A and 4A departed by more than 1-σ in q from those of 2A and 11A, while that of 4A departed by more than 1-σ in u from those of 2A and 11A. Therefore the results show no significant polarization for [FE - CR] at the 2σ (95%) confidence level.

[FE-CB] :Seven of the measurements of q at FE were not significantly departed from those at CB, the other being departed by more than 1-σ. For u, four measurements at FE departed from CB by more than 2-σ, four being not departed within the errors. It is seen that measurements 2B and 11B departed by more than 2-σ from those of 3A and 4A in u, with those four measurements themselves departed by more than 1-σ in u from 2A and 11A, while there are no significant variations at all in q.

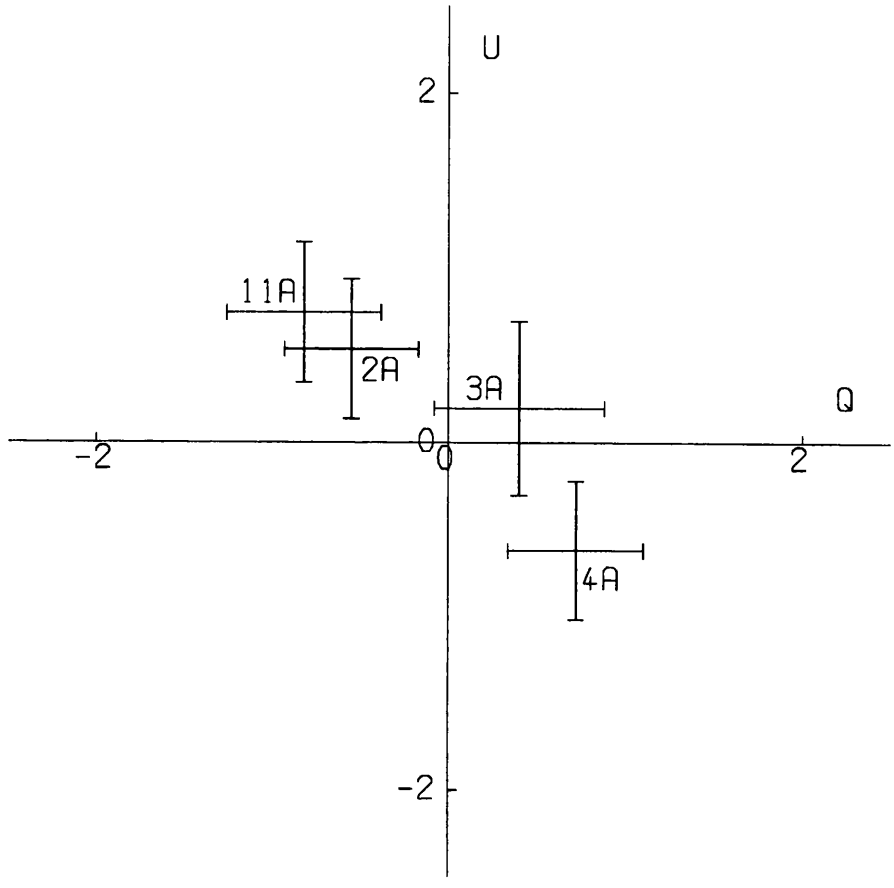

Fig. 3.13 *q*,*u* diagram showing the difference between measurements at the Fe I line-centre and red continuum [FE-CR] over four days observations. (Units 0.01%)

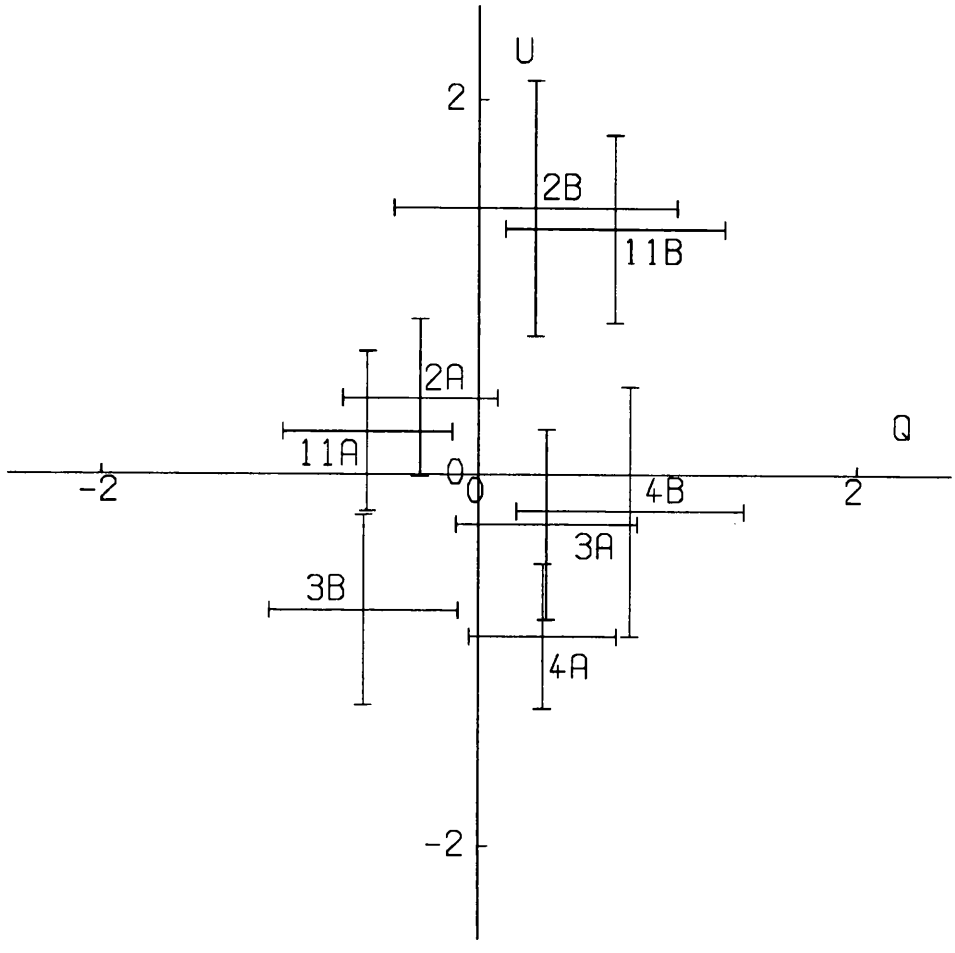

Fig. 3.14 *q*,*u* diagram showing the difference between measurements at the Fe I line-centre and blue continuum [FE-CB] over four days observations. (Units 0.01%)

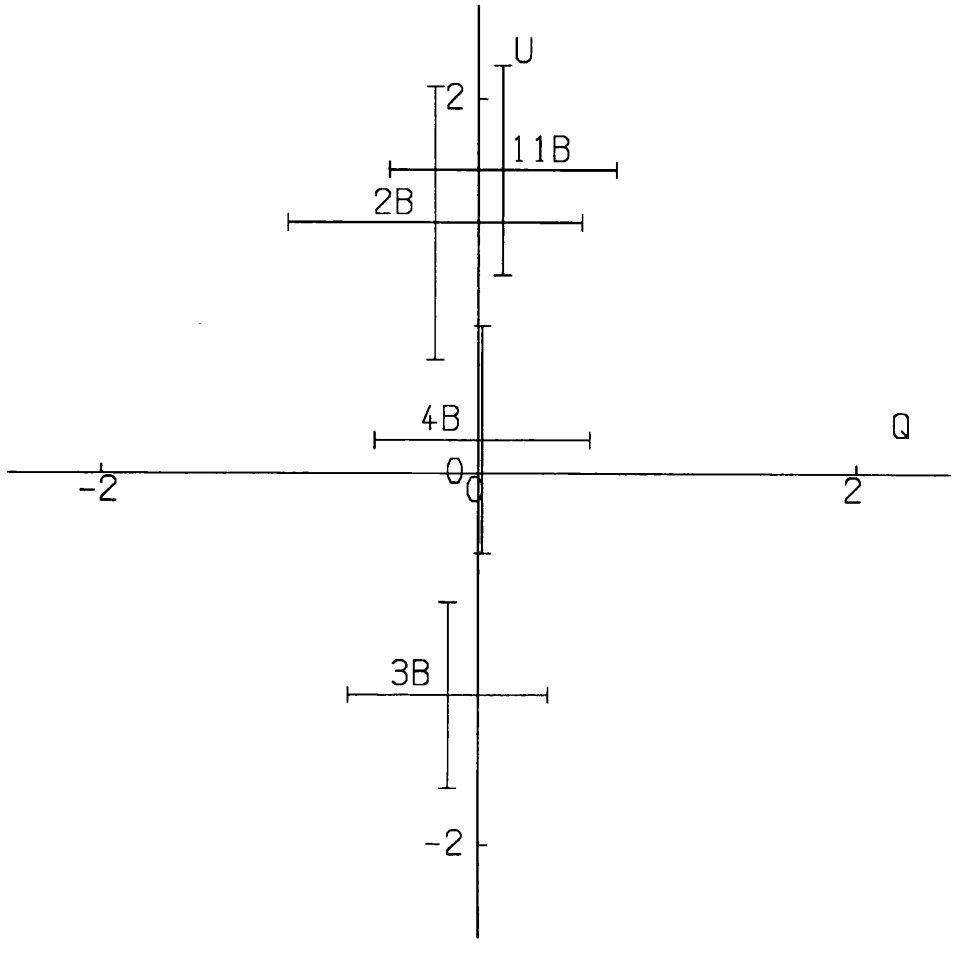

Fig. 3.15 *q*,*u* diagram showing the difference between measurements at the Hβ line-centre and blue continuum [HB-CB] over four days observations. (Units 0.01%)

[HB-CB] : All four observations show no significant differences in the q parameters between HB and CB. However two measurements of u show a greater then 2-σ departure (2B and 3B) and one measurement shows a 3-σ departure (11B), while the fourth shows no departure. It is seen that for the u parameter the measurements 2B and 11B departed by more than 2-σ from that of 3B, while that of 4B departed by more than 1-σ from the others. There are no significant variations in q.

3.3.5 Possible explanation for variations

Figure 3.16 shows the visible disk of the Sun on the four days of observations, taken from the Solar Geophysical Prompt Reports, Boulder, Colorado. If the polarization is due mainly to the position on the solar disk of magnetic active regions, is at its maximum degree when the region is near to the solar limb and zero when the region is at the centre of the disk (Tinbergen and Zwaan, 1981), then the observed variations of q and u might be explained as follows.

A number of active regions are visible during the days of the observations. On 2 September the region 6806 in visible on the west limb in the north-west quadrant, and also included in this quadrant are regions 6805, 6812 and 6813. For these regions the normal to the scattering plane will be in the north-easterly direction (i.e. tangential to the limb) so if the instrumental frame is indeed equivalent to the equatorial frame (section 3.2 shows this to be true to within 1°) then these regions will be responsible for positive q and u signals if the visible frame (i.e not necessarily the frame of the solar equator and rotation axis) of the Boulder diagrams are assumed to be the same. Regions 6803 and 6807 will also contribute to positive q but also negative u, and the other regions nearer to the disk centre will contribute a little to negative q and positive u. What we see in figures 3.5(b) and 3.6(b) is a positive u and small negative or zero q.

On 3 September regions 6806 and 6813 had disappeared so we should expect a

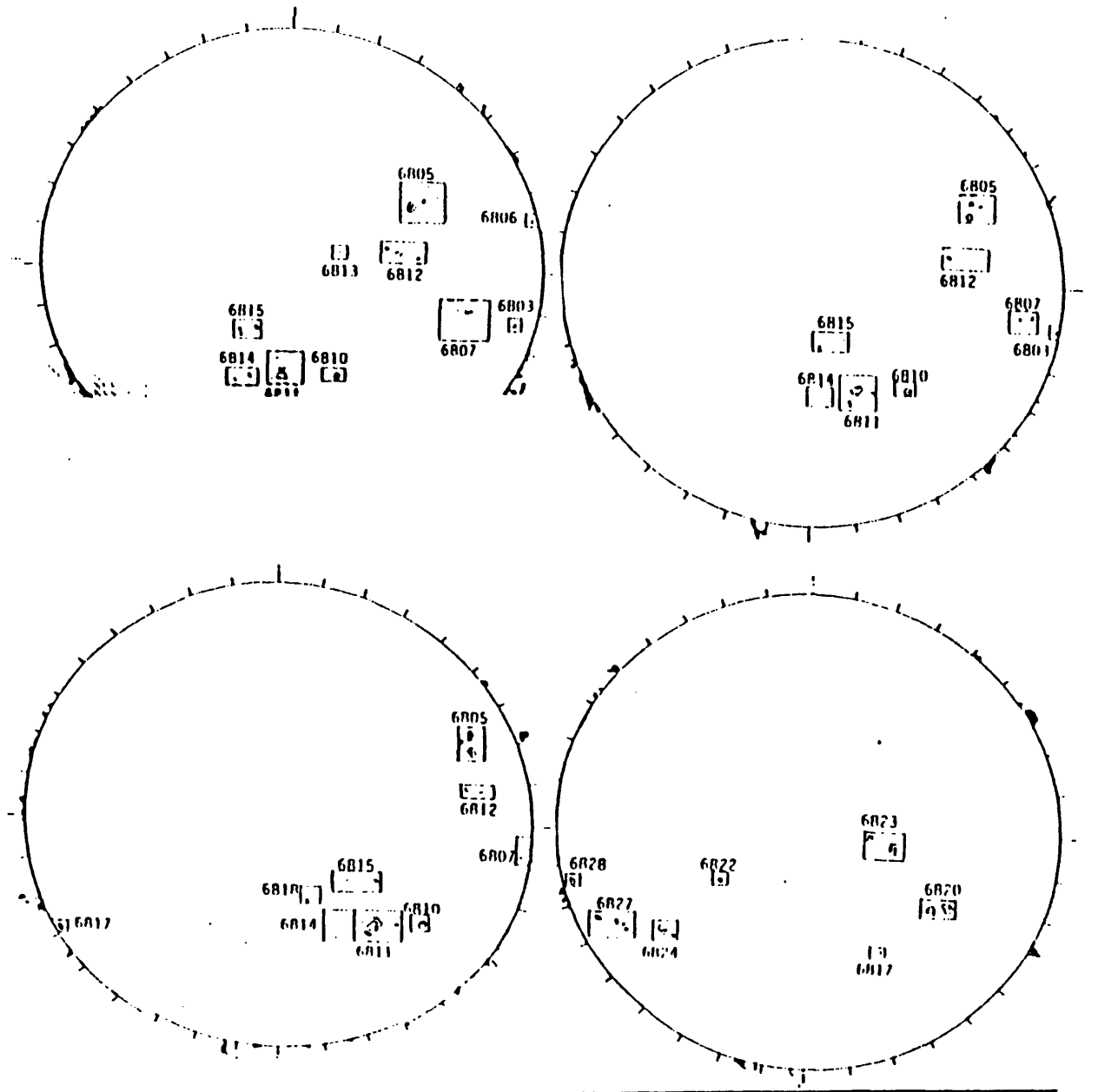

Fig. 3.16 Visible disk of the Sun on 1991 September 2 (top left), 3 (top right), 4 (lower left) and 11 (lower right) showing the positions of sunspots. (Taken from the Geophysical Prompt Reports, October 1991).

decrease in positive u, while regions 6805 and 6812 approach the west limb in the north-west quadrant to increase positive u. However regions 6803 and 6807 approach the west limb in the south-west quadrant to introduce negative u. The regions near the disk centre are all now in the south-west quadrant and will contribute to negative q and u. Figures 3.7(b) and 3.8(b) show little change in q but a negative shift in u compared with figures 3.5(b) and 3.6(b) respectively.

For 4 September regions 6805 and 6812 are very close to the north-west limb, so contributing most to positive u. Region 6803 has disappeared but 6807 contributes most to negative u and positive q in the south-west quadrant. Now the large regions 6810, 6811, 6815 and 6814 will be contributing much more to negative u, and possibly more to positive q as they move towards the limb from the disk centre. Figures 3.9(b) and 3.10(b) show that this means that a slightly more positive q and a net small negative u.

Finally on 11 September the situation has greatly changed, with a mass of regions in the south-east quadrant contributing to positive u, and with some regions in the south-west quadrant but not close to the limb contributing mostly negative q and a small negative u. This is evident in figures 3.11(b) and 3.12(b) with the measurements of positive u similar to those made on 2 September when regions were diametrically opposite, and hence contributing to the same sense of q and u. One point to mention is that [FE-CB] shifts by more than one standard error in positive q between the two measurements.

In chapter 6 a computational model designed to predict the measured q,u values depending upon the apparent positions of visible active regions is described. It will take into account the effects of magnetic intensification and of resonance scattering in the belief that both mechanisms are required to produce measurable whole-disk polarization, and the results presented above will be compared with the outcome of the model.

3.3.6 Short-period polarimetric variations

Figures 3.17 (a), (b), (c) and (d) show the variations of the individual calculated measurements of $q_{[FE-CR]}$, $u_{[FE-CR]}$, $q_{[FE-CB]}$ and $u_{[FE-CB]}$ respectively against time (GMT) for each cycle of integrations of run A made on 2 September 1991. There is a hint of a sinusoidal variation but it is obvious from the size of the error bars (equal to 1-σ) that any such variation is probably not significant. Helioseismology has shown over the past few years that physical oscillations are occurring within the Sun with dominating periods of 5 and 160 minutes. It is constructive, therefore, to ask whether these processes affect the polarization of solar light.

Unfortunately the data only have a temporal resolution of about 7.5 minutes so it would not be possible to detect 5-minute variations in the Stokes' parameters, but with some of the data acquisition runs occurring over periods of more than three hours it may be possible to detect the longer period effects. Indeed, if the oscillations cause polarimetric variations, then the polarimetric period would be one half of the physical period due to the nature of polarized light (i.e. polarimetric periods of 80 minutes).

A normal Fourier transform method cannot be applied to this data as successive data points are irregularly spaced in time. It was decided to try and fit sinusoidal waveforms to the data, in which the sinusoid with the closest frequency and phase to the variation in the data would give the greatest power. Should the amplitude of the fitted sinusoid about the mean of the data be greater than an average value for one standard mean error, then the peaks and troughs of the sinusoid would be more than two standard mean errors apart, and so significant at the 95% confidence level. The fitting technique is performed thus:

The data is represented by an amplitude, a_i, about the mean value, $\bar{a}$, which is subtracted from each data point, at a discrete time, t_i. Suppose there is an underlying period, P_o, present in the data corresponding to a frequency,

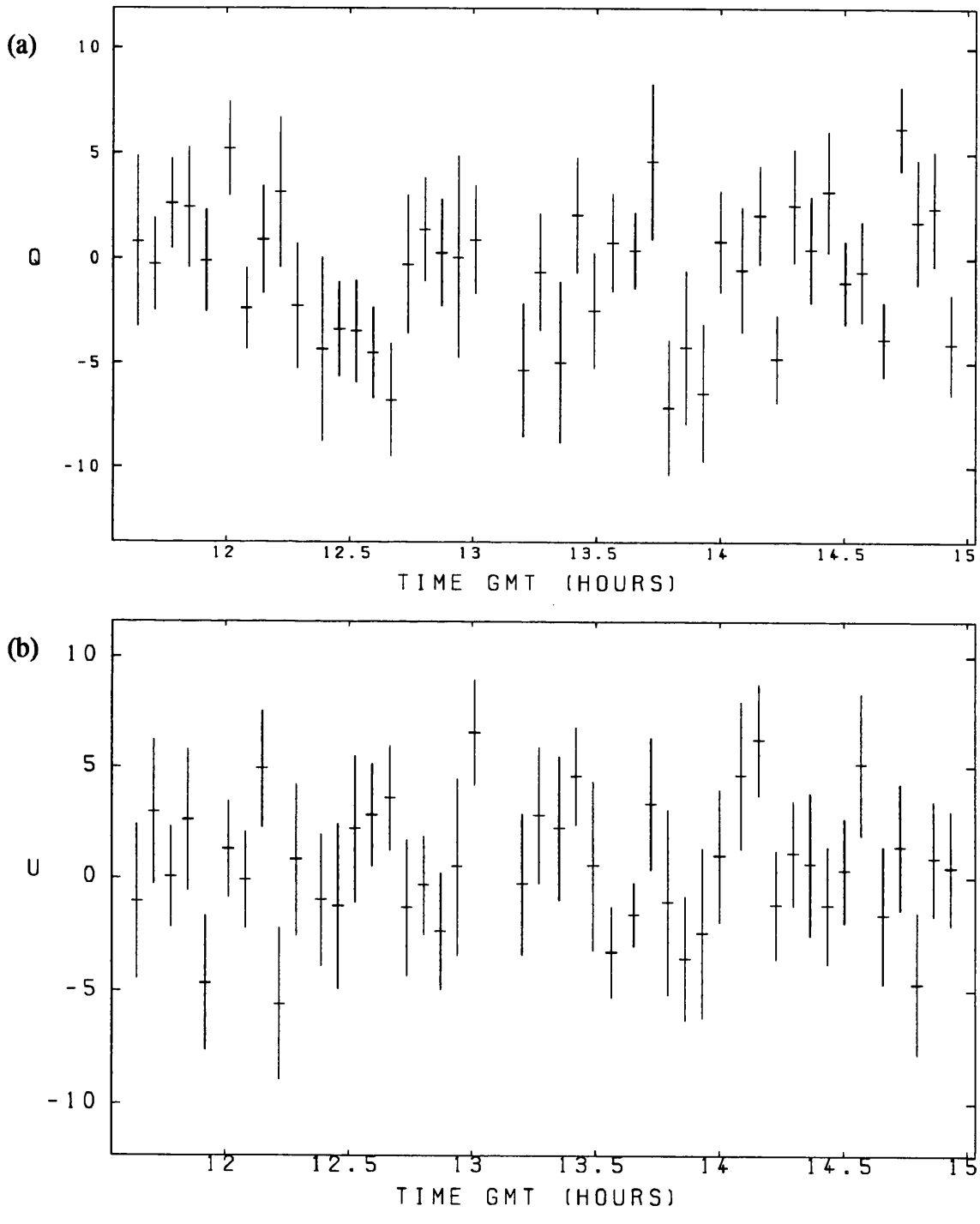

Figure 3.17 Variation of the Stokes' parameters (a) q (above), and (b) u (below), with time (GMT) for [FE-CR], run A on 2 September 1991. (Units 0.01% for q and u).

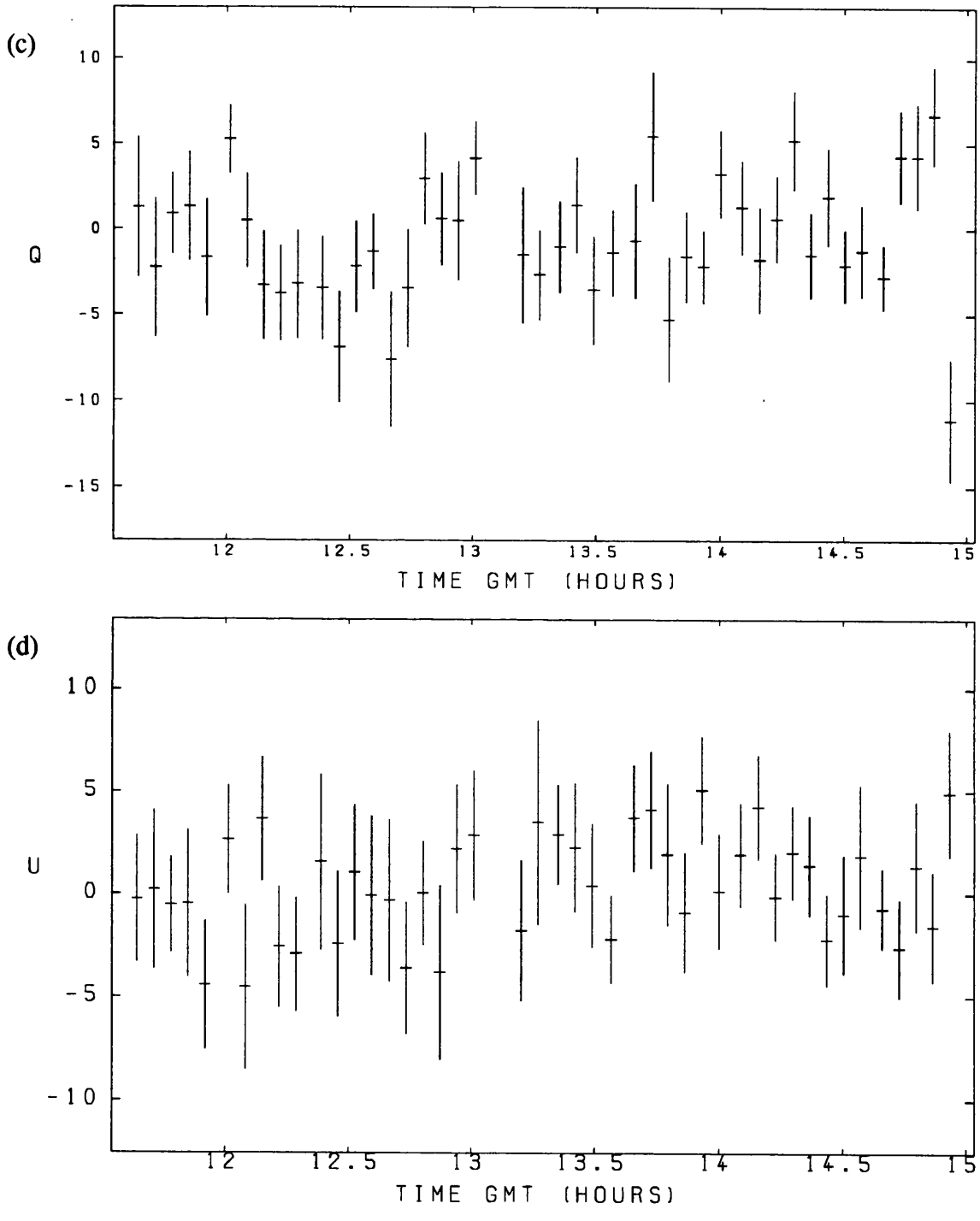

Figure 3.17 Variation of the Stokes' parameters (c) q (above), and (d) u (below), with time (GMT) for [FE-CB], run A on 2 September 1991. (Units 0.01% for q and u)

ν_o (= $^1/_{P_o}$). If there is no noise present the data values correspond to

$$a_i = a_o \cos(2\pi\nu_o t_i + \phi_o) \tag{3.6}$$

where a_o is the amplitude of the oscillation, ϕ_o its phase at t = 0.

Suppose now that a period, P (frequency ν = 1/P), is run through the data. This can be checked by calculating the cosine (C) and sine (S) summations, i.e.

$$C = \frac{2}{N}\sum_{i=1}^{N} a_i \cos(2\pi\nu t_i) \quad \text{and} \quad S = \frac{2}{N}\sum_{i=1}^{N} a_i \sin(2\pi\nu t_i) \tag{3.7}$$

If $\nu \neq \nu_o$ then these summations should tend to zero if N is large. This can be seen by substituting values of a_i given by $a_o\cos(2\pi\nu_o t_i+\phi_o)$,

$$C = \frac{2}{N}\sum_{i=1}^{N} a_o\cos(2\pi\nu_o t_i + \phi_o).\cos(2\pi\nu t_i) \tag{3.8}$$

$$S = \frac{2}{N}\sum_{i=1}^{N} a_o\cos(2\pi\nu_o t_i + \phi_o).\sin(2\pi\nu t_i) \tag{3.9}$$

which gives

$$C = \frac{a_o}{N}\sum_{i=1}^{N} \left\{ \cos(2\pi t_i[\nu_o+\nu] + \phi_o) + \cos(2\pi t_i[\nu_o-\nu] + \phi_o) \right\} \tag{3.10}$$

$$S = \frac{a_o}{N}\sum_{i=1}^{N} \left\{ \sin(2\pi t_i[\nu_o+\nu] + \phi_o) - \sin(2\pi t_i[\nu_o-\nu] + \phi_o) \right\} \tag{3.11}$$

Within the summation, the terms reduce to zero for large N unless $\nu = \nu_o$, when

$$C = \frac{a_o}{N}\sum_{i=1}^{N} \left\{ \cos(4\pi\nu t_i+\phi_o) + \cos\phi_o \right\} \tag{3.12}$$

$$S = \frac{a_o}{N}\sum_{i=1}^{N} \left\{ \sin(4\pi\nu t_i+\phi_o) - \sin\phi_o \right\} \tag{3.13}$$

in which the first term in each summation should tend to zero, hence

$$C \Rightarrow m_o \cos\phi_o \quad \text{and} \quad S \Rightarrow m_o \sin\phi_o \tag{3.14}$$

The value of m_o and $\phi_o$can then be determined from

$$m_o = \sqrt{(C^2 + S^2)} \; ; \quad \phi_o = \tan^{-1}\left[\frac{S}{C}\right] \tag{3.15}$$

The amplitude, m_o, is then checked against the average standard mean error for q (or u).

This analysis provided null results for all the solar data. If there are any underlying polarimetric variations they would be extremely difficult to detect because of the noise on each data point and the small sample number (less than 45 in this case).

Another look at figures 3.17 (a) to (d) suggest that the four calculated Stokes' parameters may be correlated. This would be expected because there is a data point common to both differences, *i.e.*

$q_{[FE-CR]}$ should be correlated to $q_{[FE]}$ and $-q_{[CR]}$,

$q_{[FE-CB]}$ should be correlated to $q_{[FE]}$ and $-q_{[CB]}$,

and $q_{[FE-CR]}$ should be correlated to $q_{[FE-CB]}$ because $q_{[FE]}$ is common to both values, and similarly for the other parameters.

However, if $q_{[FE]}$ varies with respect to $q_{[CR]}$ and $q_{[CB]}$, which themselves remain roughly constant (*i.e.* $q_{[FE]}$ is not correlated to either $q_{[CR]}$ or $q_{[CB]}$), so that $q_{[FE]}$ is correlated to $q_{[FE-CR]}$ and $q_{[FE-CB]}$ but neither $-q_{[CR]}$ nor $-q_{[CB]}$ are correlated to $q_{[FE-CR]}$ or $q_{[FE-CB]}$ respectively), then the value $q_{[FE]}$ must be intrinsically varying and the observed correlation is not an instrumental or observational effect. Similarly, if $q_{[FE]}$ and/or $q_{[HB]}$ are correlated to $q_{[FE-CB]}$ and $q_{[HB-CB]}$ respectively, while $q_{[CB]}$ is not correlated with either, then the polarization in the lines must again be varying with respect to the continuum.

A third scenario is that the continuum varies so that $q_{[CR]}$ is correlated to

$q_{[CB]}$, whereas the observed $q_{[FE]}$ remains roughly constant, which would suggest one of two things: (1) that the continuum is not an unpolarized source, or (2) that the instrumental effects vary and the line-centre measurement happens to be varying in a compensatory way (which would be extremely unlikely!).

Using NAG routines for correlation analysis, and using the tables by Stewart to compare the calculated co-efficients with the percentage levels for 95% and 99%, the following conclusions were made:

2/9/91, run 2A.

[FE-CR] correlates with [FE-CB] in both q and u at 99% level.

[FE] & -[CR] correlate with [FE-CR] in both q and u at 99% level.

[FE] & -[CB] correlate with [FE-CB] in both q and u at 99% level.

This is expected even if there is no polarization present but the data are noisy, and the q and u measurements for this run were not significantly departed from zero.

2/9/91, run 2B.

[FE-CB] correlates with [HB-CB] in both q and u at 95% level.

[FE] correlates with [FE-CB] in q at 95% level but -[CB] correlates with [FE-CB] at 99% level.

[FE] correlates with [FE-CB] in u at 99% level but -[CB] correlates with [FE-CB] at 95% level.

Both [HB] & -[CB] correlate with [HB-CB] in both q and u at 99% level.

This is again expected if there is no polarization present, and the q and u measurements for this run were not significantly departed from the zero.

Most of the findings for the data of 3, 4 and 11 September are similar so only the important results will be further described.

3/9/91, run 3B.

In u,[FE] is correlated to both [HB] at the 99% confidence level *and* [HB-CB] at the 99% level, and [FE-CB] is correlated with [HB-CB] at the 99% level, suggesting variations in each spectral line during the run. During this run significant differences were found in u at above the 2-σ level.

4/9/91, run 4B

In both q and u the usual correlations as seen in runs 2A and 2B are not seen at the 99% level. Some expected correlations are not present at all, whereas some are at only the 95% level. The Stokes' parameters in this run are virtually zero, so this run is probably an example of the measurement of an unpolarized source with very small amounts of noise on the data.

11/9/91, run 11B

In q a similar set of correlations to those in u for run 3B are seen but only at the 95% level, whereas for u the case is similar to that of run 4B with only one correlation, between [HB] and [HB-CB] at the 99% level. As in the case of run 3B this run shows significant polarizations ($>$ 3-σ in both u values, $>$ 1-σ in $q_{[FE-CB]}$), but may affected by only a relatively small magnitude of noise.

In summary, as significant results were only found for data values concerning measurements in the lines, the correlation analysis may add further weight to the argument put forward here that low levels of polarization do indeed exist, at least in spectral lines measured in narrow spectral bands, which show temporal variability. While figures 3.13 to 3.15 suggest temporal variations due to the positions of magnetic regions, shorter periodicities may be related to phenomena that change over timescales of minutes, for example solar oscillations.

3.4 Hβ Polarimetry in May 1990

With the possible detection of linear polarization during September 1991, previously recorded 3-position Hβ line polarimetric data made in May 1990 was re-analyzed. On 4 and 14 May 1990 a 2.5Å filter was used to measure q and u at the centre of the Hβ line and in the continuum on the red and blue sides of the line, while on 5 May a 10Å filter was used. Unfortunately the starting positions of the filters (i.e their initial tilt-angle) were not recorded so that a wavelength vs. tilt angle calibration could not be performed. However a solar profile over 60 tilt steps for the 2.5Å filter was recorded, with the 3 positions used, CR, HB and CB, being shown in figure 3.18.

The data were recorded in a slightly different manner in that only one integration was made at each spectral point during each cycle, which is a less time-efficient method of data acquisition as it requires filter rotation adjustment after each integration. This method also means that an error on each observation cannot be estimated, while beforehand the internal spread of the 10, 15 or 20 individual integrations could be calculated. It was therefore decided to group sets of 10 successive integrations at each filter position and to sum the counts in the three scalars to give the greatest S/N ratio when q and u are calculated (as in the previous section). The spread of the 10 individual points could then be used to estimate σ_q and σ_u as before. If the data run consisted of more than an integer multiple of 10 integrations at each position, then the Stokes' parameters and their errors were calculated for the remaining 2 to 9 integrations, with single outstanding integrations being ignored as no error could be assigned to it.

The results are shown in Table 3.5 with the column headings as for Table 3.4. The only statistical polarimetric detections are

4 May; u [HB - CR] = +0.0468 ± 0.0184 % (2.54σ)

5 May; q [HB - CB] = +0.0239 ± 0.0114 % (2.10σ)

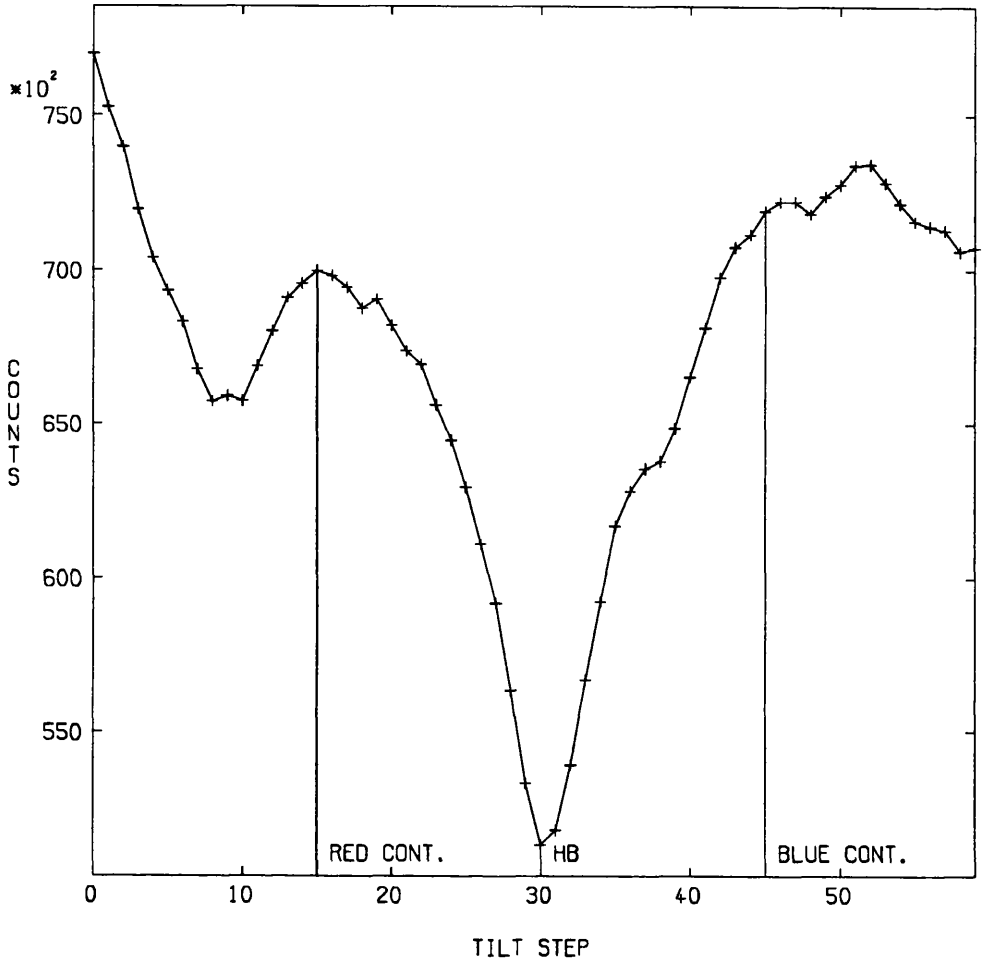

Fig. 3.18 Solar profile over 60 tilt steps made on 4 May 1990.

Date	Spectral Position	$q \pm \sigma_q$ (%)	$u \pm \sigma_u$ (%)	Normal q u
4/5/90	HB - CR	− 0.0028 ± 0.0173	+ 0.0468 ± 0.0184	N N
	HB - CB	+ 0.0016 ± 0.0179	+ 0.0106 ± 0.0220	Y Y
5/5/90	HB - CR	+ 0.0213 ± 0.0153	+ 0.0106 ± 0.0116	N Y
	HB - CB	+ 0.0239 ± 0.0114	+ 0.0025 ± 0.0141	N Y
14/5/90	HB - CR	− 0.0087 ± 0.0273	+ 0.0040 ± 0.0294	Y Y
	HB - CB	− 0.0157 ± 0.0247	− 0.0068 ± 0.0273	N Y

Table 3.5 Stokes' q and u values for May 1990 observations

Figures 3.19 to 3.21 (a) and (b) show the measurements made at the three spectral positions in (a), and the differences [HB - CR] and [HB - CB] in (b), for the three days of observations. For 4 May the point [FE] departed from [CR] in u but not from [CB], and from neither [CR] nor [CB] in q. However on 5 May [FE] departed from both [CR] and [CB]in q but not in u. On 14 May there is no difference between [FE] and either [CR] or [CB].

The Boulder Sunspot diagrams shown in figure 3.22 for those days suggests the following.

On 4 May the regions 6040 and 6050 would contribute positive q and u, as would 6045 and 6048 in a smaller amounts, while 6039, 6051 and 6049 would contribute positive q and negative u. A small net q would be expected, however a small net u is measured for [HB - CR].

On 5 May regions 6039 and 6040 have disappeared, while the effects of 6051 and 6045 would be increased. The other regions would have smaller effects on q and u as they are near the disk centre. It would be expected from these changes that the measured q and u would decrease with fewer regions near the limb, but a small detection in q is seen for [HB - CB].

On 14 May there are three large regions (6063, 6062 and 6060) at high latitudes in the north-east quadrant which should give a large negative u contribution, aided by 6054 in a smaller way. However 6049 and 6064 would contribute to positive u, but with a smaller magnitude due to their lower latitudes. It would be expected to measure a negative u and possibly a positive q, however there is no polarization measured.

The measured Stokes' parameters for the data taken in May 1990 are not conclusive and do not seem to agree with the "theoretical" estimates, this may be due to their large errors (in excess of 0.01% compared to $<0.007\%$ for the September 1991 data) and it should be noted that 5 of the 12 values in Table 3.5 are non-normal, i.e. they come from skew or kurtose distributions.

(a)

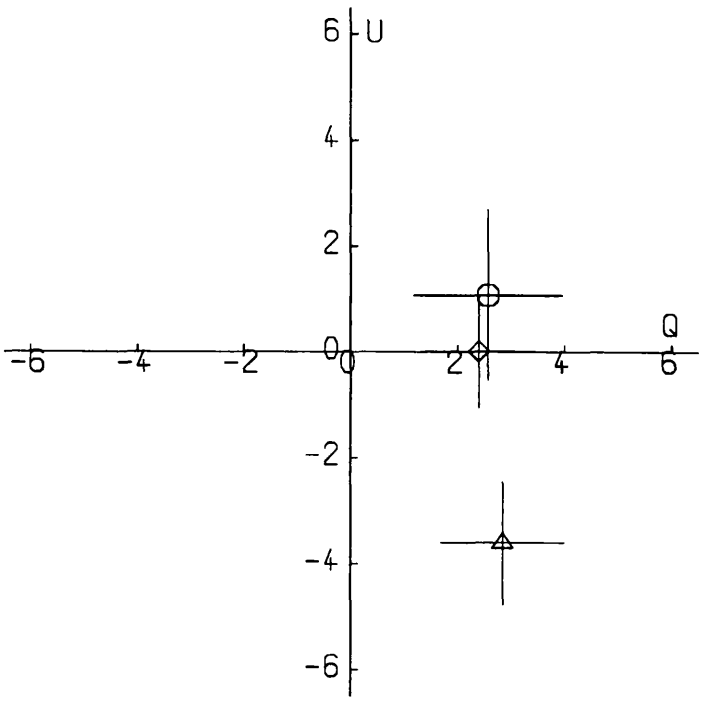

(b)

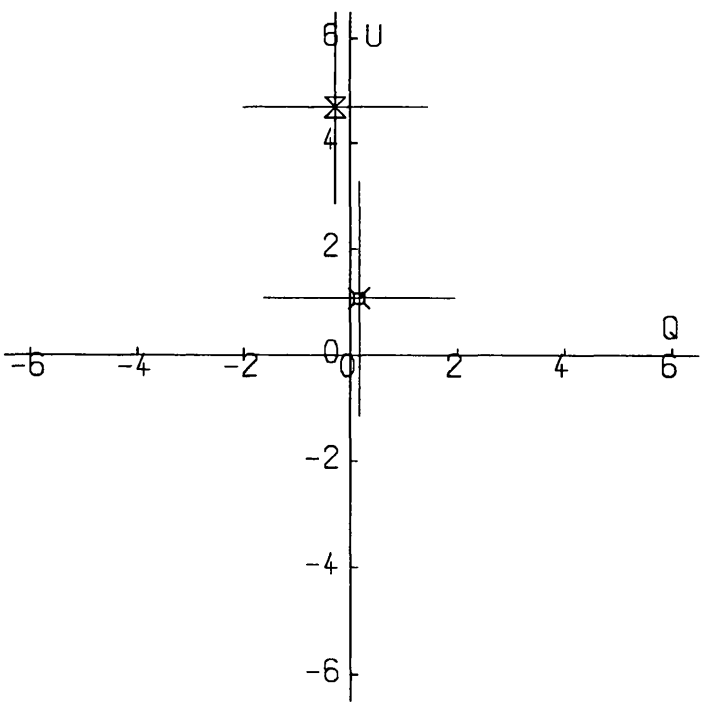

Fig. 3.19 (a) and (b) as for Fig 3.6 for 4 May 1990.

(a)

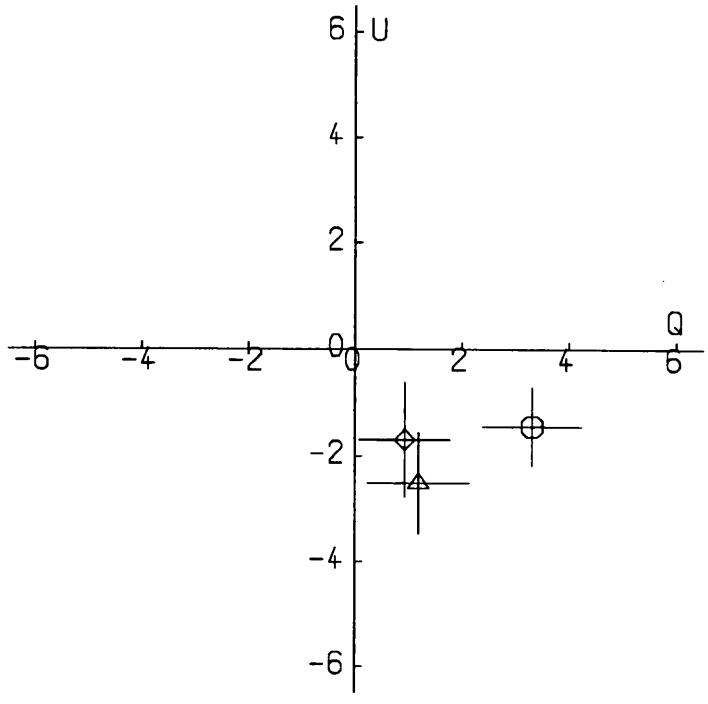

(b)

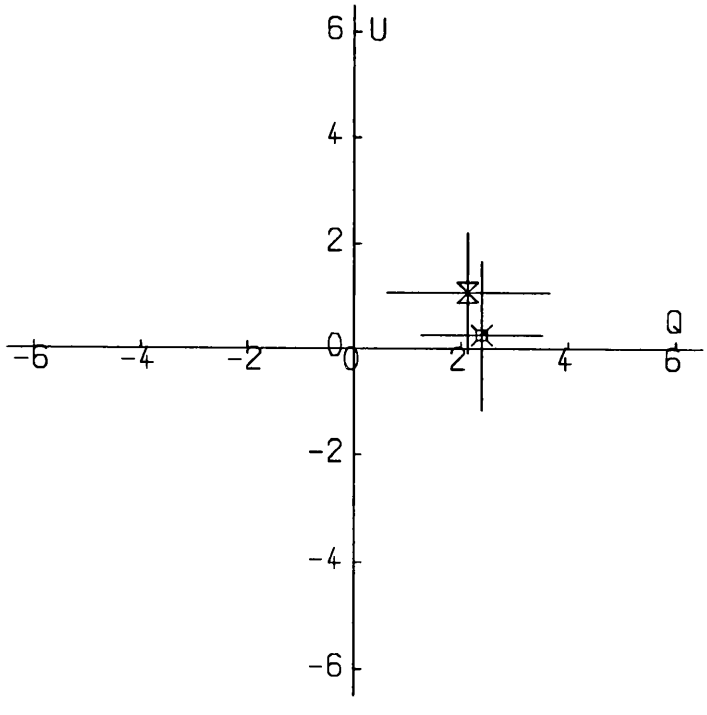

Fig. 3.20 (a) and (b) as for Fig 3.6 for 5 May 1990.

(a)

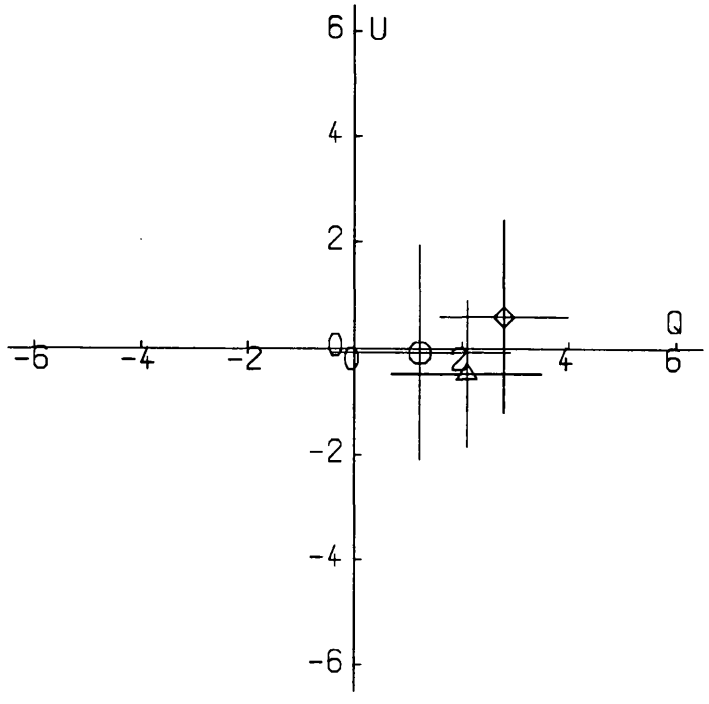

(b)

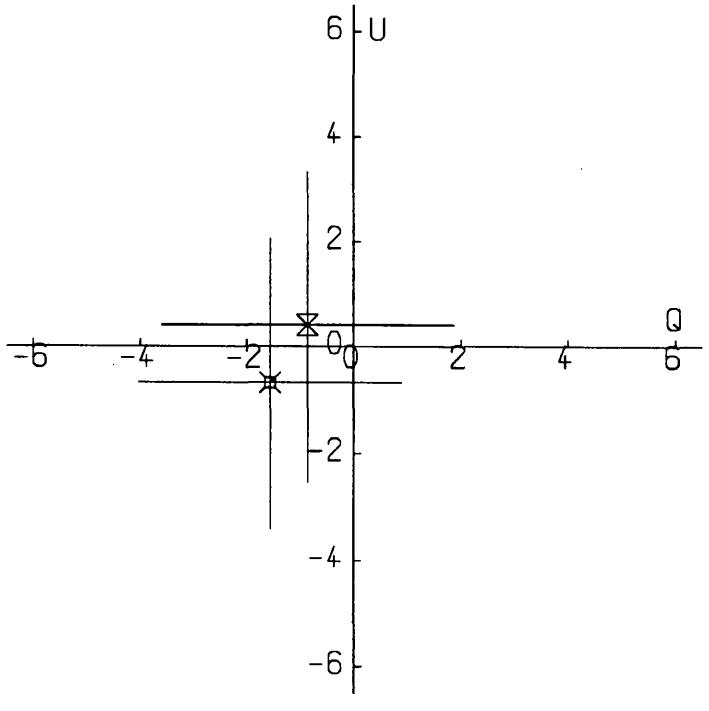

Fig. 3.21 (a) and (b) as for Fig 3.6 for 14 May 1990.

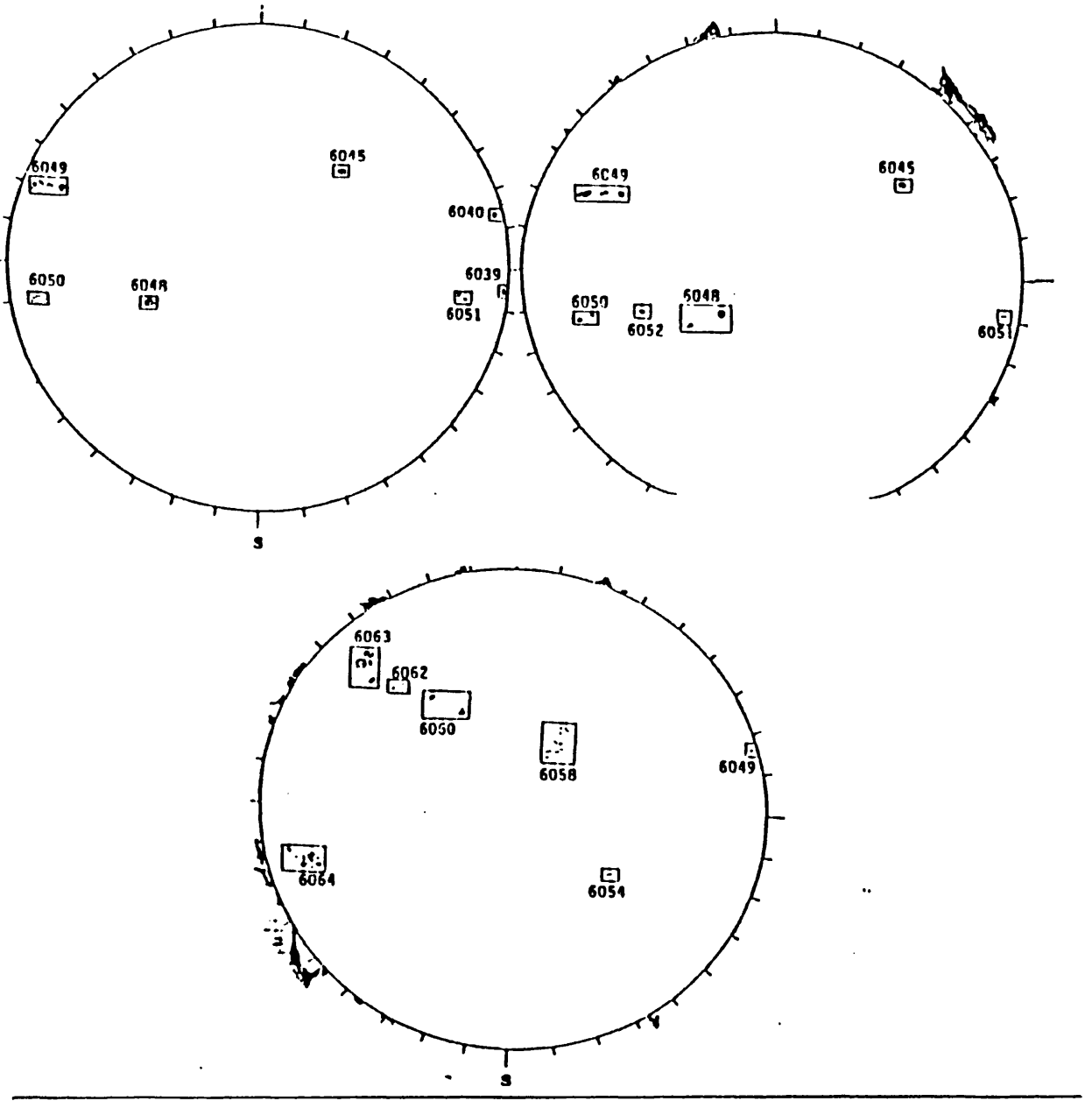

Fig. 3.22 Visible disk of the Sun on 1990 May 4 (top left), 5 (top right) and 14 (below) showing the positions of sunspots. (Taken from the Geophysical Prompt Reports, June 1990).

3.5 Conclusions Drawn from the Solar Observations

It is important to state at this point that for all the solar observations discussed in this chapter there is only one data point in which the measured line polarization is departed by more than three standard errors from its associated continuum measurement. A histogram of $p/\Delta p$ was drawn for all measurements (respecting that the calculated value of p from q and u would be biased and therefore is not shown) and compared to a Rice distribution with $p_0 = 0$, indicating that no significant global polarization in either the Fe I or Hβ line was detectable at the quoted accuracies of measurement. However I do not feel that solar whole disk polarization should be easily dismissed as non-existent. The prior evidence provided by Dr. Clarke that the polarimetric monitoring at 5000Å in a 50Å band-width showed a small yet significant variation at above the 0.01% level over a period of a few of weeks, together with the positive Welch test results (showing that the means of the separate data sets are not equal within the errors) on the data shown in figures 3.14 and 3.15 lead me to believe that polarimetric variations do exist at, or just below, this level of detection. The correlation analyses also lent a little more weight to the claim that polarizations were indeed measured. More accurate apparatus and photon detection techniques, coupled with a shorter time resolution to make more precise measurements, will ultimately allow a polarimetric precision better than 1 part in 10^5, which in turn would allow confirmation of this belief. Unfortunately, had the planned observations of isolated active regions devoid of dilution by unpolarized light from the quiet photosphere been possible, then a more decisive statement about solar polarization could have been made.

CHAPTER 4

STELLAR POLARIMETRIC OBSERVATIONS WITH THE GLASGOW UNIVERSITY PHOTOMETER/POLARIMETER

4.1 Introduction

Section 2.1.2 described the method of data acquisition for the GUPP instrument. This double beam polarimeter allows the measurement of the normalized Stokes' parameters in two colours simultaneously by the use of interference filters, whilst a continuously rotating half-wave plate acts as a polarimetric modulator. As one of the photomultipliers of the instrument is most sensitive in the red region of the spectrum, and the second at blue wavelengths, most filter combinations for the observations had the longer wavelength filter in the red channel.

For some sets of data two filters with equal (or nearly equal) central wavelengths (λ_0) and with similar passbands (FWHM, or $\Delta\lambda$), were used in an attempt to combine two measurements made simultaneously in one passband. In this way a more accurate estimate of the Stokes' parameters might be made using a count-ratioing technique to reduce noise on the integrations from atmospheric effects. This process is described in section 4.4.

The instrumental polarization of the equipment had not recently been investigated so observations of unpolarized standard stars were required. The known standards γ Gem, β Cas, α Aur and α UMa were chosen for this purpose due to their brightness and favourable position in the winter sky.

The polarized standard star 55 Cyg and Mars were observed so that the instrumental frame of the telescope/polarimeter could be related to the equatorial frame. The results of this chapter will, however, always be given in the instrumental frame as conversion to the equatorial frame may carry errors of axis transformation which may be systematically different at each wavelength, increasing the uncertainty in the analysis. In any case, the purpose of investigating variable polarization does not depend upon which frame of reference is being used, as long as one frame is strictly adhered to.

55 Cyg has a wavelength dependent polarization and position angle given by

Serkowski (1974), and the expected polarization vibration from Mars can be calculated from its position relative to the Earth and the Sun at the time of the observation.

Observations were made on twelve nights over a period from 1992 January 9 to 1993 April 28. The sparsity of clear nights in Glasgow due to its infamous weather meant that it was decided to only observe α Tau and α Boo for the investigation. This was because their brightness allowed rates of about 10^6 counts during an eight second integration for filters with 100Å band passes so that a few hundred integrations should give photon noise dominated errors of less than 1 part in 10^4. Fainter stars would require many hours of observations to reach this level of precision, as will be shown by the data for the standard stars.

The statistics used in this and the following section will be those explored by Stewart (1984) and described in section 2.5. As a bias will be introduced in calculating the polarization, p, from the normalized Stokes' parameters, q and u, all analysis will be concerned with q and u only.

It will be assumed that for each observation of n integrations the calculated mean values of the Stokes' parameters, $\hat{q}$ and $\hat{u}$, have estimated squared standard errors, $\hat{\sigma}_q^2$ and $\hat{\sigma}_u^2$, that come from the same parent statistical distribution.

If (q_0, u_0) is the true point of the Stokes' parameters, Stewart states that the confidence region for the point (q_0, u_0) for data which has $\hat{\sigma}_q^2 \neq \hat{\sigma}_u^2$ and $n_q = n_u$ at the (1-α)100% level is given by

$$\frac{(\hat{q} - q_0)^2}{\hat{\sigma}_q^2} + \frac{(\hat{u} - u_0)^2}{\hat{\sigma}_u^2} = z_{(1-\alpha)} \qquad (4.1)$$

which is an ellipse with centre $(\hat{q}, \hat{u})$ and semi-major and semi-minor axes given by $\sqrt{\hat{\sigma}_q^2 z_{(1-\alpha)}}$ or $\sqrt{\hat{\sigma}_u^2 z_{(1-\alpha)}}$. The data point is said to be unpolarized if the origin is contained within the ellipse at a chosen (1-α) confidence level. Values

of $\sqrt{z_{(1-\alpha)}}$ as a function of sample size were calculated and tabulated by Stewart. For the purpose of this study a confidence level of 95% will be used, and as each sample size is greater than 140 a value of $\sqrt{z_{(1-\alpha)}} = 2.46$ can be employed as it is almost invariant for larger sample sizes (e.g. at $n = \infty$ the value is 2.45).

Each individual data set was tested for normality by calculating the skewness and kurtosis of their q and u values and comparing them with the tables of Brooks (1985) at the 95% and 99% confidence levels. Failing a normality test may show variable polarization during the period of the observation and this possibility was investigated for all data.

To detect polarimetric variations *between* the calculated mean value of q (or u) of each data set, *i.e.* to search for day-to-day variation, the Welch test was employed. As the measurements were made with different sample sizes and have unequal standard mean errors, and Welch statistics are derived separately for both q and u, again at the 95% and 99% confidence levels.

The normalized Stokes' parameters and their standard mean errors are shown in Tables 4.1 and 4.2 for all observations. The columns of the table shows the following:

(1) the Henry Draper number of the star;

(2) its common name and spectral classification;

(3) the Julian date at the start of each observation (2440000+);

(4) the wavelength and bandwidth of the filter used;

(5) in which channel the measurement was made, (R) or (B) (important because the instrumental polarization may be different for each channel, which will be investigated later);

(6) the measured q value (in units of 10^{-6});

(7) the standard mean error, σ_q, upon q, in the same units;

(8) the measured u value (in same units as q);

(9) the standard mean error, σ_u, upon u, in the same units;

(10) the number of integrations taken during the observation.

1	2	3	4	5	6	7	8	9	10
95912	γ Gem	8671.478	5000/400	R	+ 36	153	- 150	152	512
	A 1 IVs	to .535	4500/400	B	+ 86	153	+ 211	152	512
		8925.519	4588/359	R	- 134	118	+ 211	108	512
		to .630	4520/393	B	+ 362	121	- 134	115	512
34029	α Aur	8911.459	5100/50	R	+ 115	300	- 16	302	176
	G 8 III	- .506	5100/100	B	- 81	276	- 116	269	176
		8921.395	5100/50	R	- 381	172	+ 158	188	246
		- .426	5100/500	B	+ 255	161	+ 56	172	246
		8921.444	4800/50	R	+ 214	164	- 69	151	224
		- .474	4800/100	B	+ 154	105	- 226	111	224
		8921.481	4200/100	R	+ 137	137	- 73	144	140
		- .500	4215/100	B	+ 47	125	- 197	141	140
432	β Cas	8926.297	4588/359	R	+ 77	128	+ 71	106	334
	F 2 IV	- .360	4520/393	B	- 33	120	+ 86	108	334
		8940.308	4588/359	R	- 35	109	+ 216	105	688
		- .390	4520/393	B	+ 207	108	+ 43	104	688
95689	α UMa	9050.403	4200/100	R	+ 236	167	- 105	175	480
	K 0 III	- .522							
198478	55 Cyg	8925.406	4860/50	R	+8107	776	+24751	735	127
	B 3 Ia	- .501	5020/70	B	+8126	722	+27972	675	
	Mars	8925.640	4588/359	R	+7164	49	+36984	52	128
		- .656	4520/393	B	+6481	46	+31810	49	

Table 4.1 Observations of All Standard Stars and Mars

1	2	3	4	5	6	7	8	9	10
29139	α Tau	8631.346	5000/400	R	- 91	83	+ 24	87	1580
	K 5 III	- .553	4500/400	B	- 205	85	+ 13	86	1580
		8636.345	5000/400	R	+ 66	77	+ 121	73	640
		- 6.424	4500/400	B	- 65	61	- 41	71	640
		8644.343	5000/400	R	+ 139	96	+ 25	96	512
		- 4.401	4500/400	B	- 200	95	+ 56	110	512
		8671.333	5000/400	R	+ 227	128	- 201	135	1024
		- 1.462	4500/400	B	- 444	139	- 51	154	1024
124897	α Boo	8631.690	5100/100	R	- 147	236	- 111	230	360
	K 2 IIIp	- 1.751	4200/100	B	- 174	197	+ 419	252	360
		8631.761	5600/100	R	- 356	279	- 84	266	336
		- 1.808	4800/100	B	+ 112	235	+ 101	215	336
		8671.599	5100/100	R	- 165	111	- 243	106	503
		- 1.657	4200/100	B	+ 102	114	+ 90	115	503
		8671.667	5600/100	R	+ 90	85	+ 135	89	554
		- 1.737	4800/100	B	- 191	81	- 284	95	554
		9050.539	4200/100	R	+ 363	241	- 429	238	512
		- 0.597							
		9050.607	5100/100	R	+ 142	126	+ 190	126	512
		- 0.669							
		9050.680	4800/100	R	+ 9	152	+ 424	157	512
		- 0.737							
		9072.397	5100/100	R	+ 88	52	- 24	72	704
		- 2.486							
		9106.479	5100/100	R	+ 88	36	+ 97	28	512
		- 6.539							
		9106.547	4800/100	R	+ 80	31	+ 166	31	479
		- 6.605							

Table 4.2 Observations of α Tau and α Boo

4.2 Determination of the Instrumental Polarization

4.2.1 Observations of Unpolarized Standard Stars

No interpretation of polarimetric results is complete without knowledge of the way in which the instrument might affect the values obtained. The optical elements of a reflecting telescope and those in any polarimetric instrument that are placed in the optical train before a polarimetric modulator (in this case a half-wave plate) may not have the same transmission/reflection efficiency for the orthogonal directions of vibration of the incident light. This may introduce an instrumental polarization.

The fact that the GUPP instrument has a continuously rotating half-wave plate modulator and that both Stokes' parameters are simultaneously measured using the same photomultiplier for each channel means that the optical elements placed after the half-wave plate should not introduce any instrumental effects.

It is therefore required that unpolarized standard stars are observed to measure the instrumental polarization of the telescope. It may also be possible that such an instrumental polarization is unstable, being variable over short or long time scales, and this could be due to meteorological effects on the telescope optics.

The two channels (denoted R for red and B for blue as described in the previous section) will be treated separately so that any possible effect that may introduce the instrumental polarization is taken into account.

The unpolarized standards measured were:-

γ Gem (A 1 IVs)⊕ in figures 4.1 (a) and (b);

β Cas (F 2 IV) ◊ in figures 4.1 (a) and (b) (ref. Serkowski, 1974);

α Aur (G 8 III) □ in figures 4.1 (a) and (b) (ref. Behr, 1959; Tinbergen, 1979, 1982);

α UMa (K 0 IIIa) Δ in figures 4.1 (a) and (b) (ref. Behr, 1959; Dyck and Jennings, 1971; Tinbergen, 1979, 1982).

Figure 4.1 (a) is a q,u diagram showing the nine observations of unpolarized standard stars measured by the red channel, consisting of two measurements of γ Gem, two of β Cas, four of α Aur and one of α UMa. Also plotted is the weighted mean of the nine values of q and u. Each error bar is one standard error in length. The position of the weighted mean value is at

$$\hat{q} = + 13 \pm 46 , \quad \hat{u} = + 67 \pm 46 \quad (\text{x } 10^{-6}) \tag{4.2}$$

A Welch test on the nine values of the Stokes' parameters showed that both q and u did not vary significantly, the Welch statistic being below the 90% confidence level. The measurements were made over a period of 14 months and there is no correlation between either the $\hat{q}$ or $\hat{u}$ values with time. Also, there is no correlation of $\hat{q}$ or $\hat{u}$ with filter wavelength.

It can therefore be assumed that the polarimetric origin of the red channel of the instrument is contained within the circle surrounding the weighted mean point whose radius is given by the standard mean errors $\sigma_{\hat{q}}$ and $\sigma_{\hat{u}}$ multiplied by $\sqrt{z_{(1-\alpha)}}$ for 9 degrees of freedom at the 95% confidence level. Therefore the value of the radius is given by 2.696 x 46 = 124 (x10^{-6}).

Figure 4.1 (b) is the q,u diagram showing the eight observations of the unpolarized standard stars using the blue channel. The observation of α UMa is not included here because an anomaly was noticed in the data from the blue channel for the observations that were made in 1993 and which was not present beforehand. This will be discussed later. The values of the weighted means of q and u are

$$\hat{q} = + 147 \pm 46 , \quad \hat{u} = - 38 \pm 46 \ (\text{x } 10^{-6}) \tag{4.3}$$

The Welch test again found no temporal variability above the 90% confidence level for either Stokes' parameter, and no correlation was found between either

(a)

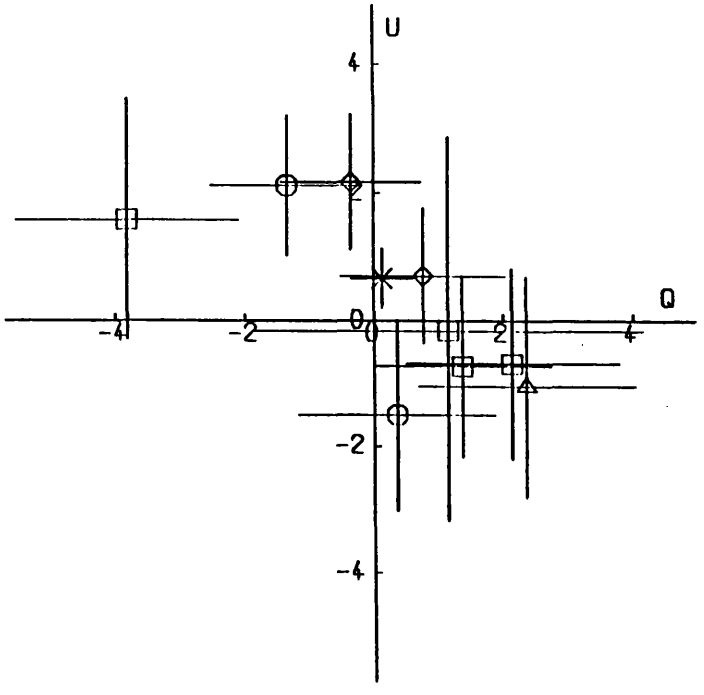

(b)

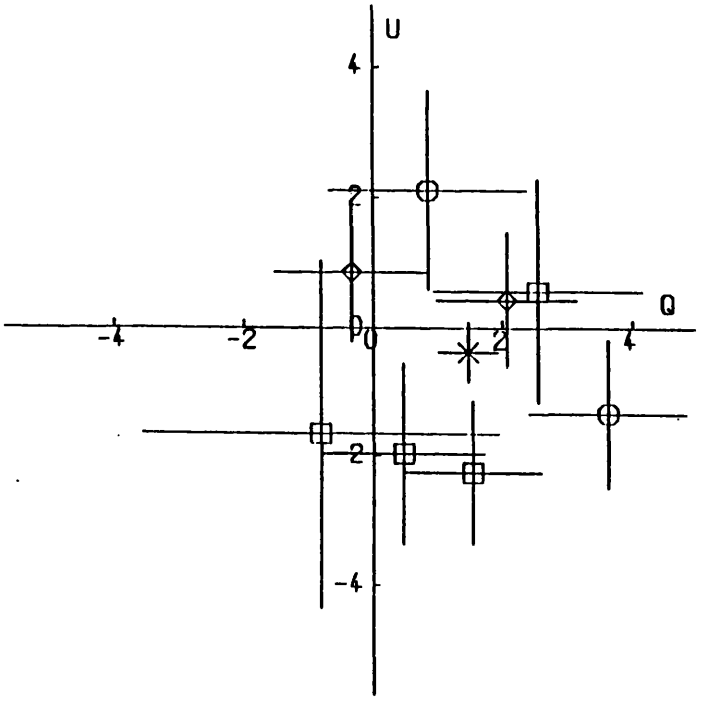

Fig. 4.1 Polarization diagram showing the q,u values of the unpolarized standard stars measured in (a) the red channel (above), and (b) the blue channel (below), in units of 0.01%. See text for legend. Weighted mean value shown by cross, ×.

Stokes' parameter and the time of the observation, nor with filter wavelength.

It is therefore assumed that the polarimetric origin for the blue channel is contained within the circle surrounding the weighted mean values whose radius is given by the standard mean errors $\sigma_{\hat{q}}$ and $\sigma_{\hat{u}}$ multiplied by 2.735 in this case. This gives a radius of 126 x 10^{-6}.

The determined q,u values for each channel will be used with the results in the next section. The weighted mean values will be subtracted from the data and the circle will be drawn around the origin to establish whether or not polarization is detected.

4.2.2 Observations of a Polarized Standard Star and Mars

Although, as mentioned in the previous section, all results presented here will be in the instrumental frame, it would be of value to know the position angle of the instrumental frame with respect to the equatorial frame where the positive q axis is parallel to the North-South axis. For this purpose the polarized standard star 55 Cyg was observed, with the polarization and position angle given by Serkowski (1974) as

$$p(\lambda) = p(\lambda_{max}) \exp [-1.15\ ln^2(\lambda_{max}/\lambda)] \qquad (4.4)$$

where λ_{max} = 5300Å and $p(\lambda_{max})$ = 2.8%. The position angle, θ, at λ_{max} is 3° and has only a very small wavelength dependence within the spectral regions used in the observation (i.e. 5020/70Å and 4860/50Å). The theoretical polarizations for the two passbands, p_{th}, the observed q, u values and the calculated p and θ are then:

λ	= 5020 Å		λ = 4860 Å	(4.5)
p_{th}	= 2.79 %		p_{th} = 2.77 %	
q	= 0.81 %		q = 0.81 %	
u	= 2.80 %		u = 2.48 %	
p	= 2.91 %		p = 2.60 %	
θ	= 36.90°		θ = 35.93°	

It is obvious that the observed p do not agree with Serkowski's values. The probable explanation for this is that the data were exceptionally noisy, due to the low photon counts for each integration. For this reason the differences between $\theta_{Serkowski} = 3^\circ$ and the observed values of θ, about 37° and 36° respectively, should not be considered as being the true instrumental frame's orientation. Also, it should be noted that some authors claim that 55 Cyg is a polarimetric variable.

Fortunately Mars was also observed for the purpose of finding the position angle. Scattered sunlight from Mars will be partially polarized and the direction of vibration can be calculated from its position relative to the Sun and Earth. Mars was observed with 4588/359Å and 4520/393Å filters and from the q and u values in Table 4.1 the position angle for the two channels are calculated to be

$$\theta_{4588Å} = 39.52^\circ \quad \text{and} \quad \theta_{4520Å} = 39.24^\circ \tag{4.6}$$

The calculated position angle, θ_{calc}, is found from the following relationship

$$\cos(\theta_{calc} + 90^\circ) = \frac{\sin(\delta_\odot) - \sin(\delta_{mars})\cos(E)}{\cos(\delta_{mars})\sin(E)} \tag{4.7}$$

where E is the elongation of Mars, i.e. the angle subtended at the Earth by Mars and the Sun, which is itself calculated from

$$\cos(E) = \sin(\delta_\odot)\sin(\delta_{mars}) + \cos(\delta_{mars})\cos(\delta_\odot)\cos(\alpha_{mars}-\alpha_\odot) \tag{4.8}$$

for which the α's and δ's refer to the right ascensions and declinations of the Sun and Mars. At the time of the observation,

$$\alpha_{mars} = 7h\ 37m\ 22.67s \qquad \delta_{mars} = 22^\circ\ 47'\ 32.44'' \tag{4.9}$$

$$\alpha_\odot = 14h\ 18m\ 25.66s \qquad \delta_\odot = -13^\circ\ 49'\ 58.97''$$

which gives $\theta_{calc} = 9.12^\circ$.

The instrumental frame can therefore be said to have a position angle of approximately +30° with respect to the equatorial frame.

4.3 Observations of α Tau and α Boo

4.3.1 α Tau (K 5 III)

This star is listed as being unpolarized in broad-band by Tinbergen (1982) but it is known to be photometrically variable. However Stewart (1984) found small, time dependent polarization differences across the Hβ line on the threshold of detectability.

Figures 4.2 (a) and (b) show the 4 measurements made at 5000Å and 4500Å respectively, corrected for instrumental polarization. The error on the origin found from the unpolarized stars is drawn as a circle while the error bars on the measurements represent one standard mean error.

The observations made with the 5000Å filter show no polarization present, and a weighted mean of the four measurements lies within the origin circle. The Welch test shows that there are no significant variations in either Stokes' parameter between observations.

The measurements made with the 4500Å filter have a weighted mean for each Stokes' parameter of

$$q = -307 \pm 42 \qquad u = 29 \pm 47 \qquad (\times 10^{-6}) \tag{4.10}$$

which, when the error is multiplied by $\sqrt{z_{(1-\alpha)}}$ for 4 degrees of freedom at the 95% level (=4.365), lies just outside the origin circle. The Welch test for q shows a polarimetric difference between the points at the 95% level.

The evidence suggests that α Tau is indeed polarized at low levels (i.e. a few hundredths of a percent) is measurable in broad spectral bands, and may be variable. As expected from either pure scattering or magnetic intensification the

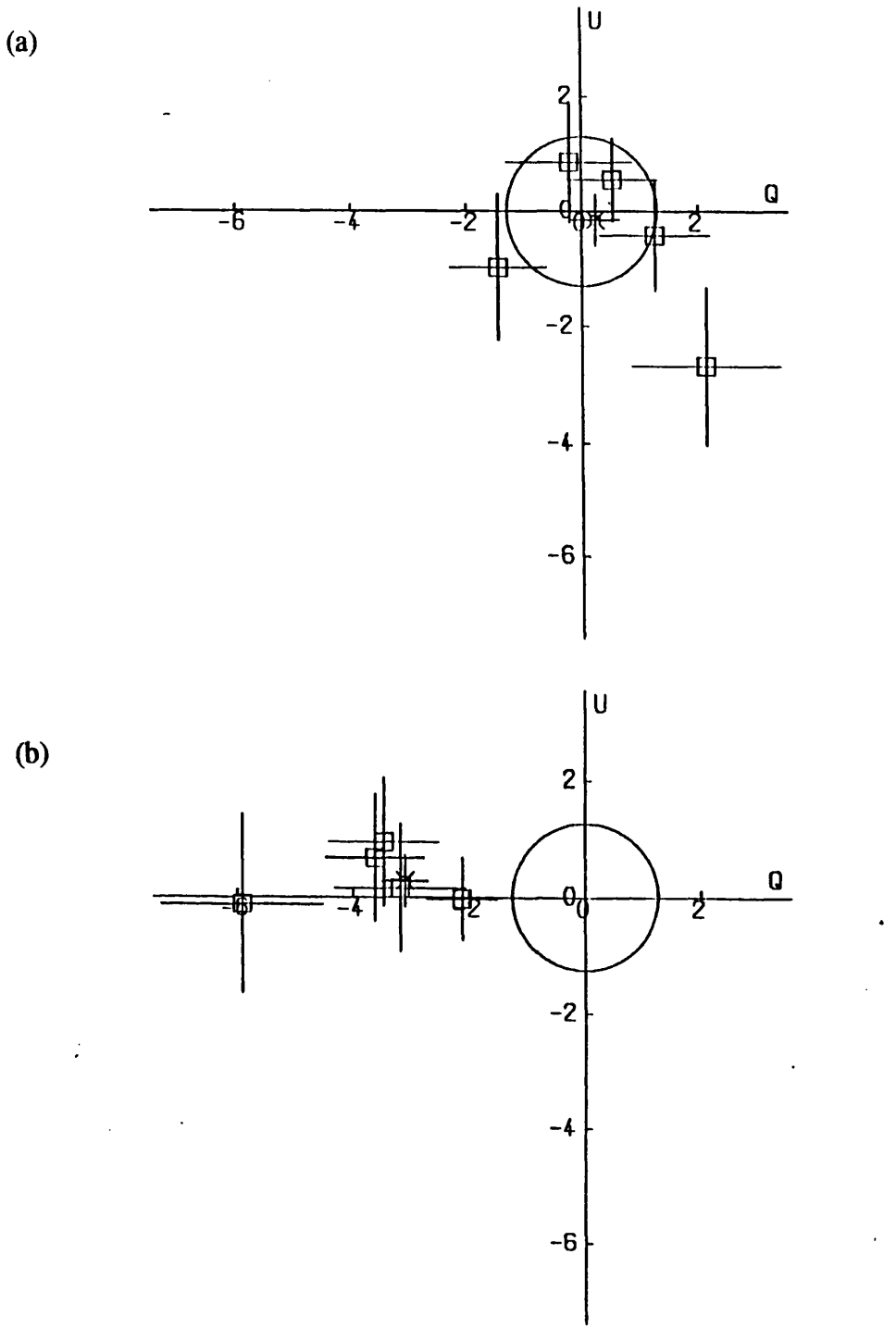

Fig. 4.2 *q*,*u* diagrams for α Tau at (a) 5000Å (above) and (b) 4500Å (below) in units of 0.01%. Measurements within origin circle are unpolarized.

polarization is higher at shorter wavelengths and hence was only seen at 4500Å, with a null result at 5000Å.

4.3.2 α Boo (K 2 IIIp)

This star is also unpolarized in broad-band according to Behr (1959) and Tinbergen (1979, 1982), but Kemp *et al.* (1986) claim it exhibits variable polarization, and it is a peculiar photometric variable. The results of Stewart (1984) suggested very low levels of polarization across the Hβ line.

This star was observed in four different passbands, three measurements being made with the 4200/100Å filter, four with the 4800/100Å filter, five with the 5100/100Å filter and two with the 5600/100Å filter. Figures 4.3 (a) to (d) are polarization diagrams showing the measured q,u values for each passband respectively.

If the star is to be considered as being unpolarized it would be possible to group all the measurements and calculate weighted mean values of q and u. Performing these calculations yields

$$\hat{q} = +32 \pm 19 \qquad \hat{u} = +26 \pm 19 \qquad (\times 10^{-6}). \tag{4.11}$$

However the Welch test shows that both Stokes' parameters show variations at greater than the 99% confidence level. This could be due to these possible effects;

(i) temporal variations of the stellar polarization in one or more passbands;

(ii) temporal variation of the instrumental polarization which has been subtracted from the measured α Boo values [as the measurements were taken over a period of 14 months];

(iii) a wavelength dependence of the stellar polarization;

(iv) a wavelength dependence of the instrumental polarization.

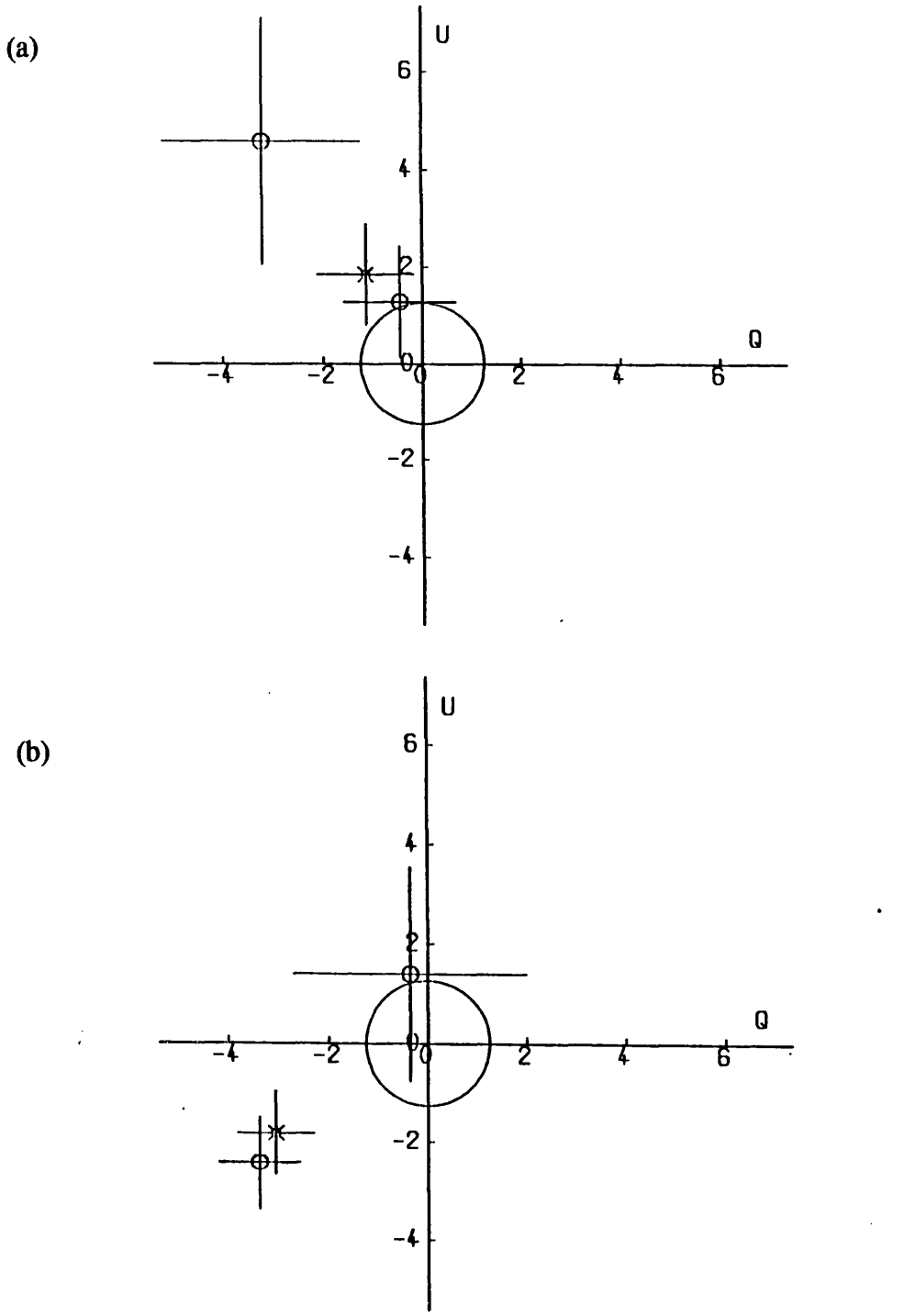

Fig. 4.3 *q,u* diagrams for α Boo at (a) 4200Å (above) and (b) 4800Å (below) in units of 0.01%. Measurements within origin circle are unpolarized.

(c)

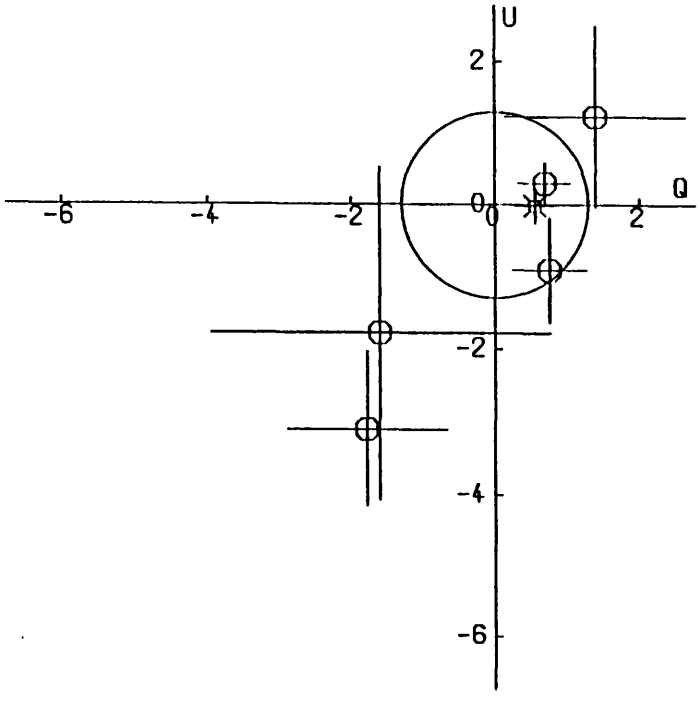

(d)

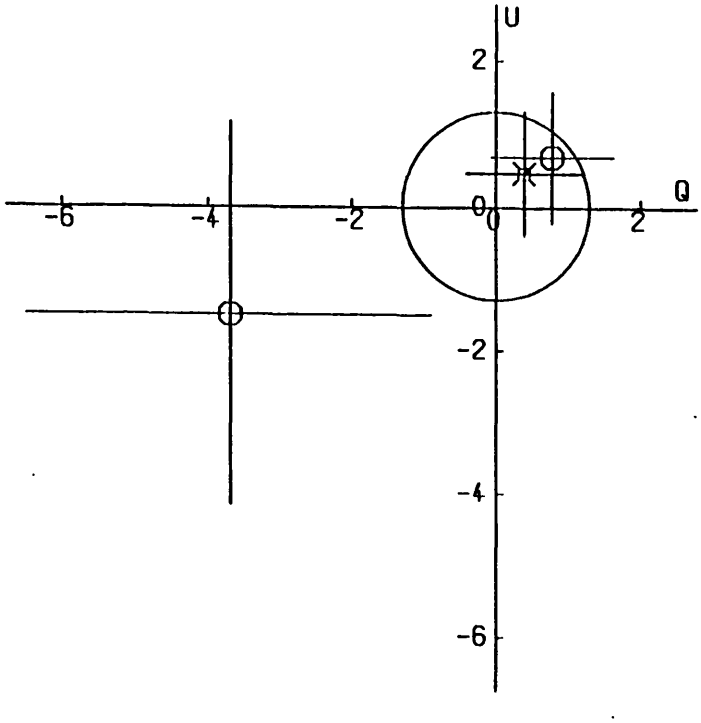

Fig. 4.3 As for (a) and (b) for (c) 5100Å (above) and (d) 5600Å (below).

The instrumental polarization was not found to vary significantly in either observing channel with wavelength or temporally, so cases (ii) and (iv) can be disregarded. The results for α Tau show a possible detection in one waveband while no detection in the second, so it could be assumed that (iii) might be true. It would be better, therefore, if each spectral band is treated separately to see if there are polarizations present, and if so whether they are temporally variant.

The weighted means and standard mean errors of q and u were calculated for the four spectral bands, and the data points were tested for variability by the Welch test for each Stokes' parameter. The results are presented in Table 4.3, where significant Welch statistics at the 95%,99% confidence levels are noted.

4200Å:the error upon the weighted mean falls within the error circle of the origin, which insinuates no polarization being present. However there *is* a significant drift in u at the 95% confidence level which can be seen in figure 4.3 (a) as being in the negative direction from point 10/1/93 through 19/2/92 to 3/3/93, with the outer two points being considered polarized.

4800Å:the weighted mean falls inside the origin circle, as do two of the four measurements. However both q and u show significant variations at greater than the 99% confidence level. Figure 4.3 (b) shows that there is not a simple drift as in (a) but a more "oscillatory" movement, with the points 19/2/92 and 3/3/93 being considered polarized.

5100Å:the weighted mean also falls within the origin circle, but again a significant variation is seen in u at the 95% confidence level. Figure 4.3 (c) shows a distinct difference between the measurements made in 1992, which are significantly negative in u and can be considered polarized, to those made in 1993 which fall within or near to the origin circle and so are considered unpolarized.

Filter (Å)	No. of Obs.	Stokes' Parameter	Weighted Mean ± Standard Error	Welch Statistic	Confidence Level
4200/100	3	q	− 48 ± 91	2.32	
		u	+ 74 ± 96	4.13	95%
4800/100	4	q	+ 14 ± 28	7.27	99%
		u	+ 68 ± 38	5.02	99%
5100/100	5	q	+ 56 ± 28	1.49	
		u	− 2 ± 25	3.21	95%
5600/100	2	q	+ 39 ± 81	2.34	
		u	+ 46 ± 84	0.61	

Table 4.3 Weighted mean q,u values for α Boo measured in each passband and their respective Welch statistics. Significant polarization differences are denoted by the 95% and 99% confidence levels.

5600Å:the weighted mean once again falls within the origin circle (figure 4.3 (d)) and in this case no point is polarized and no significant temporal variation exists.

Plot of (biased) polarization versus wavelength are shown in figures 4.4 (a) and (b) for α Boo and α Tau respectively. In the case of α Tau it seems that the measurements at the shortest wavelengths show some significant polarization, as expected. In the case of α Boo points 10-1-92 and 3-3-93 show large polarizations at 4200Å compared with measurements in other wave bands. The p versus λ dependence shown in figure 1.6 shows that a dip would be expected near 4800Å with a peak near 5100Å. This is not seen in this data which suggests that any polarization present from this star is produced by pure scattering, but the relatively large errors mean that this cannot be regarded as matter of fact.

However the temporal variations in the Stokes' parameters are likely to be intrinsic to the star, which is in agreement with the observations of by Kemp.

4.4 The Possible Effects of the Atmosphere upon GUPP Measurements

With the knowledge that Baliunas *et al.* (1981) found a 10% variability in the chromospheric Ca II K and H emission in timescales of less than 20 minutes, it may be possible that the activity responsible for these variations may also affect the polarized light from the star. A similar investigation into periodicities in the Stokes' parameters to that for the Sun was employed for all the stellar data, but with null results.

However, the close examination of the individual values of the parameters during an observation seemed to show that when the q value of the measurement in the red channel increased, that of q in the blue channel decreased, and vice versa. A similar effect was seen for u, but there appeared to be no connection between the variation of q and u for either channel. Figures 4.5 (a) to (d) show

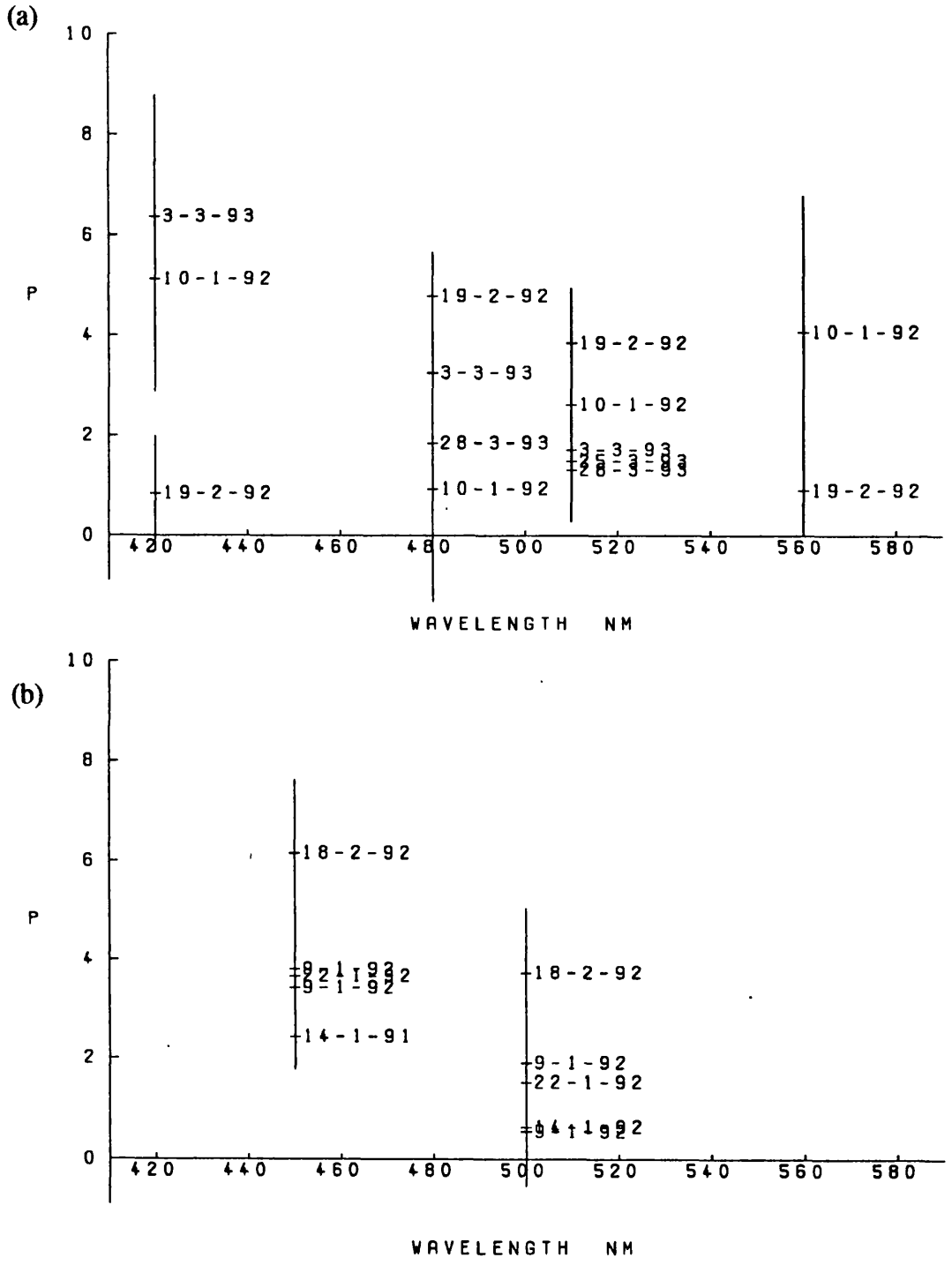

Fig. 4.4 (Biased) Polarization against wavelength diagrams for α Boo (above) and α Tau (below). (Units 0.01% in P)

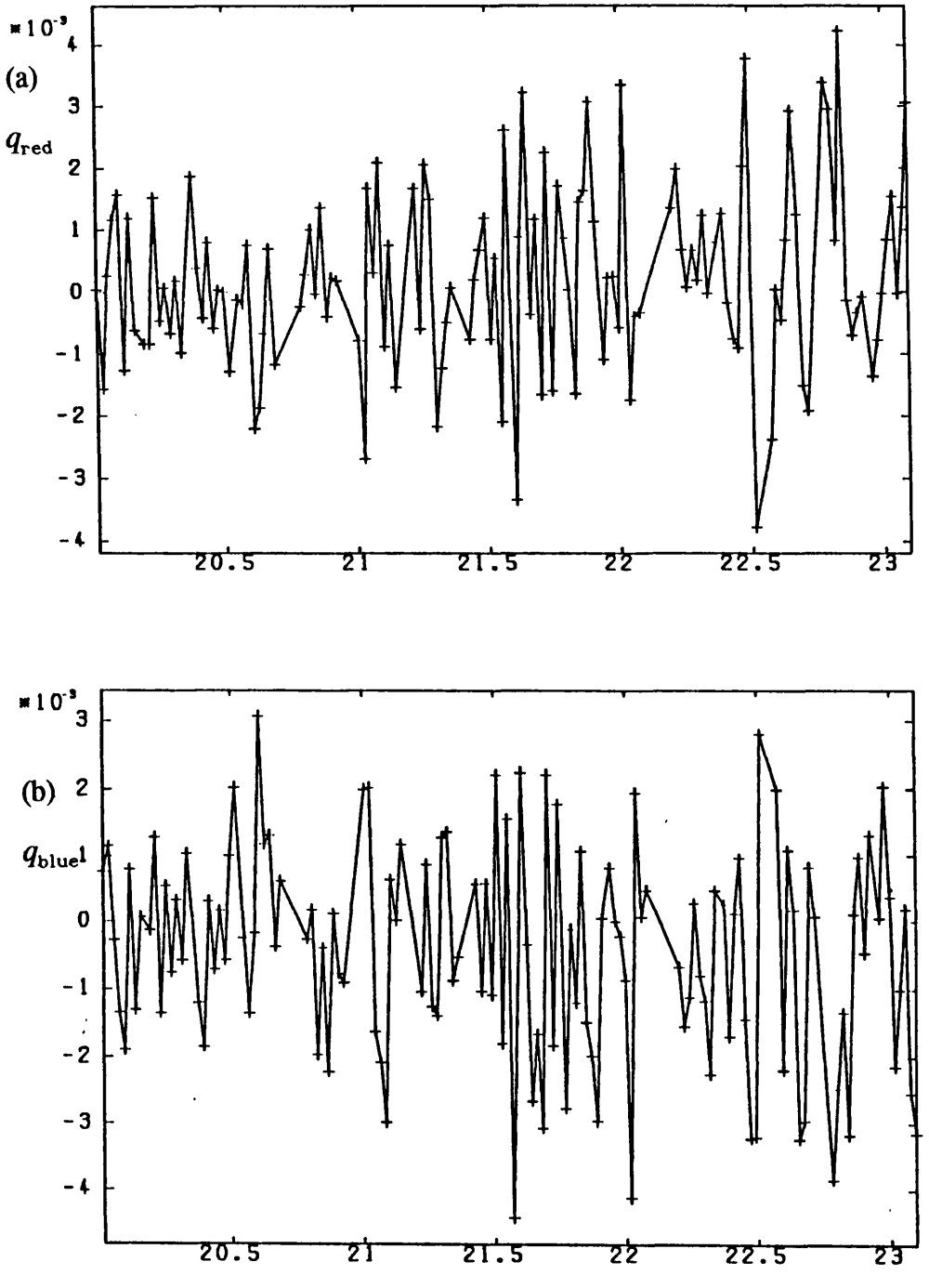

Fig. 4.5 Variation of (a) q_{red} (above), and (b) q_{blue} (below) with time (GMT), during a complete observing run, that of α Tau on 1992 February 18.

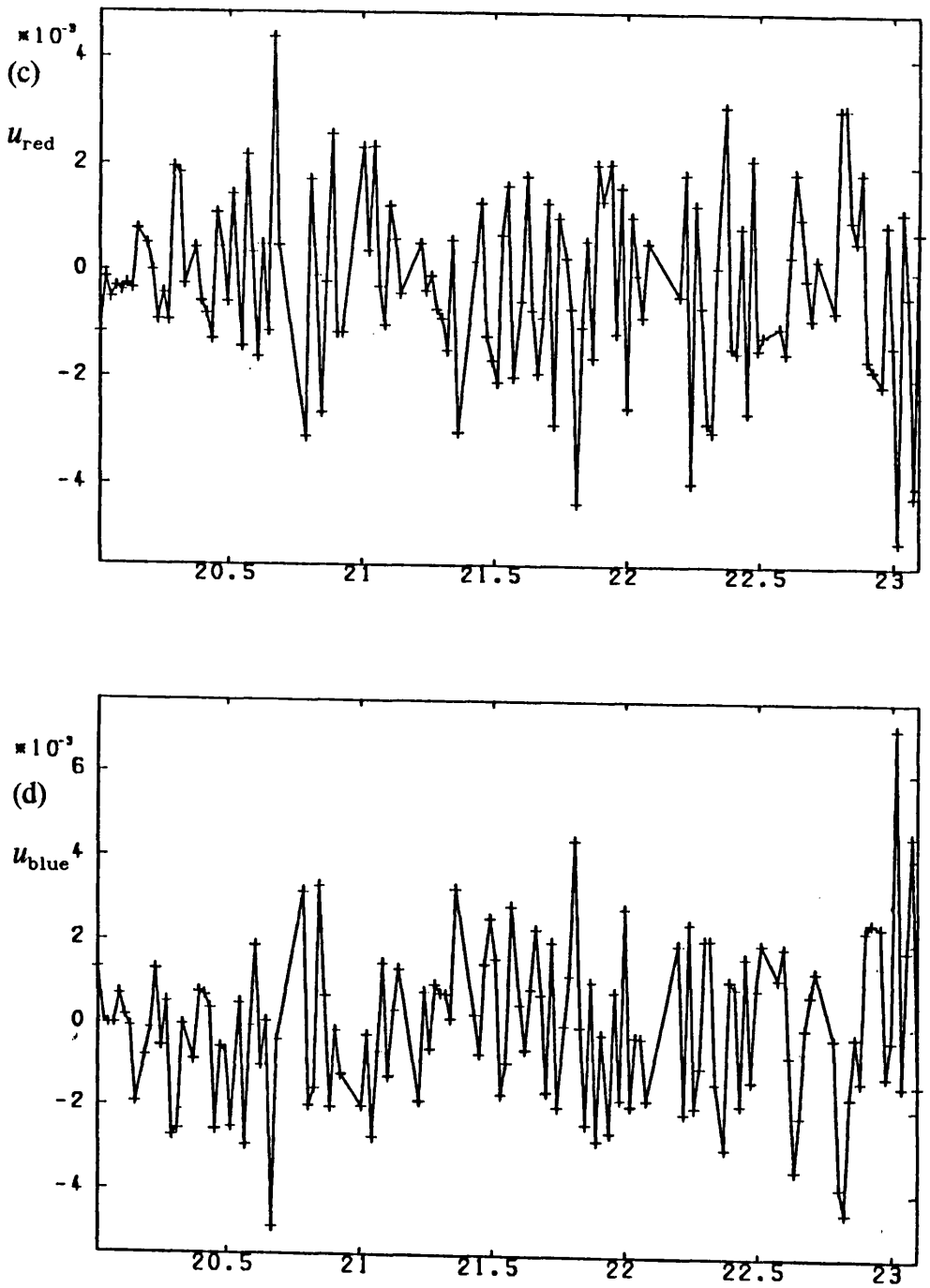

Fig. 4.5 As for (a) and (b) but for (c) u_{red} (above), and (d) u_{blue} (below).

this phenomenon clearly, the first two graphs showing q_{red} and q_{blue}, while the second pair show u_{red} and u_{blue}, for the data of the run of α Tau on 18/2/92. A full correlation analysis was deemed necessary.

The results of the analyses were that for every observation of all stars, there were anti-correlations between q_{red} and q_{blue}, and between u_{red} and u_{blue}, at greater than the 99% confidence level. Only in the case of the observation of α Tau made on 9/1/92 were q_{red} and u_{red} correlated at above the 99% level, but with a greatly reduced correlation co-efficient in comparison with those between q's and u's themselves, whilst in all other cases the co-efficients were almost zero. This fact may indeed suggest short period variability, but as already stated no periodicities were found within the errors of the observation.

Figure 4.6 clearly shows the anti-correlations between q_{red} and q_{blue}, and between u_{red} and u_{blue} (top two quarters respectively), and the non-correlations between Stokes' parameters in each channel in the bottom two quarters. The data is again that of α Tau made on 18/2/92.

That q is not correlated to u for each channel was an expected conclusion, as in his thesis Stewart (1984) calculated that the use of this method of data acquisition leads to negligible correlation between Stokes' parameters. But the anti-correlation between channels needs to be explained by a suitable physical phenomena.

The design of the polarimeter and the data acquisition method gives a clue. The beamsplitting analyzer reflects the extraordinary beam by 90°, so that while the polarized intensity $+Q$ is being recorded in the ordinary channel (red), $-Q$ is being recorded in the extraordinary (blue) channel and vice versa, and similarly for U. If the brightness of the source were to increase during that phase interval of the half-wave plate rotation when $+Q$ and $-Q$ were being recorded in the red and blue channels respectively, then this anti-correlation would indeed be expected.

But such increases or decreases in incident radiation would have to be

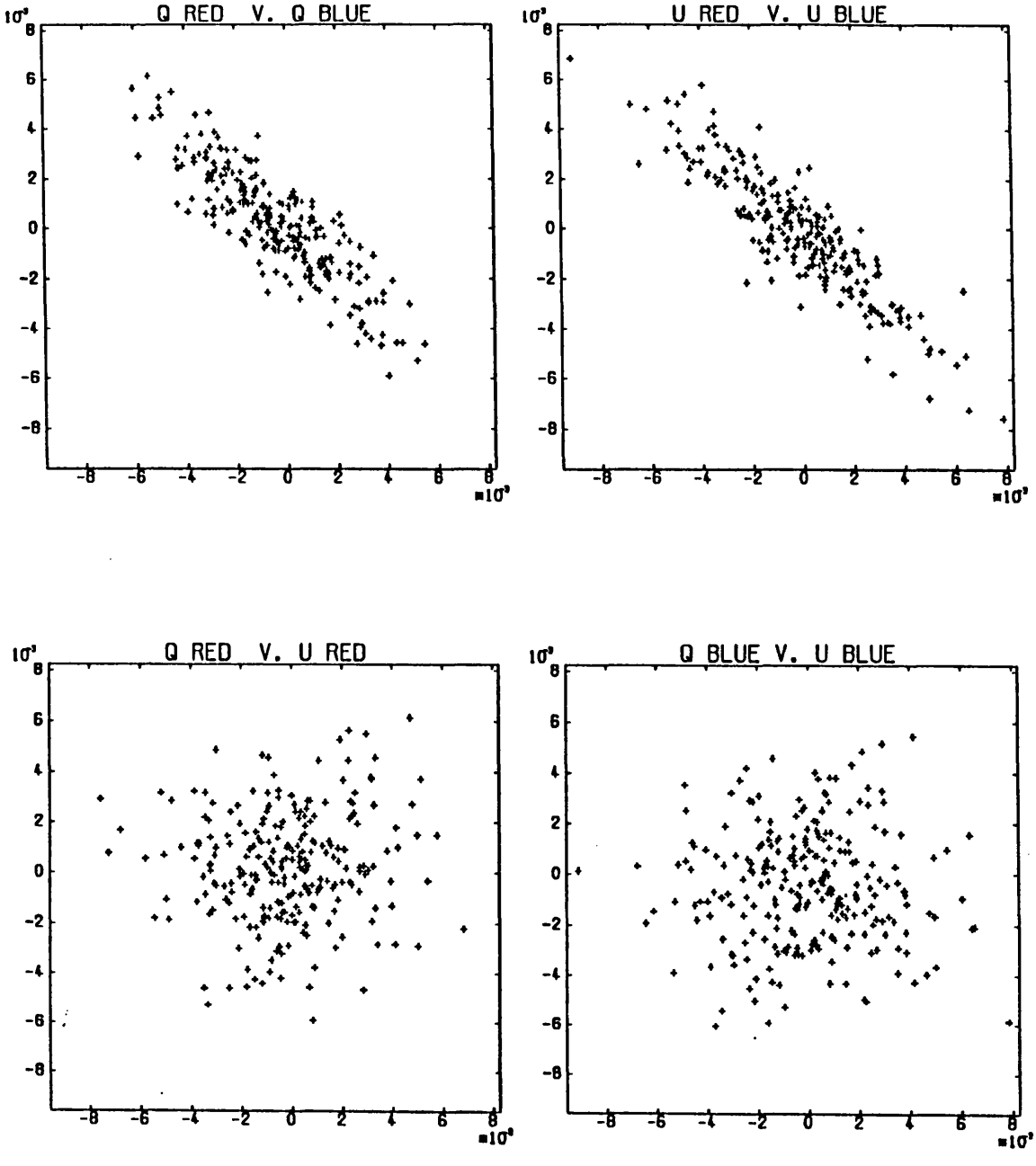

Fig. 4.6 Correlations between q_{red} and q_{blue} (top left), u_{red} and u_{blue} (top right), q_{red} and u_{red} (bottom left), and q_{blue} and u_{blue} (bottom right) for the observing run of α Tau, 1992 February 18.

persistent to produce the observed effects. Obviously the cause of brightness fluctuations could not be at the light source as they would need to have extremely small periods to result in the rapid variation of the observed Stokes' parameters. A more likely explanation is atmospheric effects.

The seeing in Glasgow is not of a high quality, and with the aid of an eyepiece it was possible to observe the rapid movement of the stellar point source within the telescope aperture. As the polarimetric modulation is only 56Hz it would also be expected that scintillation noise at higher frequencies would also affect the data. Both of these causes of rapid brightness fluctuation could result in the observed anti-correlations.

In section 2.1 a method of denoting intensities for discrete phase intervals of the half-wave plate rotation was described. These intensities, x, y, z and w, could be used to attempt to explain the observed anti-correlations. The normalized Stokes' parameters were found by the following equations:

$$q_{\text{red}} = \pi \left(\frac{1}{2} - \frac{y + z}{x + y + z + w} \right) \tag{4.13}$$

$$u_{\text{red}} = \pi \left(\frac{x + y}{x + y + z + w} - \frac{1}{2} \right)$$

$$q_{\text{blue}} = \pi \left(\frac{y + z}{x + y + z + w} - \frac{1}{2} \right) \tag{4.14}$$

$$u_{\text{blue}} = \pi \left(\frac{1}{2} - \frac{x + y}{x + y + z + w} \right)$$

So if, say, z increases, then q_{red} decreases while q_{blue} increases, and the opposite sense would occur for u if x increased. But when y changes, then all four Stokes' parameters would be affected, and so some anti-correlation would exist between q and u in each channel.

Dummy data was produced using NAG routines to provide random numbers. An intensity, for each x, y, z and w, was drawn from a normal distribution about

I_{mean} with a FWHM of $\sqrt{I}$. An individual noise value was then added to each of the four intensities, which were drawn from a log-normal distribution centred upon zero, which has been found to describe scintillation noise best (Young, 1974). The maximum level of the noise was set at various percentages of the normal intensity to investigate what effect greater noise levels would have.

The individual values of x, y, z and w were added for the 480 polarimetric modulations per integration, and the Stokes' parameters calculated from them. This was repeated for 128 integrations, and a weighted mean value and standard mean error of each parameter could then be found for noiseless and noisy data.

With no actual polarization introduced into this data the standard mean values were small and within two mean errors of zero, and as would be expected the noisy data had larger mean errors. Higher percentages of noise also increased the mean errors. The values of the calculated Stokes' parameters were

$$\text{Log-normal noise} = 1\% : \begin{array}{llll} q_{red} = -43 \pm 85 & q_{blue} = +48 \pm 98 \\ u_{red} = +33 \pm 83 & u_{blue} = -101 \pm 109 \end{array} \quad (4.15)$$

$$\text{Log-normal noise} = 10\% : \begin{array}{llll} q_{red} = +844 \pm 853 & q_{blue} = -450 \pm 1006 \\ u_{red} = +515 \pm 932 & u_{blue} = +1200 \pm 1002 \end{array} \quad (4.16)$$

What was of greater interest was whether the anti-correlations present in the stellar data are reproduced. The answer is a resounding no. The only correlation above the 95% confidence limit is between q_{red} and q_{blue} for the 10% log-normal noise level, but it is a positive correlation, not what was expected.

The q,u diagrams similar to those of figure 4.6 for α Tau is shown in figure 4.7 for the q and u values with 10% log-normal noise, and the difference between the two figures is obvious. It is most probable that the method of producing the dummy data is not an accurate representation of how real data is affected by atmospheric noise.

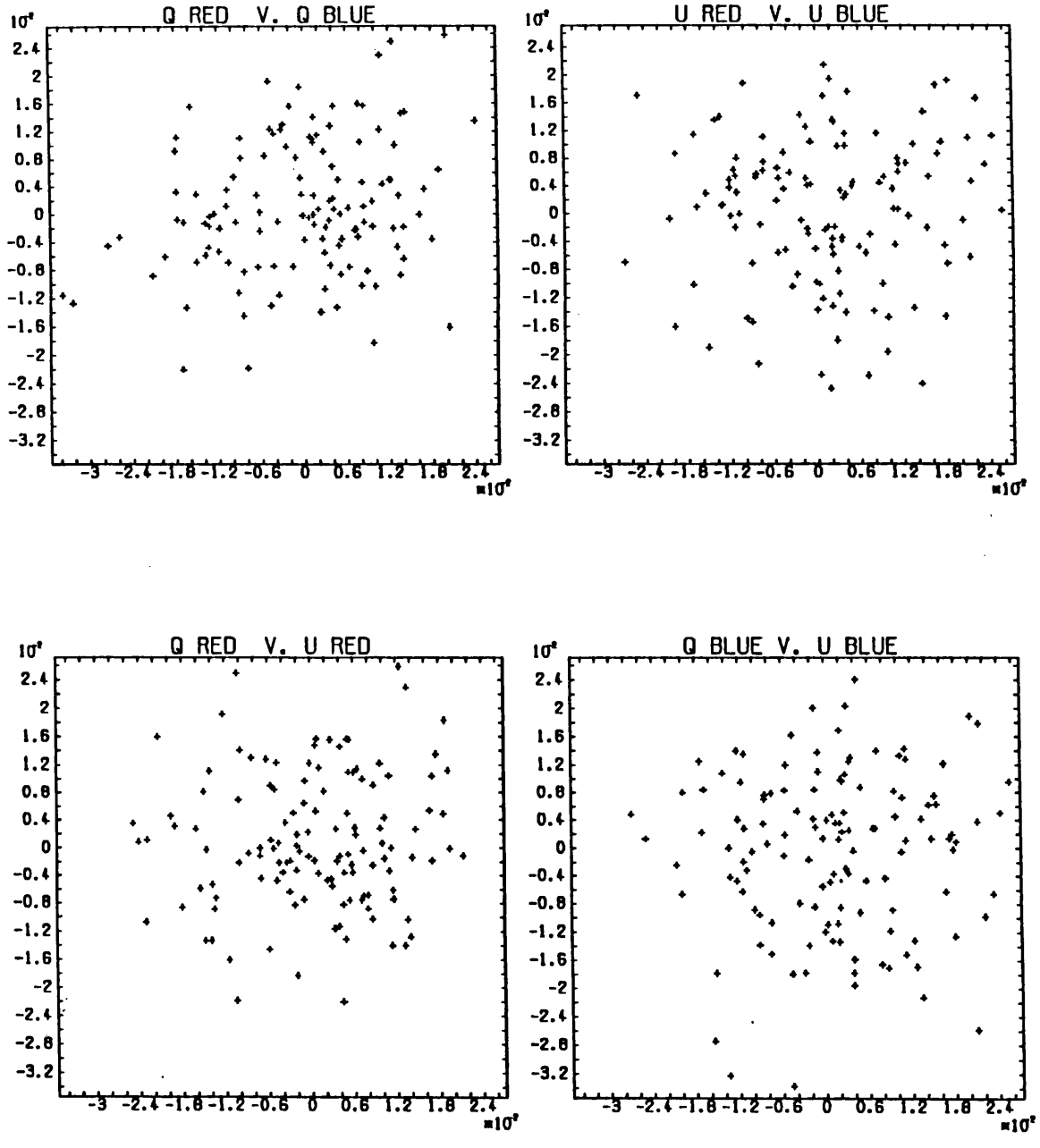

Fig. 4.7 As for figure 4.6 for dummy data with 10% log-normal noise.

It was proposed that if two filters of identical wavelengths and passbands were used in each channel then using an intensity ratio technique to calculate the combined Stokes' parameters would yield smaller errors by eliminating the noise. The method is thus: for the six scalars described in section 2.1.2 let

$$rq = (C4 * C2) / (C5 * C1) ; \quad ru = (C3 * C4) / (C6 * C1) \quad (4.17)$$

and the Stokes parameters are then found by

$$q = \frac{\pi}{2} (1 - rq) / (1 + rq) ; \quad u = \frac{\pi}{2} (ru - 1) / (1 + ru) \quad (4.18)$$

This method will reduce noise because the intensity ratios C1/C4, C2/C5 and C3/C6 cancel atmospheric effects. The result is that q is roughly the mean of q_{red} and q_{blue} (and similarly for u), while the standard mean errors may be reduced by a factor as great as four. But the techniques application is limited because the two channels' instrumental polarizations are significantly different and cannot be subtracted from the data in these equations.

Regardless of this fact observations were attempted of α Boo with two filters at 5100Å, but with 100Å and 50Å passbands, and later with two similar filters at 4800Å. If the instrumental values were assumed equal (within errors) it would be interesting to see what this technique would show when q and u were plotted against time. But when this was attempted, during the first possible run in 1993, an inexplicable problem occurred with the blue channel in which the count rate varied by large amounts over periods of minutes, an effect not mirrored in the red channel whose behaviour was normal. Without time to look into any possible instrumental problem the red channel's results were used on their own, which is why they appear in Table 4.2 without corresponding blue channel results for α Boo and α UMa.

4.5 Discussion of Stellar Results

Despite the high error levels on the Stokes' parameters it was possible to confirm that both α Tau and α Boo show wavelength dependent polarizations. Temporal variations of polarizations are also indicated, but due to the sparseness of data and the long time period over which the observations were made it is not possible to speculate on periodicities such as those found by Kemp *et al.* (1986) for polarization in α Boo, and by Baliunas *et al.* for Ca II H and K emission from α Tau, which might be caused by magnetic effects that could also affect polarization. Nor was the data able to allow measurement of the exact wavelength dependence of polarization which, with the polarization from both stars showing temporal variations, would require accurate measurements in many spectral bands during either a single or a few consecutive nights.

It is necessary to observe for many continuous nights to properly investigate what has been attempted, so the achievements are limited. It was also possible, however, to show that the polarimeter's instrumental polarization does not appear to drift over timescales of more than a year.

CHAPTER 5

OBSERVATIONS WITH THE MULTI-PURPOSE FOTOMETER ON THE JACOBUS KAPTEYN TELESCOPE, LA PALMA

5.1 Introduction

As described earlier in the previous chapter the GUPP instrument on the 51cm telescope at Glasgow was not capable of measuring the polarization of faint stars (e.g. $m_V < 3$) with sufficient precision in short time scales such as two hours. Observations of 55 Cyg ($m_V = 4.84$) highlight this problem, the errors on the normalized Stokes' parameters being about 0.07% due to the low photon count rate. It was therefore decided to submit proposals to the Panel for Allocation of Telescope Time to observe selected solar type stars with the 1m Jacobus Kapteyn Telescope (JKT).

Application J/V/9, submitted in September 1991, was accepted and seven grey nights beginning 1992 April 22 were awarded. The target stars were ξ Boo A (G8V; $m_V = 4.5$) and χ Her (F9V; $m_V = 4.6$), whose properties were described in Chapter 1.

The observations of ξ Boo A concentrated on two things. Huovelin *et al.* (1988) predicted a $\lambda^{-4.9}$ dependence for ξ Boo A and observed a $\lambda^{-5.9\pm0.6}$ dependence, with variability during the five nights of his observations which were significant in the V band and indicative in the U and B bands, while Leroy and LeBorgne (1989) reported that the star exhibited an intrinsic polarization greater than 0.01% that was possibly wavelength dependent (as predicted by his model of polarization due to magnetic intensification). Therefore polarimetric measurements in many colours across the visible spectrum were made to show such a wavelength dependence. Secondly, as the star has a rotation period of 6.2 days it was hoped that observations made on each night over the course of the week would show a polarimetric variation over the whole rotation period of the star if the polarization is due to magnetic features on the stellar surface.

In his survey of standard stars, Piirola (1977) showed that the polarization of χ Her varied between the observations with a maximum of 0.082±0.012% in the B band, yet previously the star had been reported as an unpolarized standard

(Serkowski *et al.*, 1975), so the question of its possible polarimetric variation still stands. A similar investigation as for ξ Boo A should again cast light upon the problem.

The unpolarized standard stars 46 LMi (K0III-IV; m_V = 3.8) and α UMa (K0III; m_V = 1.8) were observed, as was the polarized standard o Sco (A5II; m_V = 4.5), whose polarization had previously been measured by Clarke (1986), and was tabulated by Serkowski (1974).

5.2 The set-up of the Multi-Purpose Photometer (MPF)

It was possible to use one of two instruments on the JKT, namely the Peoples' Photometer and the MPF. The Peoples' Photometer was capable of simultaneous polarimetric observations in two channels with count rates of up to 2 MHz and a polarimetric modulation of 4 Hz. However, it was decided to use the MPF because the polarimetric modulation was 100 Hz, reducing scintillation noise to a greater extent than the Peoples' Photometer, and because it was also possible to make simultaneous measurements in up to 12 channels with a maximum count rate of 1.3 MHz. The polarimetric precision was stated to be 0.005%, with a polarization zero-point instability of 0.03% which was of unknown origin.

The design of the instrument is described in the MPF users manual, is shown in figure 5.1and can be summarized as follows. A continuously rotating half-wave plate acts as a modulator and is followed in the light path by a 100% polarizing beam splitter acting as the analyzer. The reflected beam is used for viewing the object to keep it centred within the instrument's aperture. The transmitted beam then passes through optional neutral density wedges (for the safety of the photomultipliers), and is then split by an arrangement of five dichroic filters chosen by the observer so that the resulting six beams cover the required wavelength bands. Each of the six beams are then split by neutral beam splitters in ratios of 50:50 or 90:10 into 12 channels, with each beam passing through a

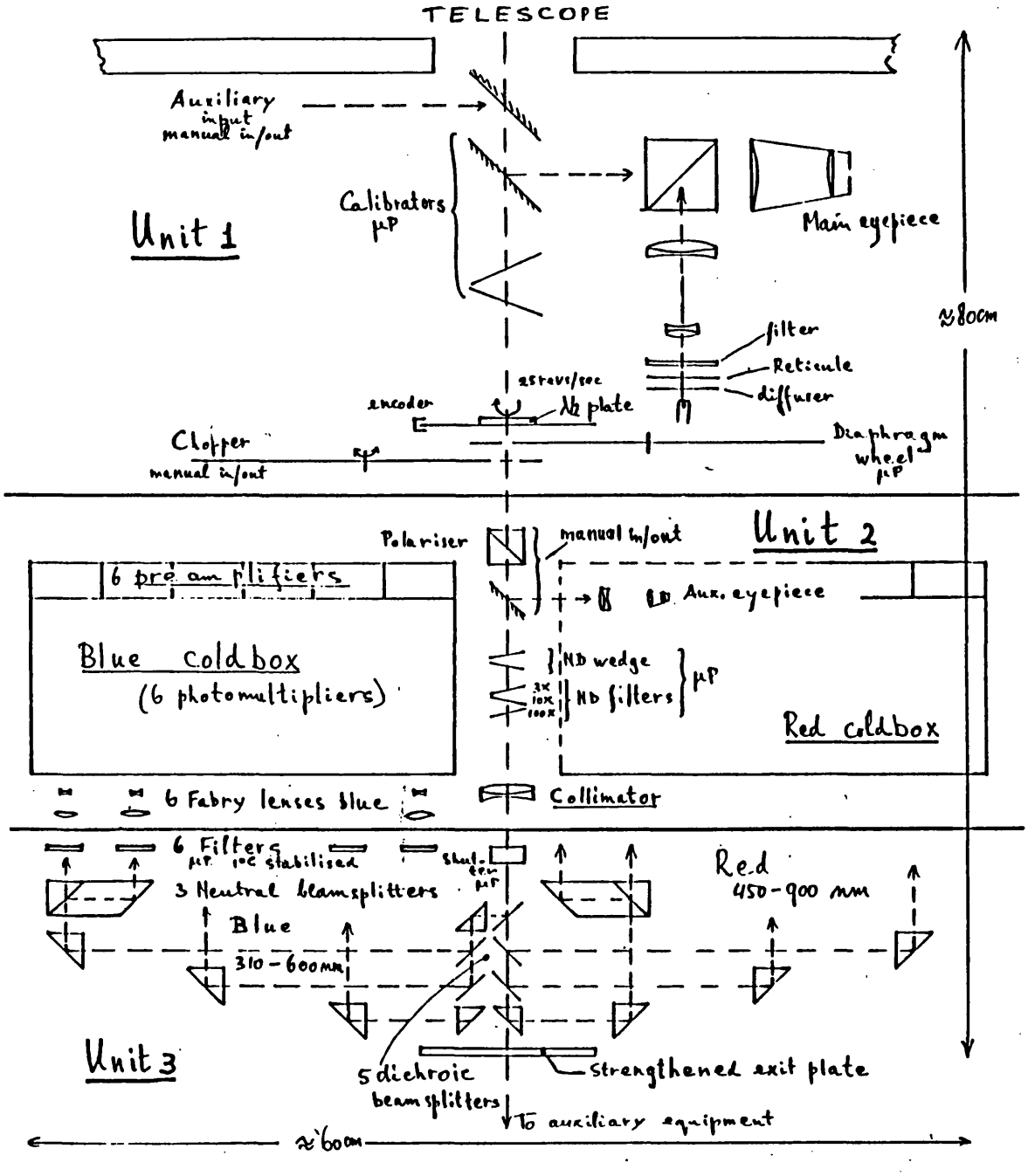

Fig. 5.1 Schematic diagram of the Multi-purpose Fotometer

chosen interference filter and a Fabry lens and being detected by a photomultiplier.

The signal from each photomultiplier is recorded by 16 scalars, each scalar counting charge during a distinct phase interval of the rotation of the half-wave plate. A sinusoidal fit to the total counts of each scalar during the integration then yields the Stokes' Q and U parameters and their error, E. The total intensity, I, is then used to calculate the normalized parameters, q and u, and their error, σ.

Observations could be made with a range of integration times, with each observation containing a set number of repetitive integrations. As the instrument read-out time and subsequent calculation of the Stokes' parameters needed about 5 seconds per integration, it was decided to use integration times as great as possible to reduce time lost for signal recording. Thirty seconds was also used by the instrument at the beginning of each set of repetitions to check that the light level of the target star was not great enough to harm the detectors, using neutral density filters accordingly.

The data acquired by the MPF is displayed in the form of the normalized Stokes' parameters q and u, the standard error in measuring the parameters, σ, the average intensity, I, the calculated polarization, p, and position angle, θ, for each channel. An observation is a repeated set of integrations ranging from 1 to 99 unless a scalar overflow error occurred during an integration which halted the observation.

For the weighted means calculated in Table 5.1 the number of observations for each star ranges from 11 to 61, depending upon how long the star was observed for (40 minutes for o Sco, and between one hour and two hours 30 minutes in other cases), and how much time was lost due to the intermittent overload problems highlighted in the following section.

Problems with the MPF

The first set of observations of ξ Boo A with the initial set-up of dichroic and interference filters showed that there were problems! The count rates in some channels were extremely small compared with others, which could not be explained simply because the wavelength range was not suited to the photomultiplier (six were blue sensitive, the other six red sensitive), or due to low efficiencies of photomultipliers. The filters were chosen to be within the pass bands of the beam as dictated by the dichroic filters, and the photomultipliers were of similar efficiencies in any case. During the course of the first night the setup was altered to attempt to cure this problem, and after a major stoppage due to a slide of neutral density filters becoming stuck on the second night, a further revision of the setup was required.

A further problem occurred that was to persist throughout the week. An intermittent and unaccountable "overload error" in the scalars was reported which halted the set of integrations currently underway. There should have been no overloads in reality as the maximum number of counts for a whole integration of 10.8 seconds never exceeded 1 million (c.f. the maximum number of counts per second should be 1.3 million, or 1.3MHz) even for the brightest star. Despite attempts by technicians to fix this problem no cure was found, the only possible explanation being a sharp increase in brightness due to an atmospheric effect. It was decided to use integration times of only 5.4 seconds after noting that in this case there were fewer instances of these errors. Now, of course, the total intensity during each integration was lower, requiring more observations to get the desired accuracy.

Time was also lost on the first night because of high winds for a total of two hours, on the fourth night due to a persistent problem with the graticule projector light for another two hours, and the whole of the last night was abandoned because high winds did not allow the telescope dome to be opened. As the problems with the MPF required its set-up to be changed, the first two nights

observations were rendered useless.

Seven of the twelve channels were deemed to have useful count rates, those being channels 1, 3, 5, 6, 8, 10 and 12. The most important filters (i.e. those that would give a reasonable spectral coverage in an attempt to highlight the wavelength dependence of polarization due to magnetic intensification) were placed in these channels, and the neutral beam splitters were placed in the 90:10 ratio configuration to favour channels 1, 3, 8, 10 and 12, while a 50:50 ratio was used to split channels 5 and 6 from their parent beam. The other 5 channels' results were not used.

The filter combinations for each channel could be altered between observations as a slide was used to carry 3 filters for each beam which could be electronically set by the observer.

5.3 Observations of Polarized and Unpolarized Standard Stars

o Sco (HD147084)

The polarized standard o Sco was observed on April 28 for 40 minutes. The polarization is due to the interstellar medium, and according to Serkowski (1974) has a maximum value of 4.3% at 6800Å and a position angle of 32° in the equatorial frame. The wavelength dependence is given in equation 1.1. The survey of standard stars by Serkowski gives the K parameter an average value of 1.15. Clarke (1986) obtained values of $p(\lambda_{max}) = 4.5\%$ and $\lambda_{max} = 6700$Å, with the K parameter being equal to 1.47 for this specific star. Figure 5.2 shows that the measurements made with the MPF (shown by circles) agree with those of Clarke (squares) within the errors, and also with the theoretical curve described by the above equation with K and λ_{max} given by Clarke's values. The position angle measured in the instrumental frame of the MPF is 145.7 ± 0.3°, which is not wavelength dependent within the errors. Therefore the position angle of the instrumental frame on this night was 113.7°. These results indicated that the MPF

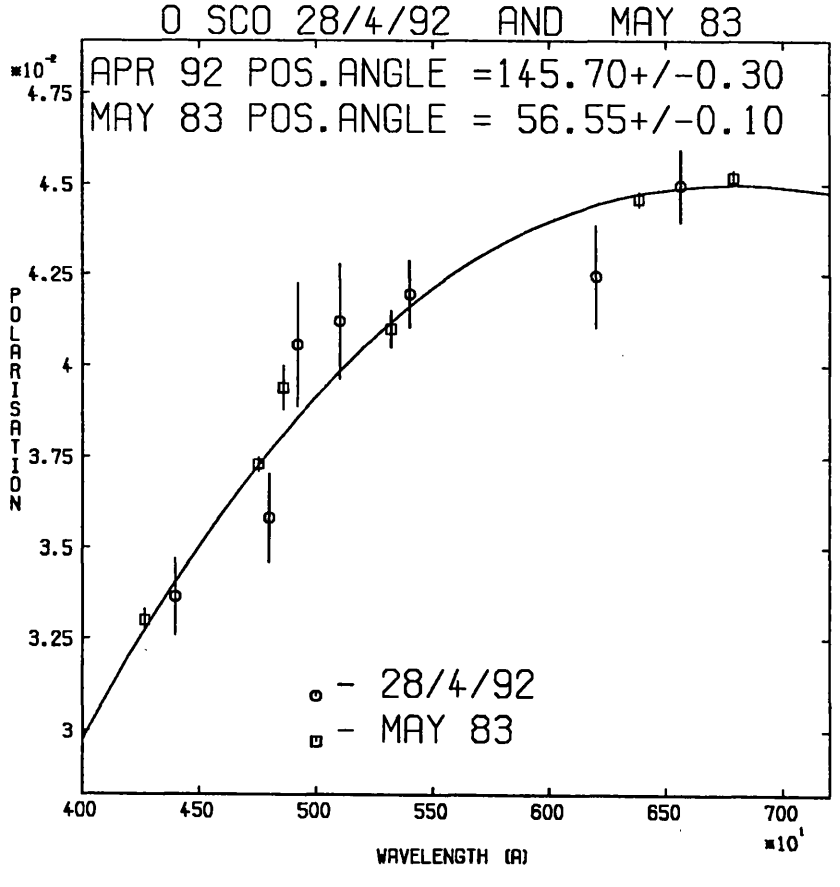

Fig. 5.2 Polarimetric measurements of 55 Cyg, showing that its wavelength dependence agrees with previous data by Clarke (1986)

HD Number	Name	Spectral Type	JD 244 8700+	Filter	q	u	σ
94264	46 LMi	K 0 III	37.421	656/4	+ 139	+ 39	77
				620/10	+ 165	+ 75	91
				540/10	+ 119	- 1	79
				510/10	- 41	- 277	99
				492/10	+ 254	- 76	98
				480/10	+ 141	+ 76	85
				440/10	+ 57	- 117	83
			37.476	656/4	+ 24	+ 5	67
				590/10	- 74	- 187	111
				560/10	+ 19	- 30	68
				510/10	- 152	- 77	85
				502/7	+ 121	- 82	94
				480/10	- 7	+ 6	73
				423/10	- 26	- 143	72
			38.415	656/4	- 242	- 1	59
				620/10	- 208	- 115	70
				540/10	- 271	- 131	58
				510/10	- 167	- 197	75
				492/10	- 159	- 109	76
				480/10	- 199	- 114	65
				440/10	- 157	+ 18	62
			38.467	656/4	+ 80	- 248	63
				590/10	+ 43	- 163	119
				560/10	+ 157	- 181	63
				510/10	- 35	- 457	82
				502/7	- 32	- 188	89
				480/10	+ 148	- 245	68
				423/10	- 130	- 217	68
			39.413	710/10	- 191	- 66	64
				590/10	- 194	+ 128	122
				532/3	- 165	- 60	66
				510/10	- 186	- 132	90
				502/7	- 216	+ 166	98
				480/10	- 171	- 84	72
				423/10	- 234	- 62	73
			39.462	656/4	- 352	- 301	68
				620/10	- 359	- 368	81
				540/10	- 266	- 333	67
				510/10	- 295	- 346	91
				492/10	- 132	- 277	88
				480/10	- 215	- 303	74
				440/10	- 251	- 290	74
95689	α UMa	KOIII	40.434	656/1	+ 130	+ 92	52
				590/10	+ 153	+ 168	58
				532/3	+ 75	+ 146	52
				515/3	- 68	+ 37	59
				502/7	- 95	+ 63	54
				486/5	+ 56	+ 134	56
				423/1	- 13	- 5	69

Table 5.1 Polarimetric Measurements of 46 LMi and α UMa

can measure polarizations of a few percent with standard errors of 0.1% without any apparent problems.

46 LMi (HD94264) and α UMa (HD95689)

The unpolarized standard star 46 LMi was observed on the nights of April 24, 25 and 26 using 2 sets of 7 filters each night, with two or three of the wave bands (4800/100Å and 5100/100Å every night, 6563/40Å two nights) being common to both sets. The weighted means and standard errors of the Stokes' parameters Q/I and U/I for these observations are shown in Table 5.1. It can be seen that some of the measurements in each wave band significantly change not only from night to night but also between observations made on the same night only one hour apart. This behaviour led to an investigation into the drift of the measurements of the Stokes' parameters with time which is described later. For this reason the data for each night will be analyzed separately.

In the following figures the different runs of data acquisition (there were two attempted for each star each night) will be denoted by the labels 24A, 24B, 25A, ... , 27B, and the seven filters will be denoted by the following symbols:

⊙ - 6563/40Å (24A,25A,25B,26B); 6563/8 (27B); 7100/100Å (24B,26A,27A)

∗ - 5400/100Å (24A,25A,26B); 5600/100Å (24B,25B,26A,27A); 5320/30Å (27B)

□ - 4800/100Å (24A,24B,25A,25B,26A,26B,27A); 4860/50Å (27B)

◇ - 6200/100Å (24A,25A,26B); 5900/100Å (24B,25B,26A,27A,27B)

△ - 5100/100Å (24A,24B,25A,25B,26A,26B,27A); 5145/30Å (27B)

⧖ - 4920/100Å (24A,25A,26B); 5020/70Å (24B,25B,26A,27A,27B)

⌑ - 4400/100Å (24A,25A,26B); 4227/100Å (24B,25B,26A,27A); 4227/10Å (27B)

Figures 5.3 (a) and (b) show q,u diagrams for 46 LMi on 24 April. The Welch test was used in this analysis of the seven filter data to test the Stokes' parameters for spectral dependence. Here the u values vary at the 95% level in

(a). The weighted mean values for the two sets of data are departed by more than two standard errors in the q direction.

Similarly, figures 5.4 (a) and (b) show the data for 25 April. The Welch test shows a spectral difference in q for (b) at the 95% confidence level. The weighted means are departed by more than 4 standard errors in q, and more than 2.5 standard errors in u. The change in the Stokes' parameters can be seen from two measurements made with the same filter. For filter 6563/40Å the two q values are: (a) - 0.242 ± 0.059 % and (b) + 0.080 ± 0.063 %, a difference of 2.6 standard errors (σ). This large difference is also seen for filter 4800/100Å. As the two data sets were recorded successively it suggests a problem with the telescope or instrument as the stellar polarization should not change by 0.3% in one hour, it should remain unchanged!

A similar change is seen on 26 April, shown in figures 5.5 (a) and (b). The Welch test shows no spectral difference between the seven data points in either (a) or (b), but the two weighted mean values of each seven filter set are departed by 6 standard errors in u. For filter 4800/100Å the u values are separated by more than two standard errors.

The six sets of data from the three nights can now be compared. Figure 5.6 shows the relative positions of the weighted mean values. If the weighted means of each set describe the instrumental polarization at the time of the measurement then it is seen that the instrumental polarization drifts erratically between observations. The two measurements made on 24 April (24A and 24B) are departed in q by 2.08σ, those of 25 April (25A and 25B) are departed by 4.79σ in q and 2.65σ in u, and those of 26 April (26A and 26B) by 5.91σ in u. It may be possible that the instrumental polarization of the telescope/instrument system may change over the course of weeks or months due to seasonal temperature changes or altering the instrument, but it should not change abruptly day-to-day or even hour-to-hour. Therefore it has to be concluded that the instrumental polarization is too unstable to measure low levels of polarization with the low photon count rates

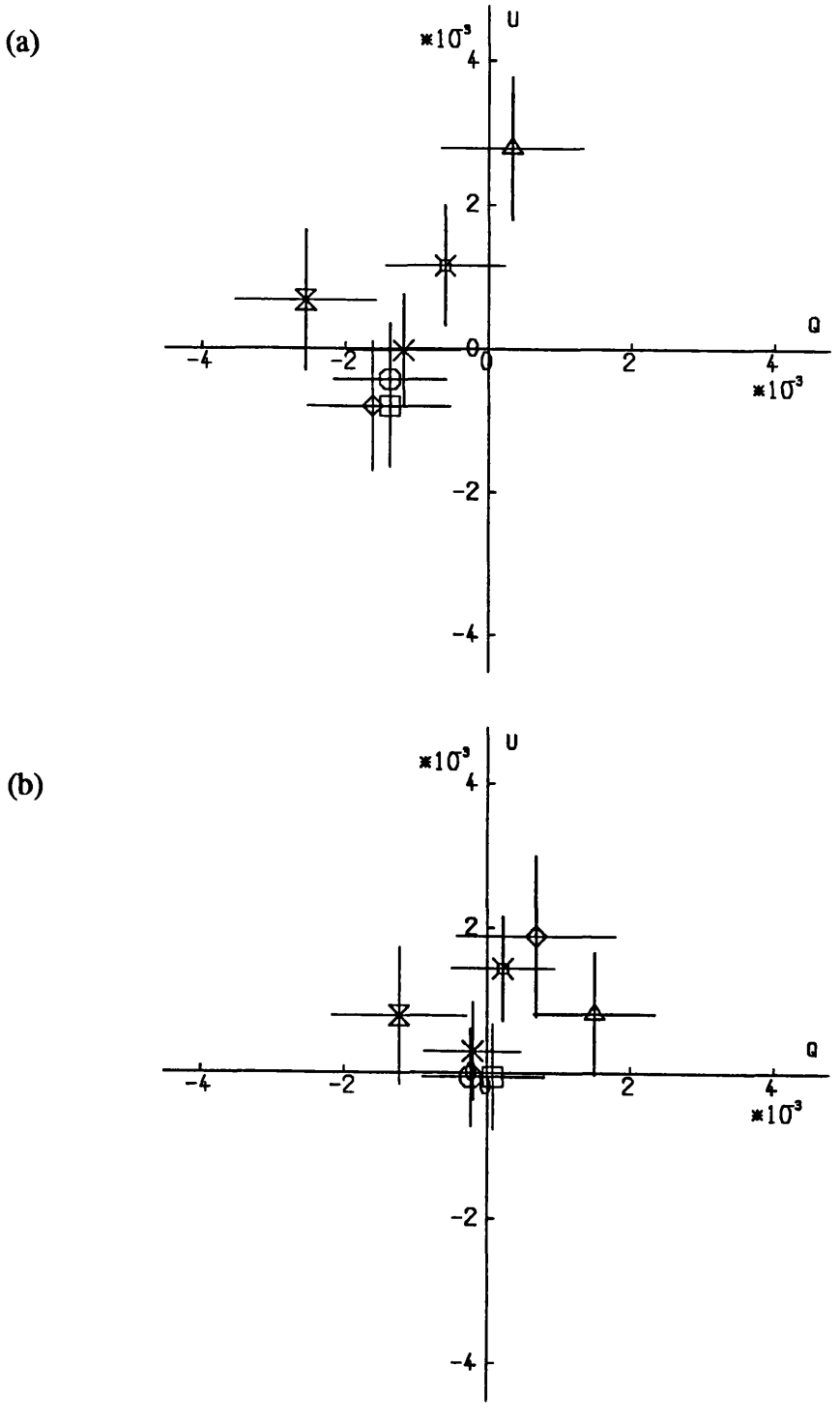

Fig. 5.3 *q*,*u* diagram showing the two sets of seven filter data of 46 LMi measured on 1992 April 24.

(a)

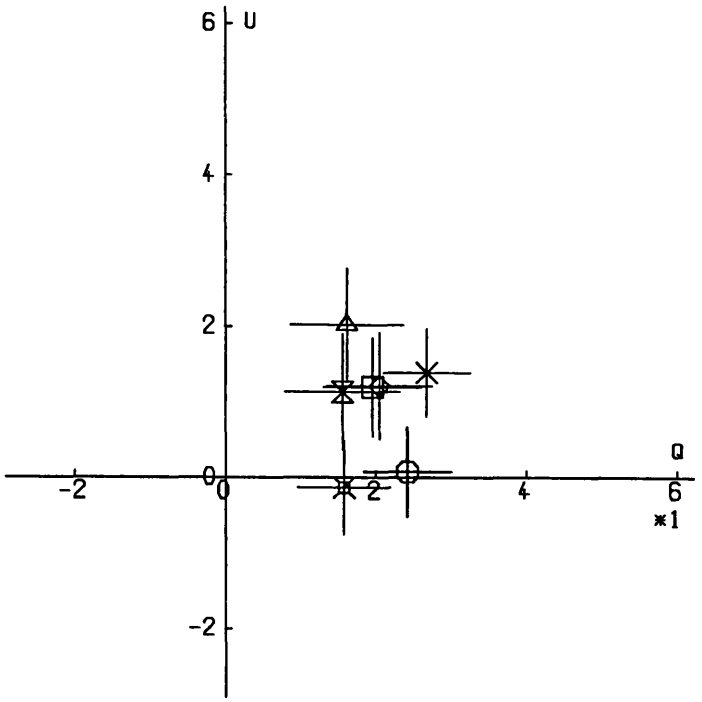

(b)

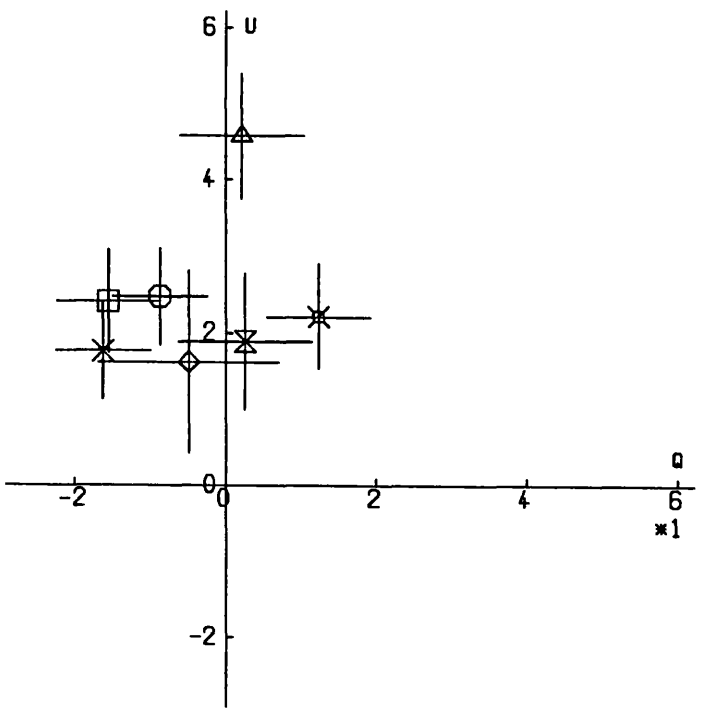

Fig. 5.4 *q*,*u* diagram showing the two sets of seven filter data of 46 LMi measured on 1992 April 25.

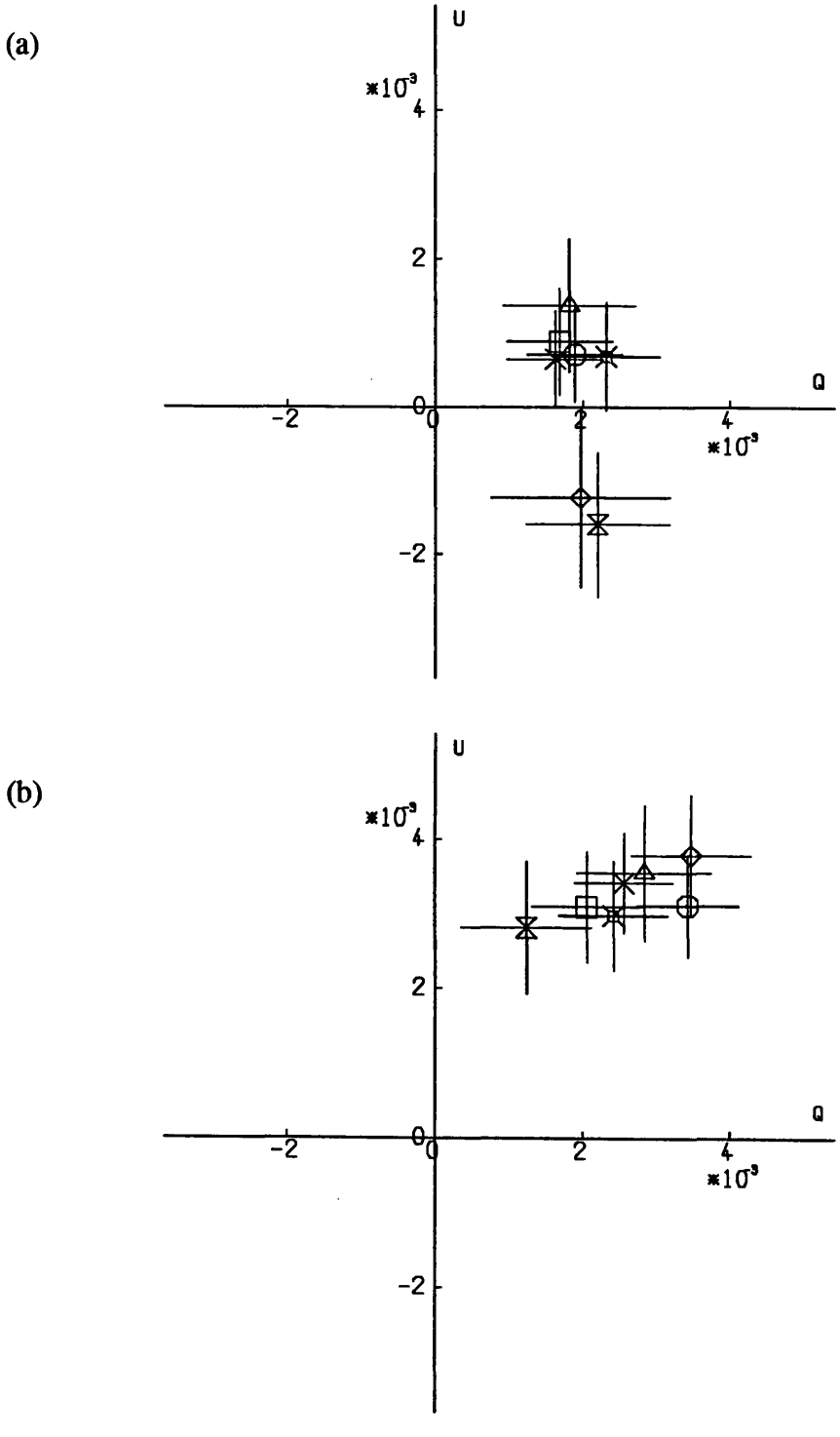

Fig. 5.5 *q,u* diagram showing the two sets of seven filter data of 46 LMi measured on 1992 April 26.

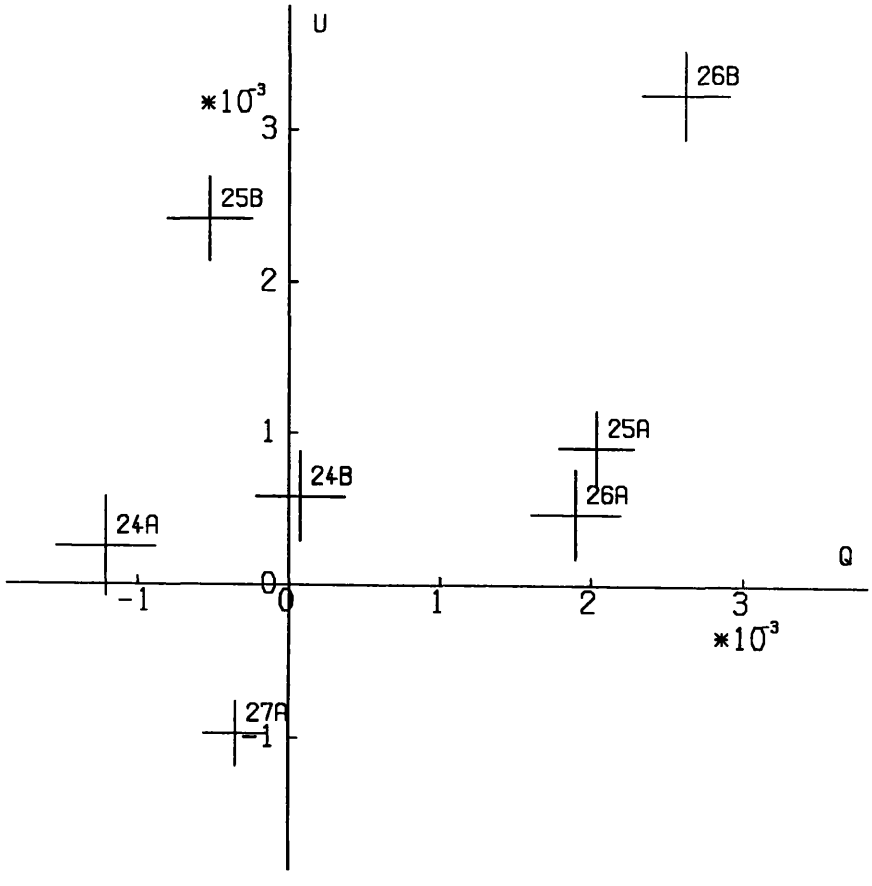

Fig. 5.6 *q*,*u* diagram showing the weighted mean values of each of the six sets of seven filter data of 46 LMi measured between 1992 April 24 - 26, designated 24A to 26B, and the mean of the data for α Uma from 1992 April 27 for comparison (27A).

that were encountered. It can also be noted that higher photon count rates resulted in overload errors from the scalars.

α UMa was observed on the night of 27 April using 7 filters, and the weighted mean of those seven values is also shown in figure 5.6. Two filters were the same as used for 46 LMi (5900/100Å and 5020/70Å), three had the same central wavelength but with narrower passbands (6563/8Å, 4860/50Å and 4227/10Å), and two other narrow band filters were used (5145/30Å and 5320/30Å). The Welch test shows a spectral variation in q at the 95% level of confidence. The weighted mean is significantly departed from the 46 LMi measurements except for those of run 24A. This confirms the erratic behaviour of the instrumental polarization.

5.4 Observations of ξ Boo A and χ Her

ξ Boo A was observed every night with two runs possible on each of the last three nights. χ Her (HD142797) was observed only on April 24, 26 and 27, with two runs being possible on the 26th. The normalized Stokes' parameters are shown in Tables 5.2 and 5.3 for ξ Boo A and χ Her respectively. The results will be treated night-by-night and compared to the unpolarized standard star measured that night with the same seven filter set, both collectively and for each filter.

April 24 (A)

Figure 5.7 shows the measurements of ξ Boo A and χ Her relative to that of 46 LMi for each of the seven filters used in this run. For ξ Boo A the Welch test shows no variation between spectral points, but in the case of χ Her the u parameter shows a variation at the 99% level. The weighted mean of ξ Boo A departed by 2.39-σ from that of 46 LMi in the q parameter. For filter 5100/100Å, the measurement of ξ Boo A departed by 2.5-σ in u from that of 46 LMi, while that of χ Her is 2.3-σ from 46 LMi in u.

April 25 (A)

Figure 5.8 similarly shows the measurements of the three stars for each filter. The Welch test shows a variation in u at the 95% confidence level for

HD NUMBER	NAME	SPECTRAL TYPE	JD 244 8700+	FILTER	q	u	σ
131156A	ξ Boo A	G8V	37.615	656/4	+ 40	+ 46	43
				620/10	- 33	+ 33	58
				540/10	+ 29	+ 45	41
				510/10	- 49	+ 74	62
				492/10	- 20	- 22	63
				480/10	- 15	- 46	49
				440/10	- 26	+ 5	44
			38.551	656/4	- 89	- 29	54
				620/10	- 159	- 79	76
				540/10	- 111	- 110	50
				510/10	+ 22	- 125	83
				492/10	- 172	- 63	82
				480/10	- 38	- 265	61
				440/10	- 74	- 47	57
			38.592	656/4	+ 138	- 46	94
				590/10	+ 93	- 341	233
				560/10	+ 89	+ 143	92
				510/10	- 143	+ 73	148
				502/7	+ 74	+ 397	168
				480/10	+ 133	- 164	108
				423/10	+ 65	- 112	101
			39.540	710/10	- 240	+ 69	51
				590/10	- 361	+ 178	127
				560/10	- 245	- 22	55
				510/10	- 405	+ 21	86
				502/7	- 505	- 132	98
				480/10	- 124	- 47	64
				423/10	- 344	+ 88	60
			39.601	656/4	+ 118	- 28	54
				620/10	+ 1	+ 15	77
				540/10	+ 44	- 50	52
				510/10	+ 79	- 164	83
				492/10	- 65	+ 58	82
				480/10	+ 109	+ 36	62
				440/10	+ 34	- 3	57
			40.573	656/4	- 26	- 14	52
				620/10	- 15	+ 75	72
				540/10	+ 4	+ 17	49
				510/10	- 90	- 217	80
				492/10	- 34	- 107	80
				480/10	+ 23	- 8	59
				440/10	- 90	- 7	54
			40.636	710/10	+ 45	+ 23	49
				590/10	- 394	+ 192	125
				560/10	+ 123	+ 23	51
				510/10	+ 95	+ 48	81
				502/7	+ 29	- 209	94
				480/10	+ 29	+ 26	59
				423/10	+ 185	+ 23	57

Table 5.2 Polarimetric Measurements of ξ Boo A

HD NUMBER	NAME	SPECTRAL TYPE	JD 244 8700+	FILTER	q	u	σ
142373	χ Her	F 9 V	37.740	656/4	+ 40	- 48	41
				620/10	- 34	- 124	57
				540/10	- 23	- 78	38
				510/10	+ 89	+ 48	59
				492/10	+ 103	- 173	61
				480/10	+ 28	- 63	45
				440/10	+ 55	- 125	41
			38.735	656/4	- 12	+ 109	124
				620/10	+ 114	- 255	170
				540/10	- 18	- 134	118
				510/10	+ 163	- 223	175
				492/10	- 125	- 115	179
				480/10	+ 248	+ 64	138
				440/10	+ 77	- 219	122
			39.674	710/10	- 444	+ 91	51
				590/10	- 427	+ 117	124
				560/10	- 373	- 40	51
				510/10	- 480	+ 123	80
				502/7	- 538	- 367	90
				480/10	- 388	- 46	61
				423/10	- 337	+ 108	57
			39.734	656/4	+ 40	+ 47	58
				620/10	- 180	+ 71	79
				540/10	+ 37	+ 56	54
				510/10	+ 91	+ 277	84
				492/10	- 19	- 16	84
				480/10	+ 33	+ 55	64
				440/10	+ 47	- 39	57
			40.740	710/10	+ 39	- 70	42
				590/10	- 45	- 186	115
				560/10	+ 105	- 81	45
				510/10	- 108	- 28	70
				502/7	+ 326	- 351	82
				480/10	+ 20	- 40	52
				423/10	- 69	- 103	48
147084	o Sco	A 5 II	40.667	656/4	+1695	-4174	99
				620/10	+1602	-3950	141
				540/10	+1529	-3952	92
				510/10	+1686	-3666	158
				492/10	+1281	-3930	169
				480/10	+1262	-3464	122
				440/10	+1142	-3215	107

Table 5.3 Polarimetric Measurements of χ Her

ξ Boo A. The weighted mean of q for ξ Boo A departed by 2.45-σ from that of 46 LMi, and that of χ Her is 3.43-σ from 46 LMi. For filter 4800/100Å the measurement of q for χ Her departed by 2.2-σ from 46 LMi.

April 25 (B)

Figure 5.9 shows the measurements of 46 LMi and ξ Boo A for each filter. The Welch test indicates a variation in u at the 99% confidence level for ξ Boo A. The weighted mean of u for ξ Boo A departed by 3.66-σ from that of 46 LMi. For three filters, 5600/100Å, 5100/100Å and 5020/70Å, the u parameters of ξ Boo A departed from those of 46 LMi by more than 2-σ.

April 26 (A)

Figure 5.10 shows the measurements of the three stars for each filter. For the weighted means in the q parameter, ξ Boo A departed by 1.59-σ from 46 LMi, χ Her by 4.03-σ. The Welch test shows that for ξ Boo A the q values vary at the 95% confidence level, with the u values varying at the 99% level, but χ Her shows no spectral variation. χ Her departed from 46 LMi by 2.18-σ in q for filter 7100/100Å, and by 2.1-σ in u for filter 5020/70Å, and ξ Boo A departed by 2.71-σ in u for filter 5020/70Å.

April 26 (B)

Figure 5.11 shows the measurements of the three stars for each filter. This set of observations show the largest measurements of the Stokes' parameters compared to the unpolarized star. For ξ Boo A the weighted mean departed by 6.24-σ in q and 6.57-σ in u, while for χ Her the q parameter departed by 5.42-σ and u by 6.83-σ. For individual filters, five measurements of q for ξ Boo A departed from those of 46 LMi by more than 2-σ with that of filter 6563/40Å being 3.78-σ, while in the u parameter five departed by more than 2-σ with that of 6200/100Å being 3.23-σ. In the case of χ Her, three measurements of q departed by more than

2-σ with that of filter 6453/40Å being 3.1σ, and for u five departed by more than 2-σ with those of 6200/100Å and 5100/100Å being 3.25-σ and 3.54-σ respectively.

April 27 (A)

On this date α UMa was used as the unpolarized standard star, and its measurements in the chosen passbands are shown with those made on the same night of ξ Boo A and χ Her in figure 5.12. The measurement that stands out is that of χ Her at 5020/70Å which departed by more than 3-σ in both q and u, whereas only one other measurement (5600/100Å in the u parameter) departed by more than 1-σ. None of ξ Boo A's measurements are significant.

April 27 (B)

Narrow bands were used in some channels for these observations of α UMa and ξ Boo A, but as is shown in figure 5.13 there is only one significant measurement, that at 5900/100Å in q, a departure of 3-σ.

In many cases we see significant differences between the normalized Stokes' parameters for the target stars compared to the unpolarized standard measured that night. This suggests that ξ Boo A and χ Her do exhibit intrinsic polarization. As Welch tests on the values from the seven filters yield instances of spectral variation then it is also possible that a wavelength dependence has also been detected. However the following section shows serious flaws in the data that cast a severe doubt on the results being meaningful.

5.5 Correlation and Regression Analysis

The data were tested for correlations by comparing the Stokes' q (or u) parameters in different pairs of wave bands during each observation run. The results showed that both the q and u parameters were correlated with greater than

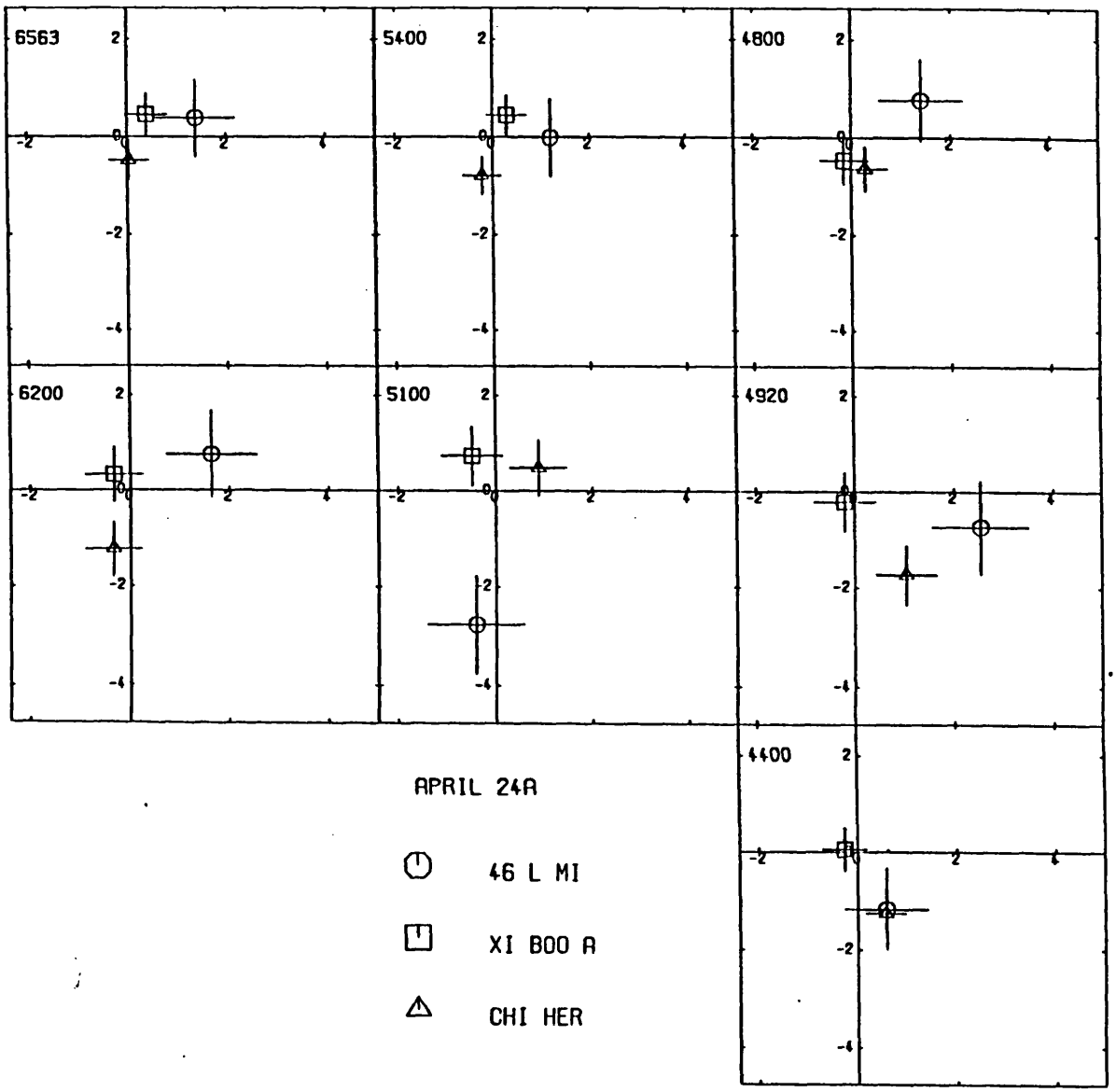

Fig. 5.7 *q*,*u* diagrams showing the measurement of all stars measured in each filter of this seven filter set on 1992 April 24, run A.

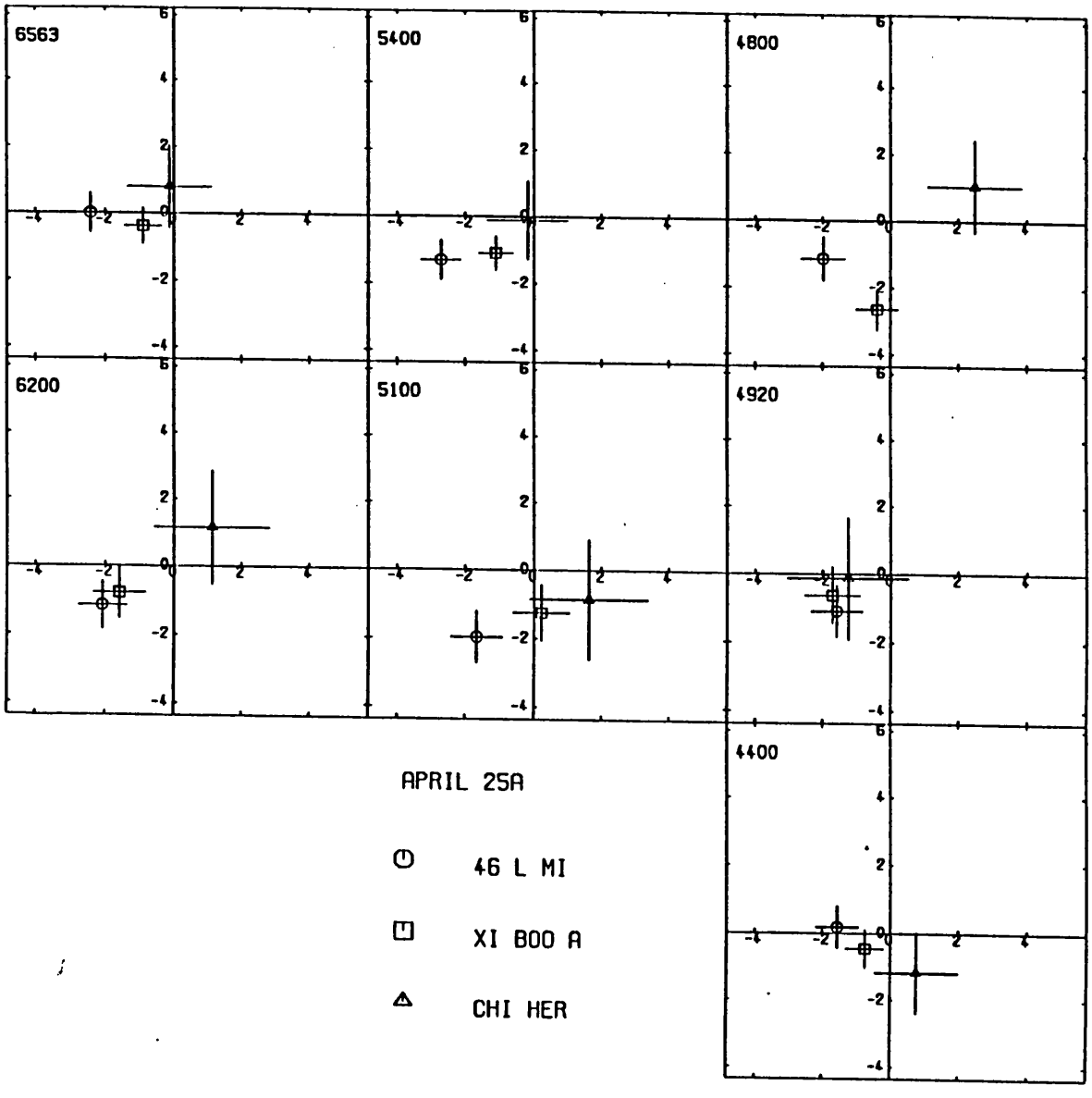

Fig. 5.8 As for figure 5.7 for measurements made on 1992 April 25, run A.

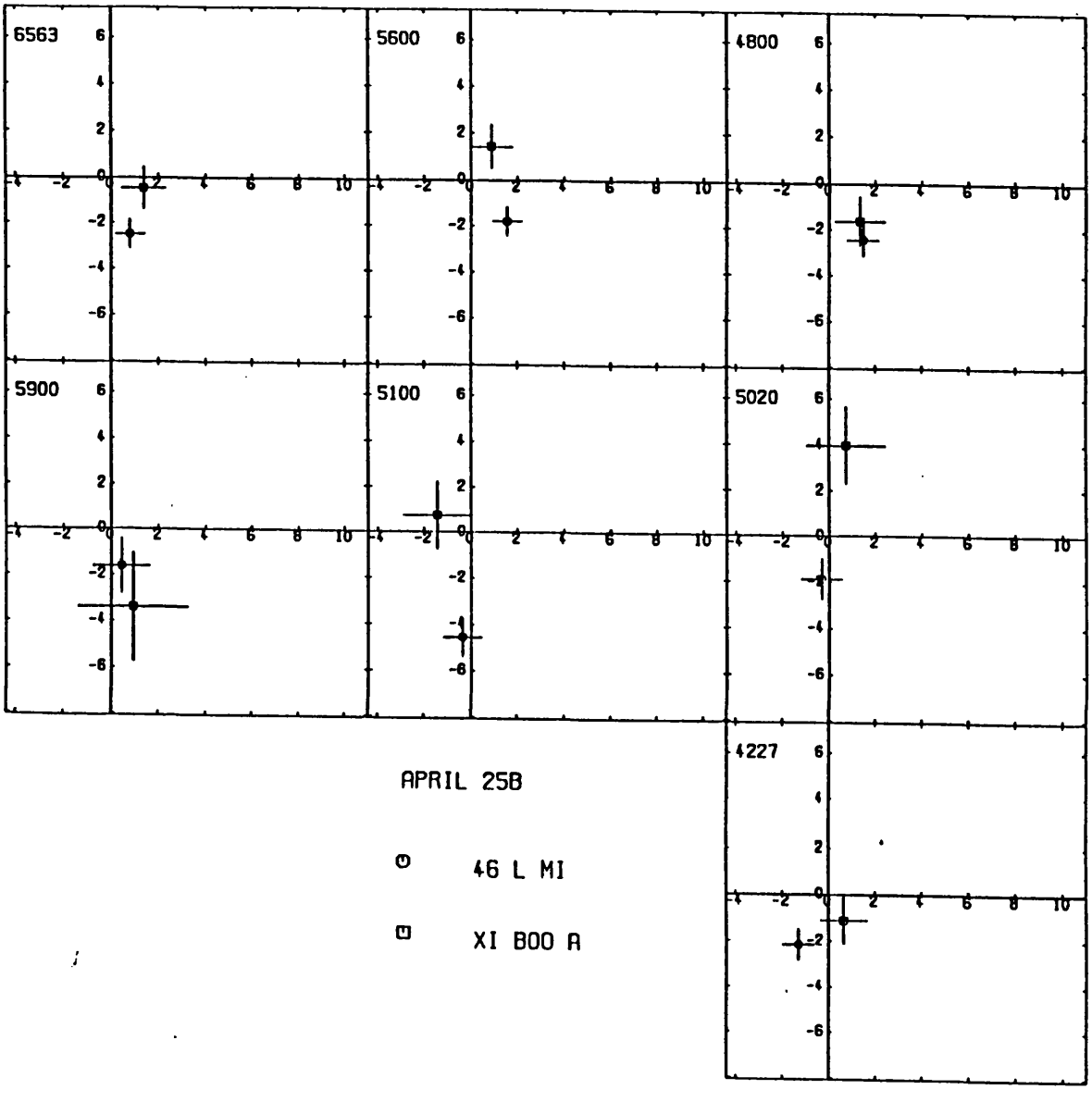

Fig. 5.9 As for figure 5.7 for measurements made on 1992 April 25, run B.

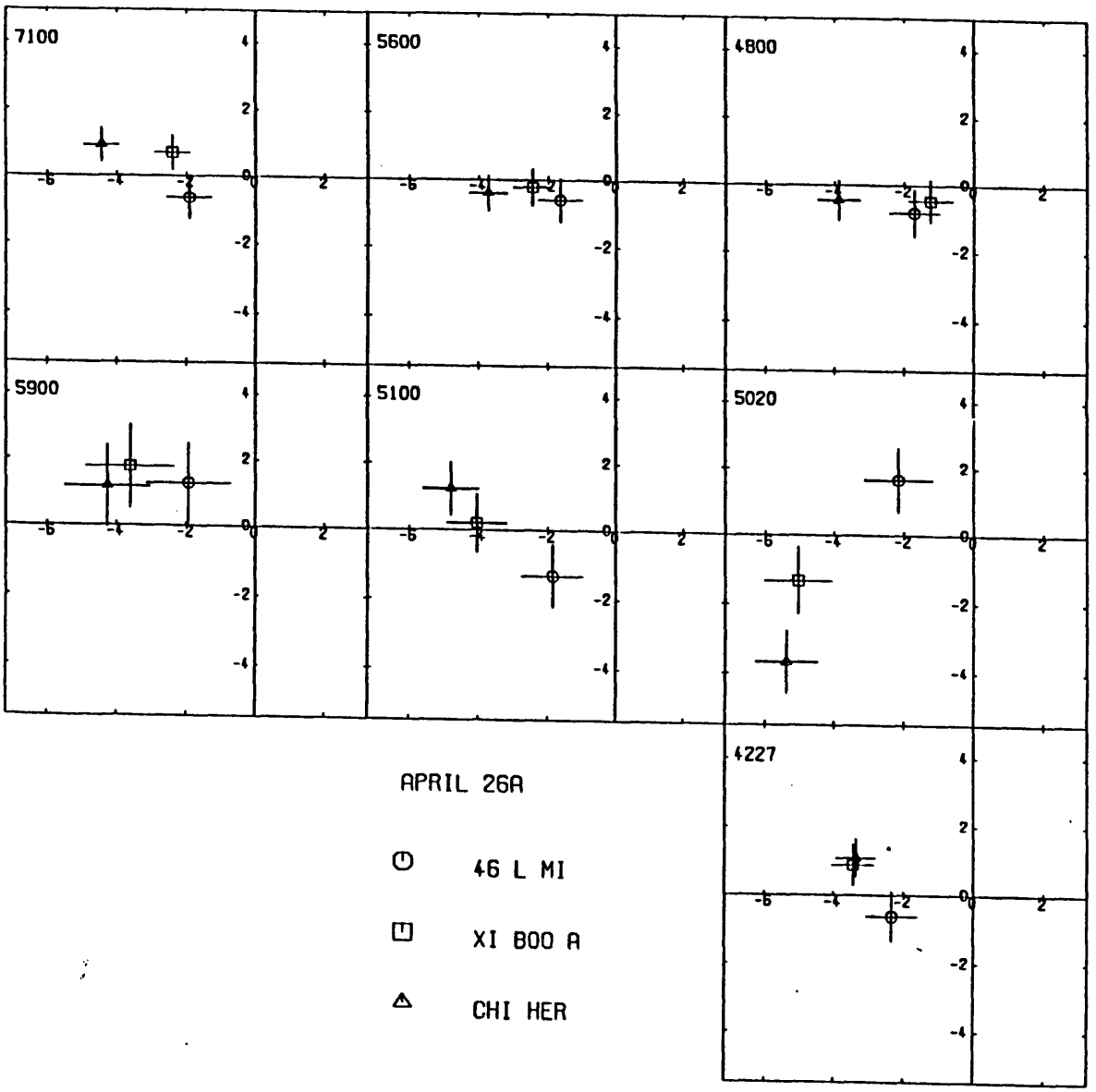

Fig. 5.10 As for figure 5.7 for measurements made on 1992 April 26, run A.

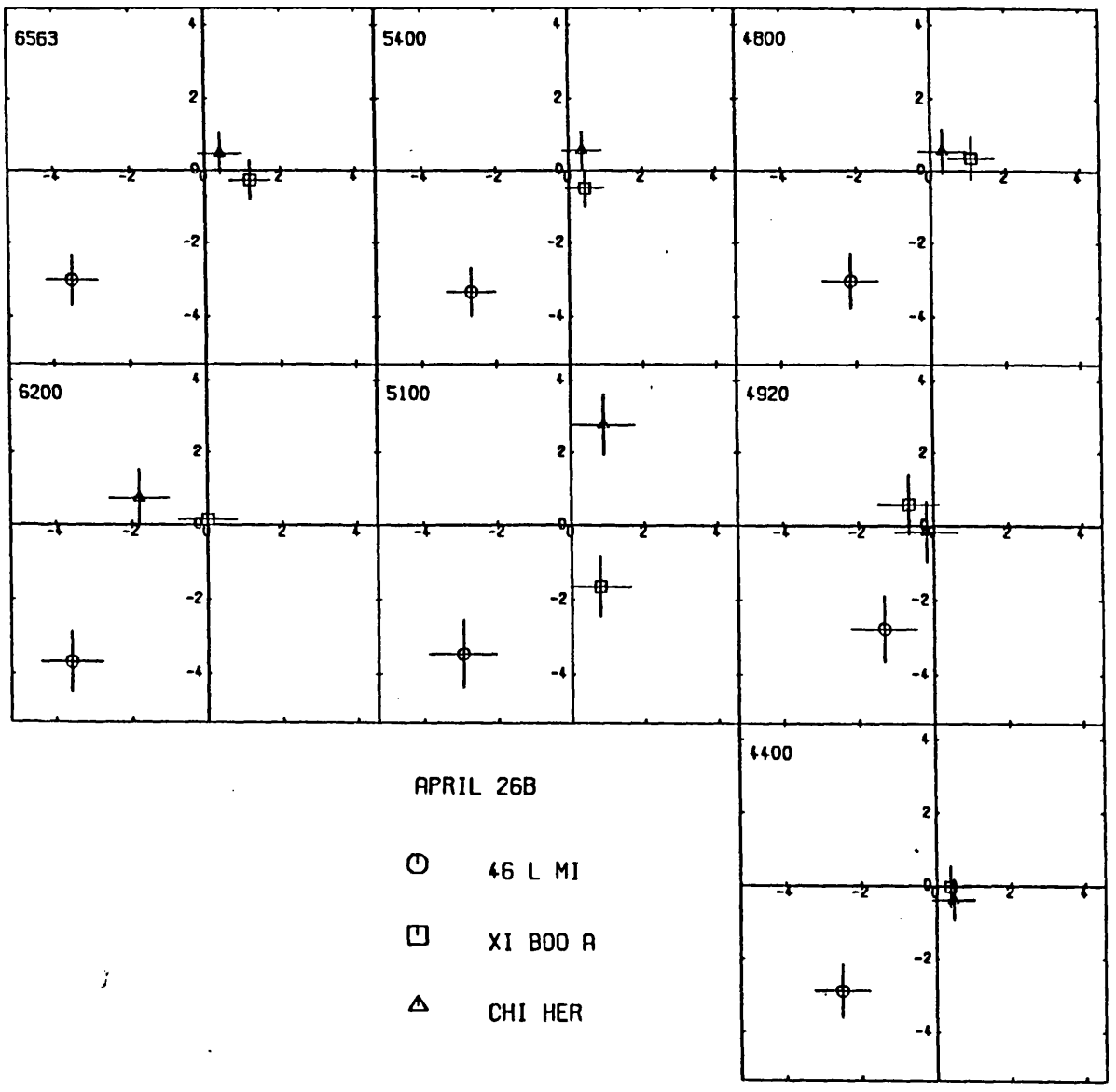

Fig. 5.11 As for figure 5.7 for measurements made on 1992 April 26, run B.

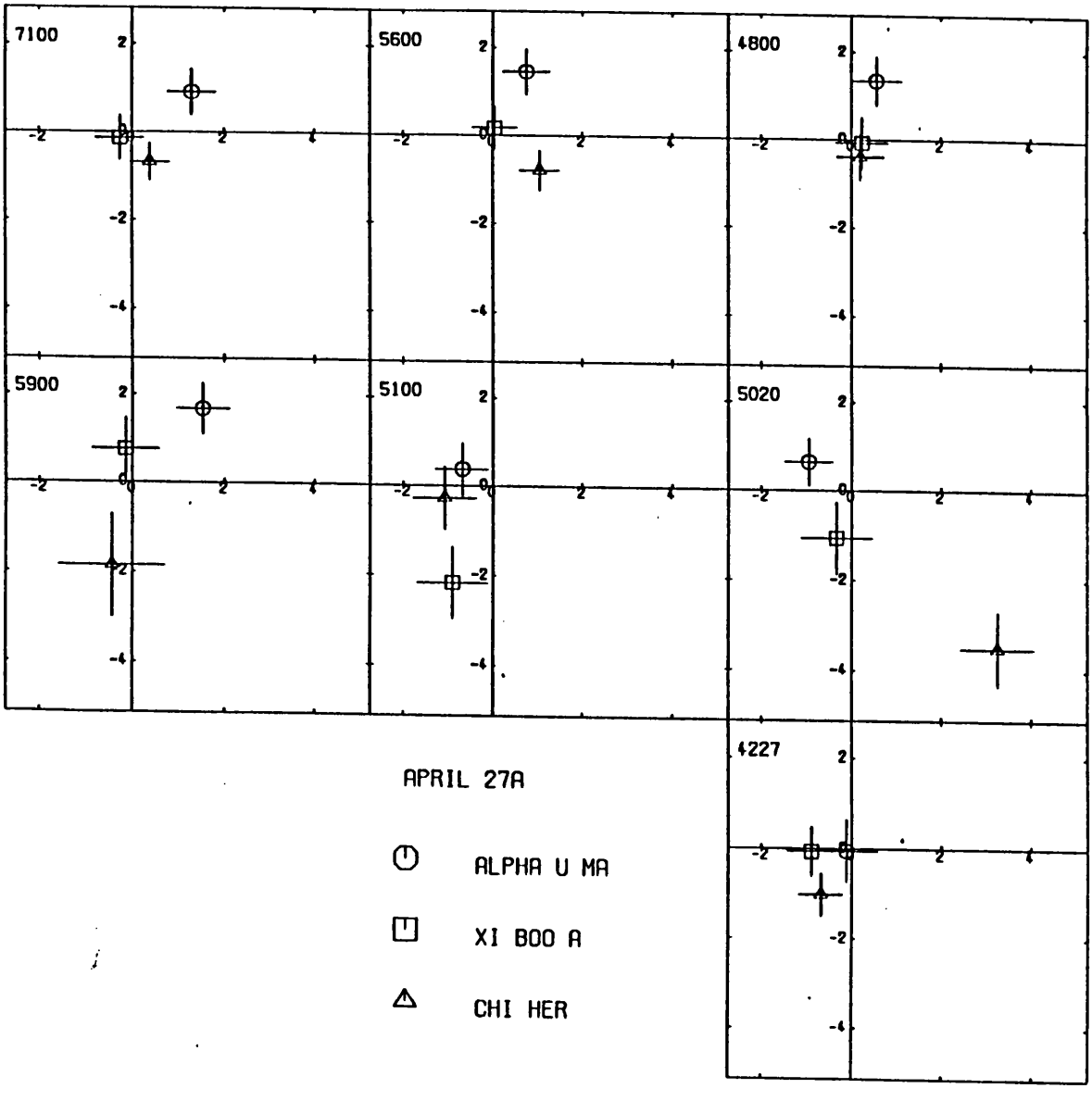

Fig. 5.12 As for figure 5.7 for measurements made on 1992 April 27, run A.

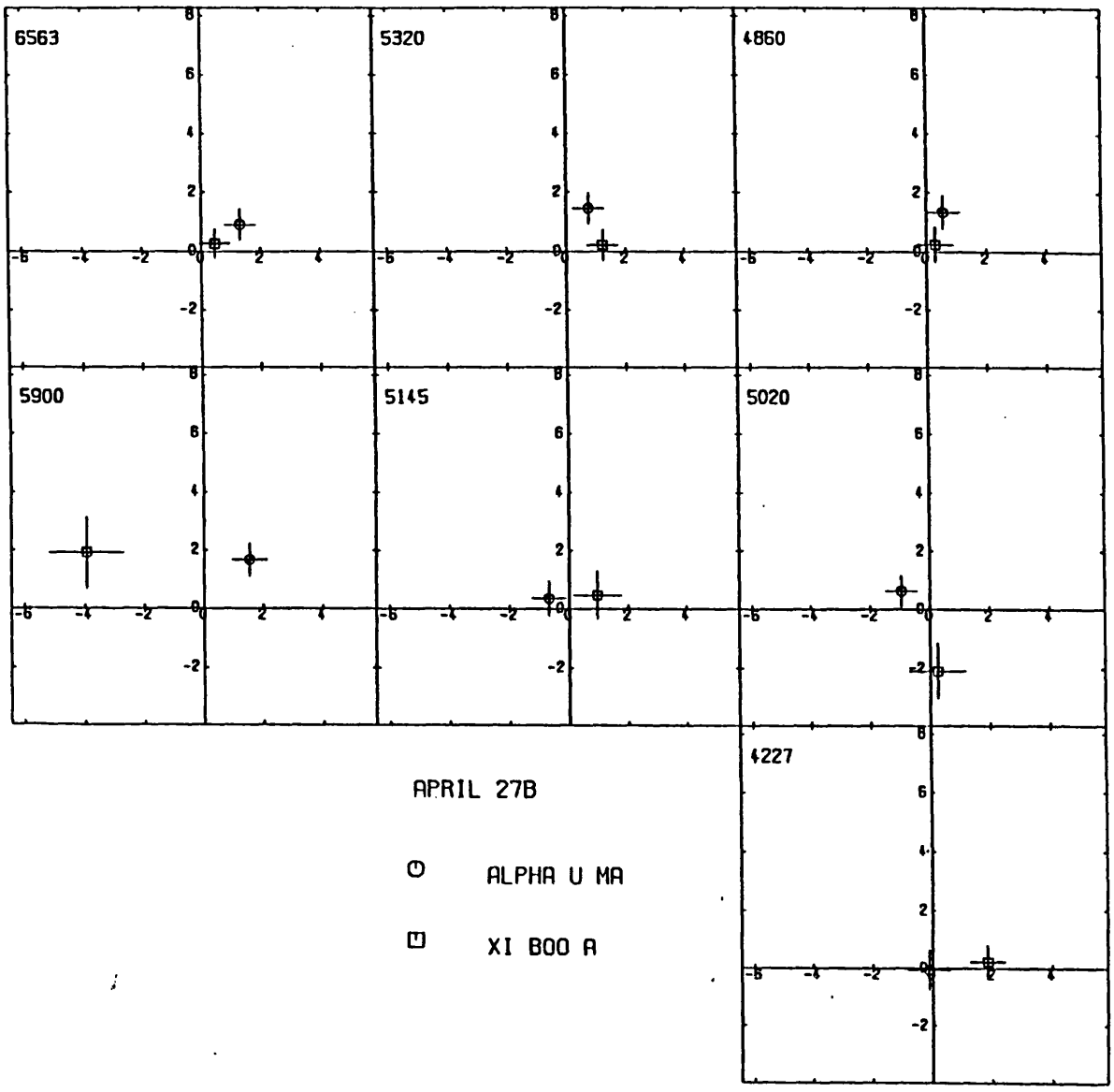

Fig. 5.13 As for figure 5.7 for measurements made on 1992 April 27, run B.

95% confidence in many cases during each set of observations of both 46 LMi and α UMa. A possible cause of these correlations is scintillation noise with frequencies greater than the modulation frequency of the half-wave plate in the MPF (100Hz), the bright star α UMa shows greater correlations than the fainter stars as scintillation noise increases with increasing brightness. Also, the wandering of the star in the diaphragm may cause some correlation, and this property is described later.

As the MPF is known to have a zero-point instability, and the data for 46 LMi changed from night-to-night, it was decided to investigate how the normalized Stokes' parameters varied during each set of observations. Regression analysis was performed using a Numerical Algorithms Group routine to see if the Stokes' parameters calculated from each repetition of integrations varied with respect to the hour angle at the time of observation. The regression coefficient divided by its calculated standard error can be tested as a t-distribution with N-1 degrees of freedom, where N is the number of observations made. Table 5.4 shows that for all stars there are significant drifts in many passbands above the 95% confidence level, some of which being above the 99% level. This suggests that the instrumental polarization drifts over a period of as little as an hour. As the slopes of the regression lines are negative when a star is observed before the meridian and positive afterwards, except in four cases, the drift may depend upon the hour angle of the star being observed (i.e. its position in the sky).

One observation of α UMa was made as it crossed the meridian. It can be seen from the graphs of q and u against hour angle for the filter 6563/8Å (figures 5.14 (a) and (b)) that the drift may be better described by a polynomial fit than a regression line, *i.e.*

$$q = q_0 + q_1 h + q_2 h^2 + \ldots + q_n h^n \quad \text{(and similarly for } u\text{)} \qquad (5.2)$$

where h is the hour angle of the star during the observation, and q_n are the

JD 244 8700+	Star	Run	Number of wave bands with significant drifts above confidence levels						Gradient of slope		Hour Angle
			q	95%	99%	u	95%	99%	q	u	
37.421	46 LMi	A						1		-	-
37.476		B					1			+	+
37.615	ξ Boo A	A		2					+		-
37.740	χ Her	A					2			+	+
38.415	46 LMi	A			5				-		-
38.467		B		1	4			2	+	+	+
39.413	46 LMi	A		1	1		1	2	-	-	-
39.462		B		1			2	1	+	+	+
39.540	ξ Boo A	A		1	3		1	3	-	-	-
39.674	χ Her	A		2	3				+		+
40.573	ξ Boo A	A		2			3		+	-	-
40.636		B		1					-		+
40.740	χ Her	A					0	1		-	+

Table 5.4 Results of regression analysis showing that in many instances both the q and u parameters exhibit significant drifts at greater than the 95% confidence level.

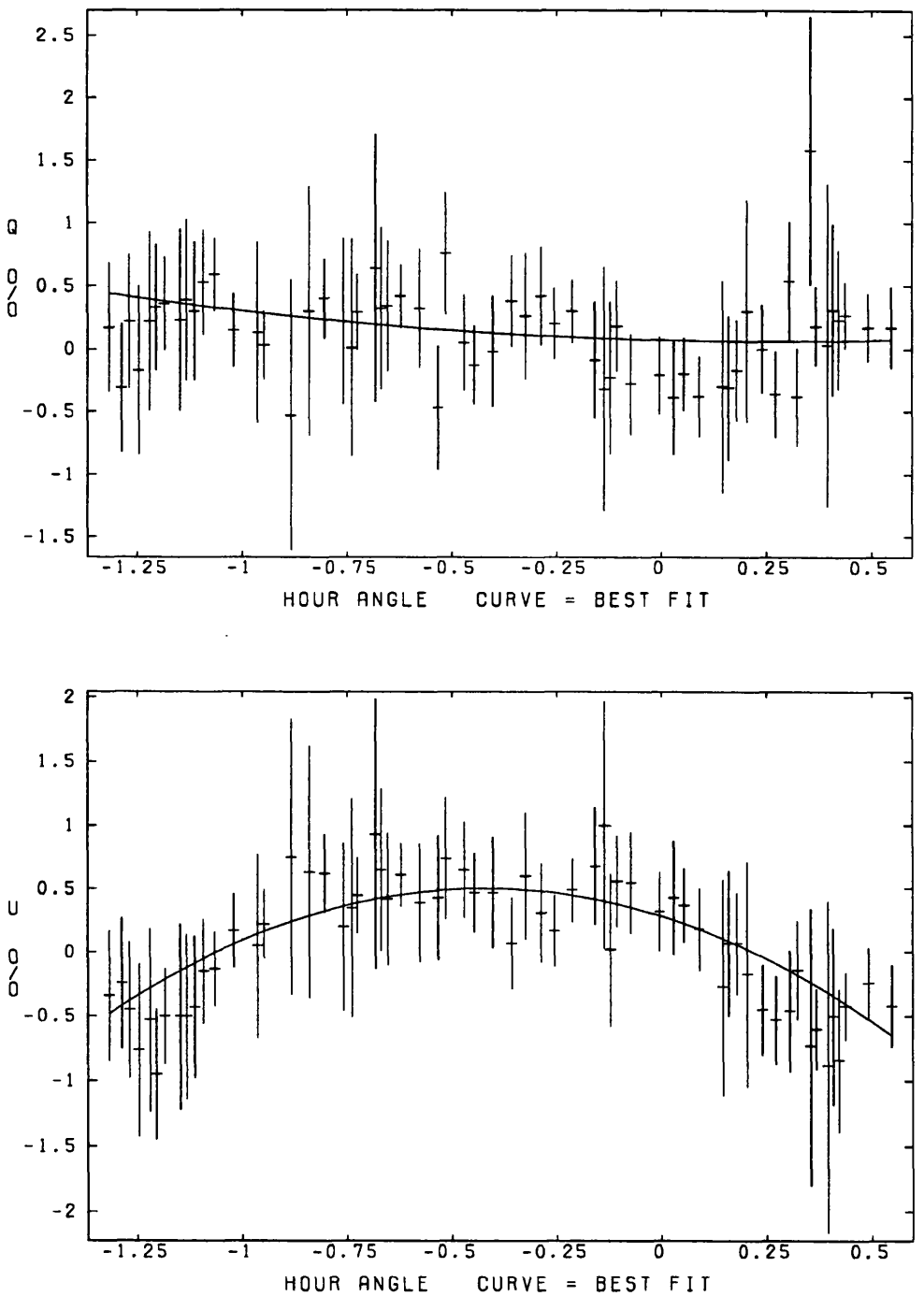

Fig. 5.14 The drift of the Stokes' parameters q (above) and u (below) during an observation of α Uma on 1992 April 27 at 6563/8Å, showing a seemingly smooth curve in u but a possible sinusoidal behaviour in q.

polynomial coefficients. The coefficients of a polynomial of order 2 (i.e. a quadratic in h) were calculated for those observations that showed a significant drift by calculating the Chebyshev co-efficients from the q (or u) values using the NAG routine E02ADF, and converting them into polynomial co-efficients using routines taken from the "Numerical Recipes, The Art of Scientific Computing" (see ref.). The curve defined by these polynomial co-efficients could then be drawn through the data, and the value of the hour angle at the minimum or maximum of the curve could be calculated by differentiation.

The hour angles at which the Stokes' parameters reached a minimum or maximum value are shown in Table 5.5. It can be seen that most of the maxima or minima occur between 40 and 20 minutes before the star reaches the meridian. It is an extreme example of this drift which is shown in figures 5.14 (a) and (b), where the degree of the Stokes' parameters vary by a few percent during 1 hour 20 minutes. Such "quadratic" drifts are not seen for all observations made, however, and for those that do exhibit this effect, the hour angle at which the Stokes' parameters reach a maximum or minimum cannot be shown to be at any particular time. Also the drift does not appear to be due to whether or not the telescope is viewing north or south of the zenith.

A possible cause of this drift, as explained in the MPF users' manual, is due to the star moving in the diaphragm during the observations. As the auto-guiding on the JKT cannot be used with the MPF, the star has to be re-centered during the observing run. This was done every 10 minutes on average, but it was noticed that the star did not wander very much during the half-hour that it passed the meridian. According to the manual, '...this polarization zero-point shift (due to the star moving across the diaphragm) seems to be independent of wavelength or channel to well below 0.1%...'. This effect may be the cause of the correlations between the data, but the degree of variation suggested is much smaller than has been observed. If the drift is attributable to the star drifting in the diaphragm, then the Stokes' parameters should not vary by more than 0.1%

JD 244 8700+	Star	Filter	Stokes' Parameter	Hour Angle at Min or Max (h)	N=Min X=Max
37.421	46 LMi	620/10	u	0.295	N
		440/40	q	0.142	N
37.476	46 LMi	560/10	q	0.922	X
		560/10	u	0.867	N
37.740	χ Her	440/10	q	1.552	N
38.415	46 LMi	656/4	q	-1.485	X
		620/10	q	-2.693	X
38.467	46 LMi	656/4	q	1.215	X
		656/4	u	0.688	N
		560/10	q	1.249	X
		560/10	u	-2.644	N
		480/10	q	1.048	X
39.462	46 LMi	656/4	u	4.307	X
		620/10	u	-0.037	N
		540/10	u	-1.381	N
		480/10	u	-0.025	N
39.540	ξ Boo A	710/10	q	-0.881	N
		560/10	q	-0.795	N
		423/10	q	-0.882	N
39.674	χ Her	710/10	q	-0.931	N
		710/10	u	0.756	N
		590/10	q	1.615	X
		560/10	q	1.555	X
		560/10	u	0.707	N
		510/10	q	0.909	X
		510/10	u	0.747	N
		480/10	u	0.667	N
		423/10	q	1.068	X
		423/10	u	0.688	N
40.667	α UMa	656/.8	q	0.252	N
		656/.8	u	-0.422	X
		590/10	q	-0.233	N
		590/10	u	-0.452	X
		532/3	q	-0.219	N
		532/3	u	-0.472	X
		515/3	q	-0.360	N
		515/3	u	-0.703	X
		502/7	q	-0.298	N
		502/7	u	-0.663	X
		486/5	q	-0.246	N
		486/5	u	-0.500	X
		423/1	q	-0.204	N
		423/1	u	-0.544	X
40.573	ξ Boo A	656/4	u	-0.552	N
		510/10	q	-1.294	N
		510/10	u	-0.583	N
		492/10	u	-0.608	N
		480/10	u	-0.446	N
		440/10	q	-0.749	N
		440/10	u	-0.469	N

Table 5.5 Results of fitting a polynomial curve to data which clearly showed a drift in the Stokes' parameters.

over an hour when re-centering is performed many times during the observation (about every 10 to 20 minutes). Also, the variation should be periodic, *i.e.* after the star has been re-centred the Stokes' parameters should increase/ decrease until the next re-centre is performed, and then decrease/increase back to their original value. This is not seen in figures 5.14 (a) and (b) where the drift looks quite smoothly parabolic in u, and sinusoidal in q. Finally, the drifting effect is not seen in all channels, or at a particular wavelength. Therefore it can be concluded that this zero-point polarization change may not be due to the star wandering in the diaphragm.

5.6 Conclusions

The object of this investigation was to explore the possibility of detecting low levels of polarization (*i.e.* a few times 0.01%) in solar-type stars to high accuracy (<0.01%), but it has been shown that the instrumental effects dominate the measurements in two ways.

First, the instrumental polarization is greater than 0.1%, *i.e.* about an order of magnitude greater than the polarimetric signal being measured, and is not constant over observing times of an hour or so. Secondly, the MPF has inherent problems with the photon counters. As they intermittently overloaded, only low count rates could be used, which meant that the errors in measuring the polarization during an observation run of up to 2 hours were never smaller than 0.04%. Also, as the total amount of time needed to make a set of observations was large compared with the actual integration time of the measurements, the efficiency in making these measurements was small, and raises the question whether the MPF's ability to measure in many wave bands simultaneously is outweighed by the ensuing low count rates and time consumption when compared to two-channel instruments.

CHAPTER 6

COMPUTATIONAL MODELLING OF POLARIMERTRIC VARIATIONS DUE TO SOLAR ACTIVE REGIONS

6.1 The Reasoning behind this Investigation

The suggested detection of solar whole-disk polarization at 5000Å by Clarke (1991) showed that the polarimetric variations could be due to the movement of sunspots from day to day, and were correlated with the AAVSO activity index. The tilting filter experiment described in Chapter 3 seems to confirm that low levels of linear polarization can be measured and attributed to the position of active regions on the solar disk. The following is an argument that these results are due to a combination of magnetic intensification and resonant scattering effects.

Leroy and LeBorgne (1989) came to the conclusion that the linear polarization due solely to differential saturation in the light of active regions would hardly reach the level of 1 part in 10^7 when the whole solar disk is integrated. Their investigation centred on the observations of whole or part of an individual sunspot in a blue spectral band with half-maximum transmission at 4400Å and 4900Å. They found significant polarization measurements of $> 1.10^{-4}$ in $1'$ to $1'.5$ fields of view that would at least include the spot penumbras. They concluded that a major part of the polarized signal comes from the penumbras where the horizontal magnetic field gives a strong contribution, and it also seemed that cancellation due to axial symmetry of even isolated spots was far from complete.

In another paper, Leroy (1989) derived the expected polarization of 6000 individual solar spectral lines due to magnetic intensification for weak (500 Gauss) and strong (10,000 Gauss) magnetic fields. The values he gives for the Fe I and Hβ lines are used in the following model.

Landi Degl'Innocenti (1982) concentrated on magnetic intensification being the sole source of broad-band linear polarization in his model of cool stars with active regions. He obtained the fractional linear polarization emerging from the magnetic region dependent upon the direction of the magnetic field and the resultant Zeeman broadenings, the fraction of the continuum subtracted by the

spectral lines within the passband, the apparent position of the region on the stellar disk and the fraction of the disk surface area covered by the region. He produced polarization diagrams expected from single regions at various positions traversing a stellar disk which would allow comparison with observed data.

Tinbergen and Zwaan (1981) also addressed the question of polarimetric variations being due to active regions. They assumed that the circularly symmetric penumbrae of sunspots would hardly contribute to the polarization signal, and that the largest contribution is to be expected from faculae in the active regions near the east and west limbs as they present the strongest transverse component of the magnetic field. This transverse component is perpendicular to the limb so that the resultant polarization has its electric vector parallel to the equator. Indeed they argue that, for a star viewed nearly in its equatorial plane like the Sun, the direction of polarization will always be roughly *parallel* to the stellar equator. This is *not* seen in the data of Clarke (1991) nor in the data treated in this thesis.

As discussed in Chapter 1 another possible method of producing polarized light in the case of the Sun (or solar type stars) is resonant and fluorescent scattering. The magnitude of polarized light produced in this way is at a maximum for scattering at 90°, i.e. from light at the limb, and its direction is perpendicular to the radial vector at that point (so at a tangent to the limb). Polarized light from this source has been observed by Stenflo (1981, 1983a, 1983b). Circular symmetry means that whole-disk polarization would cancel out, so an asymmetry is needed for net polarization to be observed. One such effect that could provide an asymmetry is the Hanle mechanism whereby the polarization associated with resonance scattering is rotated from its regular vibration of being tangential to the limb according to the strength of the local magnetic field.

Rayleigh scattering and scattering by electrons may also be present in limb polarization, and this may be enhanced by there being a disturbance near the

limb. Leroy (1972) showed how a plage altered limb polarization, and suggested that the centre-to-limb polarization may have different behaviours along equatorial and polar radii, which may result in a small net polarization.

With the above information in mind the following assumptions are going to be made in an effort to predict the polarization from the Sun due to magnetically active regions on its surface.

1. The presence of an active region, which will be regarded as a partially polarized source within magnetically sensitive lines (as found by Leroy) in contrast with quiet regions of the photosphere, will break the circular symmetry that is required to cancel whole-disk polarization produced purely by scattering of unpolarized light, either resonant or fluorescent (as described by Stenflo), or Rayleigh, which have greatest effect towards the limb. This assumption can be made as there is not necessarily circular symmetry within each active region, which will leave a net polarization in a line (Leroy and LeBorgne), and also regions are not symmetrically distributed on the solar surface, being restricted to latitudes between about $\pm 40^{\circ}$.
2. The strength of the observed polarization produced by an active region increases as a region approaches the limb, in accordance with the nature of scattering, in a sinusoidal nature (for simplicity), i.e. $p_{obs} = p_{max}.\sin\chi$, where $\cos\chi = \cos\alpha.\cos\delta$, with (α,δ) being the *apparent* longitude and latitude of the region in the equatorial frame. The geometry is similar to the formulation by Landi Degl'Innocenti except that a particular direction of the magnetic axis is not required here. Of course the direction of polarization due to magnetic intensification is not necessarily tangential to the limb at any point on the disk, but even if such directions of vibration are randomly distributed then the p

vector can be split into its components parallel and perpendicular to the limb, and the strength of p_{parallel} could be used as the partially polarized source scattered with its vector tangential to the limb, with the perpendicular component not being scattered towards the observer.

3. The magnitude of the polarization from a patch of photosphere is affected by limb darkening because the total intensity from the patch follows the law

$$I = I_{\text{diskcentre}}.(1 - u1 + u1.\cos\chi) \qquad (6.1)$$

with u1 being a wavelength dependent parameter, and χ as defined above.

A spectral band corresponding to the passband used in the tilting-filter experiment will be chosen, and the number of spectral lines within the band which exhibit polarization can be found in Leroy (1989). His calculated polarizations within a continuum band of 20Å correspond to a magnetic field strength of 500 Gauss. The magnitude of the polarization is dependent upon the magnetic field strength cubed, and for this study a value of 1500 Gauss will be used for the active regions. As the passband chosen is not 20Å a correction needs to be made to the polarization value considering also the width of the spectral line.

Extension of the model to arbitrary stars can easily be made by inclining the rotation axis away from the perpendicular to the direction of the observer, whereas for the Sun it lies almost along the x-axis of an x,y,z co-ordinate system with z being in the direction of the observer. Such an inclination can be thought of as a tilt of the rotation axis by an angle ε in the x-y plane followed by a precession of the new rotation axis about the x-axis by an angle π. The calculations can then be made for various phases throughout a rotation period of the star to show the form of the polarimetric variation. This process may be repeated for various values of ε and π.

6.2 Geometry

Figure 6.1 shows the geometry of the system. Consider a star whose rotation axis is along the x-axis of a right-handed co-ordinate system with the z-axis in the direction of the observer. The direction of stellar rotation in the y-z plane is anticlockwise (from z through y). The origin is at the centre of the star so that its equator lies in the y-z plane. The Stokes' parameters are defined such that positive Q is in the positive x-direction, or North, and that positive U is in the North-East direction, i.e. at 45° anticlockwise from North in the x-y plane.

Consider then a magnetic spot at position S, whose longitude on the actual stellar surface is α, at phase = 0, and whose latitude is δ with respect to the disk centre, C. and the rotation axis of the star, which is tilted with respect to the observer by ε in the x-y plane to x'. It is required to calculate the new apparent longitude and latitude of the spot at S (ϕ',θ) with respect to C to an observer along the z-axis, given α, δ, and ε.

For the anti-clockwise rotation about the z-axis consider the spherical triangle PP'S, where P and P' denote the poles on the x and x' axes respectively. The sides of the triangle are P'P = ε, PS = 90°-θ and P'S = 90°-δ. As OP'P and OPP' are both right angles then it follows that PP'S = 90°-α and P'PS = 90°+ϕ'.

Using the cosine formula,

$$\cos PS = \cos P'P \,.\, \cos P'S + \sin P'P \,.\, \sin P'S \,.\, \cos PP'S \qquad (6.1)$$

this gives

$$\cos(90-\theta) = \cos \varepsilon \,.\, \cos(90-\delta) + \sin \varepsilon \,.\, \sin(90-\delta) \,.\, \cos(90-\alpha) \qquad (6.2)$$

which can be rewritten as

$$\sin \theta = \cos \varepsilon \,.\, \sin \delta + \sin \varepsilon \,.\, \cos \delta \,.\, \sin \alpha \qquad (6.3)$$

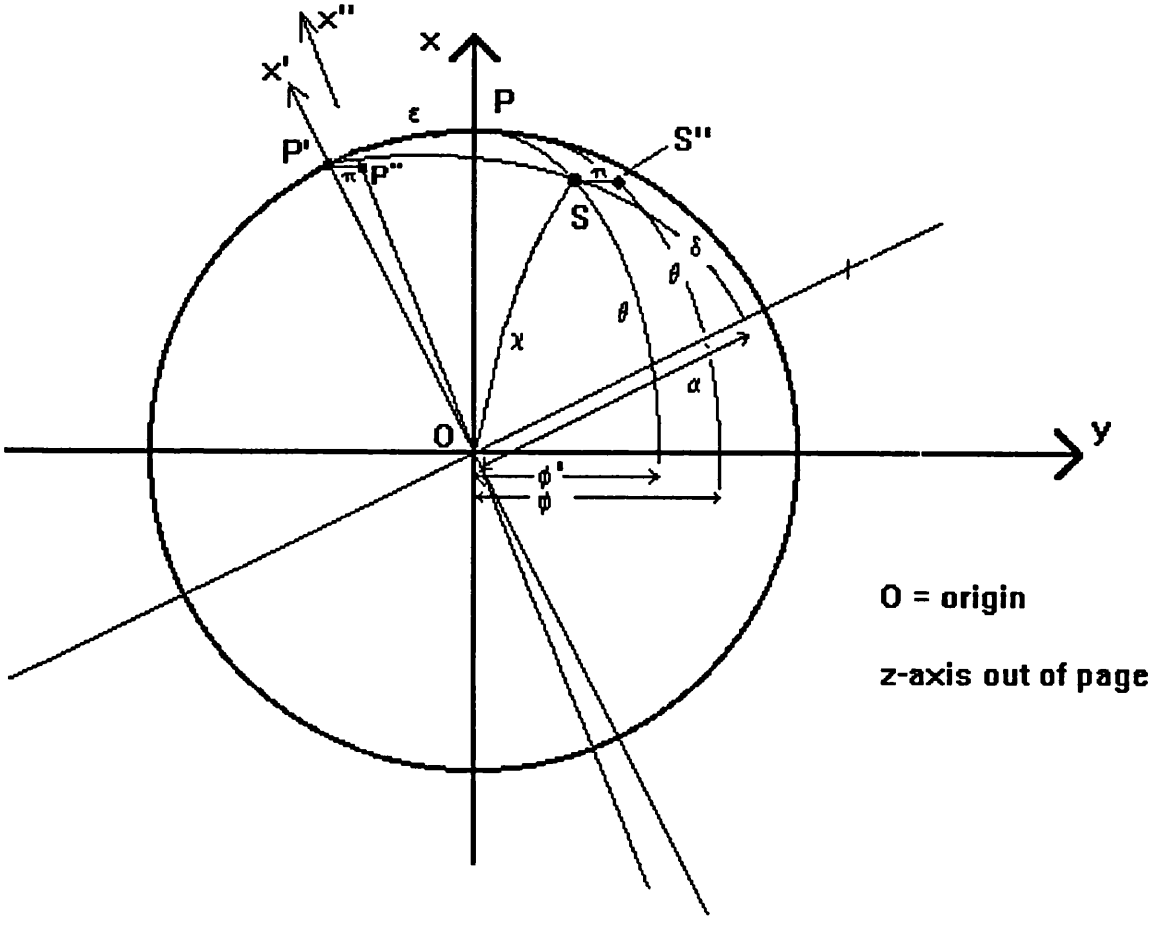

Fig. 6.1 Geometry of the model described in section 6.2. The symbols are explained in the text.

Also, if the line OS is defined by

$$\cos \chi = \cos \alpha \, . \, \cos \delta \tag{6.4}$$

and it is obvious that

$$\cos \chi = \cos \alpha \, . \, \cos \delta = \cos \theta \, . \, \cos \phi' \tag{6.5}$$

Knowing α, δ, and θ from equation 6.3, ϕ' is found and the new apparent spot position, S (ϕ',θ), is known completely.

The angle of precession of the axis x′ about x to x″, π, can then be added to ϕ' to complete the transformation to S″ (ϕ,θ).

Suppose that the light from the spot at S″ is partially polarized due to magnetic intensification. If this partially polarized light is scattered towards the observer in a plane parallel to the tangent to the stellar limb when the line OS″ is extended, then the angle between the tangent and the x-axis is the polarimetric position angle, ψ. This can be found using the equation

$$\tan \psi = \tan \theta \, / \, \sin \phi \tag{6.6}$$

The strength of the polarization depends on its proximity to the limb. As stated before it is at its strongest at the limb, say p_{max}, and zero at the centre of the stellar disk, and so a sinusoidal variation can be assigned using the angle OS″, i.e.

$$p = p_{max} \, . \, \sin \chi \tag{6.7}$$

where χ is now defined as $\cos \chi = \cos \phi \, . \, \cos \theta$.

However this will not be the observed amplitude of p as limb darkening has

to be taken into account. Limb darkening is wavelength dependent and is tabulated for some values of λ in Allen (1973). A simple interpolation was done to calculate the limb darkening parameter, u1, such that for $4000 < \lambda < 7000$Å.

$$u1 = 0.53 + ((6500-\lambda)/500).(1 + (6500-\lambda)/500)/100 \qquad (6.8)$$

and

$$I_{S''} = I_{max} (1 - u1 + u1.\cos\chi) \qquad (6.9)$$

where $I_{S''}$ is the intensity of the spot a distance χ from the disk centre, and I_{max} is the intensity at the disk centre.

The polarized intensity from the spot is now found using the equation

$$P_{S''} = I_{S''} \cdot p_{max} \cdot \sin\chi \qquad (6.10)$$

and knowing the position angle ψ we can get $Q_{S''}$ and $U_{S''}$ by

$$Q_{S''} = P_{S''} \cdot \cos 2\psi \quad \text{and} \quad U_{S''} = P_{S''} \cdot \sin 2\psi \qquad (6.11)$$

If the polarized intensities of all such spots on the *visible* hemisphere of the star are calculated, and the total intensity, I, from the hemisphere is found then the normalized Stokes' parameters are

$$q = \frac{1}{I} \sum_j Q_{S''_j} \quad \text{and} \quad u = \frac{1}{I} \sum_j U_{S''_j} \quad (j = 1 \text{ to N spots}) \qquad (6.12)$$

6.3 Comparison with the Solar Whole-disk Observations

Figure 3.16 shows the positions of the active regions on the visible hemisphere of the Sun on the days of observations (2, 3, 4 and 11 September 1991) with the tilt-tunable whole-disk polarimeter, and these positions were input into

the model. Spectral bands approximating that of the 4875Å filter at the Fe I and Hβ positions were used (approximate in that the true FWHM dependence on tilt angle was not known) and the relevant polarization values for lines included in the passbands were found to compute p_{max}.

In considering the results it should be noted that the magnitudes of the Stokes' parameters may well not agree with the observed ones, and this is to be expected since a general value of magnetic field strength was employed and not specific values for each region. The values of p_{max} should not be considered as accurate, especially as the filter passband was approximated, as were the sizes of the active regions. However these things effect q and u equally in magnitude, whereas it is the variation of the position angle in the q,u plane that is of most interest.

It would require an extremely rigorous treatment to input actual active region sizes, distributions, magnetic field strengths within regions, and accurate values of p_{max} within the filter passbands to get a true picture of the polarimetric variations, but the assumptions made here should allow an indicative estimate of the variations.

Figures 6.2 (a) and (b) show the calculated q,u values for the spectral bands containing the Fe I and Hβ lines respectively. While not totally agreeing with the observed data shown in figures 3.13 to 3.15, as the model predicts a positive q when negligible q was actually observed, it should be noted that the values for 2 and 11 September in the model have a more positive u component than those of 3 and 4 September, which *is* seen in the data, and the model seems to have successfully predicted the changes in u seen in the data.

That the computed values have a large, positive q is expected from the method of computation as active regions are concentrated near to the equator and away from the pole, contributing more to positive q than to negative q. This is not seen in the observed data but it is apparent that the variation in the computed q values is small, which does agree with the data. It might not be wrong

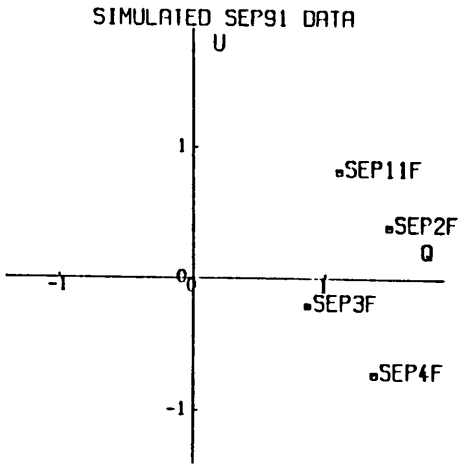

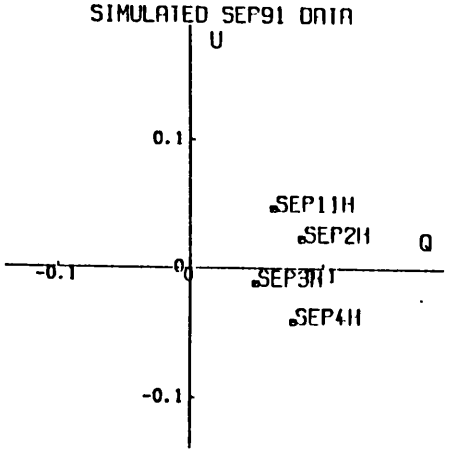

Fig. 6.2 *q,u* diagram for computed data for (a) Fe (above) and (b) Hβ (below). The date corresponding to which sunspot data were used is written by each point for comparison with solar observations. F and H correspond to Fe and Hβ. (Units are 0.01% on each axis).

to speculate that in taking a difference to arrive at the spectral line polarization in the solar work, it might be that the continuum does exhibit some polarization, which would almost certainly be caused by scattering rather than magnetic effects.

These results seem to agree with the speculative conclusions made in Chapter 3 in that polarimetric variations in the integrated light from the whole solar disk may be due to the movement of magnetically active regions, whose effects are at their greatest when they are near to the solar limb.

6.4 Results for Arbitrary Stars

The positions of the active regions on the visible hemisphere of the Sun on 2 September 1991 (figure 3.16) were used to compute the q,u values during one complete rotation period in phase steps of 3°. The computation was done for values of $\varepsilon=0°$ and $\pi=0°$ to mimic solar rotation, and for values of ε = 20°, 40°, 60° and 90°, π = 0°, 20°, 40°, 60°, 80° and 90°. Naturally, as there are only spot positions for one hemisphere, then there will be phase positions at which q and u are both zero.

The chosen spectral band is centred on 4875Å with a 10Å FWHM which would be more applicable to stellar observations. This passband includes the Fe lines as before and also a strongly polarized line at 4878Å.

Figure 6.3 shows the q,u diagram for a whole rotation with ε = 0 and π = 0. From the starting point 1 the u component decreases which is in agreement with the observed data from 2 to 4 September, with about every fourth to fifth point representing each successive day (apparent solar rotation is about 13° per day).

Figures 6.4 to 6.7 show polarization diagrams for whole stellar rotations for stars inclined in the x-y plane at 20°, 40°, 60° and 90° respectively, with each figure containing diagrams corresponding to π = 0°, 20°, 40°, 60°, 80° and 90°.

The forms of the polarization diagrams are quite diverse, so if polarimetric measurements were made of a star during one or more complete revolution periods it may be possible to compare the data with the computed diagrams. This would require longer living active regions than those that occur on the Sun, which typically last less than 25 days (about 1 revolution period), and which can grow and move apart during their lifetimes, and in turn complicate the polarization diagram.

However a star like ξ Boo A has a rotation period of only 6.2 days and has reported magnetic patches, and so would be a likely candidate for such an investigation as it would be hoped that these patches would be stable for many rotation periods. But as described in Chapter 5, accurate observations every night over the course of a week proved fruitless in this case due to instrumental problems.

Unfortunately the stellar observations made with the Glasgow polarimeter were too sporadic to be used in an investigation of this type, and it is doubtful that the weather would allow one in the future. But further solar observations may be possible (it is more likely to have 14 consecutive sunny days in summer, at least for a few hours, than 14 consecutive clear nights in autumn, winter or spring in Glasgow!), and with the knowledge of spot positions and magnetic field strengths from sources such as the Boulder Geophysical Prompt reports, coupled with a more rigorous treatment of the physics behind the problem (for which time did not allow here), a more refined model could be made.

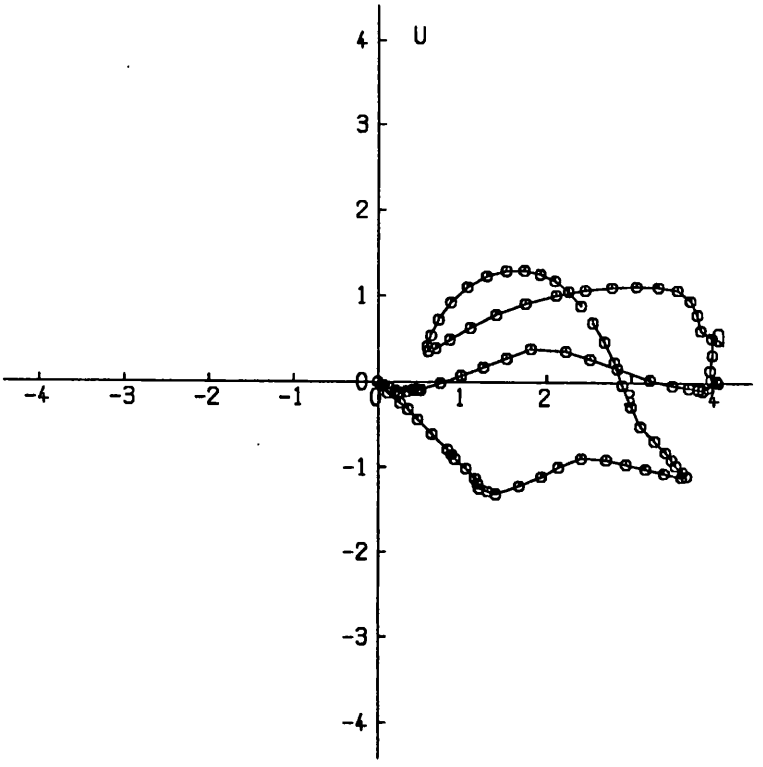

Fig. 6.3 q,u diagram for computed data corresponding to a complete stellar rotation for $\varepsilon = 0$ and $\pi = 0$ at phase intervals of 3°, with active region positions taken from 1991 September 2. Origin (0,0) is at the centre of the grid. (Units are 0.01% on each axis).

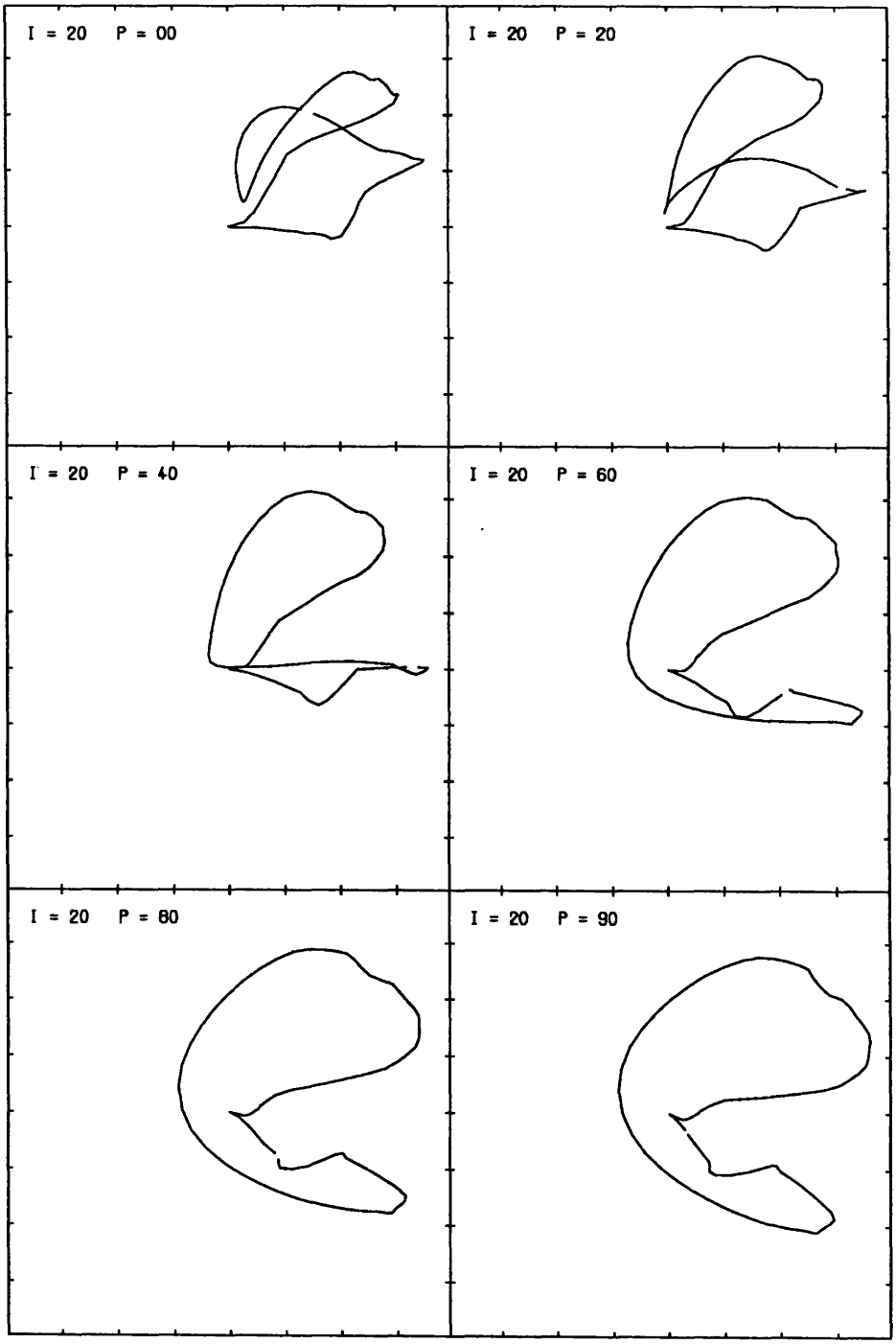

Fig. 6.4 *q*,*u* diagrams showing a complete stellar rotation with a rotation axis inclination of $\varepsilon = 20^\circ$ and precessions $\pi = 0$, 20, 40, 60, 80 and 90°, with sunspot positions as for figure 6.3. Origin (0,0) is at the centre of each grid.

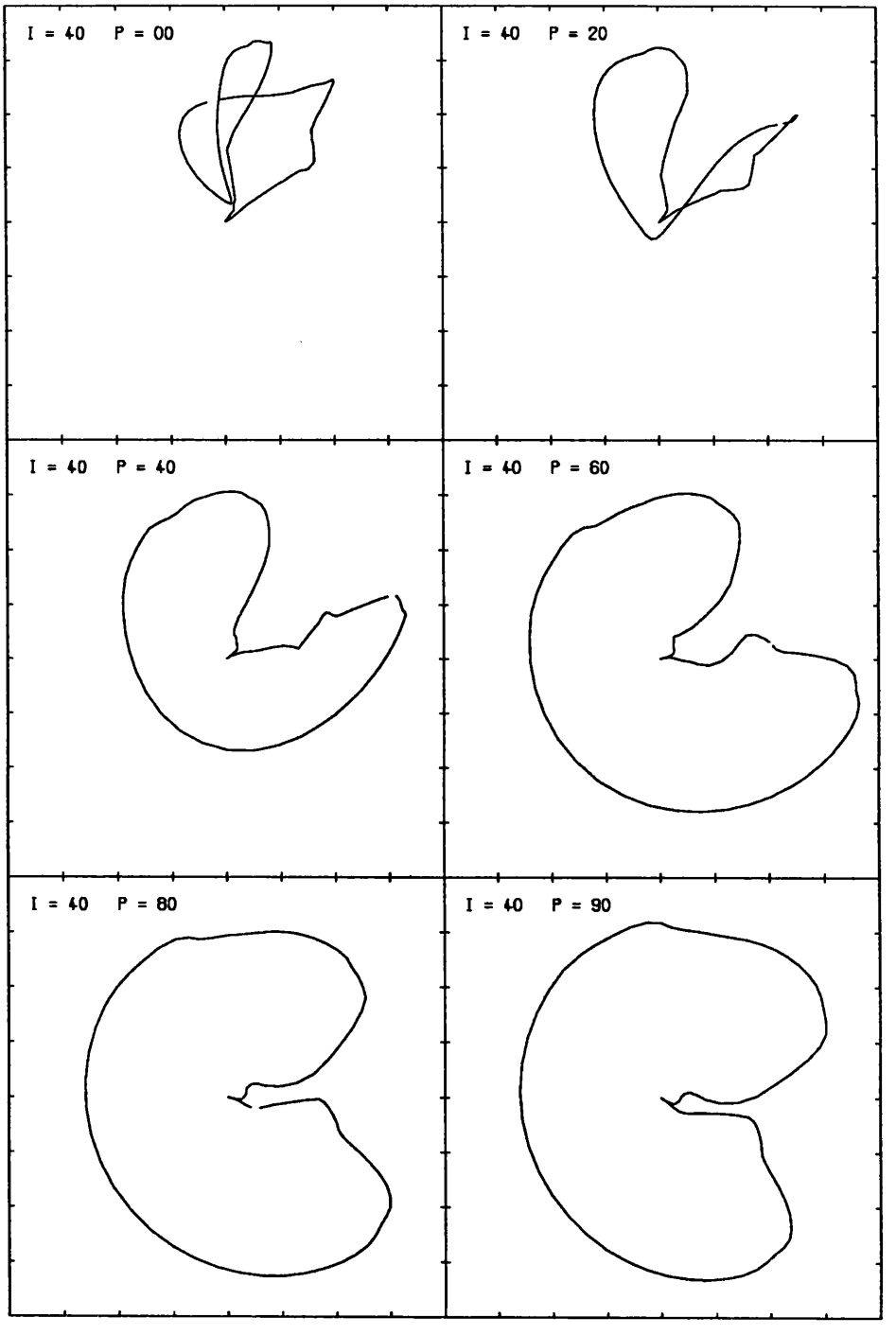

Fig. 6.5 *q*,*u* diagrams as for figure 6.4 but for inclination $\varepsilon = 40^{\circ}$.

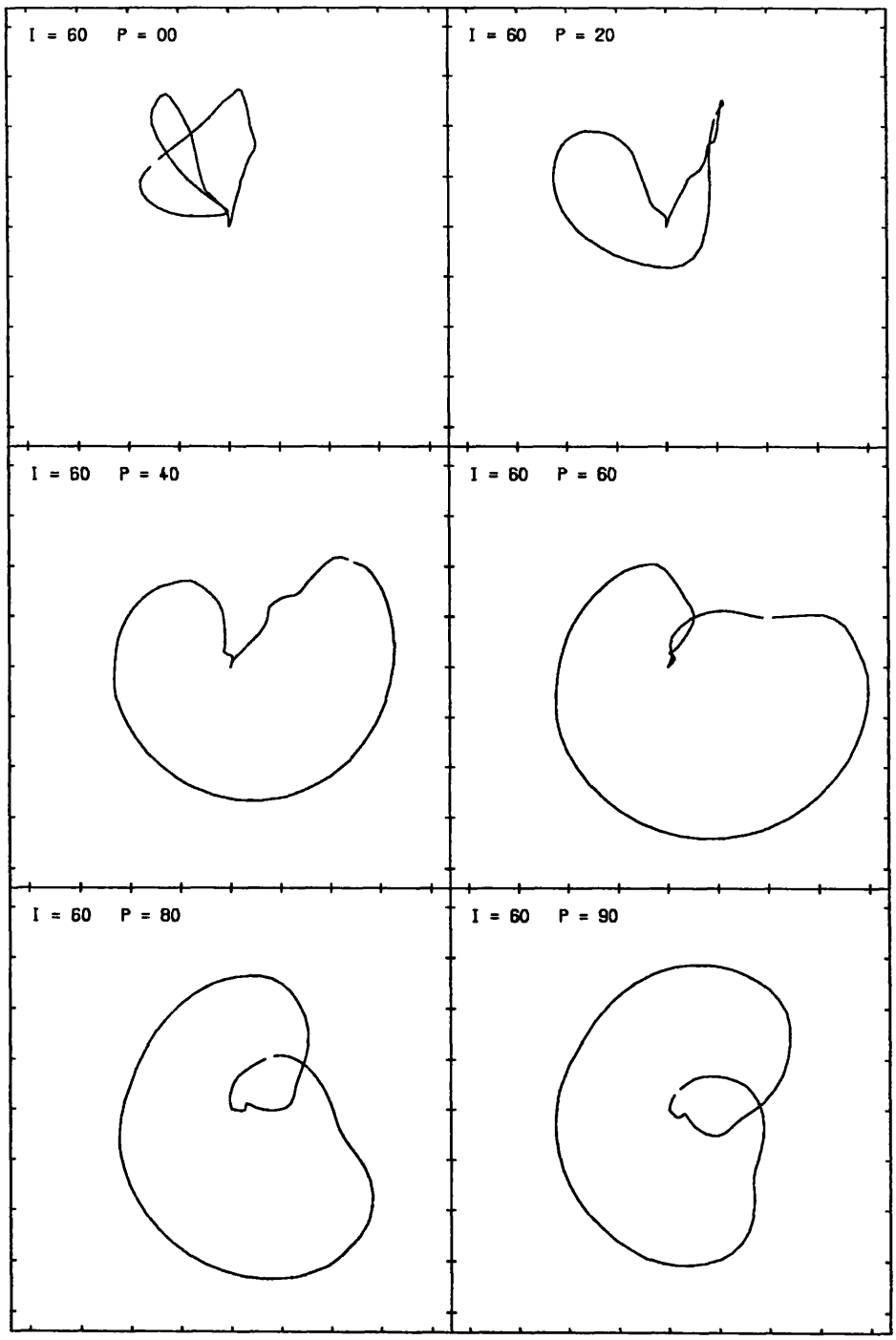

Fig. 6.6 *q,u* diagrams as for figure 6.4 but for inclination $\varepsilon = 60^{\circ}$.

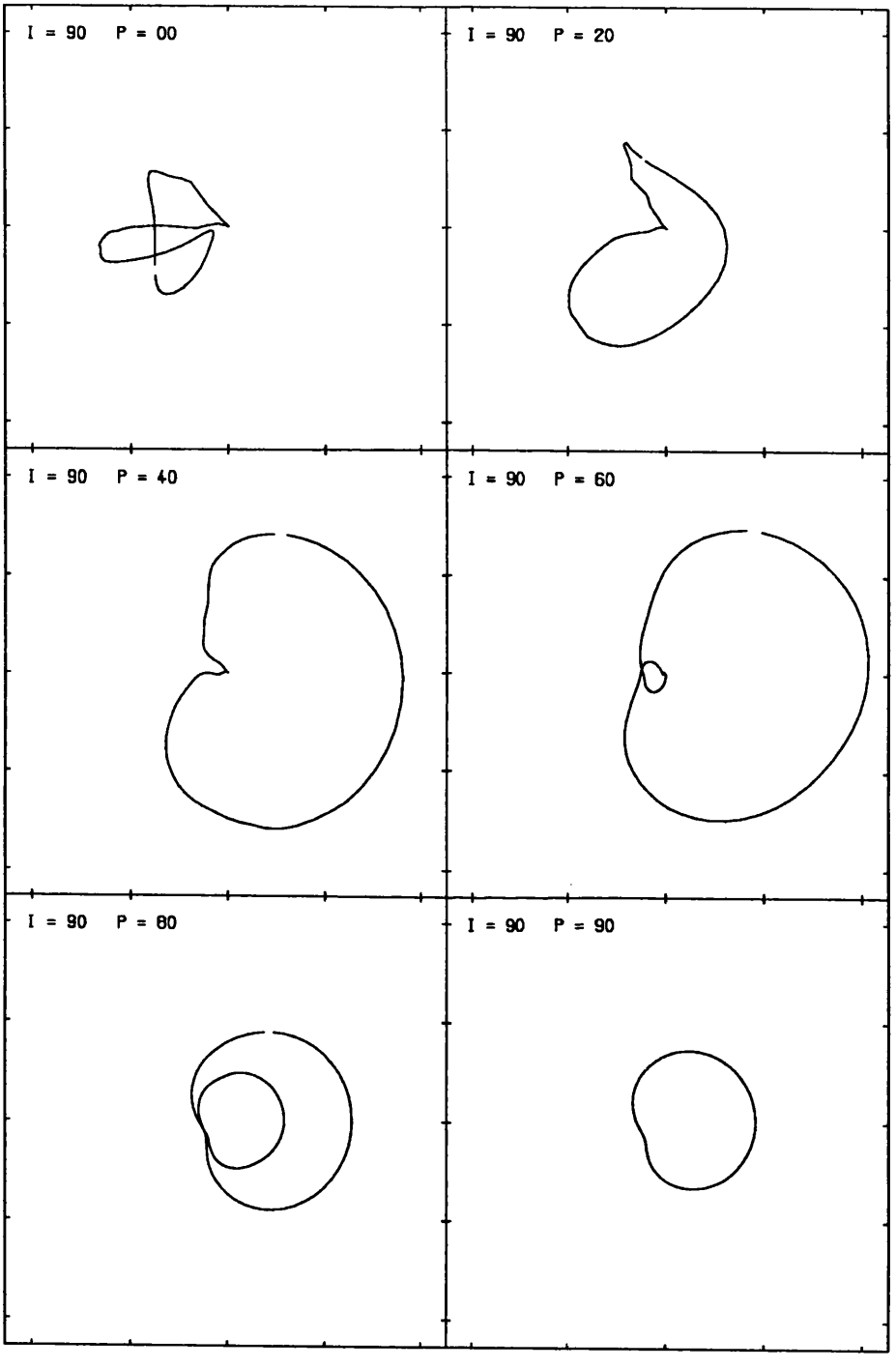

Fig. 6.7 *q,u* diagrams as for figure 6.4 but for inclination $\varepsilon = 90^{\circ}$.

CHAPTER 7

CONCLUSIONS AND FUTURE WORK

7.1 Solar Polarimetry

7.2 Stellar Polarimetry

7.1 Solar Polarimetry

The design of the double beam solar polarimeter, which could have given an important insight into the mechanisms behind and the apparent variations of solar polarizations, was unfortunately not completed due to problems of mechanical and electrical natures.

With the results from chapter 3 of the solar whole-disk experiment in mind it is even more regrettable, because those observations suggested very strongly that small polarizations exist above 10^{-5} in degree, and may well be temporally variant. However those measurements were made within a 2Å spectral band, either at the centre of the Hβ line or in the trough resulting from many Fe I lines at about 4872Å, so no conclusions could be drawn on their effect on broad band polarizations for which Clarke (1991) had previously shown to be similarly variant due to the day-to-day movement of sunspots.

A number of suggestions as to the nature of the polarization mechanisms were postulated, the most likely being magnetic intensification in areas of strong magnetic fields and limb effects such as coherent scattering. The centre-to-limb variation of scattering is well known so it would be expected that Hβ polarization is zero at the disk centre, but spectral lines that are magnetically sensitive may exhibit polarization at the disk centre, and the polarimetric CLV of magnetic intensification is unknown.

It is therefore important that future observations *do* attempt to compare the polarizations from magnetically active and quiet regions of the solar photosphere, and monitor their variations with respect to position on the disk. For example, as Stenflo *et al.* (1983 b) had shown that Hβ polarization 10 arcseconds inside the solar limb was due to coherent scattering, it is important to know whether this mechanism was completely responsible for the Hβ polarizations found in the whole-disk observations. If that is the case then why should the degree of polarization due to scattering change from day-to-day?

The simplistic model described in chapter 6 predicted polarimetric variations due to the changing positions of sunspots that were consistent with the observed data. The model postulated that if a spectral line exhibits polarization in the presence of a magnetic field, then that intrinsic polarization will break the symmetry of whole-disk polarization due to scattering, which would otherwise average to zero. While not employing radiative transfer to calculate the precise amount of polarization scattered from a polarized source, the results of the model and their agreement with the data suggest that this study should be pursued in a physical nature.

Short period variability in the solar data was hinted at but was not conclusive. The well known acoustic oscillations with periods of about 5 minutes may well affect polarization, but this is not the place to discuss how. One problem in finding out whether the effect is seen is in the method of data acquisition. The very nature of photometric techniques are putting stringent limits on the levels of polarimetric accuracy, with temporal resolution being traded for higher levels of precision. When photon count rates are only of the order of 10^5 photons per second, then 1000 seconds are needed for the errors on the Stokes' parameters to be as low as 1 part in 10^4 if photon shot noise dominates. But if photon count rates are increased in an effort to achieve those error levels in shorter time scales then it has been also shown in this thesis that dead-time can seriously affect the data and the calculation of the degree of polarization.

The use of charge coupled devices (CCD's) in polarimetry was mentioned. They have the advantage of being able to record many tens of thousands of photons per second in arrays of thousands of pixels such that a precision of the required level may be achieved in a single one second integration (if the CCD has a 16 bit read-out), and a further advantage is that CCD measurements are not affected by photon shot noise. But CCD's have their own inherent data acquisition problems in that the pixels may have different quantum efficiencies with respect to the

orientation of the electric vectors of the incident photons, and this will have to be calibrated by flat-field observations. Also CCD's usually require many seconds for the charge in each pixel to be read-out, which means that short period variability may indeed not be found using CCD methods. However, after respecting these facts, a double beam polarimeter such as that described in chapter 2 could make excellent use of a CCD detector as each beam would be incident upon its own distinct and unvarying patch of the CCD, and the pixels in each area would only have photons with a certain electric vector orientation incident upon them. Once calibration is accomplished by using light of a known polarized state then the polarimeter would be complete.

7.2 Stellar Polarimetry

The observations made at Glasgow were largely affected by noise, which were attributed to atmospheric effects, and were extremely sporadic, which therefore allowed no investigation into reported photometric and polarimetric variability of the observed stars α Boo and α Tau. Some significant results, however, can be stated.

The instrumental polarization was found for both channels to an accuracy of better than 0.005%, and as the observations of unpolarized standard stars were made over a period of 14 months it was also shown that the instrumental polarizations was stable.

Observations of α Tau found significant levels of broad-band polarization at 4500Å, which showed a statistical difference at above the 95% confidence level between measurements made over a six week period in early 1992. Measurements at 5000Å were found to be unpolarized within the errors. No short period changes were found.

The measurements of α Boo in the winters of 1992 and 1993 showed two significant results. Measurements in four spectral bands showed that the

polarizations were temporally variant at the 95% confidence level at 4200Å, 4800Å and 5100Å, but that no polarization was present at 5600Å. The levels of polarization were greatest at the shortest wavelength and zero at the longest wavelength, but those at 4800Å and 5100Å could not show the distinct form of the wavelength dependence due to magnetic intensification shown in figure 1.6, so the polarizing mechanism for α Boo may be due to scattering only.

Further observations over an extended period of time are needed for these stars, whose well documented variability and relative brightness make them excellent candidates for polarimetric monitoring in an attempt to explain polarizing mechanisms.

The atmospheric effects could not be completely explained by correlation analysis. The argument that a sharp increase or decrease in brightness will affect the measurements of q (and u) for each channel in opposite senses because of the method of data acquisition is sound, but it could not be repeated mathematically. No other reason for the observed $>99\%$ anti-correlation between the q_{red} and q_{blue} (and u_{red} and u_{blue}) could be argued theoretically. The non-correlations between q and u for either channel agree with the calculations of Stewart (1984) for continuously rotating half-wave plate polarimeters.

The observations made with the Multi-purpose Photometer were extremely frustrating as it was expected to be able to measure polarization from a reportedly polarized star, ξ Boo A, over a complete rotation period, which would allow comparisons with the data of the Sun and also with the predictions of the model. Although some measurements were significantly different than those made of an unpolarized star in the same spectral band on the same night, the apparent drift in the instrumental polarization that was highlighted in chapter 5 made it impossible to come to any conclusions about the polarization from ξ Boo A or ξ Her. In trying to formulate the "zero-point polarization" drift from the observations of unpolarized standard stars 46 LMi and α UMa it was found that no specific absolute time or hour angle of the star being observed could describe

the point at which the normalized Stokes' parameters reached a maximum or minimum value, and that the position of the star in the sky did not make any difference to the variation of either Stokes' parameter with time.

With these results in mind it is suggested that this instrument should not be used for measuring low levels of polarization as errors less than 0.1% could not be attained. It was claimed that highly polarized objects had been observed correctly beforehand, and the observations of o Sco agree with this claim. However it is believed that this instrument is no longer being used for polarimetric observations.

There is still a distinct gap, therefore, in our knowledge and interpretation of the polarization of the Sun and solar-type stars. Until quality observations over long periods are possible neither the question of the levels of polarization seen in these stars or of the mechanisms producing them can be answered. These investigations have an important role in studying "solar-stellar connections" and should be pursued as there is potentially a wealth of information to be gained.

APPENDIX A

Mueller matrices describing optical elements used in the instrumentation

1. Rotation of the Stokes' parameters through an angle ϕ measured anti-clockwise about the x-axis:

$$\left[R(\phi) \right] = \begin{bmatrix} 1 & 0 & 0 & 0 \\ 0 & \cos 2\phi & \sin 2\phi & 0 \\ 0 & -\sin 2\phi & \cos 2\phi & 0 \\ 0 & 0 & 0 & 1 \end{bmatrix}$$

2. A perfect polarizer:

$$\left[P \right] = \frac{1}{2} \begin{bmatrix} 1 & 1 & 0 & 0 \\ 1 & 1 & 0 & 0 \\ 0 & 0 & 0 & 0 \\ 0 & 0 & 0 & 0 \end{bmatrix}$$

For the Savart plate, the emerging ordinary beam has been transformed as above, and the emerging extraordinary beam has been transformed by a perfect polarizer in the orthogonal direction, given by:

$$\left[P \right] = \frac{1}{2} \begin{bmatrix} 1 & -1 & 0 & 0 \\ -1 & 1 & 0 & 0 \\ 0 & 0 & 0 & 0 \\ 0 & 0 & 0 & 0 \end{bmatrix}$$

3. A pure retarder (such as a half-wave plate) of retardance Δ:

$$\left[\Delta \right] = \begin{bmatrix} 1 & 0 & 0 & 0 \\ 0 & 1 & 0 & 0 \\ 0 & 0 & \cos\Delta & \sin\Delta \\ 0 & 0 & -\sin\Delta & \cos\Delta \end{bmatrix}$$

REFERENCES

Allen, C. W., 1973, Astrophysical Quantities, Athlone Press, 3rd Edition

Angel, J. R. P., 1974, in "*Planets, stars and nebulae studied with photo-polarimetry*", ed. T. Gehrels, Univ. of Arizona Press, Tucson, p.54

Astronomical Almanac, 1991, 1992, 1993, H.M.S.O., London

Babcock, H. W., 1947, *Astrophys. J.* **105**, 105

Balasubramaniam, K. S., West, E.A. and Hagyard, M.J., 1990, in "*Solar Polarimetry*", Proc. of the 11th National Solar Observatory/Sacremento Peak Summer Workshop, Sunspot, New Mexico, ed. L.J. November, p213.

Baliunas, S. L., Hartmann, L., Vaughan, A. H., Liller, W., and Dupree, A. K., 1981, *Astrophys. J.*, **246**, 473

Basri, G.,Marcy, G. W., 1988, *Astrophys. J.* **330**, 274

Boesgard, A. M., 1974, *Astrophys. J.*, **188**, 576

Brown, M. B., Forsythe, A. B., 1974, *Technometrics* **16**, 129

Clarke, D., 1963, Ph.D. Thesis, University of Manchester

Clarke, D., 1986, *Astron. Astrophys.*, **156**, 213

Clarke, D., 1989a, in *Practical Electronics*, October 1989, 12

Clarke, D., 1989b, in *Practical Electronics*, November 1989, 48

Clarke, D., 1991, *Vistas in Astronomy* **34**, 303

Clarke, D., and Grainger, J. F., 1971, "*Polarized Light and Optical Measurement*", Oxford, Pergamon Press

Clarke, D., McLean, I. S. and Wyllie, T. H. A., 1975, *Astron. Astrophys.* **43**, 215

Clarke, D., Stewart, B. G., Schwarz, H. E., Brooks, A., 1983, A&A **126**, 260

Coyne, G. V., McLean, I. S., 1982, in "*Polarimetry and Physics of Be star Envelopes*", IAU Symp. No. 98, Eds. Jaschek, M., Groth, H-G., p77

Dollfus, A., 1965, in "*Stellar and Solar Magnetic Fields*", IAU Symp. No. 22, ed. R. Lüst, p.176

Dollfus, A., 1974, in "*Planets, stars and nebulae studied with photo-polarimetry*", ed. T. Gehrels, Univ. of Arizona Press, Tucson, p.695

Gehrels, T. and Teska, T. M., 1963, *Applied Optics*, **2**, 67

Gondoin, Ph., Giampapa, M. S., and Bookbinder, J. A., 1985, *Astrophys. J.* **297**, 710

Gray, D. F., 1984, *Astrophys. J.*, **277**, 640

Hall, J. S., 1949, *Science*, **109**, 166

Hall, J. S., 1960, *Lowell Obs. Bull.*, **4**, 264

Hiltner, W. A., 1949, *Science*, **109**, 165

Huovelin, J., Linnaluoto, S., Piirola, V., Tuominen, I. and Virtanen, H., 1985, *Astron. Astrophys.* **152**, 357

Huovelin, J., Saar, S. H., and Tuominen, I., 1988, *Astrophys. J.* **329**, 882

Kemp, J. C., Henson, G. D., 1983, *Astrophys. J* **266**, L69

Kemp, J. C., and Wolstencroft, R. D., 1974, *M.N.R.A.S.* **166**, 1

Kemp, J. C., Henson, G. D., Kraus, D. J., Beardsley, I. S., Carroll, L. C., and Duncan, D. K., 1986, *Ap. J.* **301**, L35

Landi Degl'Innocenti, E., 1982, *Astron. Astrophys.* **110**, 25

Leroy, J. L., 1972, *Astron. Astrophys.* **19**, 287

Leroy, J. L., 1989, *Astron. Astrophys.* **215**, 360

Leroy, J. L., 1990, *Astron. Astrophys.* **237**, 237

Leroy, J. L., and LeBorgne, J. F., 1989, *Astron. Astrophys.* **223**, 336

McGale, P. A., 1986, Ph.D. Thesis, University of Glasgow

McLean, I. S., 1974, Ph.D. Thesis, University of Glasgow

Marcy, G. W., 1981, *Astrophys. J.*, **245**, 624

Marcy, G. W., 1982, *Publ. Astron. Soc. Pacific*, **94**, 989

Marcy, G. W., 1984, *Astrophys. J.* **276**, 286

Marcy, G. W., Basri, G., 1989, *Astrophys. J.*, **345**, 480

Mickey, D. L. and Orrall, F. Q., 1974, in "*Planets, stars and nebulae studied with photopolarimetry*", ed. T. Gehrels, Univ. of Arizona Press, p.686

Mie, G., 1908, *Ann. Physik.*, **25**, 377

Moore, C. E., Minnaert, M. G. J., Houtgast, J., 1966, *The Solar Spectrum* - 2935Å *to* 8770Å, National Bureau of Standards Monograph 61, Washington

Noyes, R. W., Hartmann, L. W., Baliunas, S. L., Duncan, D. K., Vaughan, A. H., 1984, *Astrophys. J.*, **239**, 961

Öhman, Y, 1942, *Stockholms Obs. Meddelande* No. **54**, 1

Piirola, V., 1977, *Astron. Astrophys. Suppl.* **30**, 213

Press, W. H., Flannery, B. P., Teukolsky, S. A., and Vetterling, W. T., 1986, "*Numerical Recipes, The Art of Scientific Computing*", Cambridge, Cambridge University Press, pp.153/4

Robinson, R. D., Worden, S. P., Harvey, J. W., 1980, *Astrophys. J. (Letters)*, **236**, L155

Saar, S. H., 1990, in "*Solar Photosphere: Structure, Convection and Magnetic Fields*", IAU Symp. No. 138, ed. Stenflo, J. O., p.427-441

Saar, S. H., Huovelin, J., Giampapa, M. S., Linsky, J. L., and Jordan, C., 1988, in "*Activity in Cool Star Envelopes*", eds. O. Havnes, *et al.*, Kluwer, Dordrecht, p.45

Schrijver, C. J., Coté, J., Zwaan, C., Saar, S. H., *Astrophys. J.*,**337**, 964

Schwarz, H. E.; 1986, *Vistas in Astronomy* **29**, 253

Serkowski, K., 1974, in "*Planets, stars and nebulae studied with photo-polarimetry*", ed. T. Gehrels, Univ. of Arizona Press, p. 135

Stenflo. I. O., Baur, T. G. and Elmore, D. F., 1980, *Astron. Astrophys.* **84**, 60

Stenflo, I. O., 1981, *Solar Instrumentation. What's Next?*, Ed. R. Dunn, Sacremento Peak National Observatory, Sunspot, New Mexico, p. 266

Stenflo, I. O., Twerenbold, D. and Harvey, J. W., 1983a, *Astron. Astrophys. Suppl. Ser.* **52**, 161

Stenflo, I. O., Twerenbold, D., Harvey, J. W. and Brault, J. W., 1983b, *Astron. Astrophys. Suppl. Ser.* **54**, 505

Stewart, B. G., 1984, Ph.D. Thesis, University of Glasgow

Timothy, J. G., Joseph, C. L., Linsky, J. L., 1981, *Bull. AAS*, **13**, 828

Tinbergen, J., and Zwaan, C., 1981, *Astron. Astrophys.* **101**, 223

Toner, C. G., Gray, D. F., 1988, *Astrophys. J.*, **334**, 1008

Van de Hulst, H. C., 1957, "*Light Scattering by Small Particles.*", Wiley and Sons, New York.

Vaughan, A. H., Preston, G. W., 1980, *Publ. Astron. Soc. Pacific*, **92**. 385

Walter, F., Charles, P., Bowyer, S., 1978, *Ap. J. (Letters)*, **225**, L119

Wang, H, 1990, in "*Solar Polarimetry*", Proc. of the 11th National Solar Observatory/Sacremento Peak Summer Workshop, Sunspot, New Mexico, ed. L.J. November, p25.

Wyllie, T. H. A., 1976, Ph.D. Thesis, University of Glasgow

Young, A. T., 1974, "*Methods of Experimental Physics*", **12**, part A, ed. N. Carleton, Acad. Press, New York, p.95.

Zirin, H.,1976, *Ap. J.*, **208**, 414